Salient Features of the North Indian Ocean associated with the Indian Summer Monsoon

Thesis submitted to the

Cochin University of Science and Technology

in partial fulfillment of the requirement for the Degree of

DOCTOR OF PHILOSOPHY
in
ATMOSPHERIC SCIENCE

BY

NEEMA. C.P

Department of Atmospheric Sciences
Cochin University of Science and Technology
Lake Side Campus, Cochin - 682 016

January 2005

CERTIFICATE

This is to certify that the thesis entitled "***Salient Features of the North Indian Ocean Associated with the Indian Summer Monsoon***" is a bonafide record of research work done by **Mrs. NEEMA.C.P** in the Department of Atmospheric Sciences, Cochin University of Science and Technology. She carried out the study reported in this thesis, independently under my supervision. I also certify that the subject matter of the thesis has not formed the basis for the award of any Degree or Diploma of any University or Institution.

Certified that **Mrs. Neema.C.P** has passed the Ph.D qualifying examination conducted by the Cochin University of Science and Technology in January 2003

Dr C A Babu
(Supervising Teacher)

Dr P V Hareesh Kumar
(co-guide)

Cochin
January 10 ,2005

DECLARATION

I hereby declare that this thesis entitled "***Salient Features of the North Indian Ocean Associated with the Indian Summer Monsoon***" is a genuine record of research work carried out by me and no part of this thesis has been submitted to any University or Institution for the award of any Degree or Diploma.

Neema C.P
Dept of Atmospheric Sciences
Cochin University of Science and Technology
Fine Arts Avenue, Cochin- 682016

Cochin
January-10, 2005

Acknowledgement

Dr. C A Babu, Reader, Department of Atmospheric Sciences, not only gave me the head start for taking up this research programme but also kept it going with his thoughtful suggestions and constant encouragement. I extend my heartfelt thanks to him for his unending support.

It was Dr. Hareesh Kumar, Scientist, NPOL, who nurtured ideas in me, making the subject comprehendible as well as enjoyable. I thank him for his ardent dedication and enthusiastic approach, which made this thesis work progress.

I thank Dr C K Rajan (Head, Department of Atmospheric Sciences) and Dr Mohan Kumar (Former Head, Department of Atmospheric Sciences) for providing necessary facilities for the smooth conduct of research.

I am certain that this work wouldn't have taken its present form without the fruitful discussions and criticisms from my friends and colleagues. They have been a part and parcel of this thesis right from the beginning. I extend my sincere thanks to Venu G, Sridevi M G, Sajith V, Madhusoodanan M S, Sanjana M C, Johnson Zacharia, Anand P, Sooraj K P, Hamza V, Mohamed Asharaf T T, Smitha B Raj, Madhu V, Rajesh G, Abhilash S, Dr.Anu Simon, Sandhya K Nair, Jossia Joseph K, Prashanth P and all other friends and colleagues, who were always there to share and lighten my academic worries; being one among you was a privilege worth cherishing.

Iam fully grateful to my family members especially my husband, who gave me unending and invaluable support and helped in all means to make this endeavour a success.

Above all, I am grateful to God for his blessings and guiding me through hardships.

CONTENTS

Preface

The north Indian Ocean is a region of complexities due to the seasonal reversal of winds associated with the monsoons. These wind reversal bring about large scale changes in the surface circulation features and thermohaline variability. It is very difficult to study these features from field measurements alone. Synoptic snapshots of the ocean and atmosphere for long durations over the basin scale are required to meet this objective. With the availability of various satellites and advanced remote sensing techniques, there is considerable improvement in the data availability. In spite of this, most of the features in the ocean still remain unexplored. In this thesis, an attempt is made to explain the salient features in the north Indian Ocean and their variability on different scales utilizing satellite as well as *insitu* measurements.

The Indian Ocean warm pool is an area of active research in the recent years, mainly due to its association with the formation of onset vortex in the eastern Arabian Sea. Studies have linked the evolution of this warm pool to the long period propagating waves, gyral circulations etc. The wind reversal during the transition months leads to the formation of equatorial Kelvin waves, coastally trapped Kelvin waves, reflected and radiated Rossby waves. Recently, many studies are focused on the role of these waves on the Indian Ocean dynamics, which are not yet fully understood. Another field that requires much attention is the factors that lead to the formation of systems in the Bay of Bengal and Arabian Sea.

The thesis "Salient features of the north Indian Ocean associated with the Indian summer monsoon" is an outcome of the investigation carried out on certain aspects of variability in the Arabian Sea and Bay of Bengal associated with the monsoon. The thesis contains eight chapters. The first chapter deals with the general introduction and objectives of the present study. A detailed literature survey pertaining to the scope of the thesis is also presented in this chapter.

The second chapter focuses on the evolution of the Arabian Sea mini warm pool and its dissipation with the monsoon onset. Predictability of the monsoon onset associated with the dissipation of this mini warm pool is also examined. Finally,

characteristics of the mini warm pool and its relation with the nature of the forthcoming monsoon is also discussed.

In chapter 3, a case study has been made to understand the marine boundary layer characteristics over the Bay of Bengal during the summer monsoon of 1999. Moreover, the response of the boundary layer characteristics to the atmospheric systems and rainfall events are discussed. The refractive index variation of the atmosphere with the system formation, which is important for radar ranging and tracking was also examined.

The response of northern and central Bay of Bengal to the atmospheric forcing during the summer monsoon of 1999 is discussed in chapter 4. The critical value of SST for the system formation is also discussed. A one-dimensional mixed layer model is utilized to study the role of local forcing on the mixed layer dynamics.

The distribution of wind and wind stress curl over the Indian Ocean and its inter-annual variability are discussed in chapter 5. This information is utilized to explain the eddies and propagating waves in the following chapters.

The nature of the propagating waves in the Indian Ocean and their inter-annual variability are discussed in chapter 6, utilizing the sea surface height (SSH) anomaly from the TOPEX/Poseidon altimeter. The wavelet technique is utilized to decompose the prominent harmonics in the SSH data and statistical test is carried out to study their significance.

The SSH anomaly is further utilized to understand the prominent eddies in the north Indian Ocean. Evolution and dissipation of these eddies and their inter-annual variability is discussed in chapter 7.

The results are summarized in Chapter 8. The future scope of the work is also discussed.

Chapter 1

Introduction

1.1 Introduction

Indian Ocean, the smallest among the major oceans and the least understood, is a region of complexities associated with the seasonal reversal of winds, known as monsoon. This seasonal change in wind pattern is best developed over the Indian Ocean, where the land ocean contrast is maximum due to differential heating. The winds over the Indian Ocean, north of 10°S reverse direction twice during a year, generally blowing from southwest during May-September and from northeast during November-February. During the transition period between the monsoons i.e. during March-April and October, the winds are weak (Hellermann and Rosenstein, 1983). About three quarters of the rainfall over the country is received during the summer monsoon months, i.e. from June to September. The monsoon shows large variability in contrast to predictions and hence creates large difficulty to the Indian community mainly depending upon agriculture and consequently to the economy of the country. Hence an accurate prediction of the monsoon has been a major area of interest for the researchers for the last few decades.

Indian subcontinent divides the north Indian Ocean into two basins, the Arabian Sea and the Bay of Bengal. Arabian Sea forms the northwestern part of the Indian Ocean and its coastal boundaries constitute the coastal belt of India, Pakistan, Oman, Yemen and Somalia. The Bay forms the northeastern part of the Indian Ocean, completely separated from the Arabian Sea by the Indian sub-continent and is in contact with the equator along its eastern boundary.

In the marine boundary of the north Indian Ocean, the prevailing wind pattern is the westerlies in lower atmosphere and easterlies in the upper atmosphere during the summer monsoon. The westerlies dominate the region from June to October. Joseph and Raman (1966) have established the existence of a low level westerly tropical Jet over the Indian Peninsula during the summer monsoon. An upper level easterly wind centered around 15°N, 50°-80°E is an important feature of the summer monsoon. It is best developed around 15 km above the earth's surface and is referred to as the tropical easterly jet. Their speed reaches 40 ms^{-1} over the Indian region. The subtropical westerly jet is found at around 30° from the equator in both the hemispheres. In the northern hemisphere, they attain maximum intensity during winter monsoon. During the northern winter,easterlies are weak and confined between

5°N and 10°S and the subtropical westerlies intrude all the way to 10°N. They recede to north of 30°N during northern summer when strong easterly jet characterizes the equatorial upper atmosphere in the region.

Occurrence of atmospheric disturbances viz, low pressure, cyclones, is also typical for the Indian Ocean. Compared to Arabian Sea, the Bay of Bengal is especially fertile with a high frequency of genesis of rain bearing systems, lows and depressions (Rao, 1976). The monsoon over the Indian region is characterized by alternating active and weak (break) spells of rain. Active spells are distinguished by high frequency of formation of synoptic scale systems triggered by maintaining sea surface temperature (SST) of roughly 28°C and high heat potential (Rao and Rao, 1986; Rao *et al.*, 1987; Sanilkumar *et al.*, 1994). The formation and dissipation of these systems or disturbances can cause variations in the marine boundary layer characteristics and on the upper ocean dynamics. However, in the Indian Ocean, the simultaneous measurements of marine boundary characteristics and thermohaline measurements are quite fragmentary during the period of system genesis. Hence, specific conclusions on this aspect could not be made.

The first major experiment conducted in the Indian Ocean was the International Indian Ocean Expedition (IIOE) during 1962-1966 that paved the way for studying the Indian Ocean (Swallow and Bruce, 1966; Duing, 1970; Wyrtki, 1971, 1973b). Later, the Global Atmospheric Research Program (GARP), which spanned the period from 1967-1982, was designed to study the dynamics and physical processes in the atmosphere with the objective of extending the range of useful weather forecasts and understanding the physical basis of climate. It was implemented as a series of major observational and experimental studies. The monsoon experiments (ISMEX-73, MONSOON 77, MONEX 79) provided valuable information on the various aspects of the boundary layer and ocean features. In the MONEX-79 program, main focus was on the study of meteorological disturbances related to the monsoon onset and its short-term variability. The Indian Ocean Experiment (INDEX) was focused on the summer monsoon response of the Somali Current (Swallow *et al.*, 1983, Schott, 1983; Schott *et al.*, 1988; Swallow *et al.*, 1988). A major field Experiment, Tropical Ocean-Global Atmosphere (TOGA) coupled Ocean Atmosphere Response Experiment (COARE) was carried out to

improve air-sea interaction and boundary layer parameterizations in ocean and atmosphere models. Pacific Ocean warm pool and the mechanisms that maintain and modulate, and its atmospheric coupling was also attempted in this experiment (Picaut *et al.,* 1989; Lukas *et al.,* 1991) to validate coupled models. The data collected during First Global GARP Experiment, FGGE represent the most comprehensive set of meteorological variables ever assembled, and have been the basis of extensive research into atmospheric dynamics and physical processes leading to major advances in operational weather forecasting. With the launch of the World Ocean Circulation Experiment (WOCE) under World Climate Research Programme (WCRP), research activities in this area increased in the early 1990s. The major objectives include developing models for predicting climate change and to collect data sets to validate models, which can be used for studying the long-term behavior of the ocean. Co-ordinated ship surveys in this experiment, during 1995-96 yielded high quality data sets of the distribution of the hydrographic properties and various tracers. In the context of Joint Global Ocean Flux Study (JGOFS) in the northern Arabian Sea during 1994-96, extensive studies on the monsoon response and mixed-layer deepening (Weller *et al.*, 1998; Lee *et al.*, 2000) as well as regional circulation and upwelling off Oman (Flagg and Kim, 1998; Shi *et al.*, 2000) were carried out. The Monsoon Trough Boundary Layer Experiment (MONTBLEX) during the summer monsoon 1990 was carried out to study the boundary layer processes in the monsoon trough region. Interest in air-sea interaction studies led to the launch of field experiments such as Bay of Bengal Monsoon Experiment, BOBMEX and Joint Air-Sea Monsoon Interaction Experiment, JASMINE (Webster *et al.*, 2000) during 1998-99. BOBMEX, the first field experiment envisaged under the Indian Climate Research Program (ICRP) aimed at collecting critical data on the sub seasonal variation of important variables of the atmosphere, ocean and their interface to gain deeper insight into the major processes that govern the variability of organized convection over the Bay and its impact. The BOBMEX observations clearly brought out the special and unique features of the atmosphere over Bay of Bengal during the Indian summer monsoon (Bhat *et al.,* 2001, Bhat, 2001, Hareesh kumar *et al.*, 2001). Arabian Sea Monsoon Experiment (ARMEX), second field experiment under ICRP started in 2002, focuses on two major facets of the monsoon. First one to understand the coupled ocean atmosphere and land processes involved in the genesis and

intensification of the systems responsible for the intense rainfall events on the west coast. The second objective was to understand the evolution of the Arabian Sea warm pool, its maintenance during the pre-monsoon season and dissipation with the onset of monsoon.

All the above experiments have considerably increased the availability of measured data in the Indian Ocean. But these traditional methods of observing the ocean from ships and buoys are inadequate as they provide only a limited assessment of the basin wide ocean dynamics on climate and synoptic scales. A good quantitative observational study, which samples in space and time, is required to understand the space-time variability of the different phenomena that occur over this region. With the advent of satellite and various remote sensing techniques, the quality and quantity of measured data over this region has increased invariably to serve this purpose. For example it is very difficult to study the characteristics features like Laccadive high and low, Arabian Sea warm pool etc. from the field measurements alone. This data is to be supplemented with data from the satellite measurements, which can provide synoptic snap shots of larger areas. In spite of all these, studies are fragmentary in the Indian Ocean and hence most of the features remain unexplored.

The monsoon winds over the Indian Ocean brings about spectacular reversal of the ocean circulation (Fig.1.1). The first major description of the currents followed after the IIOE (Duing, 1970; Wyrtki, 1971, 1973b). Progress has been made by researchers in understanding how the ocean responds to seasonal variation of the monsoon winds (Lighthill, 1969; Swallow *et al.*, 1983; Luther and O'Brien, 1985). The wind reversal associated with monsoon can be seen, especially in the annual reversal of the Somali Current (Duing and Szekielda, 1971: Leetmaa, 1972, 1973; Bruce, 1973, 1979, 1983; Duing and Schott, 1978; Evans and Brown, 1981; Quadfasel and Schott, 1982, 1983; Swallow and Fieux, 1982; 1994; Subrahmanyam *et al.*, 1996), occurrence of the strong equatorial surface jets, coastal and open ocean upwelling. Ship drift climatologies of Cutler and Swallow (1984) illustrate the prominent currents in the Indian Ocean. During the summer monsoon season, the South Equatorial Current (SEC) and East African Coastal Current (EACC) supply the northward flowing Somali Current (SC), which forms the Summer Monsoon Current. The current along the equator known as the Equatorial Current (EC), which is westward during both the monsoons, also reverse and eastward surface jets are

observed during April-May and October (Wyrtki, 1973; O'Brien and Hurlburt, 1974). The eastern boundary current or West Indian Coastal Current (WICC) in the Arabian Sea changes its direction from poleward during northeast monsoon season to equatorward during the summer monsoon season. This current turns around Sri Lanka to join the eastward Summer Monsoon Current (SMC) (Shetye *et al.*, 1990; 1993; 1996). The SMC flows eastward and southeastward across the Arabian Sea and around the Laccadive low (LL) off southwest coast India. The winter monsoon current (WMC) divides into two branches in the Arabian Sea, one continuing westward, and the other turning around the Laccadive high (LH) off the southwest coast of India to flow in to the poleward WICC. The western boundary current in the Bay of Bengal ie. the East India Coastal Current (EICC) also reverses its direction twice in a year flowing northeastward from February until September and southwestward from October to January (Shankar *et al.*, 1996; McCreary *et al.*, 1996).

In the Bay of Bengal, circulation is anti-cyclonic in the surface layer during winter months (Legeckis, 1987; Potemra *et al.*, 1991). In spring and early summer, two flows develop anti-cyclonic on the western side of the Bay and cyclonic on the eastern side. In the fall, the two-gyre system forms with the appearance of anti-cyclonic circulation in the eastern half of Bay. The currents along the east and west coasts of India (Shetye *et al.*, 1991; 1996) suggest the possible link between these two basins via coastal circulation girdling India and Sri Lanka.

The monsoon winds cause coastal upwelling of Somalia, Arabia and west coast of India (Duing and Leetma, 1980; Mathew, 1981 and Hareesh Kumar, 1994). However, unlike in the Pacific and Atlantic Ocean, upwelling is less pronounced at the equator. Downwelling is noticed in the coastal belt during winter.

Another feature associated with the Indian Ocean circulation is the formation of meso-scale eddies and gyres. These features are not easily discernable in the ocean and are associated with elevation or dip in the sea level and horizontal temperature gradients. With the onset of summer monsoon, currents in the Arabian Sea evolve into a complex pattern of meso-scale eddies and gyres (Bruce, 1973; 1979; 1983; Luther and O'Brien, 1985). After crossing the equator, Somali Current turns offshore at about 4°N forming a cold upwelling wedge on its left, while the other part re-

circulates across the equator as the Southern Gyre (SG). Another northern eddy is formed offshore often known as the Great Whirl (GW). A third gyre Socotra Eddy

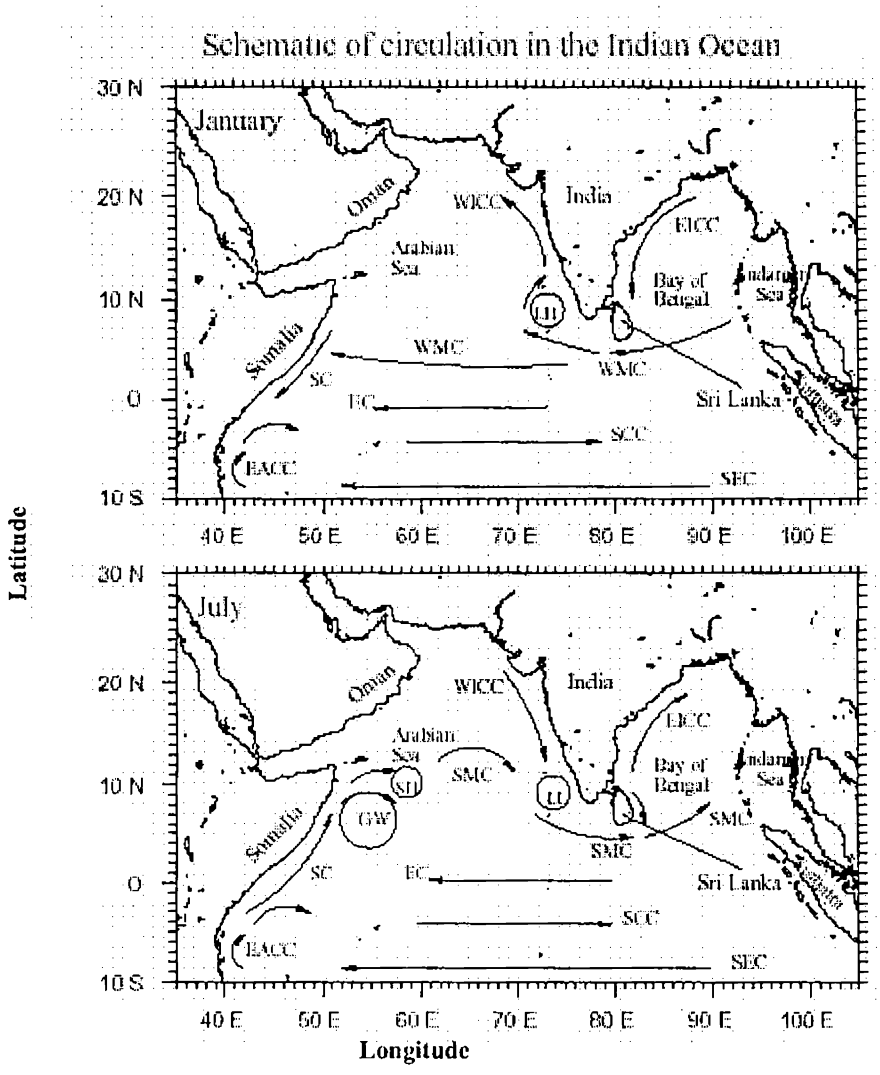

Fig.1.1 Schematic representation of the circulation in the Indian Ocean during January (winter monsoon) and July (summer monsoon). The abbreviations are as follows. SC, Somali Current; EC, Equatorial Current; SMC, Summer Monsoon Current; WMC, Winter Monsoon Current; EICC, East India Coastal Current; WICC, West India Coastal Current; SCC, South Equatorial Counter Current; EACC, East African Coastal Current; SEC, South Equatorial Current; LH, Lakshadweep high; LL, Lakshadweep low; GW, Great Whirl; and SH, Socotra high (from Shankar et al., 2001).

(SE) is seen during many years during summer monsoons northeast of Socotra. The GW and SG form the two-gyre system and in some years these two merge together (Bruce, 1973) during the later stages of the monsoon. Many researchers (Bruce, 1983; Schott, 1983) have studied these two gyres system and their generation mechanisms in the Somali Current regime. Schott and Quadfasel (1982) has attributed the

formation of the GW to baroclinic Rossby waves, generated by strong offshore anti-cyclonic wind stress curl. Subrahmanyam *et al.* (2001) has suggested the role of reflected Rossby waves from the eastern equatorial Indian Ocean in determining the strength of Somali Current and eddies.

The LH, a prominent anti-cyclonic eddy was formed off the south west coast of India during winter and a LL, a cyclonic eddy during the summer monsoon (Bruce *et al.*, 1994, 1998; Shankar and Shetye, 1997). These two eddies are the consequence of the westward radiation of Rossby wave from the coastally trapped Kelvin waves (McCreary *et al.*, 1993; Shankar and Shetye, 1997). Bay of Bengal is also well known for both cyclonic and anti-cyclonic eddies (Babu *et al.*, 1991; Sanilkumar *et al.*, 1997; Gopalan *et al.*, 2000).

The westward movement of the SMC across the Bay was a result of Rossby wave radiation from the eastern Bay and the generation of Rossby waves by Ekman pumping in the interior bay (McCreary *et al.*, 1993; Vinayachandran *et al.*, 1999). Several numerical studies (Lighthill, 1969; Jensen, 1990; McCreary *et al.*, 1993), have established the role of planetary waves in the generation mechanisms of Somali eddies, in the reversal of western boundary current (EICC) in the Bay of Bengal (Potemra *et al.*, 1991; McCreary *et al.*, 1996; Shankar *et al.*, 1996) and other circulation features.

The westerly winds over the equatorial region during the transition period between the monsoons (i.e. April/May and October) drive intense eastward jets (Wyrtki, 1973). The large scale forcing associated with these winds reversal, cause thermocline depressions in the equatorial region, leading to eastward propagating Kelvin wave. On reaching the eastern boundary, one part of this wave reflect back as Rossby wave and other propagates poleward as coastally trapped Kelvin wave (Moore and Philander, 1977). The model results (Potemra *et al.*, 1991; Yu *et al.*, 1991; McCreary *et al.*, 1993) showed that the coastally trapped Kelvin waves radiate Rossby waves as they propagate along the eastern boundaries of the ocean. These waves along with the seasonally reversing monsoon winds play a significant role in the reversal of equatorial and coastal currents in the north Indian Ocean (Cane, 1980; Potemra *et al.*, 1991; Yu *et al.*, 1991; Perigaud and Delecluse, 1992; McCreary *et al.*, 1993; Shankar *et al.*, 1996; McCreary *et al.*, 1996; Vinayachandran *et al.*, 1996;

Shankar and Shetye, 1997; Shankar, 1998; Vinayachandran and Yamagata, 1998; Han, 1999; Han *et al.*, 1999; Shankar, 2000; Subrahamanyam *et al.*, 2001). The equatorial Kelvin wave, Rossby wave and the coastally trapped Kelvin wave all connect the Arabian Sea, Bay of Bengal and the equatorial region in to a single dynamical entity i.e. the north Indian Ocean. These planetary waves also serve as energy carriers from one part of the ocean to another. Moreover, coastally trapped Kelvin waves have an important role in bringing the low salinity waters from the Bay of Bengal to the Arabian Sea during the winter monsoon, which eventually help in the building up of the Arabian Sea warm pool (Shenoi *et al.*, 1999). Schott and McCreary (2001) studied how conventional ocean dynamical mechanisms, particularly Kelvin and Rossby wave propagation, can account for much of the observed complex annual cycle of flow in the Indian Ocean, when driven by the observed winds. But direct measurements are lacking to support the above hypothesis. The ground truth measurements collected onboard various ships can provide only a limited assessment of the ocean dynamics both spatially and temporally. The advent of remote sensing techniques considerably improved the understanding of these ocean features.

In the recent years, the one area, which attracted many researchers, is the Indian Ocean warm pool and the associated ocean dynamics. Temperature in the warm pool region has been recognized as an important factor which forces the spatio-temporal evolution of both the summer and winter monsoons and the occurrence of pre-and post monsoon cyclonic storms (Godfrey *et al.*, 1995). The relationship between the inter-annual variations of SST and the Asian monsoon rainfall has been a subject of many studies (Shukla and Misra, 1977; Weare, 1979; Cadet and Diehl, 1984; Rao and Goswami, 1988). The variability in SST in the warm pool region largely determines the nature of the monsoon and hence a clear understanding on the evolution of the warm pool is important for improved prediction purposes. But the Indian Ocean warm pool has not been studied extensively compared to Pacific Ocean warm pool. It was Seetharamayya and Master (1984) who first noticed temperature in excess of 30.8°C in the southeastern Arabian Sea prior to the onset of summer monsoon utilizing MONEX-79 data and named this as the Arabian Sea mini warm pool. Joseph (1990a) also reported the formation of mini warm pool in the southeastern Arabian Sea, a week prior to the onset of summer monsoon. Recently, many studies were carried out to understand more about the feature (Rao and

Sivakumar, 1999; Sanil Kumar *et al.*, 2004). There is sufficient evidence both on empirical and theoretical basis to believe that the SST exert significant control over the atmosphere. Many workers (Ranjit Singh, 1983; Joseph and Pillai, 1984; Rao and Goswamy, 1988; Vinayachandran and Shetye, 1991; Sadhuram *et al.*, 1991) have brought out the importance of SST over Arabian Sea as an input parameter for the Indian monsoon rainfall. Joseph (1990a) has reported that the onset vortex during the summer monsoon formed in this warm pool region. With the SST greater than 30°C, this region satisfies the condition necessary for the formation of deep convection. Hence, understanding SST variations in this region is critical for monsoon onset prediction purposes. Shenoi *et al.* (1999) has stressed the importance of low saline waters from the Bay of Bengal in the building up of this warm pool and suggested that the low salinity water stabilizes the surface layer and provide a breeding ground for the warm pool formation. Shankar *et al.* (2004) has provided observational evidence for the westward propagation of temperature inversions from the southeastern Arabian Sea suggesting the role of Rossby waves in this process. Recently ARMEX program was conducted to study the dynamics of this warm pool.

The works of Bryan (1969) on long-range weather prediction indicated that the climate and its fluctuations are profoundly influenced by the interaction between the ocean and atmosphere on a variety of space-time scales. However, most of the atmospheric processes are found to occur over a time scale of 1-5 days (Denman, 1973) and hence an accurate and reliable knowledge of the upper ocean thermal structure is very much required on a synoptic scale. Even on a diurnal scale, temperature in the ocean shows marked variability over a few hundred kilometers. From the satellite data, it is now possible to monitor the SST variation at regular intervals, but does not provide information on the subsurface thermal structure. In the absence of adequate *insitu* measurements, numerical models can provide valuable information on the subsurface thermal structure from routine measurements of atmospheric parameters. Several one-dimensional numerical models are available in literature to simulate mixed layer characteristics with time-scales varying from diurnal to seasonal (Kraus and Turner, 1967; Denman, 1973; Pollard *et al.*, 1973; Mellor and Durbin, 1975; Miller, 1976; Thompson, 1976, Niiler and Kraus, 1977, Price *et al.*, 1986). These models are found to perform well on short time scales when the one-

dimensional processes appear to control the ocean dynamics (Denman and Miyake, 1973).

The mixed layer characteristics of the Arabian Sea showed marked variability in association with the seasonally varying monsoon winds (Wyrtki, 1971), due to mechanical and buoyant mixing, entrainment at the mixed layer base, horizontal/vertical advection etc.

Shetye (1986) simulated the annual cycle of SST in the Arabian Sea, utilizing Denman (1973) model and suggested that the temperature can be simulated reasonably well from heat fluxes, except during the summer monsoon season, when horizontal and vertical advection is very important. McCreary *et al.* (1993) used a 2½ layer model and simulated the near surface currents and SST fields by determining the local and remote forcing of wind. On synoptic time scales also, the simulation of mixed layer characteristics in the Arabian Sea and Bay of Bengal are limited (Rao, 1986; Rao and Mathew, 1990; Murthy and Hareesh Kumar, 1991; Sanilkumar *et al.*, 1993; Rao *et al.*, 1993, 1994, Hareesh Kumar *et al.*, 1996; Mathew *et al.*, 2003). These studies revealed that even on short time scales, the mixed layer variability in the Arabian Sea and Bay of Bengal are controlled by variety of factors viz. one dimensional processes, advective processes, internal waves, long period waves, eddies etc. In the presence of these features, reasonably good simulation could not be expected.

1.2 Objectives

The seasonally reversing monsoon winds significantly influences the seasonal reversal of surface circulation in north Indian Ocean. Moreover, the reversal of these winds lead to the long period propagating waves such as Kelvin and Rossby waves, which propagate long distances to affect the ocean remotely. The warm pool is another seasonal feature in the Arabian Sea formed during the pre-monsoon season, while Bay of Bengal is well known for the depressions which are the main rain bearing systems over this region during summer monsoon. All these features make the north Indian Ocean an interesting region for experimentalists and modelers.

The main objectives of the thesis "Salient features of the north Indian Ocean associated with the Indian summer monsoon", has been to bring out certain features of

the north Indian Ocean especially in the Arabian Sea and Bay of Bengal, associated with the Indian summer monsoon. The study region is presented in Fig.1.2.

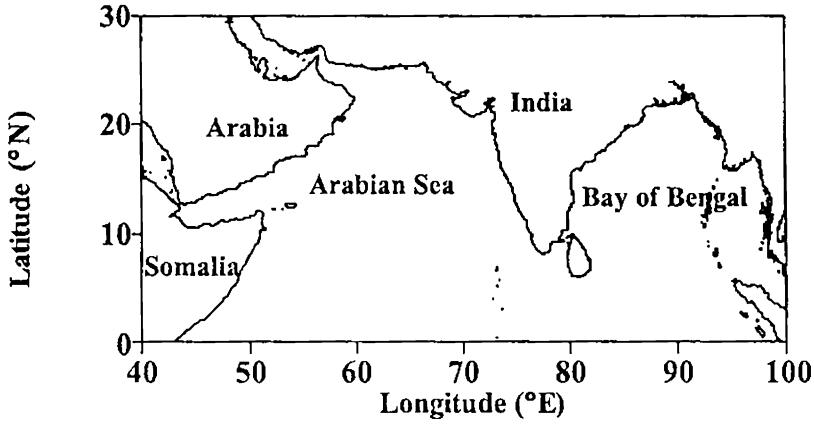

Fig.1.2 Study region

In the recent past, Arabian Sea warm pool attracted many oceanographers and meteorologists due to its association with the formation of monsoon onset vortex. Availability of highly accurate satellite data and the specific program like ARMEX have also helped to understand more about the warm pool. In this work, the evolution of the Arabian Sea mini warm pool and its dissipation associated with the monsoon onset are studied. Predictability of the monsoon onset associated with the dissipation of this mini warm pool is also examined. Finally, the characteristics of the mini warm pool (core temperature and extent) and its relation with nature of the forthcoming monsoon is also examined.

Information of the marine boundary layer is in particular needed for aviation purposes and for radar ranging and tracking. The studies pertaining to marine boundary layer over oceanic regions are also less due to lack of adequate data. The availability of radiosonde measurements on shorter time-scales during summer monsoon of 1999 has been utilized here to study the influence of atmospheric systems on the marine boundary layer characteristics at the northern Bay. The refractive index variation of the atmosphere during this period has also been examined.

The temperature information at two locations one in the central Bay of Bengal and northern Bay of Bengal are utilized to understand the role of atmospheric forcing on the upper ocean on shorter time scales. The critical SST for the system formation is

Chapter 2

Arabian Sea mini warm pool

also discussed. One-dimensional numerical mixed layer model is utilized to study the local forcing on the synoptic scale variability of mixed layer temperature and depth.

The present knowledge of the nature of the propagating waves and eddies in the Indian Ocean especially their inter-annual variability are very much limited. Investigation of the characteristics of propagating waves, especially Rossby and Kelvin waves along typical zonal transects and their inter-annual variability is discussed in terms of wind and its curl distribution, El Nino and Indian Ocean Dipole events. The prominent harmonics in the sea level at various locations in the Arabian Sea and Bay of Bengal are also decomposed using wavelet technique considering their significance level.

Eddies are another feature noticed in the Arabian Sea and Bay of Bengal. A detailed study has been carried out to understand the time of formation, extent, movement and dissipation of these eddies. The inter-annual variability in the eddy fields are also discussed by considering the propagating waves in this region and surface wind and wind stress curl variability. Finally the major findings are documented.

2.1 Introduction

Indian summer monsoon and its variability have been a major topic of study for the last few decades. An important conclusion emerging from these studies is that the variability in the Pacific Ocean is not isolated but linked with the Indian Ocean monsoon system. For example, the ENSO (El-Nino Southern Oscillation phenomena) is mainly controlled by the distribution of sea surface temperature (SST) in the tropical Pacific and Indian Ocean. Here, the maximum temperature do occur and act as the main source of heat energy for the global atmosphere. The warm SST anomaly over equatorial central Pacific ocean causes delay in the shifting of convection from equatorial western Pacific to the North Indian Ocean, which in turn causes a delay in monsoon onset (Joseph *et al.*, 1994).

Studies based on the SST climatology (Hastenrath and Lamb, 1979; Bottomley *et al.*, 1990; Shea *et al.*, 1990; Rao *et al.*, 1991) and thermal structure (Wyrtki, 1971; Hastenrath and Greischar, 1989; Levitus and Boyer, 1994) in the western tropical Pacific Ocean, central and eastern Indian Ocean indicated a zone of warm waters, where the SST was more than 28°C. This pool of warm water is generally known as Indo-Pacific warm pool; which migrates in the north-south direction in phase with the Sun.

Even though the western Pacific Ocean warm pool has been studied extensively, the Indian Ocean warm pool, which is an extension of Pacific Ocean warm pool remained little explored. Intensity and spatio-temporal variability of the Indian Ocean warm pool depends largely on the seasonally reversing monsoon (Vinayachandran and Shetye, 1991). These strong winds force the ocean locally, and they excite propagating signals (Kelvin and Rossby waves) that travel large distances to affect the ocean remotely. Shenoi *et al.* (1999) has concluded that remote forcing plays a major role in the development of high SST found in the Lakshadweep region, which is favourable for the genesis of the monsoon onset vortex. The coastally trapped Kelvin waves have an important role in bringing low salinity waters from the Bay of Bengal to Arabian Sea during the winter monsoon time which eventually facilitate the building up of the mini warm pool in the Lakshadweep area. Durand *et al.* (2004) has noticed that temperature inversions that occur in this salinity stratification contribute significantly to the warming in the southeastern Arabian Sea

during the pre-monsoon period. Shankar *et al.* (2004) has provided observational evidence of the westward propagation of these temperature inversions, which forms off the west coast of India and moving along with the down welling Rossby waves that constitutes the Lakshadweep High.

Compared to the Indian Ocean warm pool, the western Pacific warm pool is more extensive and covers an area of about 33x 10^6 km^2. Within this warm pool, the mean SST is around 29°C throughout the year in an area of 0.9 x 10^6 km^2. However, at the core of the Indian Ocean warm pool, the surface temperature is much higher than that observed in the Pacific Ocean (Vinayachandran and Shetye, 1991; Sanilkumar *et al.*, 2004). Utilising the MONEX 79 data, Seetharamayya and Master (1984) showed that a pool of water with temperature in excess of 30.8°C occurred in the southeastern Arabian Sea prior to the onset of summer monsoon. This zone, which is part of the Indian Ocean warm pool, is called as the Arabian Sea mini warm pool. Kershaw (1988) found that SST (warm) anomaly is essential for the development of onset vortex. Joseph (1990a) has reported that the onset vortex prior to the summer monsoon onset is formed in this warm pool area in the southeastern Arabian Sea.

Rao *et al.* (1994) studied the evolution of SST in the mini warm pool region (defined as the region where SST> 30°C) and evaluated the relative importance of heat fluxes and entrainment in the building up of this mini warm pool. Rao and Sivakumar (1999) summarized the previous studies related to the warm pool and analysed various factors that involve in the formation of the Arabian Sea mini warm pool. Recently, Sanilkumar *et al.* (2004) conducted a cruise in the southeastern Arabian Sea during May 2000, exclusively to study the characteristics of this mini warm pool. They defined mini warm pool as the region where the SST was in excess of 30.25°C. In this work, the mini warm pool is defined as the region where SST is more than 30°C, following Rao and Sivakumar (1999).

Several studies have been carried out to study the link between the SST in the Arabian Sea during pre-monsoon period and the monsoon activity over the Indian region (Shukla and Misra, 1977; Weare, 1979; Cadet and Diehl, 1984; Rao and Goswami, 1988). Anjaneyulu (1980) pointed out that higher the difference of maximum SST between the pre-monsoon and the monsoon seasons, greater the possibility for a good monsoon and vice versa. Joseph (1990b) found that warm SST

anomaly in north Indian Ocean or cold SST anomaly in west Pacific Ocean is favourable for good monsoon rainfall over India.

In spite of all these significance, not many studies have been carried out to understand the Arabian Sea mini warm pool in detail, primarily due to lack of sufficient data sets. With the utilization of NCEP/NCAR (National Center for Environmental Prediction/National Center for Atmospheric and Research) Reanalysis data, sea truth measurements from ships of opportunities and satellite derived SST, a better attempt has been made to map the Arabian Sea mini warm pool. In this chapter, the primary objective is to study the evolution of this mini warm pool during the pre-monsoon season and its dissipation associated with the monsoon onset. Moreover, an attempt is also made to predict the onset of monsoon over Kerala from the triggering of the mini warm pool dissipation. Finally, the mini warm pool characteristics are studied in detail so as to bring out its possible relationship with the nature of the forthcoming monsoon.

2.2. Data and methodology

The study area extends from 40°E to 80°E and from 5°S to 25°N (Fig.2.1). The NCEP/NCAR re-analysis SST data (Kalney *et al.*, 1996) (herein after referred as NNR) for a period of 39 years (1960-1998) are utilised to study the climatology. The onset dates of summer monsoon over Kerala from 1960 to 2004 is taken from India Meteorological Department (IMD). The average rainfall for the years from 1960-1994 and 1994-1998 are taken from Parthasarathy *et al.* (1994) De *et al.* (1998) respectively. Pursuing their approach, each year has been classified as excess monsoon year (wet), when rainfall of that year exceeds the long term mean (852.4 mm) rainfall by 1 standard deviation (σ), deficient monsoon year (dry) when the rainfall for that year is less than the mean rainfall by 1σ and normal otherwise. The evolution and dissipation of the Arabian Sea mini warm pool has been studied selecting typical years from NNR data set representing wet, normal and dry monsoon years. The results from the above analysis are further compared with the high resolution TRMM Micro wave Imager (TMI) SST data for the years 2001, 2002 and 2003. These data sets are having a resolution of 0.25°x0.25° (latitude x longitude). Rajeevan *et al.* (2004) classified 2003, 2001 and 2002 as above normal, below normal and drought/dry respectively. The TMI SST is further utilized to study the

characteristics of the warm pool during above normal, below normal and drought years. In addition, all the available *insitu* salinity data in this region (1940-1998) obtained from various sources after proper quality checks are also used to study the role of salinity in the corresponding wet, normal and dry monsoon years.

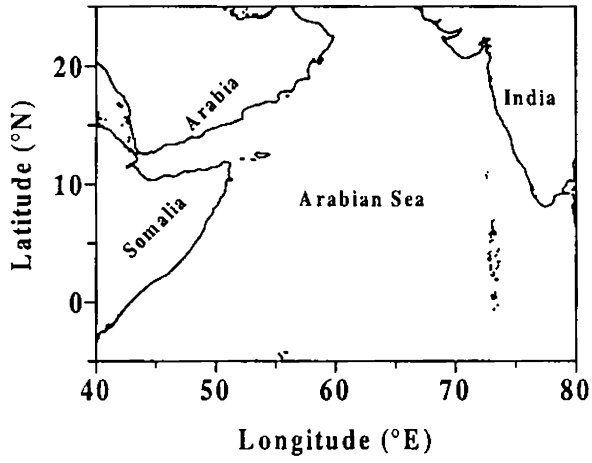

Fig.2.1 Study area

2.3. Results and Discussion

2.3.1 Variability in the onset of summer monsoon and average rainfall.

The onset date of the summer monsoon (1960-2004) and the average summer rainfall (1960-98) is presented in Fig.2.2a & b. From this figure, it can be seen that when the onset was early, the rainfall was either normal or above normal and when it was delayed, the rainfall was found to be below normal. For example, maximum rainfall (~1000 mm) is noticed during 1961 (Fig.2.2b) when the monsoon onset was very early (Fig.2.2a) i.e. during mid May. Similarly, minimum rainfall is observed during 1972 (~700 mm) (Fig.2.2b), when the onset was very much delayed (Fig.2.2a) i.e. mid June. During 2002, the onset date of summer monsoon was on 13 June (Fig.2.2 a). So as per the above discussion, it can be inferred that 2002 will be a dry year or the rainfall will be below normal. The study of Rajeevan *et al.* (2004) and IMD also confirmed that the year 2002 was a dry monsoon year. Another notable observation is the variability in the rainfall and the onset dates with a periodicity of nearly 3 year. From the trend of the curve (Fig.2.2a), it can be seen that the onset date will be early for 2004 i.e. prior to normal onset date, which can favour good monsoon rainfall. Supporting this concept, it was noticed that the onset date during 2004 was on 18 May (News report, Trivandrum IMD). The IMD weather report (2004) also

indicates above normal rainfall during this year. So from the above discussion, it can be inferred that an early onset over Kerala favours good rainfall and late onset leads to below normal rainfall.

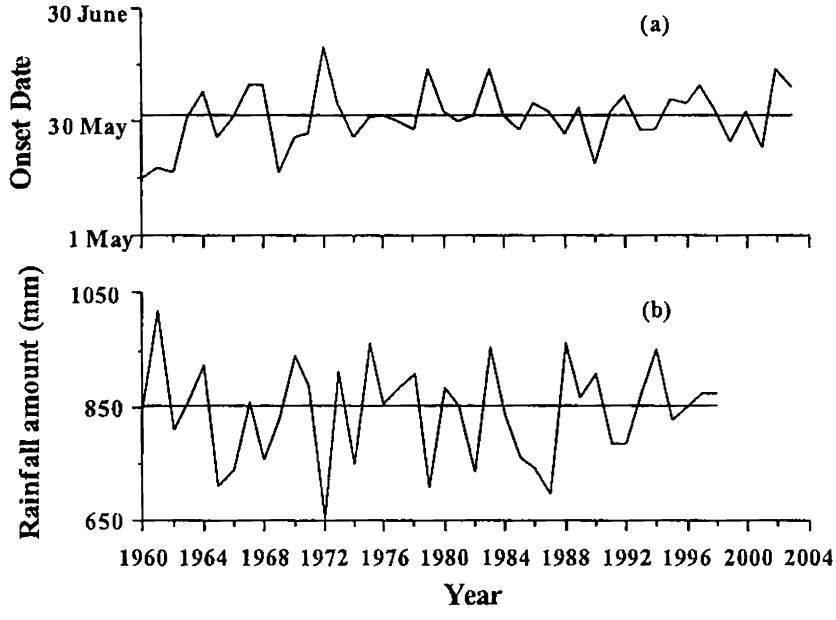

Fig.2.2 (a) Monsoon onset date (based on IMD) and (b) amount of summer monsoon rainfall from 1960 to 1993 (Parthasarathy et al.,1994), and 1994 to 1998 (De et al., 1999). The straight line indicates normal onset date (1st June) in (a) and mean rainfall (852.4 mm) in (b)

2.3.2 Monthly evolution of sea surface temperature

To study the monthly evolution of temperature in the upper layers of Arabian Sea, monthly averaged NNR SST (1960-1998) is presented (Fig.2.3). The appearance of 28.5°C isotherm near the equator between December and May clearly indicated progressive warming in the surface layers. By May, temperature in the entire Arabian Sea exceeded 29°C, with maximum temperature occurring in the eastern Arabian Sea. Here, a pool of water with core temperature in excess of 29.9°C is noticed. Various researchers (Seetharamayya and Master, 1984; Joseph, 1990 a; Rao and Sivakumar, 1999; Sanilkumar *et al.*, 2004) also reported this pool of warm water prior to the onset of summer monsoon. The core temperature of 29.9°C observed in this study is slightly less than that of Rao and Sivakumar (1999), where they reported temperature more than 30°C at the core. The difference may be due to the usage of different data sets, viz. data from Levitus and Boyer (1994) by Rao and Sivakumar (1999) and NNR Reanalysis data in this study. Even though, the core temperature is different, a well-defined warm pool is seen in both cases.

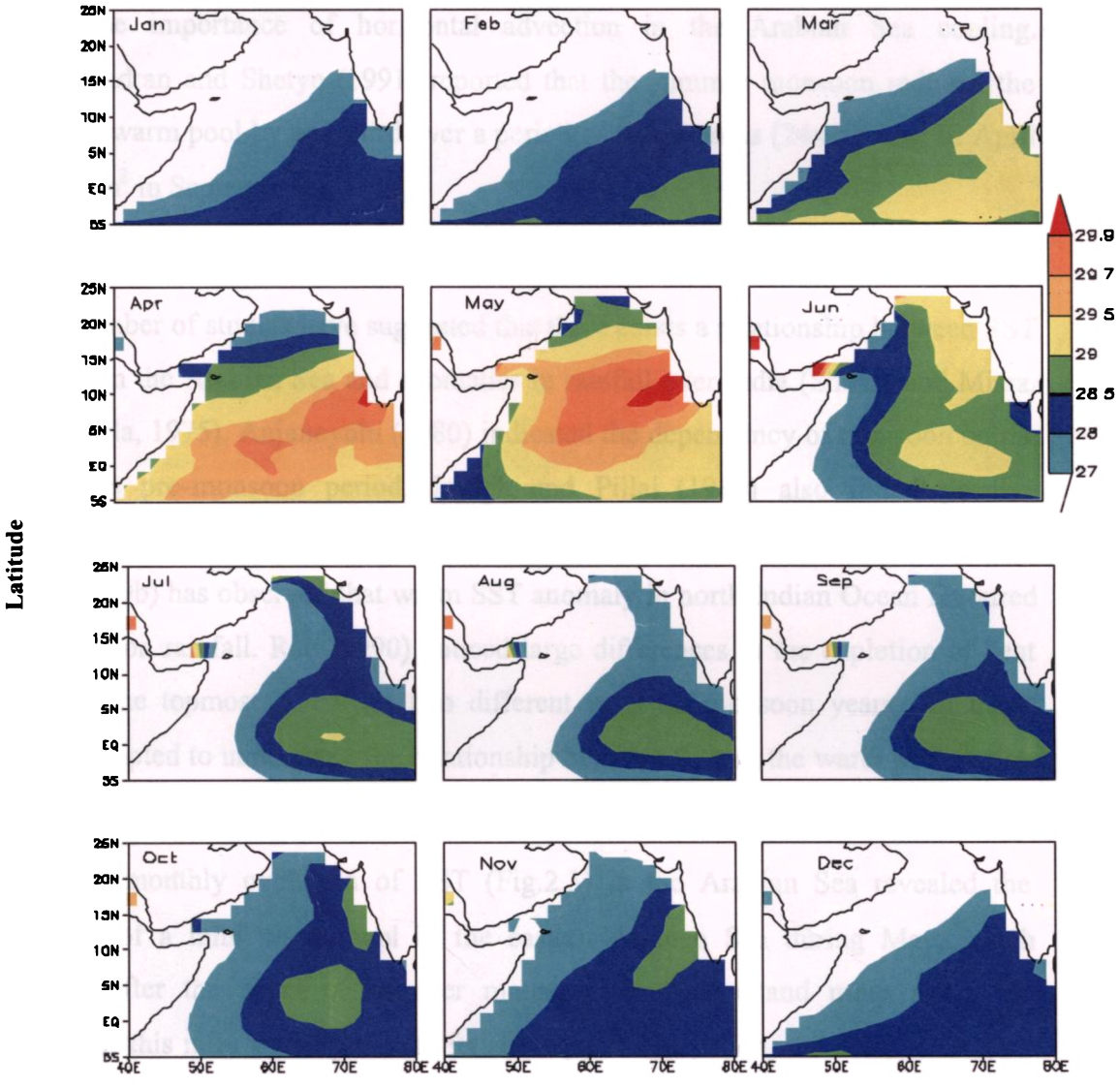

Fig.2.3 Monthly evolution of NNR SST (°C)

After the onset of summer monsoon i.e. in June (Fig.2.3), temperature in the warm pool region drops by more than 0.9°C from May (29.9° to 29°C). The increased mixing processes (both buoyant and mechanical), in association with the summer monsoon might have caused the dissipation of the warm pool. During this period, decrease in SST is also very much prominent off Somalia, Arabia and southwest coast of India. Duing and Leetma (1980), Mathew (1981) and Hareesh Kumar (1994) attributed this cooling to coastal upwelling in this region. In the central Arabian Sea, buoyant and mechanical mixing processes contributed to the cooling (Hastenrath and

Lamb, 1979). Duing and Leetma (1980) and Hareesh Kumar and Mathew (1997) estimated the summer cooling in the Arabian Sea due to various processes and stressed the importance of horizontal advection in the Arabian Sea cooling. Vinayachandran and Shetye (1991) reported that the summer monsoon reduced the area of the warm pool by one third over a period of five months ($24x10^6$ km^2 in April to $8x10^6$ km^2 in September).

2.3.3 Daily evolution of SST

Number of studies have suggested that there exists a relationship between SST anomalies in the Arabian Sea and anomalies in rainfall over India (Shukla and Misra, 1977; Shukla, 1975). Anjaneyulu (1980) indicated the dependency of monsoon on the SST of the pre-monsoon period. Joseph and Pillai (1984) also found positive correlation between pre-monsoon SST and the following monsoon rainfall. Again Joseph (1990b) has observed that warm SST anomaly in north Indian Ocean favoured good monsoon rainfall. Rao (1990) noticed large differences in the depletion of heat content in the topmost layers for two different types of monsoon years. All these studies prompted to understand the relationship between SST in the warm pool region and the monsoon characteristics.

The monthly evolution of SST (Fig.2.3) in the Arabian Sea revealed the occurrence of a mini warm pool in the eastern Arabian Sea during May, which dissipated after the onset of summer monsoon. To understand more about the evolution of this mini warm pool and its subsequent dissipation, the daily NNR SST for some typical years corresponding to wet (1988), normal (1981) and dry (1985) monsoon from 1 May to one week after the onset are presented.

In general, during wet year (1988), temperature in the entire basin between 5°S-17°N and 50°-80°E is more than 29.5°C during May (Fig.2.4a). However, in the eastern Arabian Sea, a pool of water with temperature in excess of 30°C is noticed from 1 May onwards with core temperature of ~ 30.5°C. This pool (Fig.2.4a) attains its maximum dimension laterally on 6 May, i.e. from 5°-15°N and 50°-75°E, covering an area of more than 30,00,000 km^2. The temperature increase in this zone got arrested after 6 May. Slight dissipation of this warm pool is noticed from 11 May

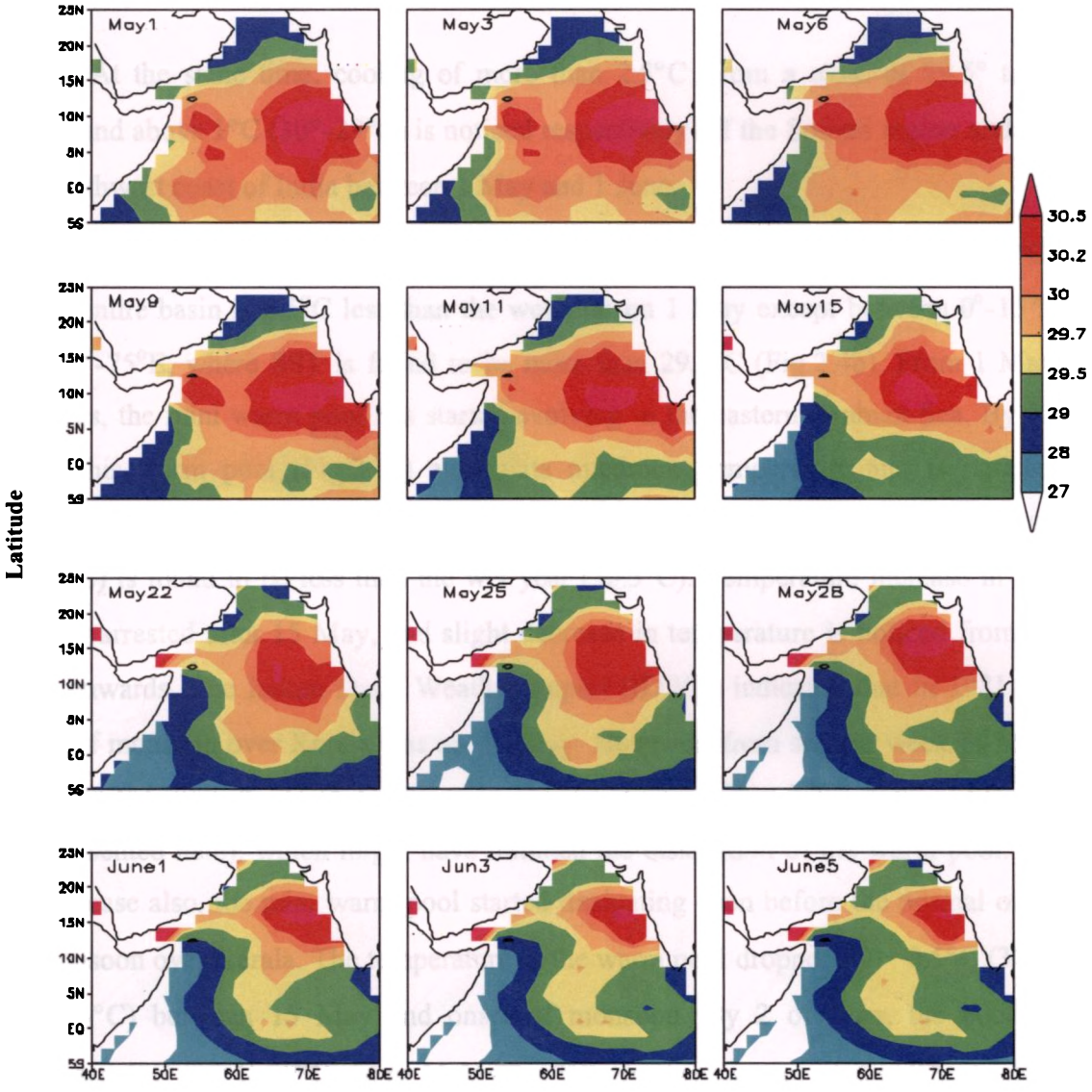

Fig.2.4a Daily evolution of SST (°C) representing some typical days of marked changes during May-June 1988

onwards. However, IMD reported the onset of summer monsoon over Kerala on 26 May during 1988. This suggests that even before the onset of monsoon, the mini warm pool starts dissipating. The analysis of NNR wind at 850mb (Figure not presented) revealed that the winds started strengthening over the Arabian Sea from the second week of May itself. This in turn can increase both buoyant and mechanical mixing processes and thereby causes the dissipation of the warm pool. Between 6 May (when the warm pool attain maximum lateral dimension) and 25 May, cooling of ~0.5°C (30.5°C-30°C, at the core) is noticed in the mini warm pool region (Fig. 2.4a).

It exceeds 1.5°C (30.5°C-29°C) between 6 May and 1 June (average monsoon onset date).

At the same time, cooling of more than 2.5°C (from a max. of 29.5° to < 27°C) and above 1°C (30°-29°C) is noticed respectively off the Somali region and off the southwest coast of India between 1 May and 1 June.

In the case of normal monsoon year (1981), the observed temperature (29°C) in the entire basin is 0.5°C less than the wet year on 1 May except between 0°-15°N and 52°-75°E, where SST is found to be more than 29.5°C (Fig.2.4b). From 1 May onwards, the mini warm pool has started evolving in the eastern Arabian Sea. By 15 May, this warm pool (Fig.2.4b) attains its maximum temperature and is noticed between 8°-15°N and 55°-75°E (> 16,94000 km^2). In this case, the core temperature (30.2°C) is found to be less than the wet year (30.5°C). Temperature increase in this zone is arrested after 15 May, and slight decrease in temperature is noticed from 17 May onwards. The Indian Daily Weather Report (IDWR) indicated that in 1981 the onset of monsoon over Kerala was on 30 May. However, from second week of May, winds in the western Indian Ocean strengthened (evident from NNR wind at 850mb, not presented here), which might have initiated the dissipation of the warm pool. So, in this case also, the mini warm pool started dissipating even before the normal onset of monsoon over Kerala. The temperature in the warm pool dropped by ~ 0.5°C (30°C to 29.5°C) between 15 May and onset of monsoon. By 2 of June, the cooling exceeded 1°C (30°C-29°C) from 15 May in the mini warm pool region. The cooling exceeds 2°C (29°-27°C) off Somalia and 1°C (30°-29°C) off the southwest coast of India, due to coastal upwelling.

In the case of dry year (1985), maximum temperature in the eastern Arabian Sea is found to be 29.7°C (Fig.2.4c). However, in the central Arabian Sea, temperature in excess of 30°C is noticed i.e. between 2°-8°N and 50°-60°E. This suggests a westward shifting of the warm pool. Here warming can be seen from 1 May and can be seen upto 14 May. In the central and eastern Arabian Sea, temperature increases till 19 May and cooling starts afterwards.

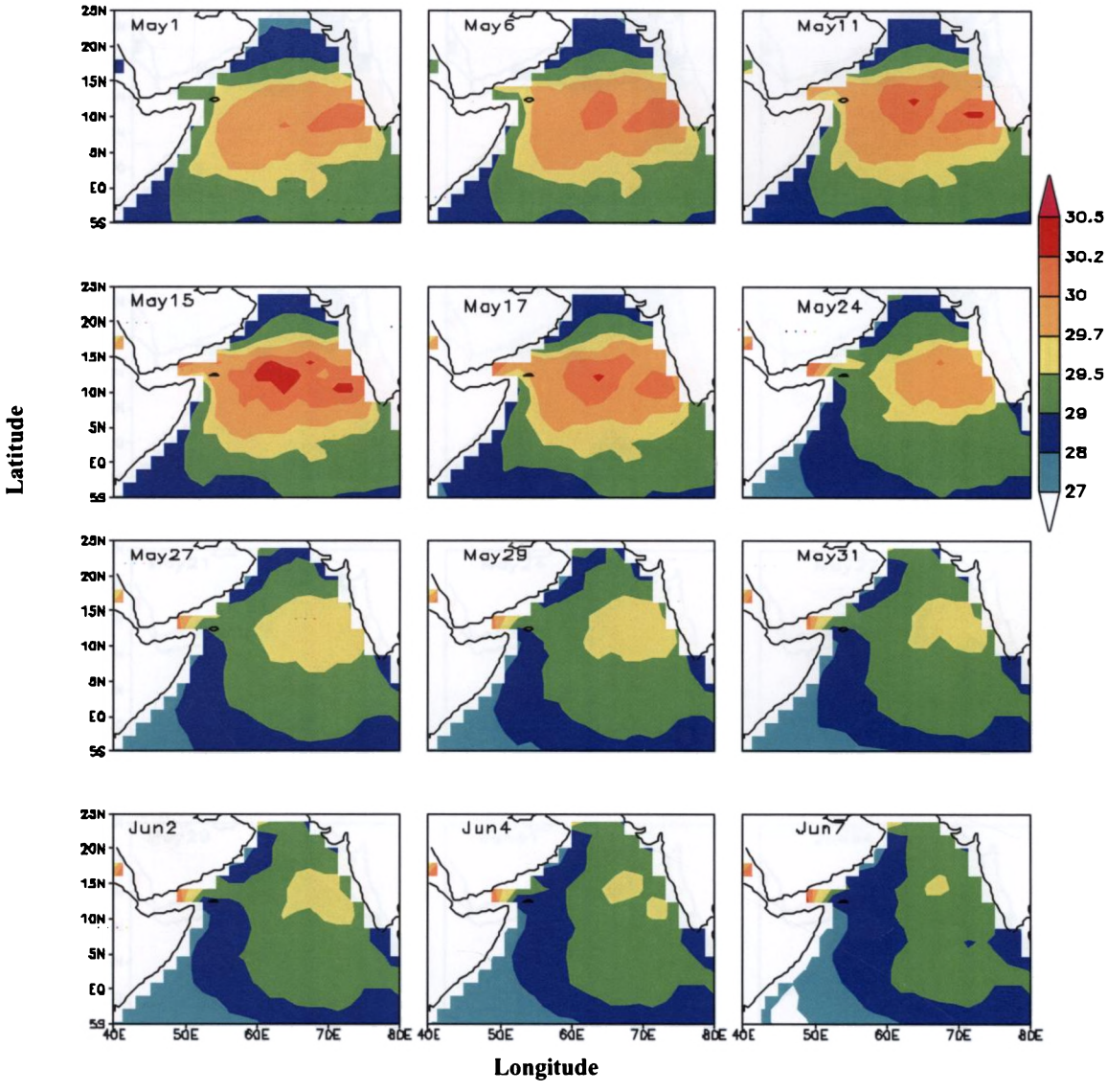

Fig.2.4b Daily evolution of SST (°C) representing some typical days of marked changes during May- June 1981

Corresponding to the dissipation of the mini warm pool, winds (NNR) also strengthened in the Arabian Sea. During this year, the onset of monsoon over Kerala was on 28 May. Hence, in this case also, dissipation of the warm pool started much before the onset of monsoon over Kerala. In the region of the warm pool, the temperature difference between 14 May (maximum temperature observed in the western Arabian Sea) and 28 May (onset date) exceeds 2°C (30°- 28°C). Off the Somali coast and southwest coast of India also, the cooling exceeds 3°C (30°- 27°C) and 1.7°C (29.7° -28°C) respectively.

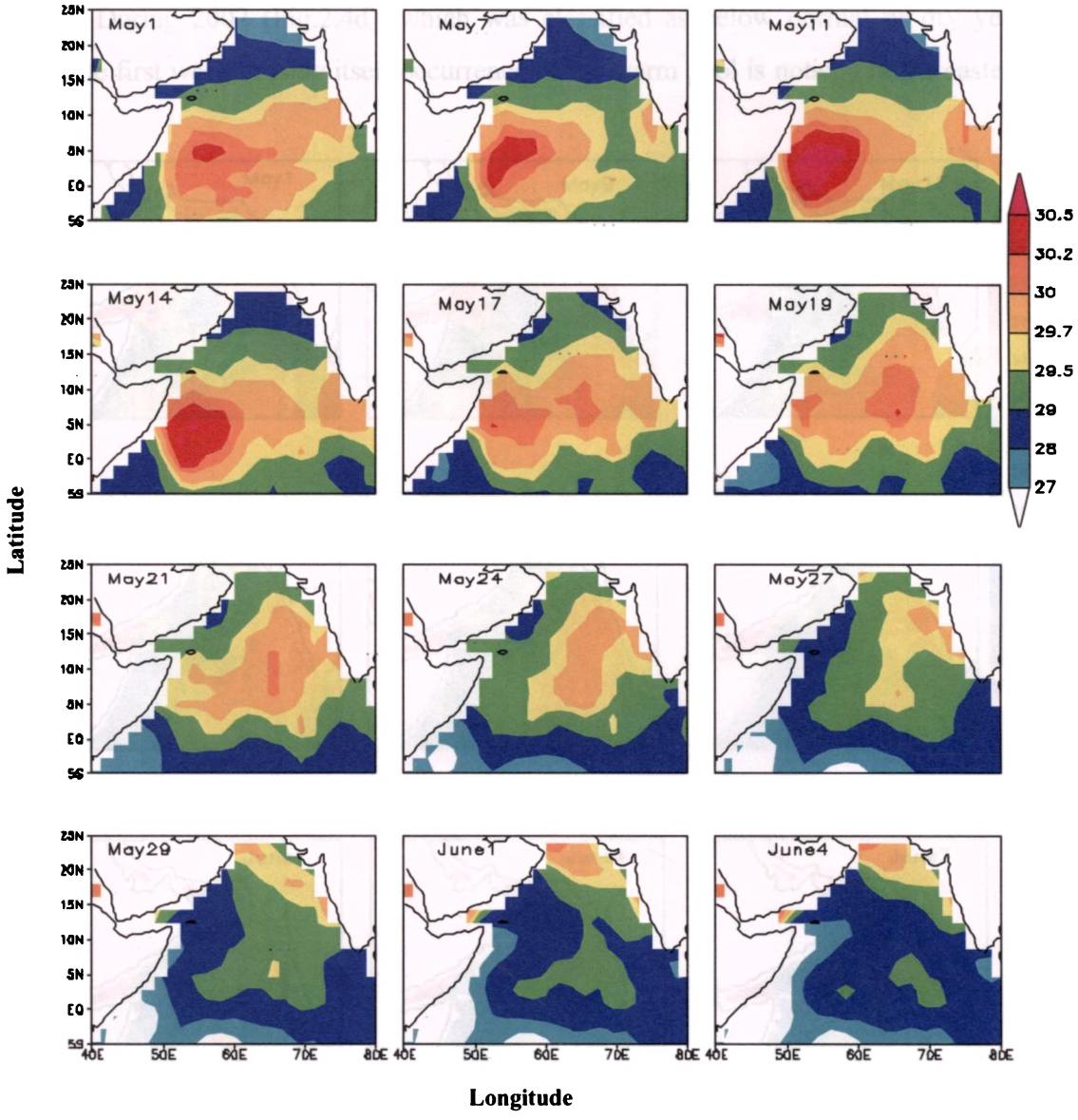

Fig.2.4c Daily evolution of SST (°C) representing some typical days of marked changes during May- June 1985

The above analysis indicates that the extension and core temperature of the mini warm pool shows large variability depending on the nature of the forthcoming monsoon. The dissipation of the Arabian Sea mini warm pool triggered 1-2 weeks before the normal onset of monsoon over Kerala. It is also noticed that during the wet years mini warm pool occupy maximum area and core temperature compared to normal and dry year. These results were verified using the TMI data for the years 2001, 2002 and 2003 (Fig.2.4d, e and f), which are classified as below normal, drought (dry) and above normal respectively by Rajeevan *et al.* (2003).

During 2002 (Fig.2.4d), which was classified as below normal or dry year, from the first week of May itself occurrence of the warm pool is noticed in the eastern

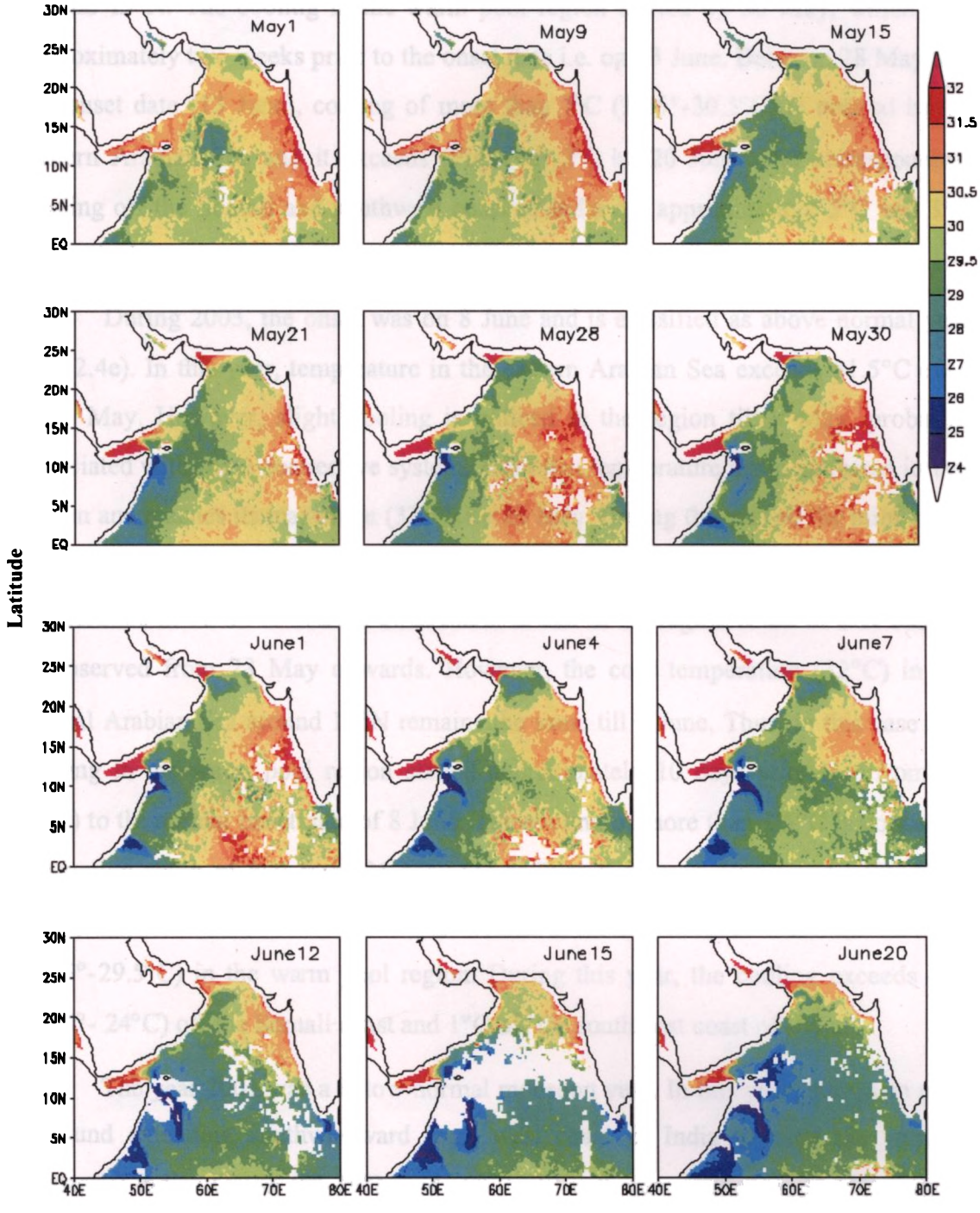

Fig.2.4d Daily evolution of SST (°C) representing some typical days of marked changes during May- June 2002 (TMI)

Arabian Sea (0°-22°N and east of 60° E) and even on 28 May, the warm pool is found to be prominent between 0°-20°N and 60°-75°E. During the period, the warm pool cover an area of more than 36,00000 km^2 with core temperature of 31.5°C centered around 15°N. The cooling in the warm pool region started by 30 May, which was approximately two weeks prior to the onset date i.e. on 13 June. Between 28 May and the onset date (13 June), cooling of more than 1°C (31.5°-30.5°C) is noticed in the eastern Arabian Sea and it exceeds (Fig.2.4d) 2°C by 20 June. The corresponding cooling off the Somali and southwest coast of India are approximately 5°C and 3°C respectively.

During 2003, the onset was on 8 June and is classified as above normal year (Fig.2.4e). In this year, temperature in the eastern Arabian Sea exceeds 31.5°C even on 1 May. However, slight cooling is noticed in the region till 9 May, probably associated with some convective system. After that temperature again increases in this region and reaches its maximum (32°C) by 26 May. During this period the mini warm pool is observed between 0°-20°N and 52°-75°E (>5500,000 km^2) with core temperature of 32°C. A notable observation is that in the region south of 8°N cooling is observed from 28 May onwards. However, the core temperature (32°C) in the central Arabian Sea around 11°N remains the same till 4 June. Thus, in this case also cooling in the warm pool region started approximately 10 days prior (i.e. from 28 May) to the normal onset date of 8 June. The cooling of more than 1.5°C is noticed in the region south of 8°N from 26 May (31.5°C) to 8 June (< 30°C) and ~1°C (32°-31°C) in the central Arabian Sea. By 17 June, cooling exceeds 2°C from 26 May (31.5°-29.5°C) in the warm pool region. During this year, the cooling exceeds 6°C (30.5°- 24°C) off the Somali coast and 1°C off the southwest coast of India.

The year 2001 was a below normal monsoon year. In this year, the warm pool is found extending southwestward from west coast of India towards the western equatorial Indian Ocean (0°-19°N and 50°-75°E) with core maximum 31.5°C noticed around 12°N on 17 May (Fig.2.4f). The area covered is of the order of ~5000,000 km^2, excluding the region in the southeastern Arabian Sea, where temperature is less than 30°C. The dissipation of the warm pool starts from 18 May onwards approximately 6 days prior to the onset date of 23 May.

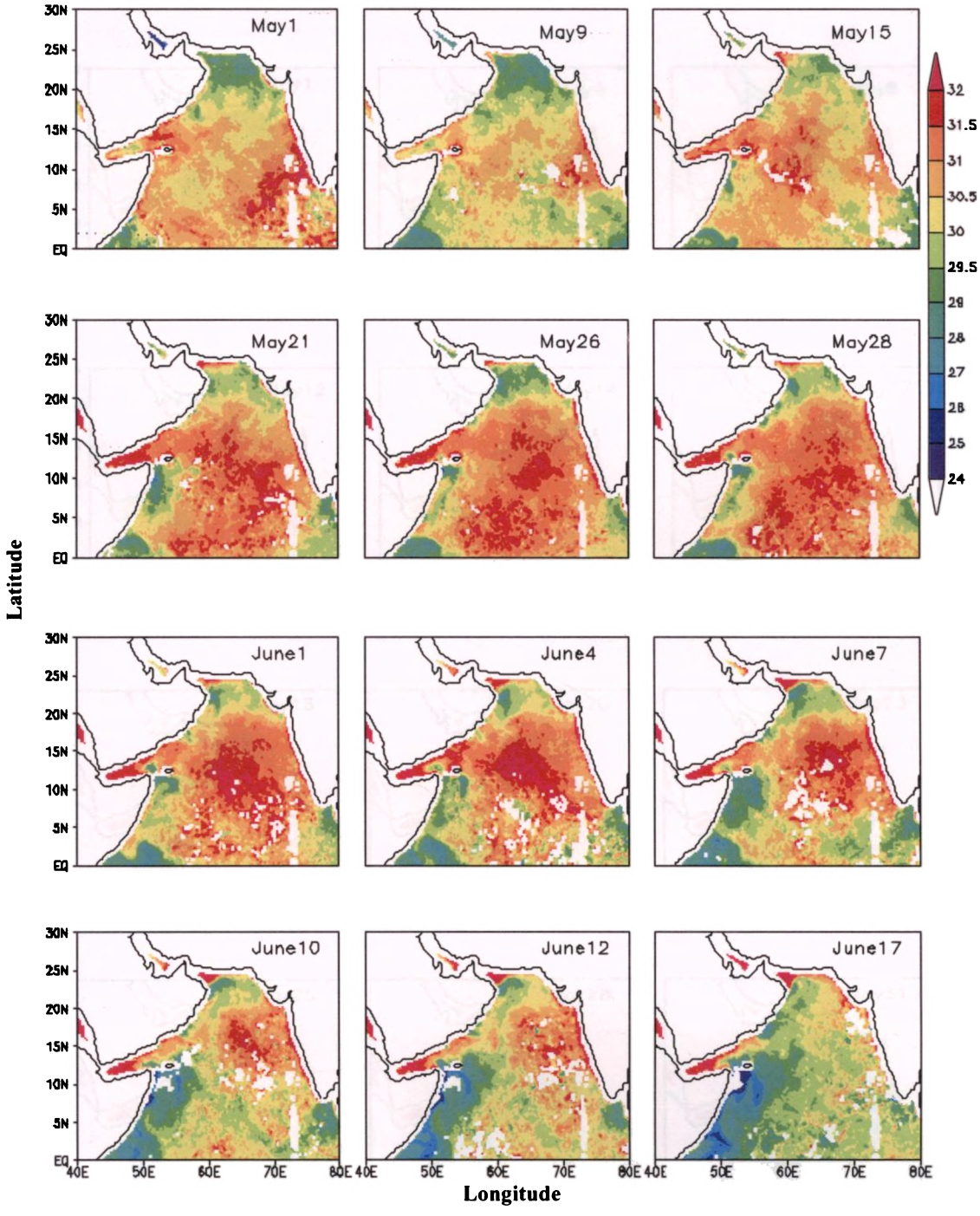

Fig.2.4e Daily evolution of TMI SST (°C) *for some typical days of marked changes during May- June 2003*

By 23 May, cooling of more than 1.5°C (31.5° on 17 May-30°C on 23 May) occurred in the warm pool region and it exceeds 3°C (31.5°- 28°C) by 31 May. The

cooling exceeds 7°C (31°C on 8 May to 24°C on 31 May) off the Somali region and 1.5°C (31°C on 17 May-29.5°C on 31 May) off the southwest coast of India.

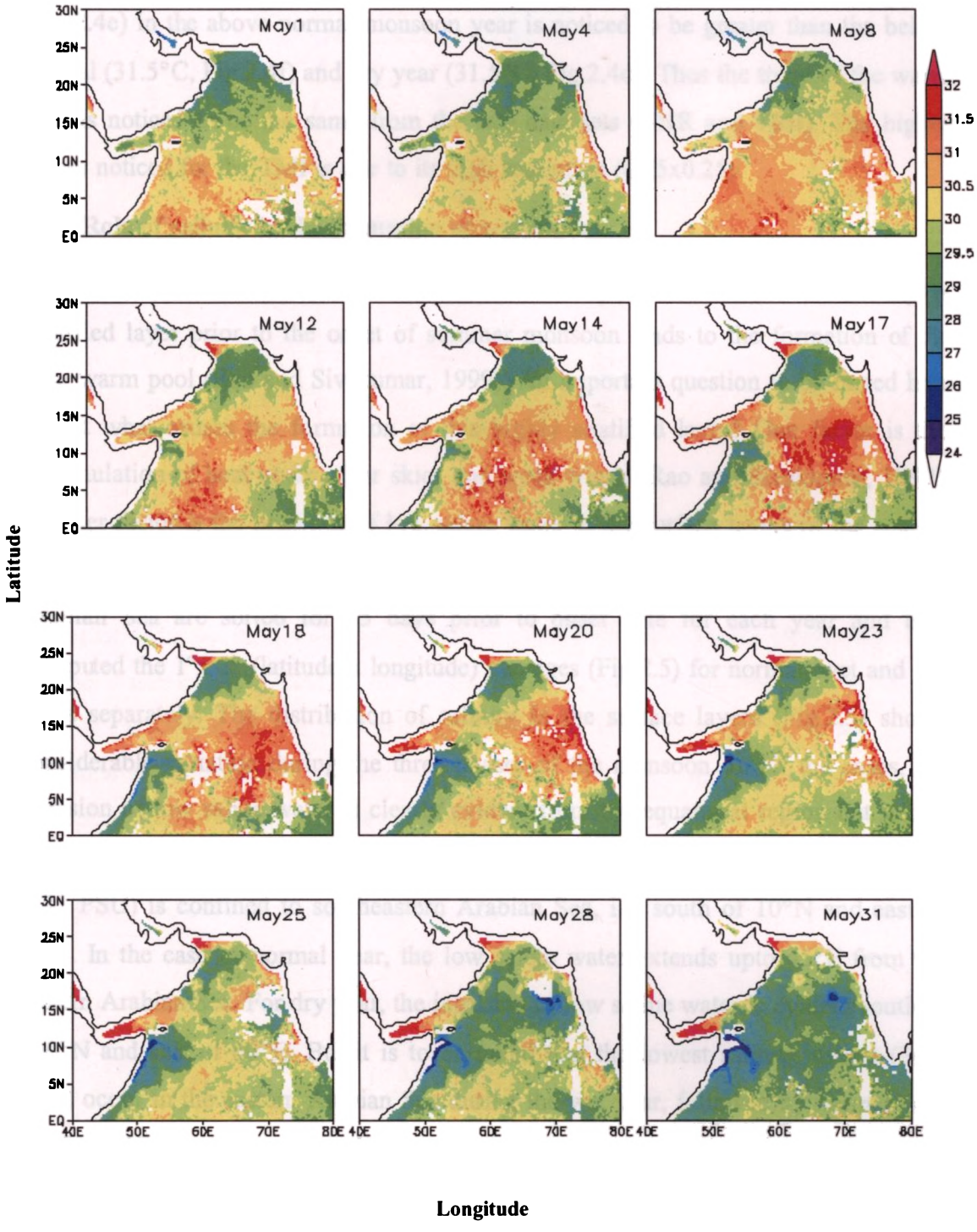

Fig.2.4f Daily evolution of TMI SST (°C) *for some typical days of marked changes during May- June 2001*

Hence TMI SST also supported the earlier findings that the dissipation of the warm pool starts one to two weeks prior to the onset date. It is also noticed that the temperature and extent of the mini warm pool region for the above normal year is higher than below normal and dry year. The core temperature (32°C) and its extent (Fig.2.4e) in the above normal monsoon year is noticed to be greater than the below normal (31.5°C, Fig.2.4f) and dry year (31.5°C, Fig.2.4d). Thus the trend of the warm pool is noticed to be the same from the two data sets (NNR and TMI). The higher values noticed for the TMI is due to its high resolution (0.25x0.25).

2.3.4 Role of salinity in the formation of warm pool

It is well understood that the heat accumulated within a shallow and highly stratified layer prior to the onset of summer monsoon leads to the formation of the mini warm pool (Rao and Sivakumar, 1999). An important question to be raised here is that what causes the formation of this highly stratified layer? One factor is the accumulation of heat under clear skies and weak winds (Rao and Sivakumar, 1999). Another factor is the presence of low saline water in the surface layers of the eastern Arabian Sea. To study this aspect, all available *insitu* surface salinity values in the Arabian Sea are sorted for 15 days prior to onset date for each year and then computed the 1°x 1° (latitude x longitude) averages (Fig.2.5) for normal, wet and dry years separately. The distribution of salinity in the surface layers (Fig.2.5) shows considerable variation during the three phases of the monsoon. In all the cases, the intrusion of low saline water is clearly evident from the equatorial region but with a different spatial extent. During wet year, the northward extent of low saline waters (<35 PSU) is confined to southeastern Arabian Sea, i.e. south of 10°N and east of 60°E. In the case of normal year, the low saline water extends upto 45°E from the eastern Arabian Sea. For dry year, the intrusion of low saline water is evident south of ~10°N and east of 60°E. But it is to be noted that the lowest salinity values (34.5 PSU) occur in the eastern Arabian Sea during the wet year, followed by normal year (34.75 PSU). During the drought year, this low saline waters is confined to south of 5°N in the eastern Arabian Sea.

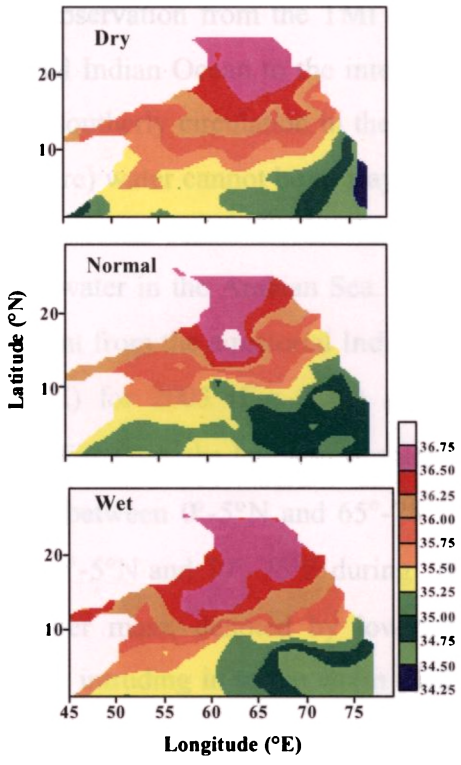

Fig.2.5 Distribution of salinity prior to the onset of summer monsoon (insitu)

During winter, the low saline water from the Bay of Bengal is brought to west coast of India by the prevailing circulation pattern (Shenoi *et al.*, 1999). This low saline water is transported to the central and western Arabian Sea by the Rossby waves radiated from the downwelling coastal Kelvin waves (Bruce *et al.*, 1994; Shankar and Shetye, 1997; Shenoi *et al.*, 1999). The circulation pattern changes to southerly along the west coast of India by April/May. With the dissipation of the Lakshadweep high and change in circulation pattern, this low saline water gets trapped in central and western Arabian Sea. So, during May, the low saline waters in the warm pool region cannot be brought by the prevailing circulation pattern. The other possibility is the re-circulation of the trapped low saline waters from the interior Arabian Sea. Recent studies (Bruce *et al.*, 1994; Sanilkumar *et al.*, 2004) reported both cyclonic and anti-cyclonic eddies in the Arabian Sea during the pre-monsoon season. The gyral circulation pattern associated with these eddies can re-circulate the low saline water trapped in the western and central Arabian Sea to the warm pool region. The highs and lows in the TMI SST for all the years (Fig. 2.6) clearly indicate the eddy type of circulation in this region.

Another notable observation from the TMI charts are the waters intrusion of waters from the equatorial Indian Ocean to the interior Arabian Sea (Figs.2.6 a, b & c). Due to the prevailing southerly circulation in the eastern Arabian Sea during May, this low saline (temperature) water cannot be of Bay of Bengal origin. So the possible origin can be from the equatorial Indian Ocean. These waters are typically low saline compared to the existing water in the Arabian Sea. The intrusion of low temperature/ low saline waters is evident from the equatorial Indian Ocean into the central Arabian Sea (near 5°N and 70°E) for 2003 (Fig. 2.6c) as indicated by the cold tongue (~29.5°C). During 2001 (Fig.2.6a), the low temperature water mass (29.5°C) from the equatorial region is seen between 0°-5°N and 65°-75°E. While the low temperature zone is noticed between 0°-5°N and 70°-75°E during 2002 (Fig.2.6b). Thus in all the cases the low saline water mass, denoted by low temperatures, from the central equatorial region was seen intruding in to the warm pool region. The intrusion of low saline waters is found to be more northwards (~10°N) during 2002 (Fig.2.6b), which was a dry year.

So the above analysis suggests that the low saline water present in the warm pool region can be from two sources. One source is the re-circulation of the Bay of Bengal water trapped in the interior Arabian Sea by the eddy type of circulation. Second is the intrusion of equatorial water into the Arabian Sea and the re-circulation by the prevailing eddies.

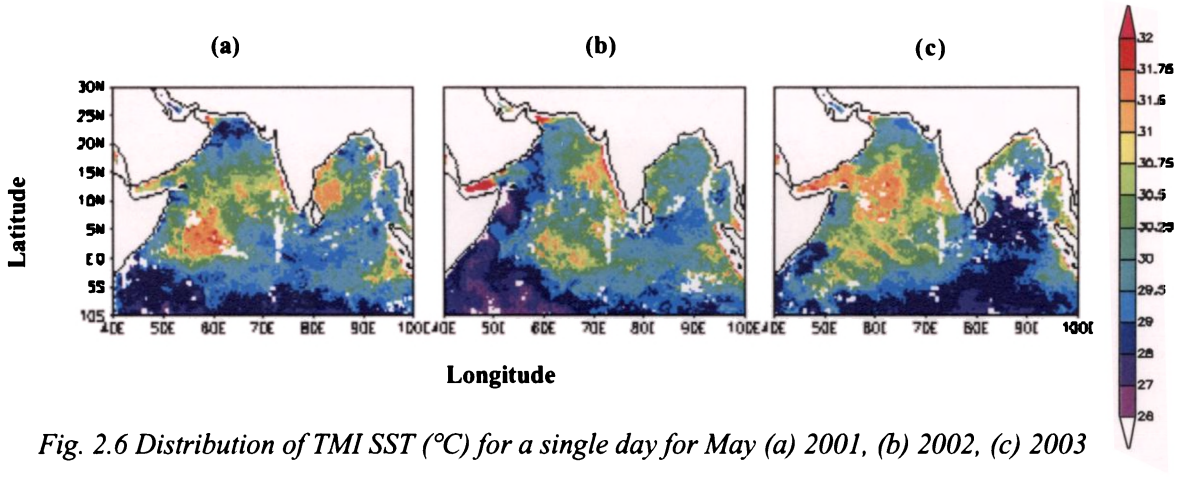

Fig. 2.6 Distribution of TMI SST (°C) for a single day for May (a) 2001, (b) 2002, (c) 2003

Chapter 3

Marine boundary layer characteristics during summer monsoon - a case study

3.1. Introduction

Studies on the marine boundary layer (MBL) are of particular interest in the fields of aviation, atmospheric prediction and radar ranging. The boundary layer over the ocean is mostly turbulent causing inhomogeneous distribution of temperature and humidity. These variations lead to large changes in the moisture content and many other atmospheric properties. The changes in these parameters may lead to inhomogeneous distribution of refractive index properties, which causes duct formation in the boundary layer. Radio rays or electromagnetic rays get trapped in these ducts and travel long distances without attenuation. For adequate radar and communication ranging, information on the refractive index profile is essential. In spite of all these significance, studies on the marine boundary layer characteristics are meager due to lack of sufficient observational programmes over the Ocean.

Most of the studies on MBL are based on the data collected during the experiments ISMEX-73, MONSOON-77, MONEX-79 and MONTBLEX-90. Using ISMEX-73 data Ramanathan (1978) analysed the temperature inversion for different stability conditions. MONSOON-77 data sets were utilized to study the changes in the horizontal wind fields, vertical velocity and large-scale heat and moisture budgets between disturbed and undisturbed conditions (Mohanty and Das, 1986). However, using MONEX-79 data, the disturbed conditions could not be studied as this period coincided with weak monsoon condition. Nimmi *et al.* (1997) studied the vertical discrepancy in meteorological parameters in the boundary layer over the Arabian Sea during the monsoon period using aircraft data collected during MONEX-79. Similarly, Holt and Sethuraman (1987) investigated the monsoon boundary layer over the central Arabian Sea and north central Bay of Bengal from wind and temperature profiles collected during MONSOON-77 and MONEX-79. They noticed marked differences in the boundary layer characteristics between the break and active phases of the monsoon. The active and onset phases showed highly unstable situations with high winds and shift to southwesterly flow and slightly unstable temperature profiles in the lower layers. MONTBLEX-90 was carried out to understand the various atmospheric as well as the marine boundary layer characteristics in detail. Using this data Rao and Murty (1992) has studied the temporal

variability of air temperature and water vapour content in the lower troposphere over the northern Bay of Bengal. Utilizing Radiosonde data collected during the Bay of Bengal Monsoon Experiment (BOBMEX), Bhat *et al.* (2001) studied the CAPE and CINE condition over the northern Bay during convectively active and weak phases of monsoon. They found that the recovery time for the CAPE to be 2 days after the disturbance has passed, which have important implications for the genesis of convection over the Bay.

BOBMEX-99 experimental program provided a unique opportunity to study the MBL characteristics during active and weak phases of the summer monsoon. Many atmospheric systems, varying from low pressure to deep depressions were also formed during this period. In this chapter, the radiosonde data collected over the northern Bay of Bengal during July-August 1999 is utilized to describe the general characteristics of the MBL and the changes induced in this layer by the atmospheric systems. Finally, variability in the refractive index duct formation in the marine boundary layer associated with these systems are also examined.

3.2. Data and methodology

During BOBMEX-99, ORV Sagar Kanya occupied a stationary position (Fig.3.1) in the northern Bay of Bengal (17°N, 89°E) in two phases (i.e. from 27 July-6 August and 13-22 August 1999). Radiosonde measurements were collected from this location at

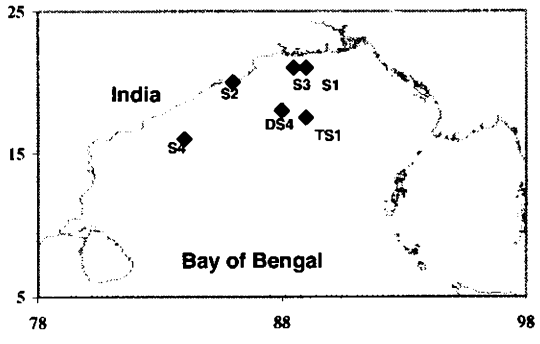

TS1 location of SK
S1 depression on 24 July
S2 low pressure on 1 August
S3 depression on 5 August
S4 low pressure on 24 august

Fig.3.1 Location of time series station and the center of atmospheric system

~6 hourly intervals. The measurements include vertical profiles of temperature, humidity and wind speed and direction. In the first phase, the wind speed and direction are not available and hence not utilized in the analysis.

The wind shear, s (s^{-1}) is computed from the horizontal (u) and vertical (v) component of the wind field and from the vertical distance, dz (m).

$$s = \sqrt{\left(\frac{du}{dz}\right)^2 + \left(\frac{dv}{dz}\right)^2}$$

Clear Air Turbulence (CAT) are zones of strong wind shear. Depending on shear, the intensity of CAT is divided into light (L), medium (M), strong and severe (S) following Stull (1993). Based on this classification, the intensity of CAT is categorized as

N	$0 < s < 0.0118$
L	$0.0118 < s < 0.0169$
L-M	$0.0169 < s < 0.0336$
M	$0.0336 < s < 0.0506$
M-S	$0.0506 < s < 0.0844$
S	$s > 0.0844$

Frictional velocity, u_* (ms^{-1}) is computed as

$$u_* = \sqrt{\tau/\rho}$$

The wind stress $\tau = \rho C_d U^2$

here C_d is the drag coefficient and U is the wind speed (ms^{-1})

Boundary Layer Height, BLH (m) is computed following Stull (1997) and Arya (1988)

$BLH = \dfrac{0.2u_*}{2\Omega \sin(\phi)}$ where Ω is the angular velocity of the earth = 0.0000727 s^{-1} and ϕ is the latitude in degree.

Radio Refractive index (N) is a function of temperature, pressure and humidity and is estimated following Hitney (1985)

$$N = \frac{77.6 \times p}{T} + 3.73x10^5 \times \frac{e}{T^2}$$

where e is vapour pressure (mb); p, is pressure (mb) and T, temperature (°C).

Understanding of the vertical gradient of RRI is having more application for diagnosing refraction of radio waves in the boundary layer compared to RRI. Based on the vertical gradients of radio refractive index (dN), the refraction of radio waves in the boundary layer is classified into four categories (Table 3.1)

Table 3.1 classification of dNased on Hitney (1985)

Gradient (N units /m)	Condition
dN < -157	Trapping
-157 < dN < -79	Super-refractive
-79 < dN <0	Standard
dN > 0	Sub-refractive

The radio rays propagating in a trapping condition bends downward with a greater curvature than the earth's curvature and propagates long distance along the duct. This condition is ideal for tracking. In super-refraction, the ray bends downward and this has the effect of extending the normal horizon and is favourable for extended radar ranges. In sub-refraction cases, the radio ray bends upwards which result in shortening of the normal horizon. This is the difficult condition when long range is required such as for tracking of an aircraft or missiles.

3.3. Results and Discussion

3.3.1 Weather summary

A well-marked low-pressure area formed over northern Bay of Bengal and adjacent coastal region of Gangetic West Bengal and Orissa on 14 July and by 17 July

1999, it weakened into a low pressure over East Rajasthan and northwest Madhya Pradesh. On 24 July, a feeble low-pressure area again formed over Gangetic west Bengal and neighbourhood with associated upper air cyclonic circulation extending up to mid-tropospheric levels. The low-pressure system became well marked by 27 and became a depression centered at 21°N and 89°E (Fig.3.1). This intensified into a deep depression by 28 with its center near 23°N and 86.5°E and moved northwestward and weakened into a well-marked low-pressure system by 30 July. Another low-pressure system was formed over northwest Bay of Bengal in the evening of 1 August and became well marked by 2 August. Afterwards, it weakened and merged with the monsoon trough. A new cloud band was generated on 4 August and a low-pressure system formed over northwest Bay of Bengal and neighbourhood on 5 August and intensified into a depression by 9 August with its center at 21°N and 88.5°E. It then weakened into a low-pressure system and lay over north Madhya Pradesh. During this time, the eastern end of the surface monsoon trough shifted northward. As a result, weak monsoon conditions prevailed over major parts of the country during mid August and the axis of the monsoon trough lay close to the foothills of the Himalayas. A new system was formed off the coast of north Andhra Pradesh on 24 August (16°N and 84°E) and moved slightly northward and finally merged with the low-pressure over the Orissa coast. Heavy rainfall was noticed during 1, 6, 15 and 16 August. During 31 July-1 August and 14-16 August, the station received more than 80 mm and 200 mm rainfall respectively (Bhat *et al.*, 2001). Thus the period of study comprises of both active and weak phases of the monsoon.

3.3.2 Variation in the marine boundary layer characteristics

In order to understand the influence of the systems formed over the northern Bay on the MBL characteristics, the time-height sections of temperature, potential temperature gradient, wind speed, wind direction, relative humidity, wind shear, intensity of CAT are presented (Figs.3.2-3.6).

Generally, the atmospheric temperature (Fig.3.2) decreases with height, with maximum temperature (28.5°C) at the surface (0 m) and minimum (-82.5°C) between 16500 m and 17000 m. Temperature starts increasing from 17000 m height onwards. In the lower layer (below 800 m), temperature shows large variation compared to the layer

above 1000 m. So, in order to highlight the variations, the lower 1000 m is enlarged. During the observational period, three drops in temperature are noticed. The first decrease, noticed during 31 July - 1 August is mainly due to the formation of low pressure system on 1 August. This activity reduces the temperature, especially in the lower atmosphere i.e., below 200 m, by more than 3.5°C (from 28.5°C-25°C). The thermal gradient is noticed to be higher in the levels below 200 m, where temperature decreases rapidly with height. The cooling is also observed in the upper layer up to a height of 1000 m though the magnitude is very small (<1°C). Above 1000 m level, the decrease of temperature in association with the formation of weather system is negligibly small. The temperature drop in the surface layer below 200 m can be attributed to the loss

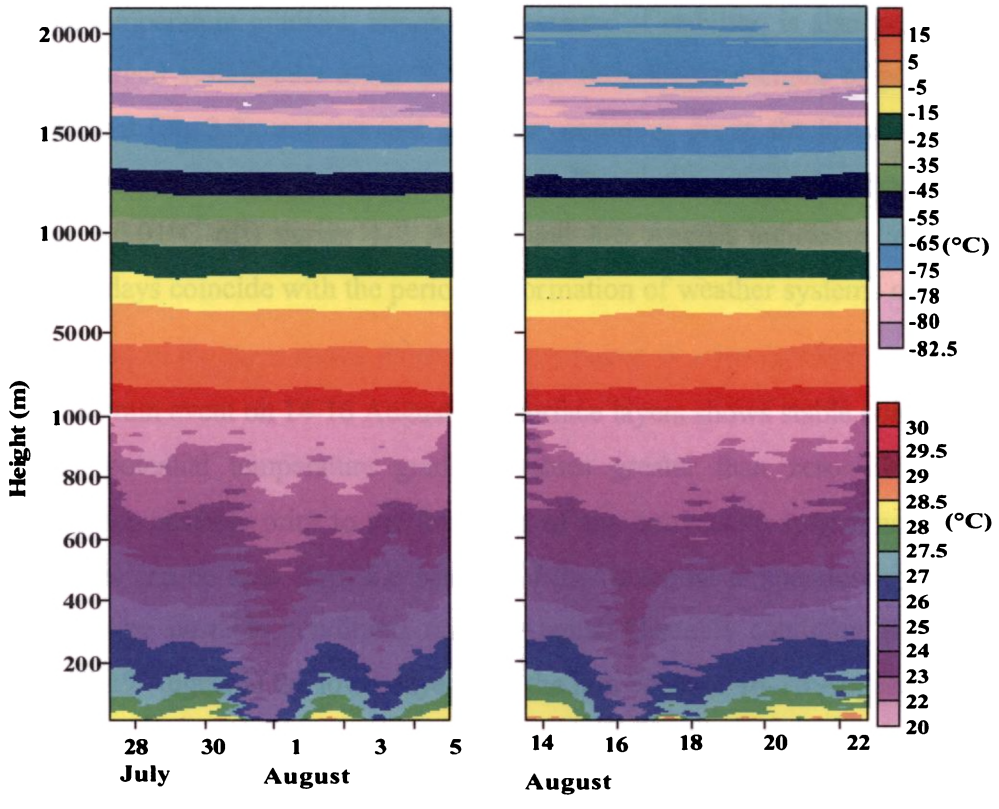

Fig.3.2 Height-time sections of temperature

of latent heat and sensible heat from the ocean and immediate surface layer in the atmosphere associated with the formation of a system (Stull, 2000). After the withdrawal

of the system, the air temperature restored to its pre-storm value (28.5°C). Similarly, the low pressure formed on 4 August reduced the temperature in the lower atmosphere by more than 1.5°C (28.5°C-27°C). Bhat *et al.* (2001) reported intense rainfall event during 14 to 16 August at the northern Bay of Bengal. A drop of more than 3°C (28.5°-25°C) between 14 and 16 August is also noticed during this major rain event. The cooling in this case is found up to the height of about 600 m. Temperature restored to its pre-system value (28.5°C at the surface) after 18 August with the decay of the convective system.

This analysis reveals that the influence of low-pressure systems/depression and convective system (associated with heavy rainfall) on the temperature field is maximum in the lower 1000 m. Above 1000 m, the variations are found to be negligible. After the withdrawal of these systems, atmospheric temperature regains its pre-system values.

Potential temperature gradient, which is a measure of stability, is also presented (Fig.3.3) with enlarged scale for the lower 300 m. The time-height sections of potential temperature gradient (Fig.3.3), indicate that unstable conditions are in the lower 150 m, with maximum gradient in the lower 50 m. Below 50 m, the potential temperature gradient is less (-0.01°C m^{-1}) during 1-2 August and 4-6 August indicating unstable conditions. These days coincide with the period of formation of weather systems over the region.

During the rain event on 14-16 August, the surface layers shows stable conditions as indicated by potential temperature gradient values greater than zero. However, atmosphere becomes unstable prior to the formation of any convective system and after its dissipation. This can be seen from the patches of low potential temperature gradient (<0 °Cm^{-1}) indicating unstable conditions on 13 August. Unstable condition is again noticed during 17-19 August in the lower layer after the rain event of 14-16 August.

During the entire observation period, near saturated condition (RH > 85%) prevailed in the lower boundary layer (Fig.3.4), i.e. below 1000 m. However, marked variability is noticed between this level and 8000 m in association with the system activity. Above 11000 m, RH values are found to be less than 30% without appreciable variation in association with the formation of weather systems.

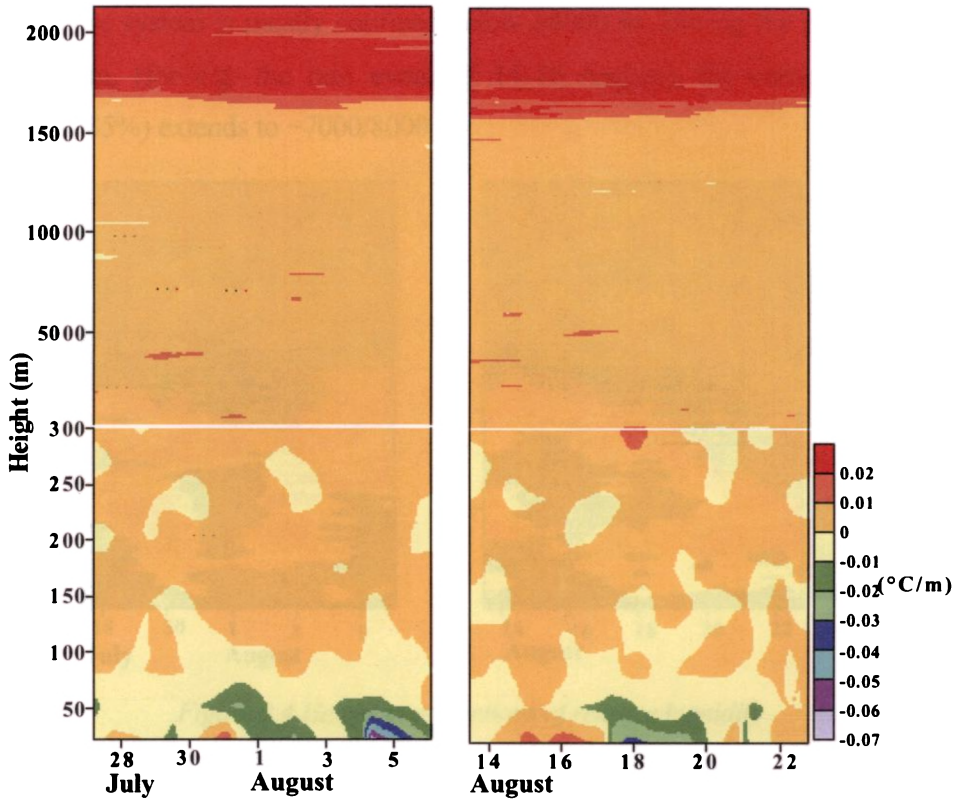

Fig.3.3 Height-time sections of potential temperature gradient

The variability in RH associated with systems is found to be more in the lower 8000 m compared to the layer above. Prior to the formation of a low pressure system on 30 July, RH was around 60-70% in the lower layer between 1000 m and 10000 m. However, during 31 July – 1 August, RH increased to more than 85%, with the maximum values occurring upto 7000 m. RH is found higher (> 85-90%) in the lower layer during 28-29 July (~4000 m) and 5 August (below 6000 m), when there was a deep depression and low pressure system respectively around this location. RH decreases to less than 70% in the levels particularly above 1000 m after the withdrawal of the system.

Similar condition is noticed during 14-16 August, when there was a heavy rainfall event associated with convective cloud band. RH increased to more than 85% in the lower 8000 m (maximum >90% between 4000 m and 6000 m). After the rainfall, low humidity regime (<60%) extended to the lower layers (~5000 m) coinciding with the weak monsoon phase. So the distribution of RH clearly indicates that the variability

associated with the system is mostly confined below 10000 m. During the period of any convective system, (for e.g. the rain event of 14-16 August), the vertical extent of maximum RH (>85%) extends to ~7000/8000 m

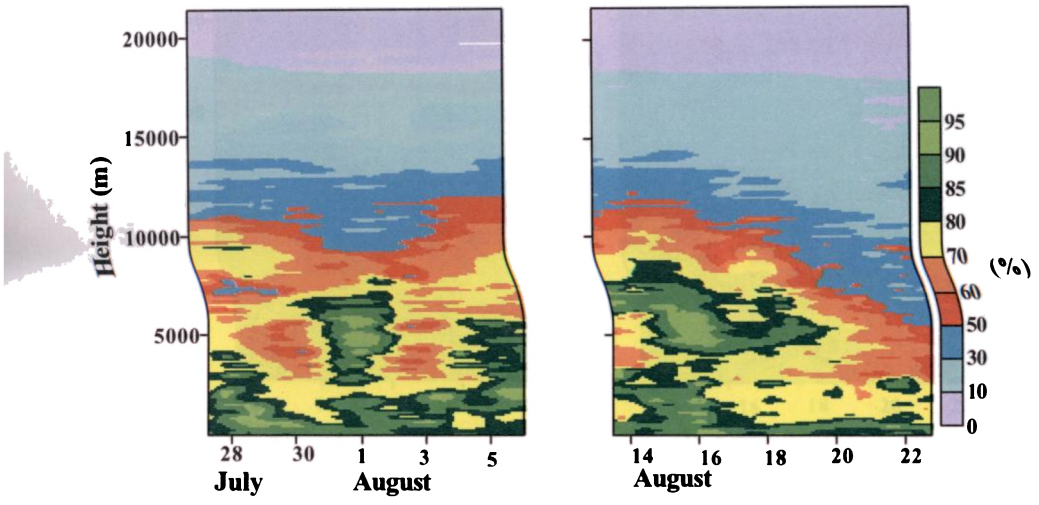

Figure 3.4 Height -time sections of relative humidity

The upper air wind speed (Fig.3.5a) and direction (Fig.3.5b) also shows marked variability in association with the formation and dissipation of the systems. In the lower atmosphere (below 5000 m), westerly winds (225-270 deg) with speed 11-16 ms^{-1} dominated. During the periods of convective systems, the westerly wind regime extends upto 7500 m with an increase in their speed (11-16 ms^{-1}) in the lower 4000 m. Once the weak monsoon situation (after 18 August) sets in, weak westerlies (1-6 ms^{-1}) are noticed in the lower layers. The westerly wind regime also shrinks and confines to the lower 5000 m. Maximum magnitude of the wind (>31 ms^{-1}) is noticed between 15000 m and 17000 m (Fig.3.5a). This high wind speed regime above 15000 m represents the core of the easterly (45-90 deg) jet stream. The core of this easterly jet stream confined to 16000 m associated with the weak phase of monsoon, i.e. after 17 August. The easterlies (90-135 deg) extend downwards to nearly 5000 m associated with weak monsoon condition.

Wind shear, (Fig 3.6b) also shows similar pattern of variation as that of wind speed and direction. A zone of higher wind shear (0.0118-0.0169 s^{-1}) is noticed above a height of 15000 m throughout the observation period. This higher shear zone coincides

with the core of easterly jet stream. This zone of high wind shear extends from 15000-20000 m during the rainfall event. The vertical extent of maximum wind shear is found to

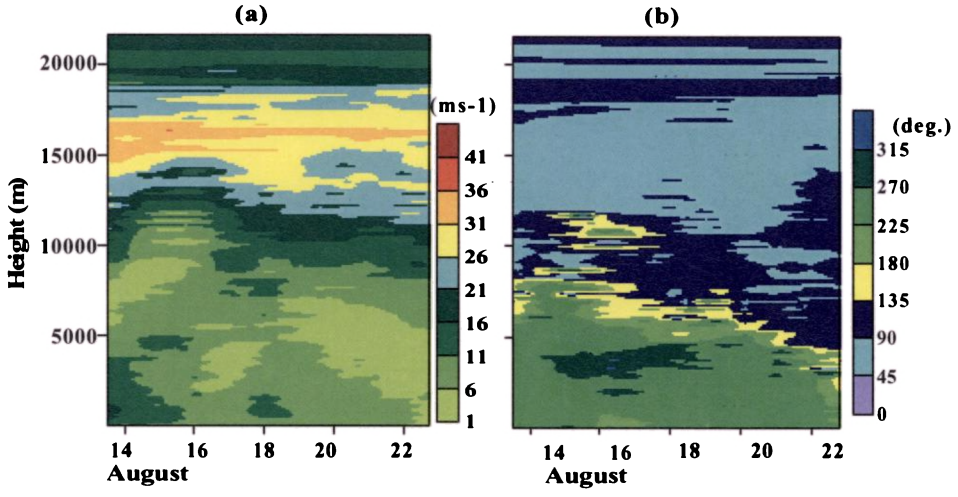

Figure 3.5 Height-time sections of (a) wind speed and (b) direction

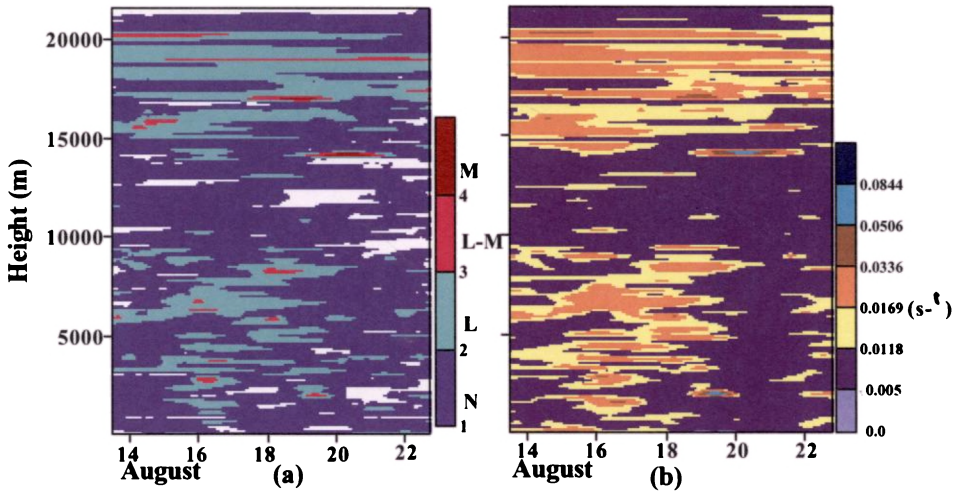

Figure 3.6 Height-time sections of (a) intensity of CAT and (b) wind shear

decrease after 18 August once the weak monsoon conditions sets in (17000-20000 m). In association with the convective system during 14-17 August, wind shear increases to more than 0.0118 s^{-1} in the lower 10000 m and decreases considerably (< 0.005 s^{-1}) after 17 August, coinciding with the weak monsoon period. Another notable observation is the weak shear (0.005 s^{-1}) between 10000 m and 14,000 m, as the influence of the both TEJ (Tropical easterly jet) and LLJ (low level jet) in this layer is small (Figs.3.5 a & b).

Variability in the CAT (Fig.3.6a) followed the shear distribution. Light conditions for the intensity of CAT as indicated by L when wind shear lies between 0.0118 and 0.0169 s^{-1} (Stull, 1993), is found in the jet stream region i.e. between 15000 m and 20000 m heights. Associated with weak monsoon conditions, thickness of this layer decreases (2000 m, 17000-19000 m). Below 10000 m also, conditions for light intensity of CAT is noticed coinciding with the high wind shear zone. In all other periods, intensity of CAT is found to be normal (N, when wind shear is less than 0.0118 s^{-1}). Thus the convective activity leading to high wind shear zones are more probable to the occurrence of light intensity of CAT.

The radiosonde data is further utilized to estimate the lifting condensation level (LCL), LCL temperature, boundary layer height (BLH) and frictional velocity (u^*) (Fig.3.7). During the observation period, LCL (Fig.3.7) lowered (below 965 –970 mb) during 31 July, 2 August and 5 August. These dates coincided with the formation of systems in the Bay of Bengal. So, the lowering of LCL can be linked to increase in surface moisture content (Fig.3.3) associated with the system formation. Similarly, LCL lowered to 997 mb on 16 August coinciding with the rain incident. Bhat *et al.* (2001) reported intense rainfall during 14-16 August. Another lowering of LCL (~990 mb) noticed on 18 August, may be due to some localized convective activity over the region. So, in general it was seen that LCL lowered to ~970 mb pressure level or below during the periods of convective activity, otherwise the LCL remains above 970 mb. The temperature at the LCL (Fig.3.7) also decreases during 31 July, 2 August, 5 August, 16 August and 18 August.

The boundary layer height (BLH) is around 2143 m just before the formation of a convective system i.e. on 13 August (Fig.3.7). The BLH decreases to 578 m on 16 August, coinciding with the period of intense rainfall. The downdraught associated with the system brings the boundary layer downward causing the sharp decline of BLH. After the rainfall event, the BLH increases to more than 1500 m, which is the normal boundary layer height (Stull, 1993) for the tropical ocean. The frictional velocity, u^* also decreases from 0.469 ms^{-1} prior to the rain events to about 0.126 ms^{-1} during the periods of intense

rainfall due to decrease in wind speed (Fig.3.5). This analysis suggest that the convective activity reduces the BLH by the order of 1500 m and U*by the order of .3 ms^{-1}.

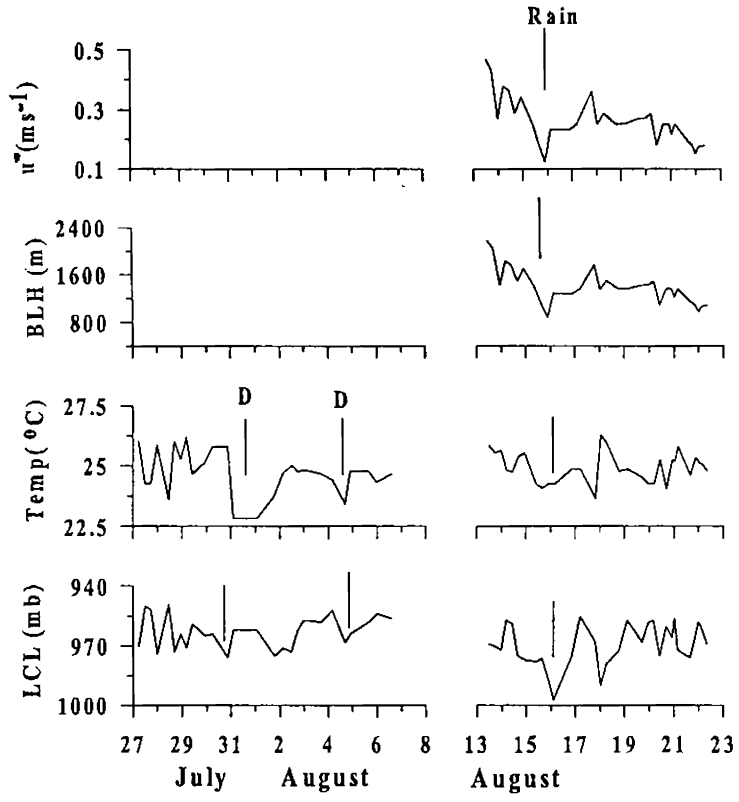

Fig. 3.7 Time series of LCL, LCL temperature, inversion height, boundary layer height (BLH) and frictional velocity (u), system period is indicated by D and Rain*

3.3.3 Radio Refractive Index (N)

The marine boundary layer, in particular is susceptible to changes in water vapor content and temperature variations to a large extent causing changes in refractive conditions of the atmosphere. Electromagnetic wave path varies with the refractive index variations in the atmosphere. Hence more information on this is needed to estimate their relationship to predict accurate radar ranges. Here, gradient of refractive index (dN) (Table3.1), is presented to study its vertical variations associated with the system activity.

Generally standard conditions (between -79 and 0 N units m^{-1}) are observed above 400 m throughout the observation period. Below 400 m, trapping (<-157 N units m^{-1}), super-refractive (-157 to -79 N units m^{-1}), standard and sub-refractive conditions (>0 N units m^{-1}) are observed (Fig.3.8). Further, it is noted that the distribution of dRRI and

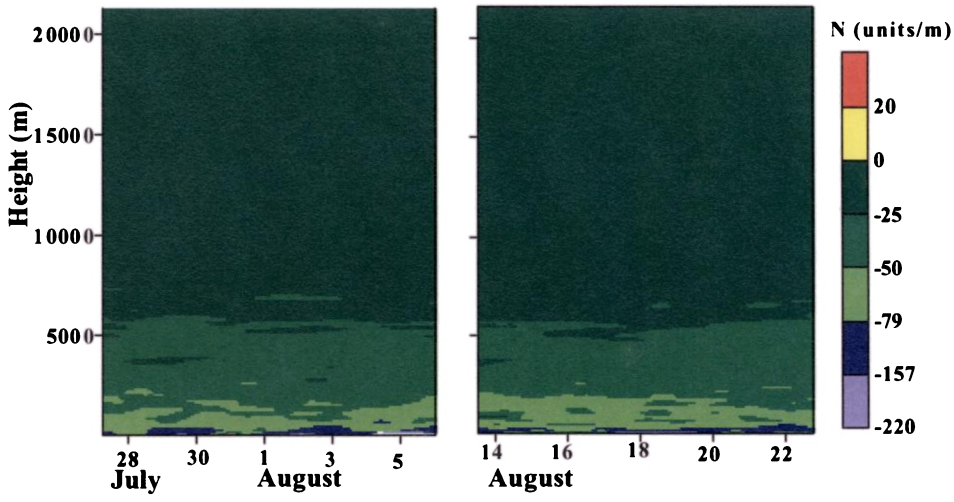

Figure 3.8 Height-time sections gradient of radio refractive index.

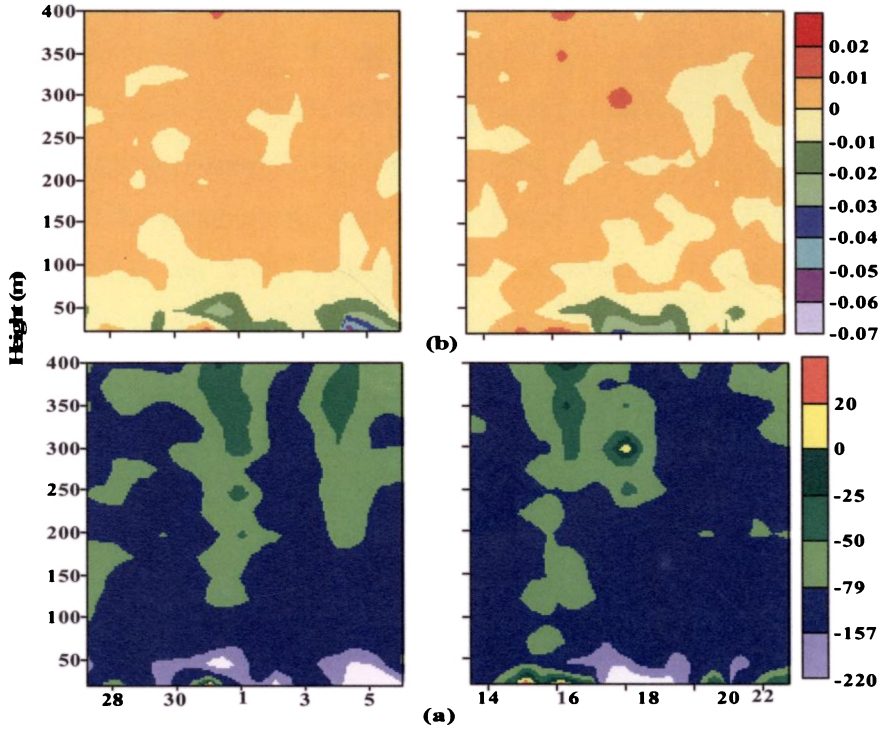

Figure 3.9 Height-time sections of (a) radio refractive index and (b) potential temperature gradient below 400 m

potential temperature gradient (Fig.3.3) shows similar patterns in the lower 400 m. So, the levels up to 400 m for both the parameters are enlarged and presented in Fig.3.9. The

trapping condition existed in the lower most layers (~70 m) during 29-30 July, 1 -2 August, 4-6 August, and coincides with unstable conditions as indicated by low potential temperature (<-0.01°C m^{-1}). The trapping condition is also noticed between 17 and 19 August in the lower 70 m and coincides with unstable condition (potential temperature gradient of ~ -0.01°C m^{-1}). Moreover, this trapping condition coincides with the drops in temperature near the surface layer (Fig.3.2) associated with the system formation. In this condition, the radio rays traveling at this height bend downwards with a greater curvature than the earth, get trapped in the duct and travel long distances in the duct. A sub-refractive condition (> 0 N units m^{-1}) is noticed in the lower most layer during 31 July, 15 to 16 August. During this period, just above the sub-refractive zone, standard refractive conditions also exists upto 30 m during 31 July and upto 50 m during 14-17 August. During the periods of convective activity, another zone of standard refractive condition is noticed above 100 m on 1 August (low pressure area), above 200 m during 4 August (depression) and above 50 m on 16 August (rain event). During the weak monsoon period, the super-refractive conditions are more prominent in the lower 400 m.

The above analysis revealed that refractive index variations are inhomogeneous in the lower layers and the variations are found insignificant in the upper layers. Above 600 m, standard conditions are found throughout the observation period. The trapping condition in the lower layers coincides with the unstable situations and the sub-refractive condition noticed in the surface layer and coincides with the rainfall. Coinciding with the weak monsoon condition super-refractive condition existed below 400 m.

Chapter 4

Upper ocean characteristics of the Bay of Bengal during summer monsoon - a case study

4.1 Introduction

International Indian Ocean Expedition (IIOE) conducted during 1962-66 was the major episode that paved the way for studying the Indian Ocean, particularly the Bay of Bengal, which was the least exposed area till then. After IIOE, various national and international agencies started giving more attention to Bay of Bengal in an organized manner. These includes the monsoon experiment (ISMEX-73, MONEX-77 and MONEX-79) of the Global Atmospheric Research Program (GARP), the First GARP Global Experiment (FGGE), the Indian Ocean Experiment (INDEX), Tropical Ocean and Global Atmospheric research program (TOGA), World Ocean Circulation Experiments (WOCE), Monsoon Trough Boundary Layer Experiment (MONTBLEX), Bay Of Bengal Monsoon Experiment (BOBMEX). All these surveys have substantially improved the understanding of various physical aspects and increased the availability of measured data in this region.

Bay of Bengal being a semi-enclosed basin is an area of intense air-sea interaction, which has an important role in the climatology of the Indian subcontinent. The physical and dynamical conditions over this region are very much influencing the intra-seasonal variability of Indian summer monsoon. An interesting feature of this area is the influx of low salinity surface water caused by large river runoff from the Indian subcontinent and Myanmar. Monsoon depressions form over head Bay of Bengal, into which the seasonal monsoon trough extends. Most of the monsoon rainfall is associated with these synoptic scale systems. SST over the Bay remained higher than 27.5°C throughout summer (Gadgil *et al.*1984; Graham and Barnett 1987). Many have studied the meteorological and oceanographic conditions favourable for the genesis of monsoon depressions. Genesis of synoptic scale systems occurred over regions of the Bay of Bengal with high SST and high heat potential (Rao and Rao, 1986; Rao *et al.*, 1987; Sanilkumar *et al.*, 1994). Rao *et al.* (1981) found that the growing thermal contrast in the surface waters between the northern and eastern locations might have infused baroclinic instability in the overlying atmosphere resulting in the formation of monsoon depression. Raman *et al.* (1978) has reported that a fall in wind shear acts as a precondition for the formation of the disturbance over Bay of Bengal.

The monsoon influences significant changes in the thermohaline/density and current fields of the upper ocean. Ocean responds to changes in wind stress and buoyancy fluxes by shoaling/warming and deepening/cooling of the mixed layer depth (Joseph *et al.*, 1996). Synoptic scale verification of the correlation between surface mixed layer characteristics and vertical fluxes of energy and mass through the interface were carried out over the western Indian Ocean using one-dimensional model simulations (Rao, 1986; Joseph *et al.*, 1990; Sanilkumar *et al.*, 1991) including advection and effects of wind stress convergence/divergence. Several one-dimensional numerical modeling of the mixed layer characteristics are available in the literature with time scales ranging from diurnal to seasonal (Kraus and Turner, 1967; Denman, 1973; Pollard *et al.*, 1973; Mellor and Durbin, 1975; Miller, 1976; Thompson, 1976; Niiler and Kraus, 1977; Price *et al.*, 1986). However, most of these studies are limited to Pacific and Atlantic Oceans where long time series measurements of temperature profiles and surface meteorological elements are made from weather ship stations. Studies of Denman and Miyake (1973) and Rao and Mathew (1990) suggested that the model of Miller (1976) is in general suitable for the simulation of the mixed layer characteristics on a synoptic scale when one dimensional processes are dominant. Sanilkumar *et al.* (1994) suggested that one-dimensional processes cannot explain the observed variance in MLD and MLT at a location in the head Bay during the monsoon of 1990 due to massive fresh water influencing meso-scale features. Recently, Mathew *et al.* (2003) using a one dimensional model found that significant departure from the observation and simulation arises when advective processes and large amplitude waves dominate.

Bay of Bengal Monsoon Experiment (BOBMEX) was conducted in the Bay of Bengal with an objective to study the air sea interaction and intra-seasonal oscillations during the summer monsoon season. The response of the northern and central Bay of Bengal to summer monsoon of 1999 has been studied here. Depressions form over the Bay of Bengal during summer monsoon time and strengthen the monsoon activity over the subcontinent. So far no study was carried out to link the northern Bay of Bengal and central Bay of Bengal to the monsoon depressions that originate in the Bay. In this aspect, the simultaneous measurements carried out from the northern and central Bay of Bengal during the BOBMEX

programme provided valuable information of the various physical processes in the Bay of Bengal at northern and central Bay of Bengal. Here, an attempt is made to compare and contrast the response of the upper area of the northern and central BOB to the atmospheric forcing during the summer monsoon 1999. A one-dimensional model was also utilized to simulate mixed layer depth (MLD) and temperature (MLT) to study the importance of local forcing on the upper ocean dynamics of the northern and central Bay to the monsoon of 1999.

4.2 Data and methodology

In the BOBMEX program, two research vessels, viz. *ORV Sagar Kanya* of Department of Ocean Development (DOD) and *INS Sagardhwani* of Defence Research and Development Organization (DRDO) participated (Fig.4.1). The DOD vessel, *ORV Sagar Kanya* occupied a location in the northern BOB (17.5°N & 89°E) between 29 July and 22 August in two phases (29 July-6 August and 13-22 August). The DRDO vessel, *INS Sagardhwani* occupied a stationary position in the central Bay (13°N, 87°E) between 17 July and 29 August in four phases each extending for a period of five to six days (17-22 July, 30 July-5 August, 12-16 August and 25-28 August). These two locations are defined as TS1 and TS2 respectively in the text. Three hourly measurements of surface marine meteorological parameters viz. pressure, air temperature, sea surface temperature, dew

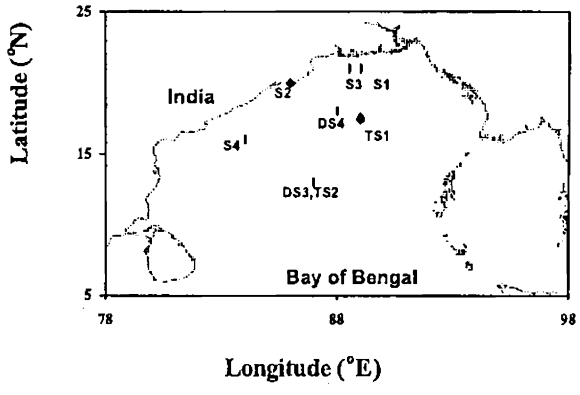

TS1 location of SK
S1 depression on 24 July
S2 low pressure on 1 August
S3 depression on 5 August
S4 low pressure on 24 august

Fig.4.1 Location of time series station and the center of atmospheric systems

point temperature, visually observed cloud, wind speed and wind direction were made (using METKIT) from both locations. In addition, the data sets (air and sea surface

temperature, wind speed and direction) obtained from the nearby moored buoys DS3 (13°N, 87°E) and DS4 (18°N, 88°E) are also utilized.

Prior to the commencement of the BOBMEX programme, an inter-comparison of data collected using various instruments onboard *ORV Sagar Kanya* and *INS Sagardhwani* were carried out (Hareesh Kumar *et al.*, 2001) and found that the observations were in fairly good agreement.

4.3 Results and discussion

The weather summary during the period of study has been described in chapter 3. In general, the monsoon was very active in the head Bay during July and beginning of August. During the active phase (July) only one deep depression was formed in the Bay of Bengal, in the northwest Bay and adjoining west Bengal coast. Mid August (18 onwards) was characterized by weak monsoon condition. Again by the end of August monsoon became active. Hence, the data collected during the BOBMEX program provided typical signatures of the active and weak phases of the summer monsoon.

4.3.1 Surface Meteorology and heat Budget

The surface weather charts of IMD indicated that the observational period was characterized by active and weak monsoon conditions. Moreover, many systems were formed in the Bay of Bengal during this period. To understand the response of the upper layers of northern and central Bay to these systems, the meteorological and oceanographic conditions at these locations (Figs.4.2-4.7) are presented.

4.3.1.1 Northern Bay

Surface marine meteorological observations taken onboard Sagar Kanya (TS1) and moored buoy (DS4) are presented in Figs.4.2 & 4.3. As the time series locations and the buoy location were nearby, only minimum variations are expected in the corresponding observations. Four systems were reported over the Bay between the last week of July and the last week of August. Correspondingly drops in pressure are observed both at TS1 and DS4 (at the northern Bay of Bengal), even though the ship and buoy positions were well away from the center of depression site. Pressure drops are noticed at TS1 (Fig.4.2) during 1 August and then on 5 August corresponding to the systems of 1 August and 5 August. But

these drops are more noticeable at DS4, since it was nearer to the location of systems compared to TS1 (Fig.4.1). Pressure drops continuously, from 23 July (1000 mb) to 26 July (995 mb) corresponding to the deep depression of 24 July (Fig.4.3). It regains its original value after the dissipation of the system on 30 July. Again the pressure drops on 1 (above 1000 mb to 998 mb) and from 4 August (1000-997 mb), in the wake of the formation of a system. A pressure drop noticed from a high of ~1010 mb during 14 August can be due to the development of convective activity associated with the rain event on 14-16 August. Increase in the atmospheric pressure from second week of August (>1005 mb)

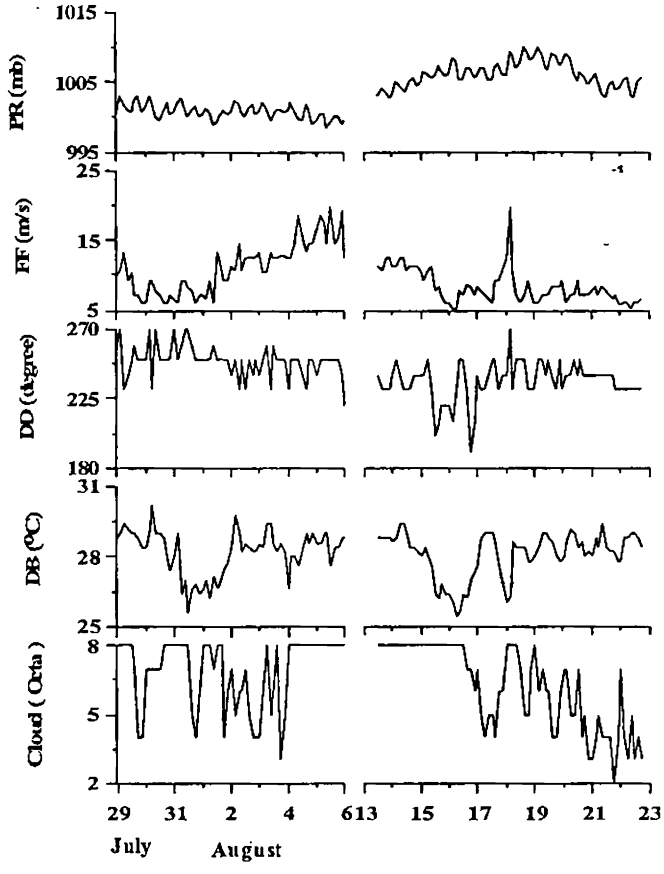

Fig.4.2 Time series of atmospheric pressure (PR), wind speed (WS) and direction (WD), air temperature (DB) and total cloud amount (CL) at TS1

(Fig.4.2 & 4.3) at both the stations TS1 and DS4 are typical during weak monsoon condition and was in agreement with the IMD report. Moreover, oscillations of semi-diurnal periodicity are also embedded on the pressure field. The wind speed increases (> 10 ms^{-1}) during the period of depression (Figs.4.2 &4.3), and restores its pre-depression value (< 7 ms^{-1}) after its passage. Wind speed decreases during the weak phase of the monsoon. Even though, the winds are mostly southwesterly, it is slightly west southwesterly (225-270

degree) during the depression and southwesterly (225 degree) during the weak monsoon period. Nearly overcast condition prevailed over most parts of the study area with fully overcast conditions during the period of systems. The sky became partially cleared off towards the end of the observational period suggesting the weak monsoon situation. SST and air temperature at TS1 also showed fluctuations during the system formation period. Meanwhile rapid fluctuations in air temperature at DS4 are also noticed. One of the notable results is the sharp decline in air temperature over a shorter period (4°C within a day both at TS1 and DS4). During the observation period, two such spells are noticed, one during the last week of July (29.5°C on 30 July to 26°C on 31 July) and the other during mid August (29°C on 14 August to 25.5°C on 16 August). Rainfall measured onboard ORV Sagar Kanya indicated continuous rainfall on 31 July and between 14-16 August, which might have reduced the air temperature. Otherwise it is steady around 28.5°C with oscillation of diurnal periodicity embedded. The drastic reduction in air temperature also coincides with the formation of atmospheric systems over the head Bay.

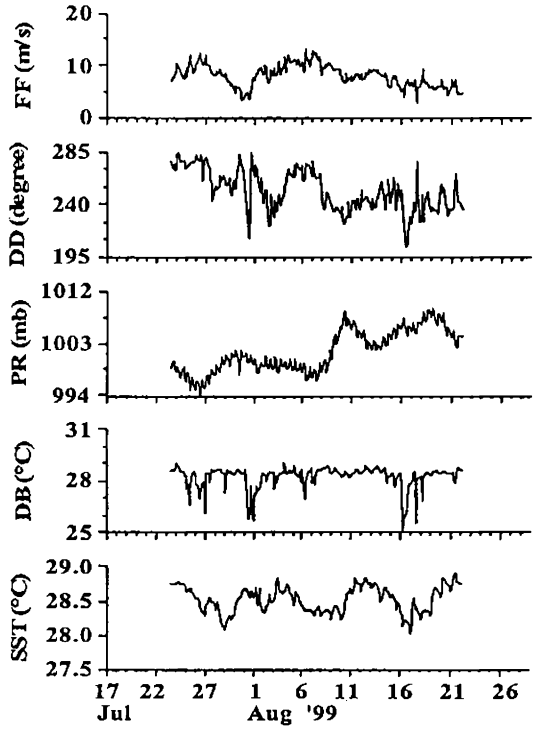

Fig.4.3 Time series of wind speed, direction, surface pressure, air temperature and sea surface temperature at the buoy station (DS4)

Heat exchange across the air-sea interface is estimated to assess the relative importance of local meteorological forcing in producing the observed variability in the

surface layers. As the direct measurement of various component of the heat budget terms are not available it was estimated using empirical relationship following Pickard and Emery (1982). The heat budget equation of the air-sea interface can be written as

$$Q = Q_I - Q_B - Q_E - Q_S$$

Here, Q is the net heat flux (positive when gained by sea), Q_I is the incoming short wave radiation, Q_B is effective back radiation, Q_E is latent heat flux and Q_S is sensible heat flux.

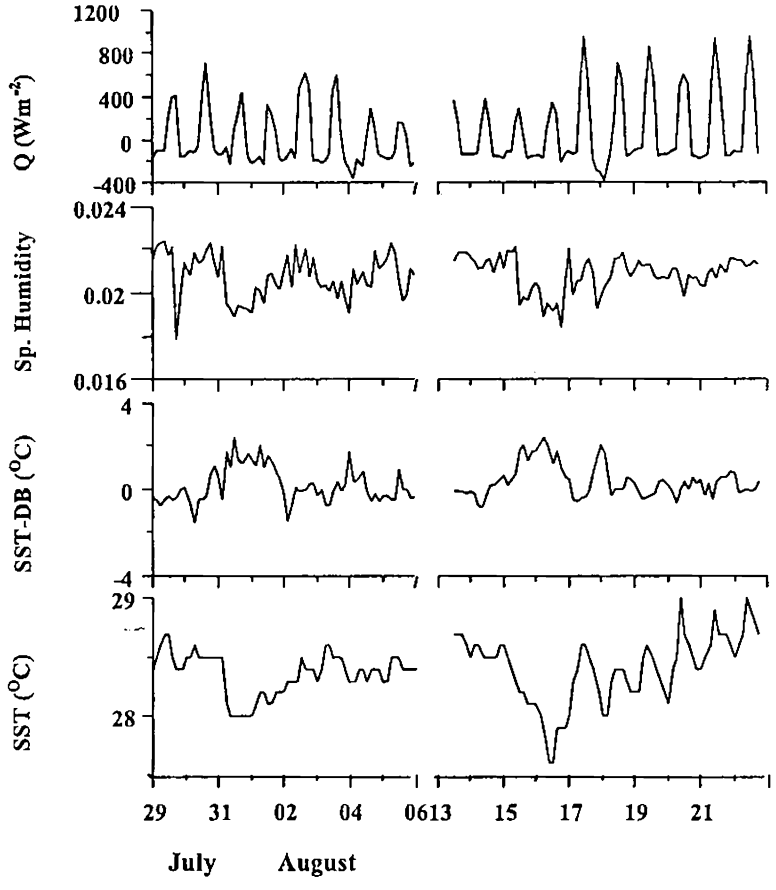

Fig.4.4 Time series of net heat flux (Q), specific humidity, sea minus air temperature (SST-DB) and sea surface temperature (SST) at the TS1

$$Q_I=(1-\alpha)\ S\ (1-0.62C+0.0019\theta_N)$$

Where S is the solar constant, C is the fractional cloud cover, α is the albedo and θ_N is the noon solar elevation in degrees.

$$Q_B =\varepsilon\sigma Ts^4\ (0.39-0.05e^{1/2})\ (1-kC^2) + 4\varepsilon\sigma\ Ts^3\ (Ts-Ta)$$ (Josey et al., 1999)

Where ε is the emittance of sea surface (.98), σ is the Stefan Boltzmann constant (5.67×10^{-8} W m^{-2} K^{-4}), Ts and Ta are the temperature of air and sea, e is the water vapour pressure, k is the cloud cover coefficient.

$$Q_S = \rho C_s C_P (Ts-Ta)U,$$

$$Q_E = \rho C_e L(q_s-q_a)U$$

Where C_P is the specific heat of water, L is the latent heat of vaporization, C_s and C_e are the empirical exchange co-efficients, U is the wind speed , q_s and q_a are the specific humidity of sea surface temperature and air temperature

In general, Q (Fig.4.4) is positive (more than 400 Wm^{-2}) during daytime and negative (-200 Wm^{-2}) during night indicating heat gain and heat loss respectively. Moreover, marked heat loss (reduction in heat gain) is noticed during the active phase (1 August, 5 August) of the monsoon coinciding with the system formation. The net heat gain is considerably less during 13-17 August, mainly due to the reduction in incoming radiation under cloudy skies (Fig.4.2). The variation in net heat flux is clearly reflected in the variation of SST (Fig.4.4) and also on air temperature (Fig.4.2). Net heat flux increases during the second phase of the observation period coinciding with weak monsoon condition and clear skies. The sea minus air temperature (SST-DB) is an indicative of static stability of the overlying atmosphere (Fig.4.4). When SST is higher than air temperature, there is a net exchange of heat from the sea surface to the overlying atmosphere and the reverse phenomena occurs when air temperature is greater than the sea surface. SST-DB (Fig.4.4) is greater than 2°C between 31 July and 1 August and more than 1°C on 4 August associated with system activity. Again during the period of rain event during 14-16 August, SST-DB drops by more than 2°C. These values return to equilibrium after the dissipation of the system. In general, the specific humidity is above 0.02 (or 20 g/kg) throughout the observation period, except during the period of system activity. Prior to the formation of a system, the specific humidity is ~ 0.022, and it dropped below 0.019 during the system formation on 1 August and 4 August. Again, specific humidity increases to more than 0.022 on 13 August, prior to the rain event and drops to less than 0.019 during the rain event of

16 August. Thus the specific humidity drop of 0.019 can be taken as one of the factors for the occurrence of any system in the Bay of Bengal.

4.3.1.2 Central Bay

The meteorological conditions are slightly different in the central Bay. The influence of the depressions formed in the northern Bay of Bengal is not reflected in the central regions (Fig.4.5 & 4.6). However, both active and weak phases of summer monsoon are experienced here with a reduced magnitude compared to northern Bay. In general, the observational period (17 July-28 Aug 1999) is mostly characterized by overcast sky conditions with the domination of stratocumulus clouds. The medium douds were mostly altocumulus and altostratus. Observations at TS2 station (Fig.4.5) are discontinuous whereas continuous observations are available at DS3 station (Fig.4.6). Atmospheric pressure decreases from a high of 1008 mb during the initial phase of the observation period to 1003 mb on 25 July (Fig.4.6). A slight increase after that is again followed by a dip on 30 July, all this accounted to the active spell of the monsoon. This is followed by an increase and a maximum of 1010 mb is observed with the weak phase of the monsoon (after 16 August). A pressure fall again figured on 21 August and a system was generated over the central Bay following this on 24 August. The prevailing winds are southwesterly during the observation period. Strong winds (>10 ms^{-1}) are observed during active phase (Fig.4.5 & 4.6). During the weak monsoon condition (mid August) winds became weak (<7 ms^{-1}) but maintaining the same southwesterly direction. Since most of the depressions are formed in and around the head Bay, winds in the central Bay is not as strong as noticed in the northern Bay. The SST is above 28.4°C throughout the period. A decrease in SST observed during the third phase of the cruise (12-16 August, in Fig.4.7) and first two weeks of August (in Fig.4.6) coincides with the system activity /rainfall event. An increase in SST to 29°C (Fig.4.6) coincides with the weak phase of the monsoon. Air temperature shows sharp fall during the initial phase as well as towards the end of the observation period. One of the striking results is that, the mixed layer, defined as the depth at which a drop of 0.2°C occur from SST, continues to deepen (Fig.4.9) during the period of decreasing winds (12 July-16 August, Fig.4.5). Moreover, towards end of the observation period, i.e. 25-28 August, the surface temperature increases (Fig.4.7) and the mixed layer shoals (Fig.4.9) even when the

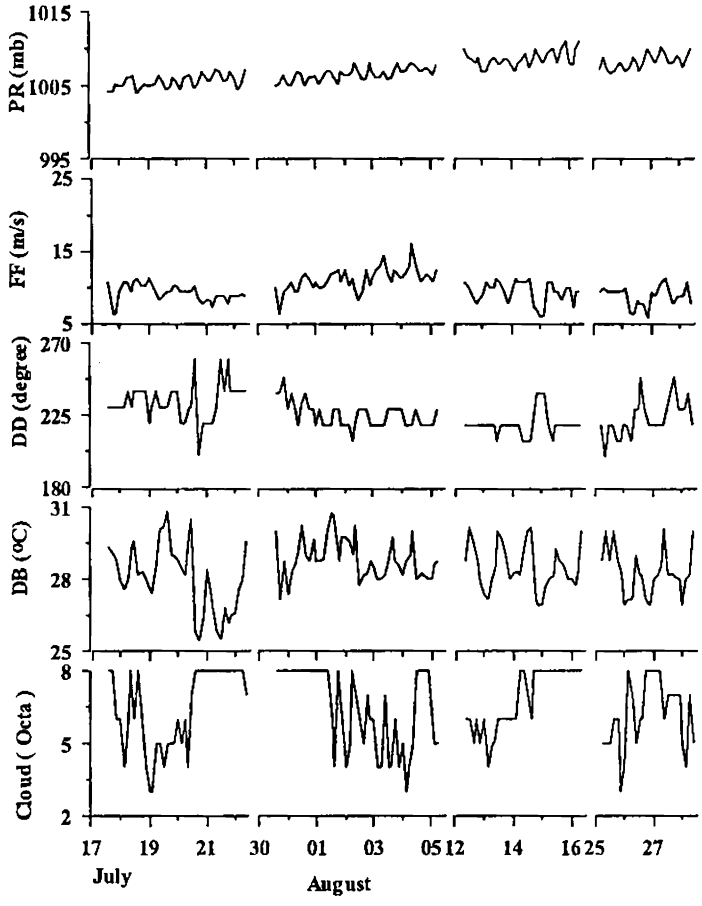

Fig.4.5 Time series of atmospheric pressure (PR), wind speed (WS) and direction (WD), air temperature (DB) and total cloud amount (CL) at TS2

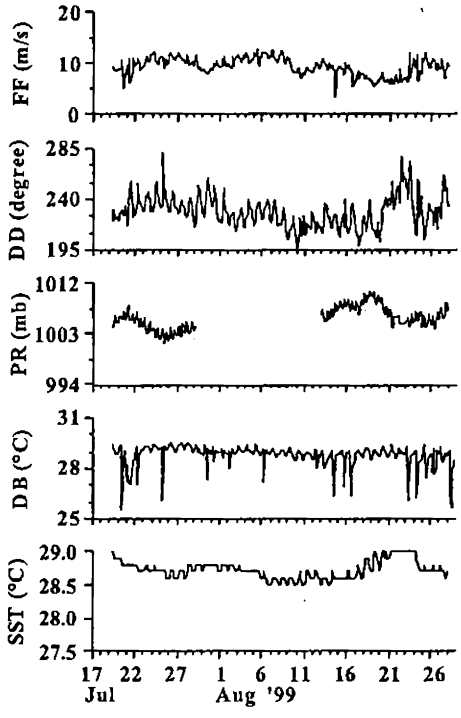

Fig.4.6 Time series of wind speed, direction, surface pressure, air temperature and sea surface temperature at the buoy station (DS3)

winds are increasing (Fig.4.5). This suggests that in the central Bay of Bengal, in addition to atmospheric forcing, remote forcing also plays a major role in the mixed layer variability.

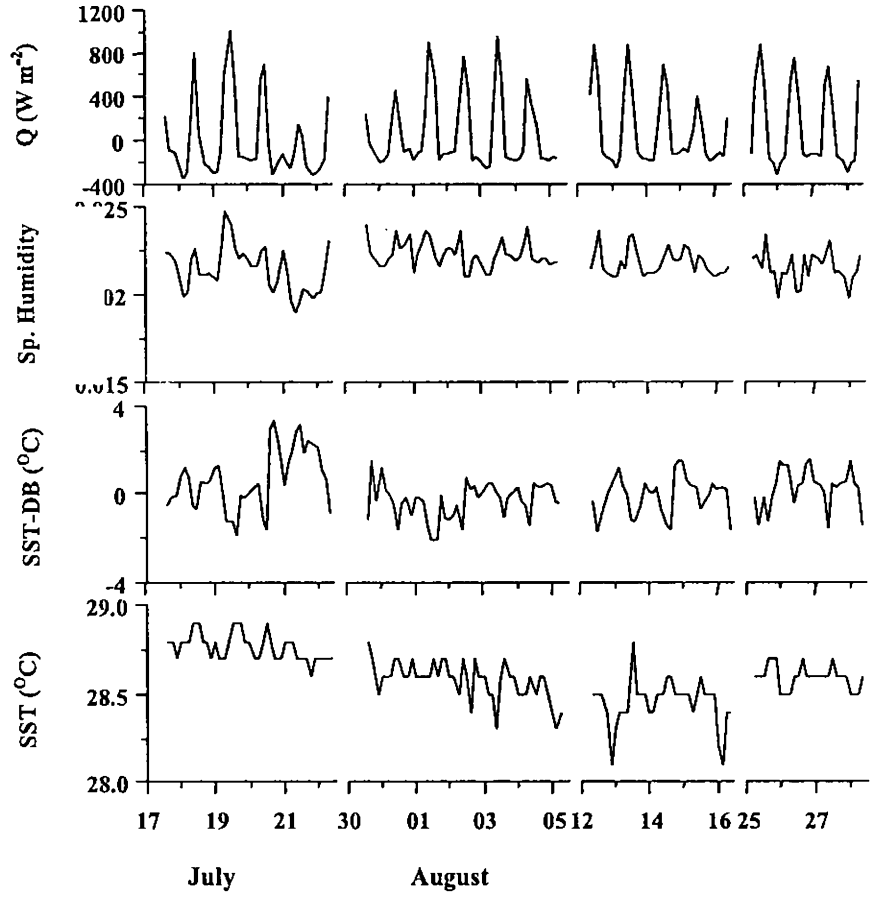

Fig.4.7 Time series of net heat flux (Q), specific humidity, sea minus air temperature (SST-DB) and sea surface temperature (SST) at TS2

Intense air-sea exchange in the near surface boundary layer is quite evident from the repeated cycles of net heat flux (Fig.4.7). In general, the heat accumulated during daytime is lost during night. Variation in net heat flux (Q) is found related to wind speed, cloud cover and air-sea temperature difference. The net heat flux is found higher over the central Bay (~ 400 Wm^{-2} throughout the period during day time) compared to northern Bay. Fluctuations in positive and negative values of SST-DB are noticed (Fig.4.7) indicating rapid changeover from unstable to stable conditions. The lower atmospheric boundary layer, with unstable conditions is observed during daytime, as indicated by positive sea-air temperature difference. On the other hand, stable boundary layer is observed during night time. Stable conditions prevailed during most of the time except during 21-22 July, when there was strong rainfall event at this station. Specific humidity is generally higher over central BOB

(>0.02) almost throughout the observation period. Here also a drop below 0.02 in specific humidity is coinciding with the unstable condition as indicated by high SST-DB (>2°C) around 21 July.

4.3.2 Response of ocean and overlying atmosphere to the atmospheric disturbances

Several factors contributed to the formation of systems and it is understood that one such factor is SST. Active monsoon conditions prevailed during July over the northern Bay of Bengal. A low pressure generated over northern Bay of Bengal (Fig.4.1) on 25 July intensified into a deep depression on 27 July. One of the key parameter to understand the genesis of atmospheric disturbance is the sea surface temperature. The temperature of 28.7°C observed prior to the formation of a system i.e. on 24 July (at DS4) drops to 28.1°C on 29 July and increases after the dissipation of the system on 30 (Fig.4.3). Again the temperature increases in association with the formation of the well marked low pressure on 1 August. The temperature again rises above 28.7°C on 4 August, prior to the formation of another low pressure over the Bay of Bengal. This intensified into a depression over land on 9 August and then the temperature decreases. From the above analysis, it can be inferred that whenever the SST crosses 28.7°C, a system has formed in the Bay. The temperature regains its normal value after the passage of the system. It is interesting to notice that before the major rain event of 16 August also, the temperature is found well above 28.7°C. Thus 28.7°C can be considered as the critical limit for the formation of a pressure disturbance or convective system (rain event). Another noticeable observation is the lag between pressure minima and SST minima (Fig.4.3). Corresponding to a pressure drop (995mb) noticed on 26 July, the SST dropped to minimum of 28.1°C on 29 July. Similarly corresponding to pressure drop during 1 August, 6 August and 14 August, temperature minima occur only on 2 August, 8 August and 17 August (Fig.4.3) respectively. This suggests that there is a lag of 2-3 days between the pressure minimum and SST minimum.

4.3.3 Role of one-dimensional processes on the upper ocean variability

In this chapter, the one-dimensional numerical model of Miller (1976), the modified version of Kraus and Turner (1967) and Denman (1973) is utilized to study the role of one-dimensional processes on the mixed layer characteristics at TS1 and TS2.

4.3.3.1 Integral equations of the mixed layer

To obtain explicit expressions for the characteristics of the mixed layer, the equations for the conservation of thermal energy, salinity and mechanical energy have to be integrated over the mixed layer depth. The simplified one-dimensional equations (Miller, 1976) used in the mixed layer simulations are

$$\frac{dh}{dt} = \frac{2[G - D + \gamma^{-1} Q_i (1 - e^{-\gamma h})] - h[Q_b + Q_e + Q_h + Q_i (1 + e^{-\gamma h}) + \frac{\lambda}{\alpha} S(P - E)]}{h[T - T_h + \frac{\lambda}{\alpha}(S - S_h)]} \tag{1}$$

$$\frac{dT}{dt} = \frac{1}{h}\left[-\frac{dh}{dt}(T - T_h) + Q_b + Q_e + Q_h + Q_i (1 - e^{-\gamma h}) \right] \tag{2}$$

$$\frac{dS}{dt} = \frac{1}{h}\left[-\frac{dh}{dt}(S - S_h) + S(P - E) \right] \tag{3}$$

$$\frac{dT_{-h}}{dt} = \gamma Q_i e^{-\gamma h} - \frac{dh}{dt}\left(\frac{\partial T}{\partial z} \right)_{-h} \tag{4}$$

$$\frac{dS_{-h}}{dt} = -\frac{dh}{dt}\left(\frac{\partial S}{\partial z} \right)_{-h} \tag{5}$$

Here, dh/dt is the rate of mixed layer deepening; G-D, fraction of the turbulent energy derived from wind ($-m\tau U/\alpha\rho g$); m, fraction of energy transferred from wind; τ, wind stress; g, acceleration due to gravity; ρ, mean density of mixed layer; γ, extinction coefficient; Q_I, solar radiation incident on the sea surface; h, depth of mixed layer; Q_B, effective back radiation; Q_E, latent heat flux; Q_S, sensible heat flux; α, coefficient of thermal expansion; β, coefficient of saline contraction; P, precipitation and E, evaporation.

For the wind dominated regime ($dh/dt > 0$), the cold water from below the mixed layer is entrained into the mixed layer as a result of work done by the turbulent eddies against the buoyancy forces. Then the layer deepens and its temperature decreases. In such

cases, the equations 1 -5 were solved using the Runge-kutta numerical integration scheme with a time step of 5 minutes.

For the heat-dominated regime (dh/dt < 0), entrainment mixing at the base of the mixed layer does not appear in the equations. Hence, all the available turbulent kinetic energy is used in mixing the lighter water near the surface uniformly and leaves the mixed layer unchanged or a shallow layer will develop under light winds. In such cases, terms involving the below layer density gradient loses its significance and 'h' is determined using Newton Raphson iterative technique.

$$h = \frac{2[G - D + Q_i \gamma^{-1} e^{-\gamma h})}{(Q_b + Q_e + Q_h + Q_i(1 + e^{-\gamma h})}$$

$$\Delta T_S = \frac{\Delta t}{h}\left[Q_b + Q_e + Q_h + Q_i(1 - e^{-\gamma h})\right]$$

The two unknowns or uncertain parameters used in this model are the fraction of wind mixing energy (m), which is used to increase the potential energy of the upper layer and the extinction coefficient for solar radiation (γ) in the ocean.

The momentum imparted by the wind into the ocean is used to generate surface waves. A part of this wave energy is utilized to increase the turbulence through wave breaking which in turn increases the potential energy of the system. Turner (1969) suggested that only a fraction of the energy transferred from wind is used to increase the potential energy. In the absence of any information about the time variation of 'm', the model calculations are made on the assumption that the rate of increase of potential energy due to mechanical mixing is constant. The laboratory experiments of Kato and Phillips (1969) suggested a value of 0.0015 for 'm' while Denman (1973) used m = 0.0012 on an idealized case of wind mixing and diurnal heating which are much lower than the values of 0.01 obtained by Turner (1969). In the present numerical simulation m = 0.0012 was found to give best results.

Solar radiation reaching the ocean surface consists mainly of visible and infrared part of the spectrum. However, the radiation mainly in the wavelength range of 0.3 to 1 mm

penetrates to deeper levels. So, an average extinction coefficient g is defined for these wave lengths, such that the solar radiation available at a depth z = -h is

$$I(z)=Q_i\, e^{-\gamma h}$$

Usually in the open ocean γ varies between 0.001 cm^{-1} and 0.003 cm^{-1} (Jerlov, 1968). As the direct measurement of γ is not available, it computed from this Secchi disc values (D) using the relationship $\gamma = 1.7/D$. In the present numerical simulation, the values of γ obtained from the above relation for the appropriate locations are used. (0.0005/cm).

The extinction coefficient used to run the model and the Root Mean Square error (R.M.S. error) for MLT and MLD are presented in Table 4.1.

Time series of the observed and simulated MLT and MLD at TS1 and TS2 are presented in Figs.4.8 & 4.9 respectively. At TS1, the observed temperature vary from 28° to 28.5°C in the first phase (29 July–6 August) and 27.5° to 29°C during the second phase (13-22 August), with large diurnal amplitude during the second phase (~0.5°C). This is due to the occurrence of active and weak monsoon conditions in the second phase compared to only active condition in the first phase. At TS2 the MLT continuously decreases upto 5 August and increases thereafter. Hareesh Kumar *et al.* (2001) attributed this to the presence of wave with intra-seasonal periodicity. In both the phases, the simulated temperature values are in general higher than the observations (> 28.5°C). Moreover, the simulated diurnal amplitude in temperature is much less than the observed amplitudes. Sanilkumar *et al.* (1991) and Hareesh Kumar (1994) also noticed the same and attributed to the irregular parameterization of the penetration of solar radiation. Large disparities are noticed between the observed MLD and simulated values. During the first phase of the observation period (29 July-6August) at TS1, the observed MLD is ~ 35 m, while it varies from 10 m to 50 m in the second phase (13-22 August). In both the phases the agreement between the observation and simulation are very poor, as indicated by the large RMS error (7.7 and 12.8 in Table 1).

In the central Bay also large disagreement is noticed between the observed and simulated mixed layer characteristics (Fig.4.9). At TS2, the observed MLT is higher than 28.7°C during the first phase of the cruise (17-22 July), around 28.5°C during the second

phase (30 July-5 August), decreases less than 28.5°C during the third phase (12-16 August) and increases slightly above 28.5°C during the fourth phase (25-28 August) of the cruise. It is to be noted that the MLD is quite shallow at TS1 (< 40 m) compared to TS2 (> 50 m), inspite of the formation of many systems near to TS1. Probably this may be due to the fact that the surface waters of TS1 are highly stratified due to marine fresh water influx and thereby limiting the deepening of mixed layer. At

Table 4.1 Tuning coefficients used in the model and rms error

	MLT (°C) TS2	MLD (m) TS2	MLT (°C) TS1	MLD (m) TS1
Phase I	0.17	16.2	0.25	7.7 (23.5)
Phase II	0.30	6.0	0.47	12.8 (22.3)
Phase III	0.20	22.2		
Phase IV	0.13	21.8		

(Values for MLD in bracket is based on density criteria)

TS2, MLD varies from less than 50 m (12 August) to more than 75 m (16 August). On closer examination, it can be seen that the deepening of MLD are associated with weak winds (Fig.4.5) and shallow MLD with strong winds (Fig.4.6). This suggests the influence of a propagating wave with a periodicity of nearly 30 day periodicity as suggested by Hareesh Kumar *et al.* (2001). Here also the simulated MLT is in general higher than the observations. In the case of MLD also, the simulated amplitudes are less than the observed one. The good agreement noticed in the MLD simulation during 30 July to 5 August can be a mere coincidence. The observed MLD and MLT suggested the presence of long-period waves in this region. Recently Sanilkumar *et al.* (1997) suggested the presence of eddy features in this region during the summer monsoon season. The presence of long period waves, discussed in the next section and internal waves further complicated the dynamics of this region. As the model utilized here is one-dimensional where the influence of these wave effects are not included, a better simulation could not be expected.

The simulation of the mixed layer characteristics using the Kraus-Turner-Denman-Miller model revealed very weak coincidence between the observed and simulated values. This suggests that one-dimensional forcing could not explain the observed variability both at the head and central Bay of Bengal during the monsoon season of 1999.

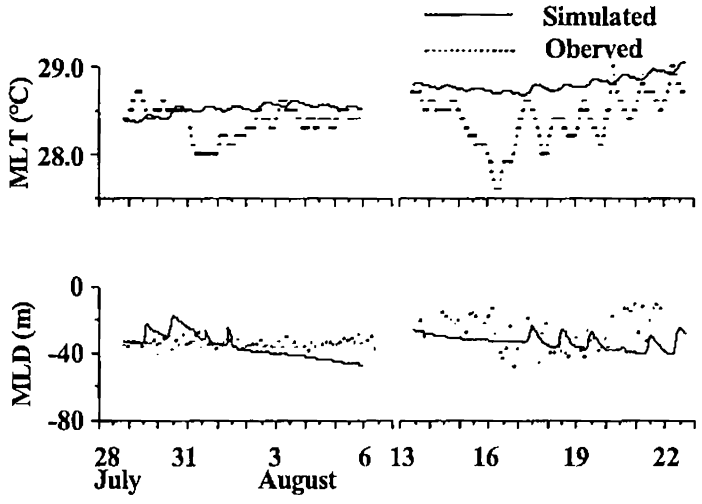

Fig.4.8 Time series of observed and simulated mixed layer characteristics at TS1

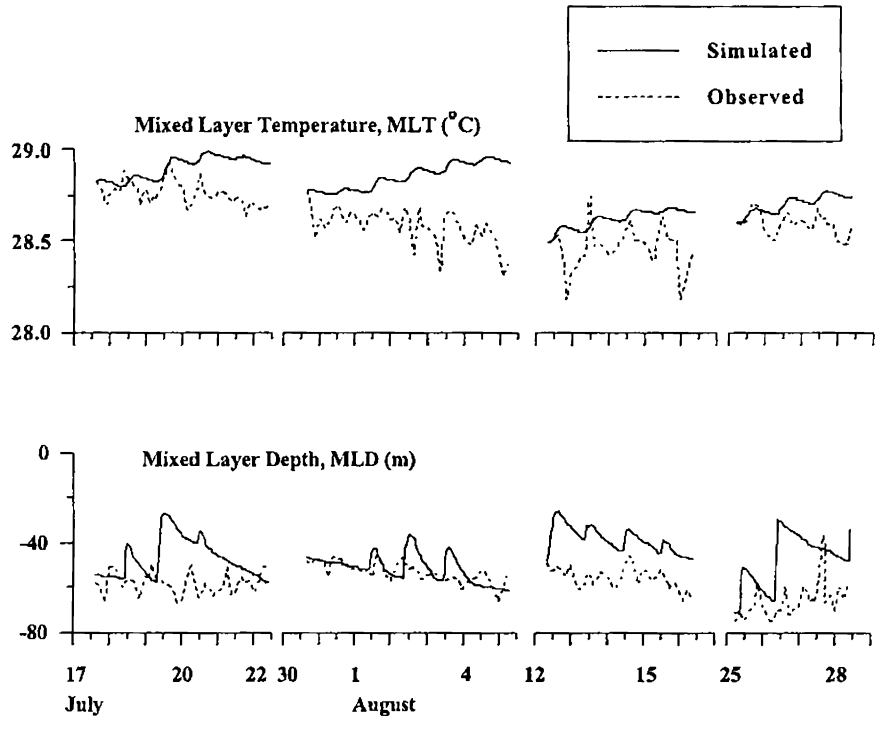

Fig.4.9 Observed and simulated mixed layer characteristics at TS2

Chapter 5

Inter-annual variability in the surface wind and wind stress curl

5.1. Introduction

North Indian Ocean is well known for the spectacular reversal of seasonally varying monsoon winds. During winter monsoon, i.e. from November onwards the winds blow away from the continent (northeasterlies) and during summer monsoon, the winds blow from the ocean towards the land (southwesterlies). South of 10°S the southeast trade winds persist throughout the year (Rao, 1976). They attain their seasonal maximum and most northward extent during the summer monsoon period. During the transition period between the monsoons i.e. during March/April and October, winds become westerlies in the equatorial Indian Ocean region. The zonal wind stress in the equatorial region is westerlies from March to October and largest during spring and fall that drive the equatorial spring and fall jets in the Indian Ocean (Wyrtki, 1973). The atlas by Hastenrath and Lamb (1979) gave a complete description of the atmospheric fields over this region.

The curl field also changes in response to wind stress reversal. During the summer monsoon, anti-cyclonic curl resides over most of the Arabian Sea and equatorial Indian Ocean north of 15°S. A sharp curl gradient was noticed in the southwesterlies of the Findlater Jet over the Arabian Sea (Findlater, 1971). Its maximum is over the central Arabian Sea. This reverses to become cyclonic during winter monsoon, whereas over the western Bay of Bengal, the curl is cyclonic in summer and anti-cyclonic in winter.

The climatological wind stress and curl of the wind stress (Hellerman and Rosenstein, 1983) showed maximum amplitude off the coast of Somalia. However, the curl changes its sign between the northeast and southwest monsoons. The region of negative wind stress curl extended over most of the Arabian Sea during the southwest monsoon. During the northeast monsoon, the surface flow exhibits two distinct jets, one in the Arabian Sea and the other in the Bay of Bengal. Even though the strongest winds are noticed over the western Arabian Sea, the region of maximum negative curl was reported over the southeastern Arabian Sea (Schott and McCreary, 2001).

Though a lot of studies have been carried out on the surface wind field and wind stress curl, their inter-annual variability particularly over the Indian region, have

not been studied much. In this chapter, the main emphasis is given on the inter-annual variability in the surface wind field and wind stress curl. Moreover, it has been reported that 1994 and 1997 are the years in which unusual climatic events, i.e. the Indian Ocean Dipole events (Saji *et al.*, 1999) took place in the Indian Ocean. The variability in the surface wind field and wind stress curl associated with these events is also discussed here.

5.2.Data and Methodology

The study region extends from 25°S-25°N and 40°-120°E over the Indian Ocean. The monthly averaged wind at 10m levels is obtained from NCEP/NCAR Reanalysis corresponding to the period 1993-1997. The wind stress curl is also computed from the wind field as follows.

Wind stress is computed as

$$\tau_x = \rho\, Cd\, U \times U_x \text{ and}$$

$$\tau_y = \rho\, Cd\, U \times U_y$$

where $U=\sqrt{(U_x^2+U_y^2)}$

where $Cd = 0.0013$ and $\rho = 1.2\ kgm^{-3}$

wind stress curl $\simeq d\tau_y/dx - d\tau_x/dy$

Curl values (Nm^{-3}) are either positive/cyclonic and negative/anti-cyclonic

5.3. Results and Discussion

5.3.1 Surface wind

Winds over the Indian Ocean reverse semi-annually associated with the monsoons. In this section, the surface winds (monthly averaged) over the Indian Ocean and their inter-annual variability are discussed during the period from 1993 to 1997 (Figs.5.1-5.5). During winter monsoon, (November to March) the winds are northeasterlies over the north Indian Ocean with maximum (>6-8 ms^{-1}) over the western Arabian Sea in January. The southwesterly winds are noticed from June to September over the North Indian Ocean with maximum magnitude (>10-12 ms^{-1}) over the western Arabian Sea and off the Somali coast during July. During the transition period between the monsoons i.e. March/April and October, winds are noticed to be

weak over the Arabian Sea and Bay of Bengal. In the equatorial region, wind direction changes from northeasterlies to westerlies (~2 ms^{-1}) during March/April and from southwesterlies to westerlies (~2-4 ms^{-1}) during October. While over the south Indian Ocean (SIO) southeasterly winds (or the southeast trades) prevail the whole year. During the winter monsoon (northern hemisphere) they are southerly (6-8 ms^{-1}) near the eastern Indian Ocean and turn to easterlies (~2-4 ms^{-1}) at about 60°E and converge with the northeast monsoon winds crossing the equator near Madagascar. During April, the southeasterlies from the south Indian Ocean and northeasterlies from the north Indian Ocean converge near the equatorial region west of 50°E. The southeasterlies strengthen from April onwards and cross the equator during May to form the continuous summer monsoon current from June to September. Thus the southeast trade winds shift northwards and southwards with the season and have their maximum magnitude (> 8 ms^{-1}) during summer monsoon season. The figures (Figs.5.1-5.5), in general show the seasonal variability and inter-annual variability in the surface wind speed and direction for all the years.

It appears that during the years 1993, 1995 and 1996 (Figs.5.1, 5.3 & 5.4), wind pattern are similar while 1994 and 1997 are typical (Figs.5.2 & 5.5) and different from these years. The maximum magnitude of the northeasterlies and southeasterlies are observed over the Arabian Sea and their variability maximum is noticed over the Bay of Bengal. Over the equatorial region, during the transition period between the monsoons, the wind pattern shows large inter-annual variability.

The northeasterlies are observed to be relatively strong (6 ms^{-1}), extending over a wide area over the Bay of Bengal during January 1993, 1995 and 1996 (Figs.5.1, 5.3 & 5.4) compared to 1994 and 1997 (Figs.5.2 & 5.5). During 1993, it extends from 2°-15°N and 82°-95°E with a core magnitude of 8 ms^{-1}. Similarly, during 1995 and 1996, the northeasterly winds (6ms^{-1}) extend from about 2°-18°N and 82°-95°E and 3°-16°N and 82°-92°E respectively. During 1994 and 1997, magnitude of the northeasterlies are weak (4 ms^{-1}) over the Bay of Bengal region. The southwesterlies over the Bay of Bengal, shows strong monsoon winds during July 1994 and 1997 and comparatively weaker winds during 1993, 1995 and 1996. During 1994 and 1997, the magnitude of the southwesterlies exceeds 8 ms^{-1} over the Bay of Bengal region between 5°-20°N. On the other hand, during 1993, the values are below 6 ms^{-1} but with a core speed of 8 ms^{-1} occur over northern Bay (around 15°N) and south of Sri

Lanka (around 5°N). During 1995, the core magnitude of 8 ms^{-1} is noticed over a small area in the northern Bay and south of Sri Lanka during July as observed from Fig.5.3 and even less during 1996, over south of Sri Lanka (around 5°N) only. During the transition period of October 1993, 1995 and 1996, strong southwesterlies (>2-4 ms^{-1}) are found over the southern and central Bay of Bengal compared to 1994 and 1997 (<2 ms^{-1}).

It is also interesting to note that the northeasterlies are slightly weak at the core during January 1994 (8 ms^{-1} over a small area) and 1997 (6 ms^{-1}) over the western Arabian Sea compared to other years. In all other years, the northeasterlies of 8 ms^{-1} at core extends over the western Arabian Sea northwards up to ~15°N.

Over the equatorial region the winds show semi-annual periodicity with westerlies occurring twice in a year during the transition period between monsoons. Over the western Indian Ocean during the winter monsoon period, the northeasterlies crosses the equator towards south to meet with the southeast trades over the southern Indian Ocean. They converge near the equator during April. During the transition period of March/April, a part of the northeasterlies turn first to northwesterlies and subsequently to westerlies, first noticed south of the equator and extending northwards. From May onwards, the southeast trade winds starts crossing the equator to form the southwest monsoon current. Again, during the transition period of October, the southwesterlies changes to westerlies over the equatorial region. The magnitude and direction of these westerlies over the equatorial region shows large inter-annual variability, with similar pattern observed during 1993, 1995 and 1996 (Figs.5.1, 5.3 &5.4) and different during 1994 and 1997 (Figs.5.2 &5.5).

During January 1993 (Fig.5.1), winds are observed to be very weak (< 2 ms^{-1}) south of equator up to 10°S (up to 15°S over the western Indian Ocean) and between 45°-85°E. By March, the northeasterlies changes to northwesterlies (> 2 ms^{-1}) near 57°E and to westerlies (> 2 ms^{-1}) east of 70°E and south of the equator to 10°S. The westerlies (> 2 ms^{-1}) strengthens during April between 5°N and 5°S over the central Indian Ocean. West of 70°E, winds are noticed to be weak (< 2 ms^{-1}) in the equatorial region and to ~10°S. The southeasterlies from the south Indian Ocean and northeasterlies from the north Indian Ocean converges near the equatorial region west of 50°E in April. By October, when the southwesterlies weakens over the Indian

Ocean, westerly winds (>4 ms^{-1}) are noticed over the central Indian Ocean between equator and 8°N. From November onwards northeasterlies appears over the Arabian Sea and Bay of Bengal, while in the equatorial region between 5°N to 5°S and 55° to 95°E westerly winds are noticed. The northeasterlies and southeasterlies from both hemispheres converge in the equatorial region west of 50°E in November. Equatorial westerly wind zone shifts southwards by December.

During 1995 (Fig.5.3), the magnitude and extent of northeasterlies over the western Indian Ocean (south of the equator) are more (> 2 ms^{-1}) during January compared to 1993 (Fig.5.1). The northeasterlies changes to northwesterlies and is strong (> 4 ms^{-1}) between 0°-12°S and west of 70°E. By March, the northeasterlies over the Arabian Sea weakens similar to that in 1993 and westerlies (> 2 ms^{-1}) are observed between 70°-100°E and 0°-5°S. The westerlies shift northward by April to extend east of 65°E over the equator, while between 55° and 65°E over the equatorial region, northwesterlies are also noticed. In April, the magnitude of the northeasterlies (2-4 ms^{-1}) over the Arabian Sea is found to be greater than other years. Westerlies are noticed between 0°-10°N and 60°-90°E (> 2-4 ms^{-1}), during October. They shift southwards by November and extend up to 100°E and weakens afterwards. In 1996, westerly winds (< 2 ms^{-1}) are noticed south of the equator during March but with northwesterlies (> 2 ms^{-1}) in the central equatorial region. In April, the northwesterlies and westerlies are stronger (2-4 ms^{-1}) than in all other years between 55° and 100°E in the equatorial region. But the northeasterlies are observed to be comparatively weaker over the western Arabian Sea in April. By October, again westerlies are also noticed to be stronger (4-6 ms^{-1}) between 0°-10°N and 60°-100°E, which weakens and shifts southwards by November/December.

The wind pattern during 1994 and 1997 (Figs.5.2 & 5.5), show slight differences from other years, more noticeable during the transition period between the monsoons. During March 1994, the northwesterlies over the western Indian Ocean and westerlies (< 2 ms^{-1}) over the central Indian Ocean appears weak. In April, the winds (< 2 ms^{-1}) are weak over the western equatorial Indian Ocean (between 50° and 70°E) and slight southwesterly winds are also noticed, in the usually westerly wind regime (between 70° and 100°E). Another noticeable observation is the southeasterlies (> 2-4 ms^{-1}) blowing alongshore of Sumatra from June to October, where otherwise winds are weak (<2 ms^{-1}). Similarly, westerly winds (<2 ms^{-1}) are noticed to be weak

in the equatorial region during October also. Moreover, during this period also southeast trade winds from the southern Indian Ocean extends north of equator over the eastern Indian Ocean and west of Sumatra, where otherwise weak winds are noticed. These conditions are even more pronounced during 1997. In March, winds are easterlies over the Indian Ocean west of 80°E. Westerlies (2 ms^{-1}) are noticed during April between 70° and 90°E only and is very weak (< 2 ms^{-1}) west of 70°E. A southward flow is also observed over the western equatorial Indian Ocean. During October 1997, easterlies are also observed in the equatorial region. The winds over the eastern Indian Ocean and west of Sumatra are similar to 1994, with the southeasterlies from the south Indian Ocean extending north of the equator also from May/June to December, which is not observed in other years.

Over the South Indian Ocean, the southeast trades exist throughout the year extending northward during the northern summer and southward during northern winter. These winds are also noticed to have inter-annual variability in their magnitude and direction. During 1993, the trades are noticed south of 10°S (Fig.5.1) with a magnitude of 6 ms^{-1} (8 ms^{-1} to the core) in January over the eastern Indian Ocean and decreasing to 2-4 ms^{-1} over the western Indian Ocean. During this period, the northeasterlies from the north Indian Ocean and southeast trades converges over the Madagascar Island. Magnitude of the southeasterlies is noticed to decrease (4 ms^{-1}) during February over the eastern Indian Ocean and increases again by March. The southeast trades (6 ms^{-1}) over the western Indian Ocean extends towards the equatorial region in April. The cross equatorial flow increases from May (6-8 ms^{-1}) onwards, with maximum magnitude (8-10 ms^{-1}) over the western Indian Ocean during July. By August eastern region also attains a maximum of 8 ms^{-1}. By October, these winds weakens and shifts southward.

The magnitude of the southeast trades is comparatively higher (>8 ms^{-1}) in February 1994 over the eastern Indian Ocean upto 80°E (Fig.5.2). This decreases in March (6 ms^{-1}) near the eastern Indian Ocean. The magnitude of the southeast trades over the western Indian Ocean is found to be small during April (4 ms^{-1}) and May (6 ms^{-1}) compared to 1993. Cross equatorial flow increases from May (6 ms^{-1}) onwards. The trade winds weaken (6 ms^{-1}) from September onwards. Another noticeable difference observed here is the southeasterlies (> 4-6 ms^{-1}) from the south eastern

Indian Ocean extending northwards across the equator over the Sumatra region from July onwards and are remains there till October/November.

During 1995 (Fig.5.3), magnitude of southeast trade winds (6 ms^{-1}) are comparatively smaller in January and extends from 110°E westwards upto 90°E in the south Indian Ocean. This extends to 60°E by February. Again, during April and May, the magnitude becomes less (4-6 ms^{-1}) over the south Indian Ocean and in June extends (6 ms^{-1}) only upto 70°E. The magnitude increases (8 ms^{-1}) during the monsoon months of July and August.

During 1996 January (Fig.5.4), the wind speed of 6-8 ms^{-1} is noticed over the eastern Indian Ocean. By February, this speed decreases over the eastern Indian Ocean and increases over the western part. The trade winds extend more northwards by March with a core of 8 ms^{-1} over the eastern Indian Ocean. During June and July the core maximum (8 ms^{-1}) shifts westwards (west of 90°E). Magnitude of the southeast trades weakens in September. By October again an increase in the magnitude (>8 ms^{-1}) of the trades are noticed west of 100°E.

During January and February 1997, the magnitude of southeast trades is found higher (>8 ms^{-1}) south of 17°S. In March the trades (>4 ms^{-1}) extends more northwards (north of 10°S). The summer monsoon flow, increases (>8 ms^{-1}) from June onwards. Here also similar to 1994, the southeast trades (>4-6 ms^{-1}) extends more northwards and is noticed west of Sumatra island, where otherwise the magnitude is comparatively small (< 2 ms^{-1}) during the summer monsoon. This southeasterlies remains over the eastern Indian Ocean north of the equator during October and November and their magnitude decreases and shifts slightly southwards by December.

Thus the wind pattern during 1993, 1995 and 1996 showed similar pattern and 1994 and 1997, different from these years. The westerlies over the equatorial region during the transition period between monsoons appeared weak (< 2 ms^{-1}) during 1994 and 1997 and even easterlies were noticed for 1997. Similarly another noticeable difference observed was the extension of southeast trades more northwards (north of equator) over the eastern Indian Ocean and over the Sumatra region from June/July to December during both 1994 and 1997. The variability in the monsoon winds was noticeable over the Bay also with weak northeasterlies (4 ms^{-1}) and strong

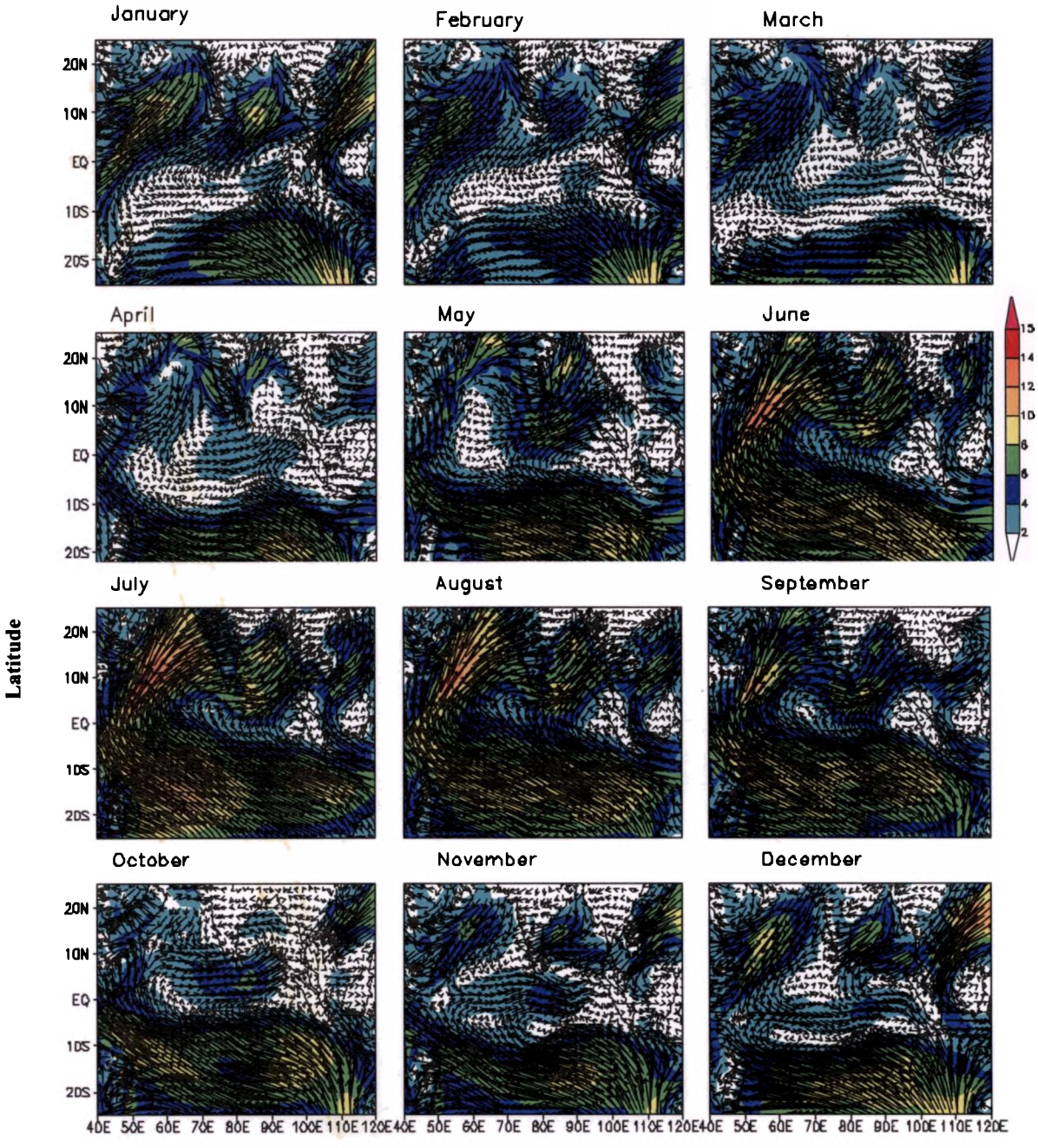

Figure 5.1 surface winds (ms^{-1}) for 1993

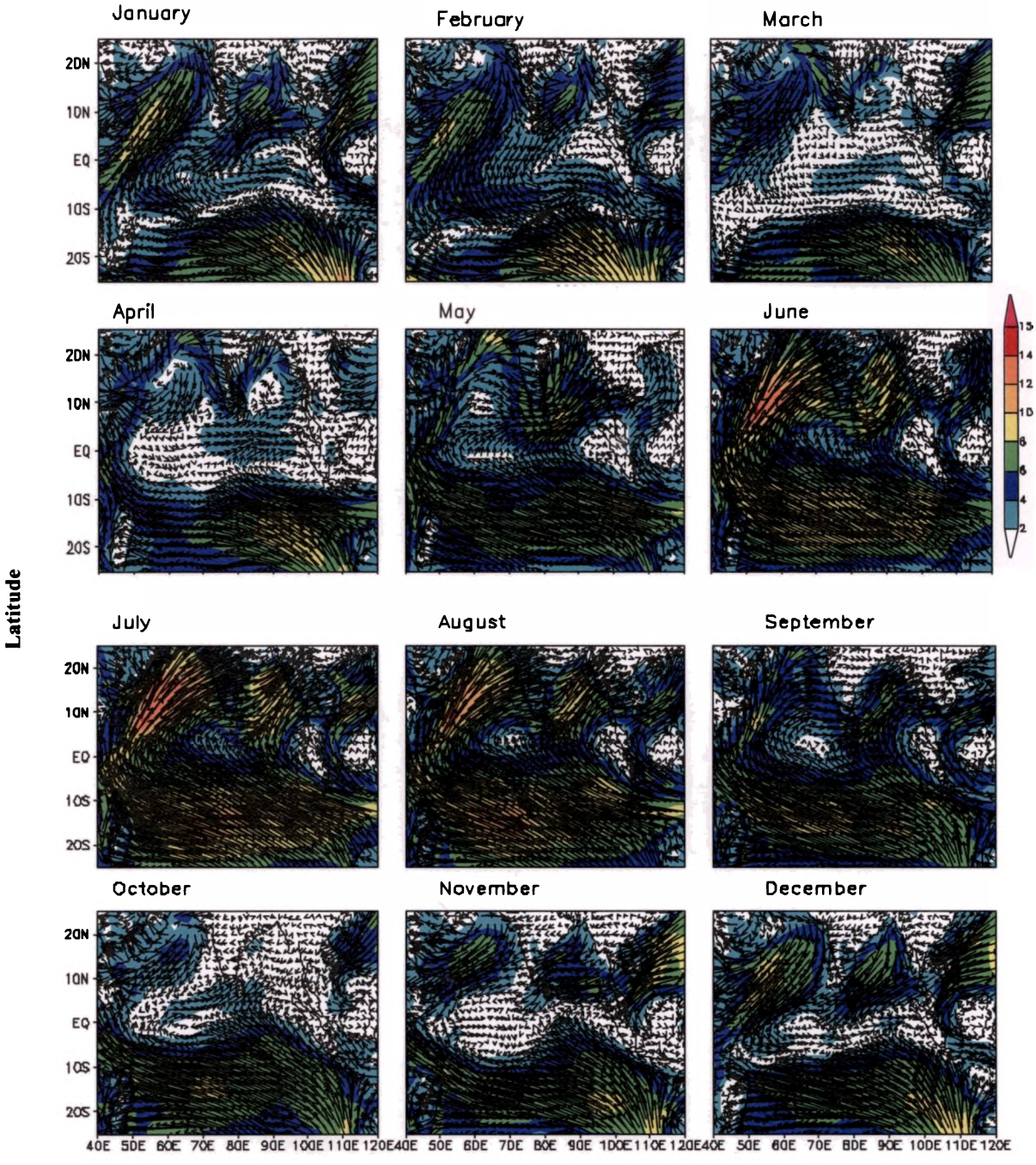

Figure 5.2 surface winds (ms^{-1}) for 1994

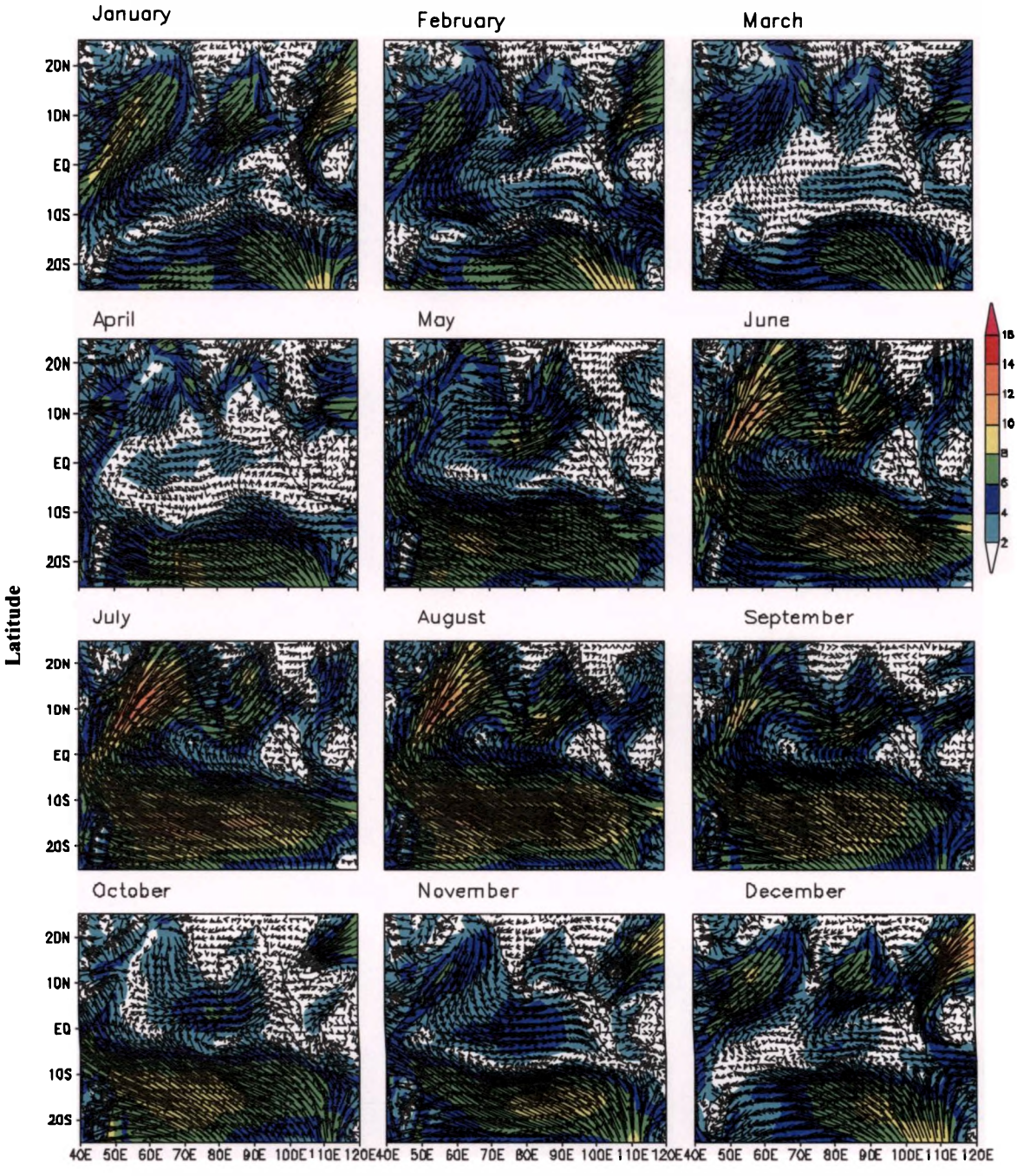

Figure 5.3 surface winds (ms^{-1}) for 1995

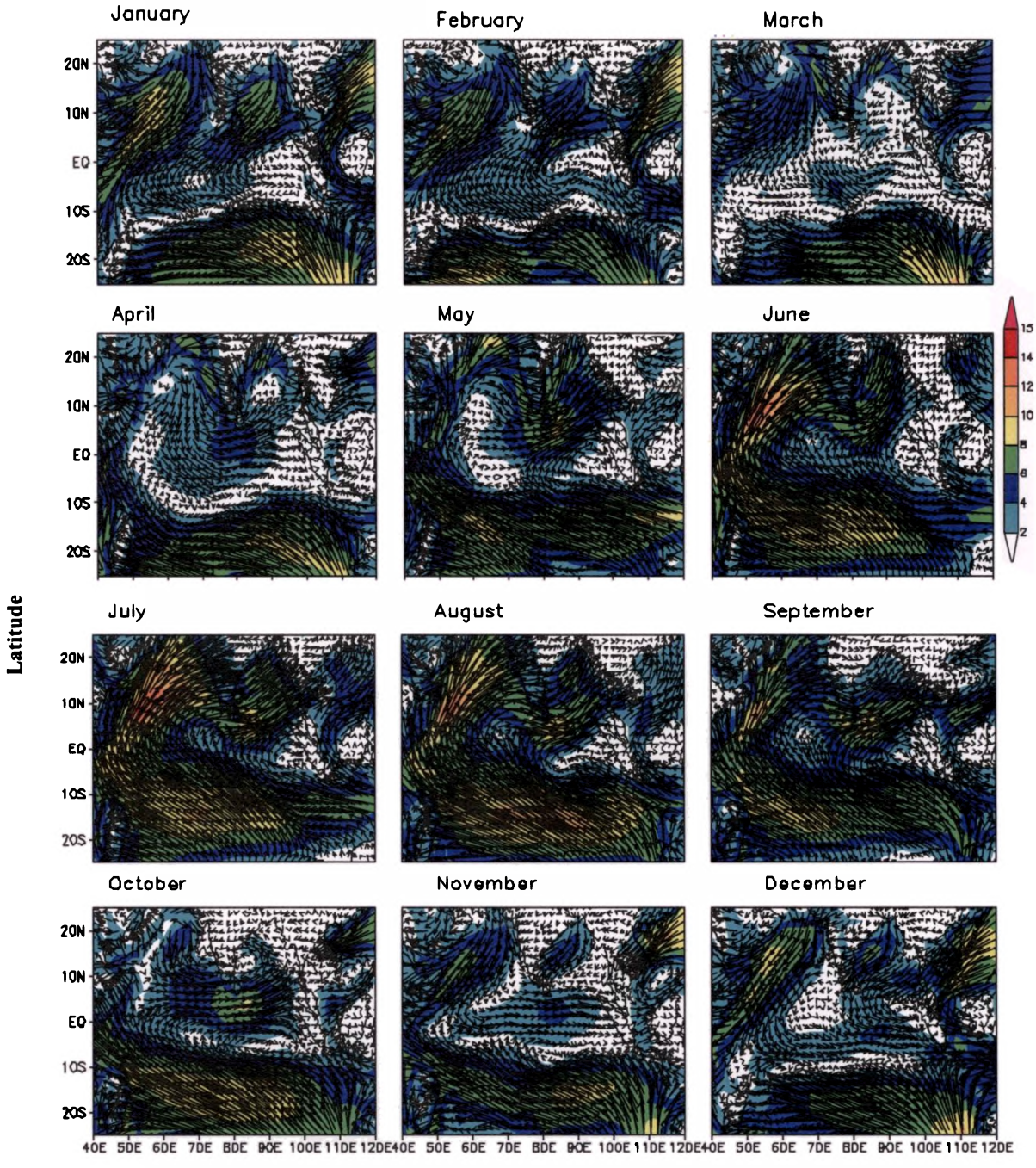

Fig.5.4 surface winds (ms^{-1}) for 1996

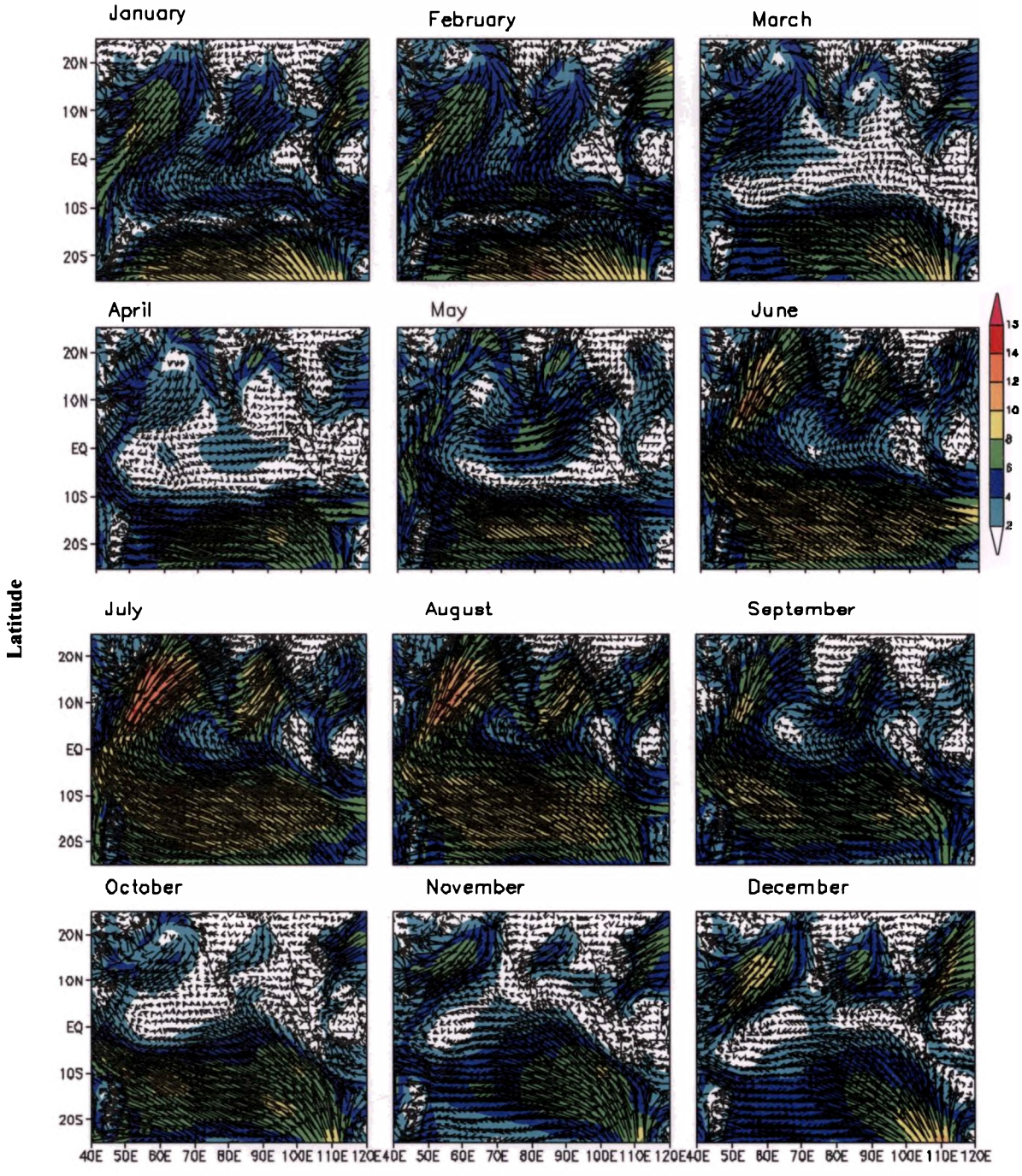

Fig.5.5 surface winds (ms^{-1}) for 1997

southwesterlies (>8 ms^{-1}) occurring during 1994 and 1997 compared to 1993, 1995 and 1996. During 1994 and 1997, El Nino has occurred over the Pacific Ocean. In addition Saji *et al.*, (1999) has reported the occurrence of Indian Ocean Dipole (IOD) events in the Indian Ocean during these years. They have also reported the appearance of abnormally extended trade winds over the Sumatra region during IOD. Murtugudde *et al.* (2000) has also reported strong upwelling in the eastern Indian Ocean during 1997 and suggested that it was forced locally by alongshore winds and remotely by equatorial and coastal Kelvin waves. The surface winds analysed here also show typical patterns during 1994 and 1997 coinciding with the anomalous events in the Indian Ocean.

In the south Indian Ocean also winds showed anomalous behaviour during 1994 and 1997, when the southeast trades over the eastern Indian Ocean extended further northward in the eastern equatorial region (near the Sumatra region) from June/July onwards. These winds remained there till December although with slightly less magnitude.

5.3.2 Wind stress curl

The wind stress curl computed from the wind field shows the rotating effect of the wind, either cyclonic represented by positive values or anti-cyclonic circulation represented by negative values in the northern hemisphere. The curl fields (Figs.5.6-5.10) are also noticed to change in correspondence with the wind reversals, with large reversals observed with the seasons over the northern Indian Ocean. In this section, the curl corresponding to the north Indian Ocean only is discussed.

Generally over the north Indian Ocean, during the northeast monsoon period and till May, curl values (Figs.5.6-5.10) are noticed to be negative or anti-cyclonic over the western Bay (-0.02 $x10^{-5}$ Nm^{-3}) to the southern tip of India (-0.01 $x10^{-5}$ Nm^{-3}), around Sri Lanka (-0.015 $x10^{-5}$ Nm^{-3}) and also over the northwestern Arabian Sea (-0.025 $x10^{-5}$ Nm^{-3}). However, curl is positive over the offshore regions of the Somali coast (0.015 $x10^{-5}$ Nm^{-3}) and negative over the Somali coast during the same period. With the establishment of southwest monsoon winds, the curl also reverses its sign. The positive or cyclonic curl (0.015 $x10^{-5}$ Nm^{-3}) starts appearing first over the west coast and over the east coast of India during the pre-monsoon period itself. From May onwards, cyclonic curl (>0.015 $x10^{-5}$ Nm^{-3}) extends over the western Bay to the

southern tip of India and around Sri Lanka and also extends towards the central Bay. However, near the Somali region from June onwards, anti-cyclonic/negative curl is noticed (< -0.03 $x10^{-5}$ Nm^{-3}) extending to the central Arabian Sea, with cyclonic curl west of it over the coast of Somali and extending to the Arabia coast and northern Arabian Sea. With the weakening of summer monsoon winds by September, both the curl values decreases. The intensity and extent of the curl (Figs.5.6-5.10), either positive or negative shows large variability in all the years indicating inter-annual variability. The prominent regions of positive and negative curl, which favour cyclonic and anti-cyclonic circulation over the region, are separately discussed here to explain their inter-annual variability in each case.

Around the tip of India, curl is negative (-0.005 $x10^{-5}$ to –0.01 $x10^{-5}$ Nm^{-3}) (Fig.5.6) during January 1993 (core around 8°N, 75°E). This value decreases with the progress of time, but the curl is still negative over regions offshore of the west coast of India. By May, positive curl (0.02 $x10^{-5}$ Nm^{-3}) appears over this region, which prevails there till September/October. From December, again negative curl (-0.005 $x10^{-5}$ Nm^{-3}) is noticed over the southern tip of India. In January 1994 (Fig.5.7), the region of negative curl (-0.005 $x10^{-5}$-0.015 $x10^{-5}$ Nm^{-3}) is shifted a little southward (core around 5°N, 75°E). The negative wind curl again forms from November 1994 onwards, earlier than 1993. The years 1995 (-0.005 $x10^{-5}$ to -0.01 $x10^{-5}$ Nm^{-3}) and 1996 (-0.005 $x10^{-5}$-0.015 $x10^{-5}$ Nm^{-3}) also, exhibits similar pattern (Figs.5.8 & 5.9) as that of 1993. While for 1997 (Fig.5.10) the negative curl (-0.005 $x10^{-5}$ to -0.01 $x10^{-5}$ Nm^{-3}) is noticed southward (~5°N and 75°E) similar to 1994 during January. Thus negative curl, which represents anti-cyclonic circulation over the region is found more southward during 1994 and 1997 compared to 1993, 1995 and 1996. The curl remains anti-cyclonic (negative) till March/April around the tip of India.

The positive curl for 1993-1997 over the southern tip of India during the southwest monsoon season also reveals similar patterns during 1993, 1995 and 1996 (Figs.5.6, 5.8 & 5.9). During these years, the positive curl (0.005-01 $x10^{-5}$ Nm^{-3}) remains around the tip of India till October and November. While during 1994 and 1997 (Figs. 5.7 & 5.10), values are comparatively less during September and October (0.005 $x10^{-5}$ Nm^{-3}) around the southern tip of India. It is also noticed here, that during 1994 and 1997 the negative curl start forming in November itself.

Curl is negative found over the northwestern Arabian Sea (off the Arabia coast) during the northeast monsoon and changes to positive with the onset of summer monsoon. The extent and core maximum of this negative/anti-cyclonic curl, also shows inter-annual variability (Figs.5.6-5.10). During 1993 (Fig.5.6), the core maximum (-0.025 $x10^{-5}$ Nm^{-3}) is noticed around 15°N in January and curl is negative off the Arabia coast and over the northern Arabian Sea (70°). During February/March, the negative curl (-0.01 $x10^{-5}$ Nm^{-3}) is seen extending from the northern Arabian Sea to the west coast of India. This negative curl changes by June to cyclonic/positive curl (0.015 $x10^{-5}$ Nm^{-3}). From December, again negative curl forms over the Arabian coast. During January 1994 (Fig.5.7), the extent of the negative curl (-0.015 $x10^{-5}$ Nm^{-3}) over the northern Arabian Sea is less and is upto 68°E only. During 1995 (Fig.5.8), the core maximum (-0.02 $x10^{-5}$ Nm^{-3}) is seen over the Arabia coast region in January and comparatively weak values (-0.015 $x10^{-5}$ Nm^{-3}) over the northern Arabian Sea during May. The maximum negative curl is noticed during January over the western Arabian Sea (-0.025 $x10^{-5}$ Nm^{-3}) in 1996 (Fig.5.9). During 1997 (Fig.5.10), negative curl is noticed to be less (-0.02 $x10^{-5}$ Nm^{-3}) in January. However, it is interesting to note that during 1995 and 1997, the negative curl (<-0.015$x10^{-5}$ Nm^{-3}) over the northwestern Arabian Sea prevails during June also, while during 1993, 1994, and 1996 (Figs.5.6, 5.7 & 5.9), positive curl develops well over the region from June onwards. Thus the negative curl denoting anti-cyclonic circulation over the western Arabian Sea (off the coast of Arabia) shows typical patterns during the years 1995 and 1997.

From May/June onwards, curl becomes positive (>0.02 $x10^{-5}$ Nm^{-3}) over the Somali coast and extending northwards over the Arabia coast and northern Arabian Sea while negative curl (-0.025 to -0.03 $x10^{-5}$ Nm^{-3}) is noticed away from the shore (Somali) and extending to the central Arabian Sea (Figs.5.6-5.10). Both this values and its extent starts decreasing from August/September and changes sign by October/November. This condition reverses from November onwards. The extension of this curl and its value indicates large inter-annual variability over the Somali region and Arabian Sea. During 1993 (Fig.5.6), the negative curl values (<-0.025 $x10^{-5}$ Nm^{-3}) extend from the equator to 12°N off the Somali coast during July with core maximum of -0.04 $x10^{-5}$ Nm^{-3}. The values are negative (-0.02 $x10^{-5}$ to -0.025 $x10^{-5}$ Nm^{-3}) over the Arabian Sea also up to 12°N. The magnitude of this curl starts decreasing from

August onwards and reverses by November. For 1994 (Fig.5.7), the curl values (-0.025 $x10^{-5}$ Nm^{-3}) are similar to 1993 in June and extends more northwards during July (~15°N). During 1995 (Fig.5.8) and 1997 (Fig.5.10), the negative curl (-0.025 $x10^{-5}$ Nm^{-3}) does not extend much northeastwards over the Arabian Sea in June, but extends upto 12°-15°N by July. During 1997, the negative curl was high (-0.025 $x10^{-5}$ Nm^{-3}) in August also, over the central and eastern Arabian Sea compared to other years. During 1996 (Fig.5.9), the extension of this curl values over the central Arabian Sea during June is greater than 1995 (Fig.5.8) and 1997 (Fig.5.10), but less than 1993 and 1994 (Figs.5.6 &5.7), and remains till September. But the northward (~10°N) extent of the negative curl values (-0.025 $x10^{-5}$ Nm^{-3}) is less during July 1996 compared to 1995 and 1997. Thus the negative/anti-cylconic curl values over the offshore regions of Somali and over central Arabian Sea during the summer monsoon season favouring anti-cyclonic circulation exhibits large inter-annual variability.

Over the western Bay and extending almost over the entire Bay, the curl is negative (-0.02 $x10^{-5}$ Nm^{-3}) during the northeast monsoon and positive (0.02 $x10^{-5}$ Nm^{-3}) during the southwest monsoon (Figs.5.6-5.10). Negative curl is noticed from November onwards till April/May. During April and May both positive (over the coast line) and negative curl (in the offshore regions) is seen over the western Bay. From June, positive curl values intensifies over the coastline and is noticed till September/October. During 1993 (Fig.5.6), curl is negative (–0.02 $x10^{-5}$ Nm^{-3}) over the western Bay and extending eastwards. From April/May, positive curl (0.02 $x10^{-5}$ Nm^{-3}) is also noticed over the east coast with negative curl (-0.02 $x10^{-5}$ Nm^{-3}) existing over the offshore regions. By June, curl is positive over the east coast of the India, extending over the western Bay till September. This prevails till August and dissipates afterwards. The negative curl during the northeast monsoon period (maximum in January) is higher (-0.02 $x10^{-5}$ Nm^{-3}) over the western Bay during 1995 and 1996, with core maximum (-0.025 $x10^{-5}$ Nm^{-3}) noticed over the northwestern Bay. During 1994 and 1997, the negative curl values are less (-0.015 $x10^{-5}$ Nm^{-3}) over the western Bay during January.

Around Sri Lanka, the curl is positive (>0.02 $x10^{-5}$ Nm^{-3}) from May onwards with a shift towards the northeast. Its maximum extension is noticed during July/August, northeastward from the Sri Lankan region towards the central Bay. This curl is noticed till October and November with decreased magnitude (<0.005 $x10^{-5}$

Nm^{-3}). During 1996 September, positive curl ($0.005 \times 10^{-5} Nm^{-3}$) extends from the Sri Lanka region continuous across to the eastern Bay. During 1994 and 1997, the curl value weakens from September onwards. In all other years i.e. 1993, 1995 and 1996, the positive curl remains there even though with decreased magnitude (0.005×10^{-5} Nm^{-3}) till November/December.

Thus curl values are noticed here with large inter-annual variability during the period 1993-1997. The major areas of negative and positive curl representing anti-cyclonic and cyclonic circulation respectively have been identified and their inter-annual variability discussed. It was found that the negative curl over the southern tip of India remained there till March/April for all the years and is shifted more southwards during 1994 and 1997 compared to other years. The positive curl during the summer monsoon period around the tip of India also showed similar patterns during 1994 and 1997 and different from 1993, 1995 and 1996. During 1993 and 1995 and 1996, the positive values are noticed upto 15°-20°N along the west coast and remains over the southern tip of India even in October, while the curl values are comparatively less along the west coast and curl is negative from November onwards during 1994 and 1997. Negative curl values were less during January 1994 and 1997 over the western Bay compared to other years. Over the western Arabian Sea, negative curl was prevalent over the region during June 1995 and 1997 when positive curl appeared over this region during the same period for other years. In the offshore regions of Somalia, the negative curl from May/June onwards also showed large variability with 1993 and 1994 showing similar pattern in June. However, during 1996, the extension of the negative curl was higher than 1995 and 1997 but less than 1993 and 1994 in June. While the extension of the negative curl in August 1997 was higher than all other years. Over the Sri Lanka region curl value weakens earlier for 1994 and 1997 compared to other years. All these information about from this chapter has been utilized as further reference in the following chapters.

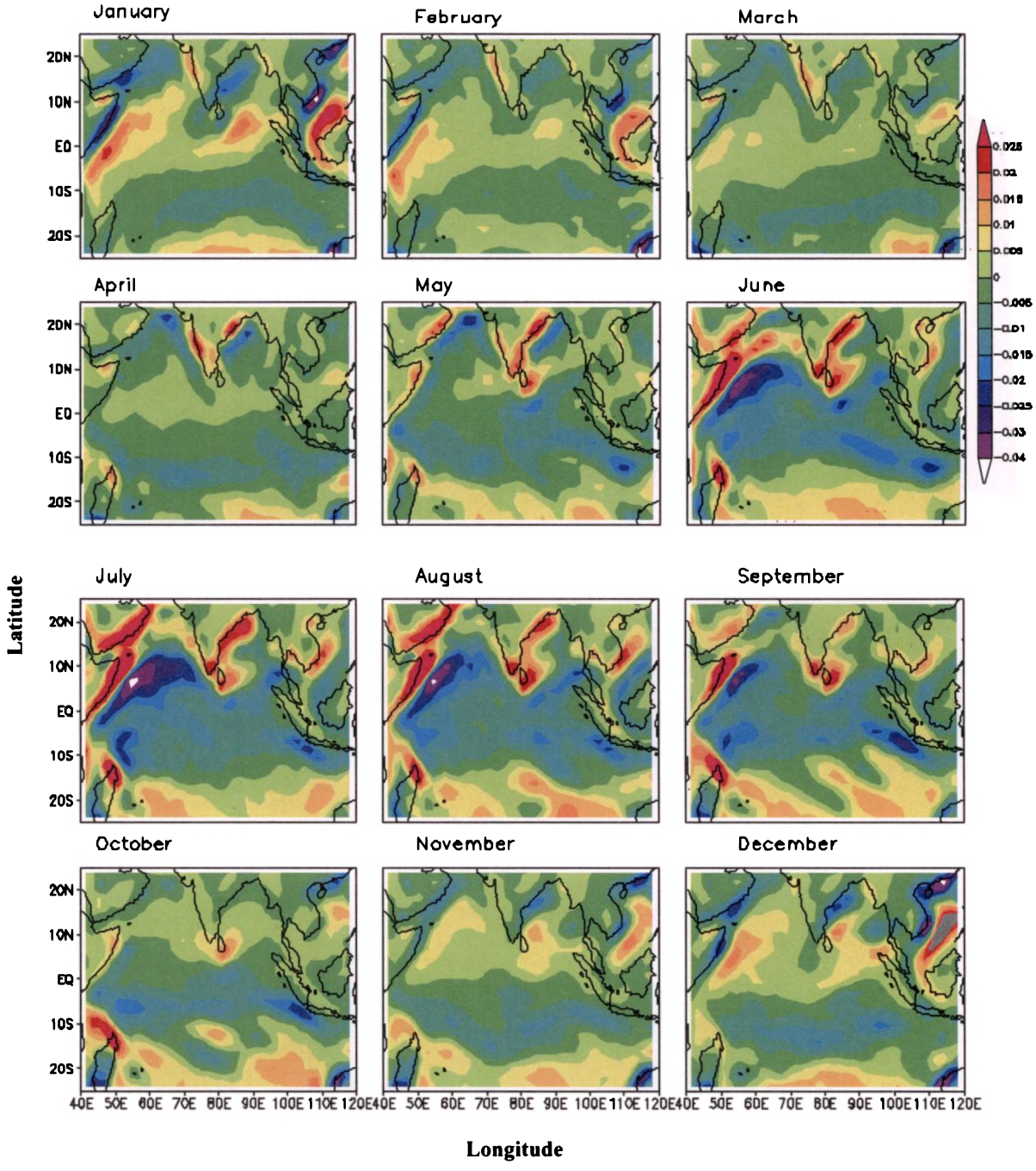

Fig. 5.6 Wind stress curl (x10^{-5} Nm^{-3}) during 1993

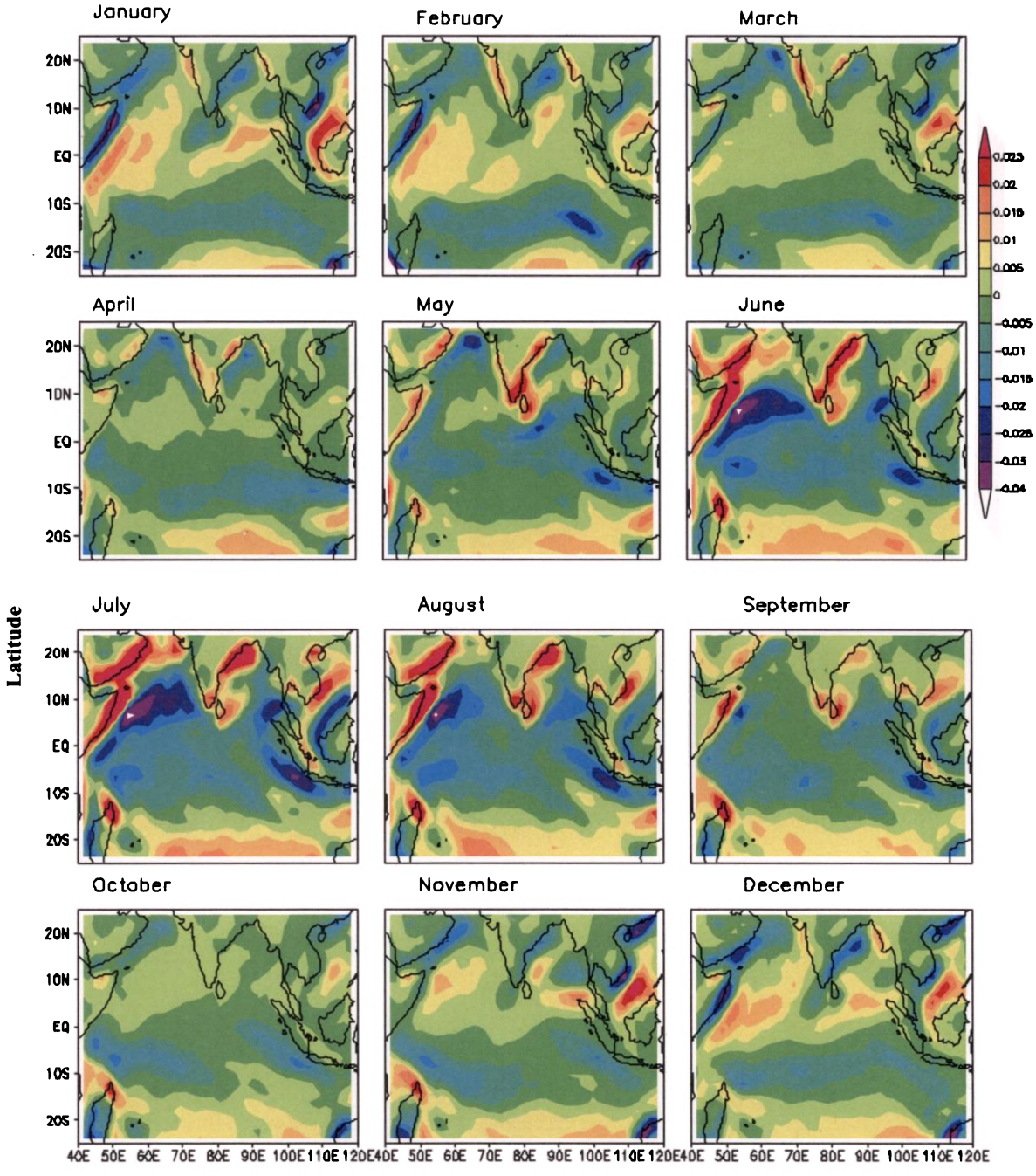

Fig. 5.7 Wind stress curl ($x10^{-5}$ Nm^{-3}) during 1994

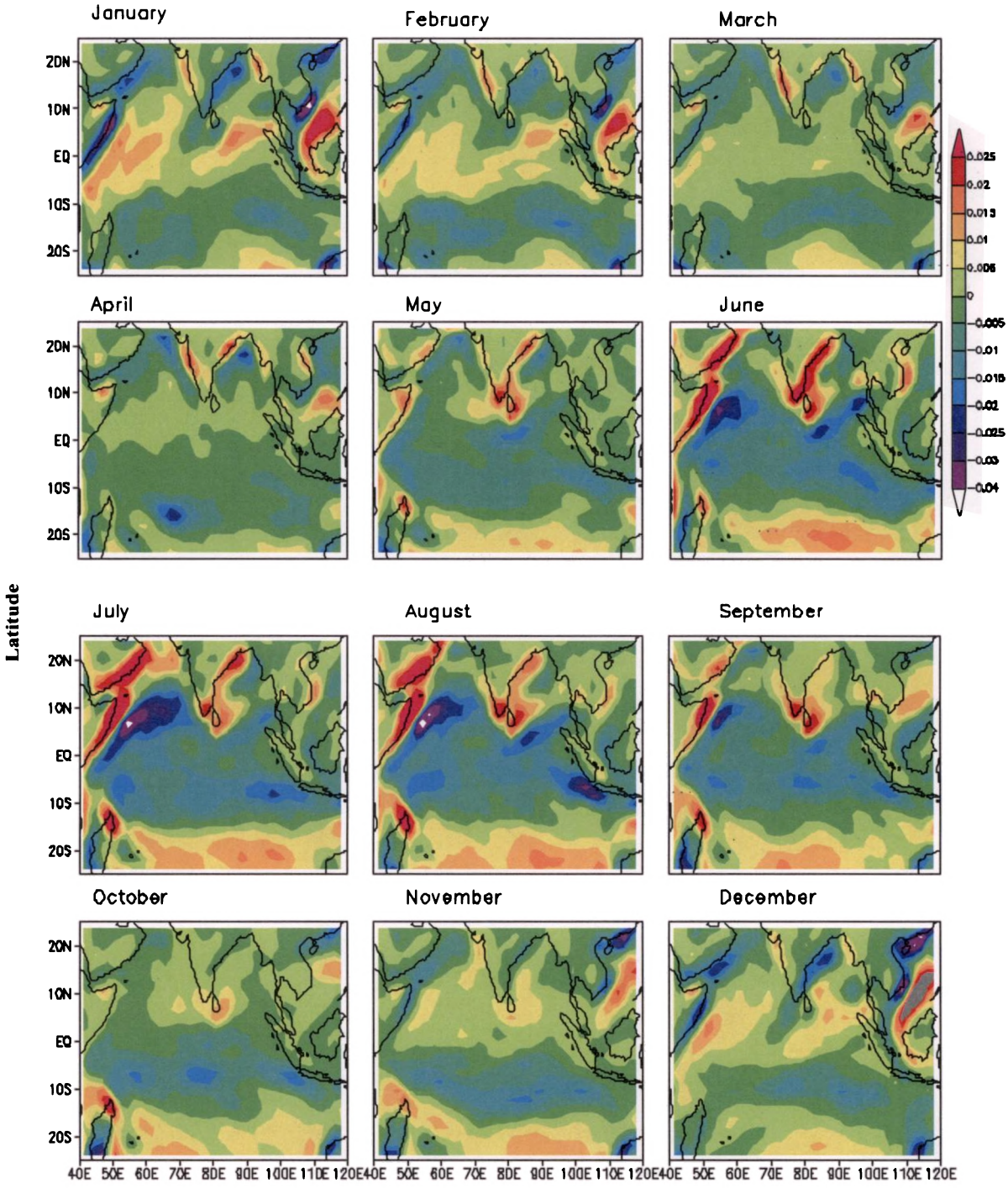

Fig. 5.8 Wind stress curl ($x10^{-5}$ Nm^{-3}) during 1995

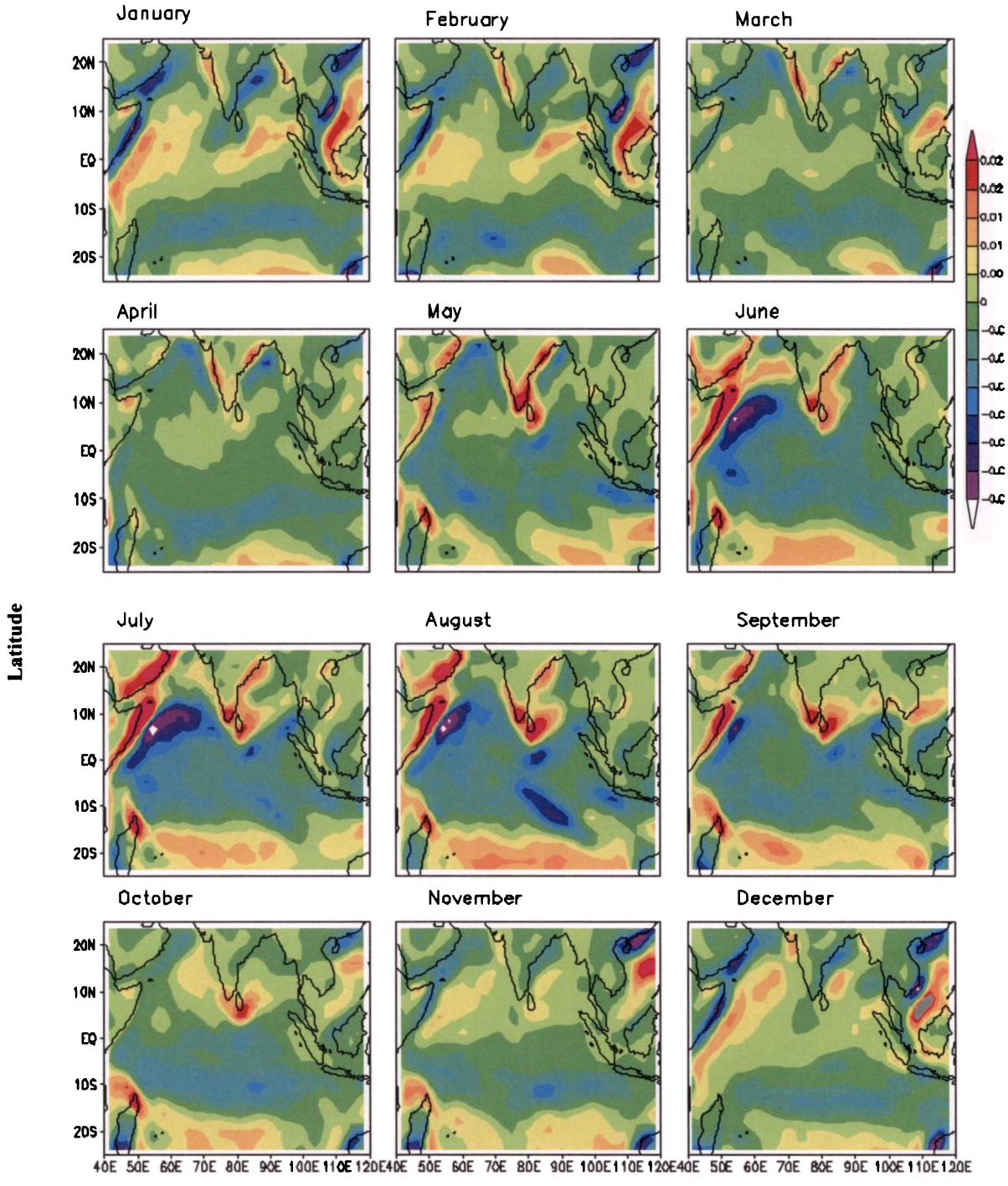

Fig. 5.9 Wind stress curl ($x10^{-5}$ Nm^{-3}) during 1996

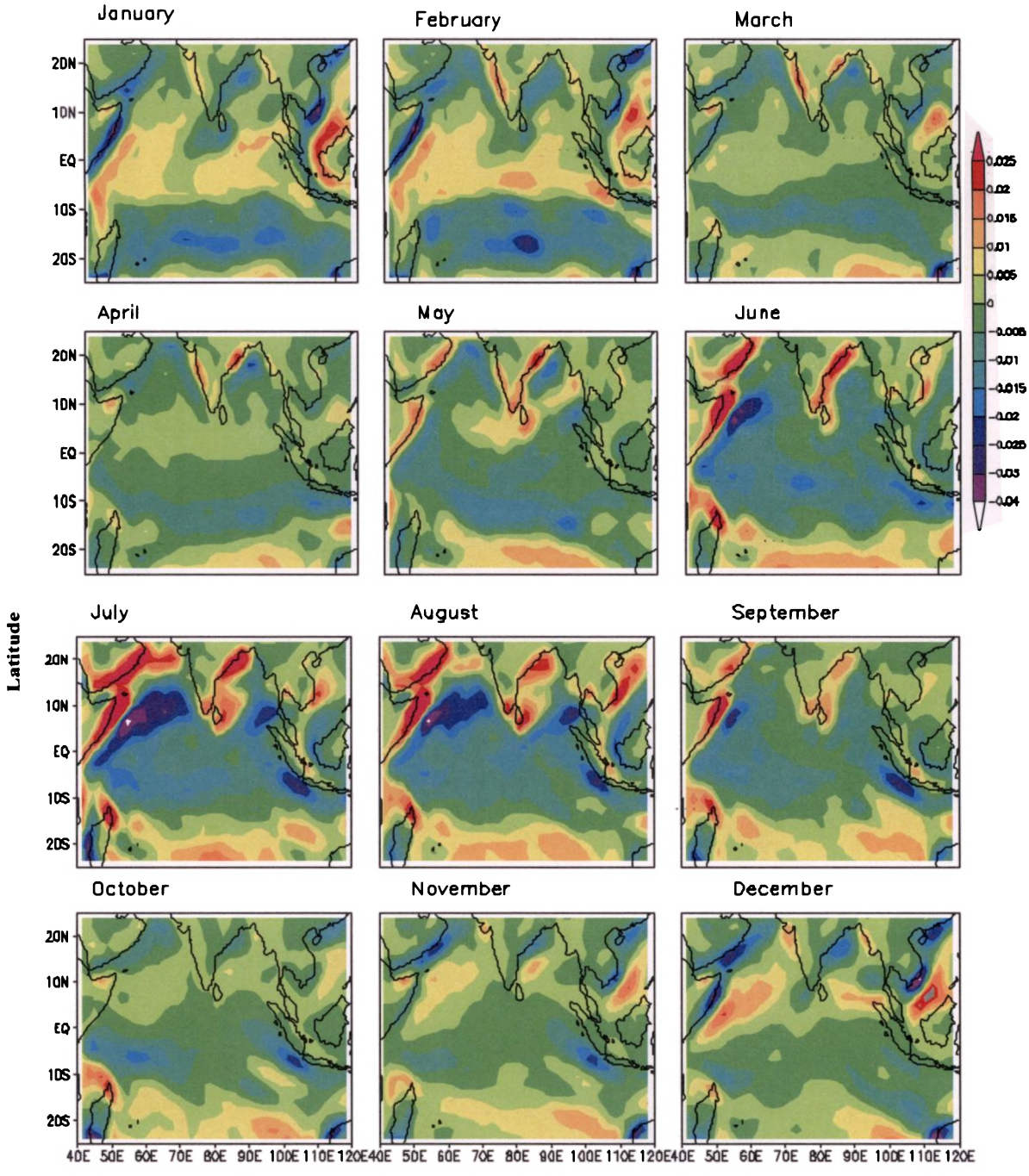

Fig. 5.10 Wind stress curl ($x10^{-5}$ Nm^{-3}) during 1997

Chapter 6

Oceanographic features obtained from satellite

Part I- Propagating waves

6.1. Introduction

The circulation in the North Indian Ocean is unique in that the winds reverse semi-annually from southwesterly to northeasterly, with which surface currents also reverses semi-annually. Large scale forcing associated with this wind reversal leads to the propagation of Kelvin waves along the equator (Yu *et al.*, 1991; Potemra *et al.*, 1991). The Kelvin waves on reaching the eastern boundary of Bay of Bengal get reflected as Rossby waves, which propagates westward and the remaining as coastally trapped Kelvin waves towards north and south along the coastal boundaries (Moore and Philander, 1977; Yu *et al.*, 1991). The coastally trapped Kelvin waves also radiate Rossby waves, as they propagate along the eastern boundary of the Bay of Bengal and contribute substantially to the circulation (Potemra *et al.*, 1991; Kumar and Unnikrishnan, 1995; Shankar *et al.*, 1996; Vinayachandran *et al.*, 1996). They also act as a link in the circulation in Bay of Bengal, Arabian Sea and equatorial Indian Ocean (Yu *et al.*, 1991; McCreary *et al.*, 1993, 1996). The coastally trapped Kelvin waves after travelling all along the periphery of Bay of Bengal reaches the southern tip of India and radiate Rossby waves into the interior Arabian Sea as they propagate northwards along the west coast of India (Shankar and Shetye, 1997; Shenoi *et al.*, 1999). The Lakshadweep high and low owe their existence to these radiated Rossby waves (Shankar and Shetye, 1997). These coastally trapped waves are believed to play a significant role in the transport of low saline waters from the Bay of Bengal to the Arabian Sea during the northeast monsoon which eventually facilitate the building up of mini warm pool in the Lakshadweep area (Shenoi *et al.*, 1999). These waves also contribute substantially in the generation and propagation of Somali eddies in the Arabian Sea and the western boundary current in the Bay of Bengal (Potemra *et al.*, 1991; McCreary *et al.*, 1996; Shankar *et al.*, 1996; Subrahmanyam *et al.*, 2001).

Thus the variability in the occurrence and propagation of planetary waves can contribute significantly to the circulation pattern and hence the climate over the region concerned. Modelling studies (McCreary *et al.*, 1993; Potemra *et al.*, 1991; Shankar *et al.*, 1996) have proved the existence of propagating waves and their role in the north Indian Ocean circulation. The hydrographic data provides only a limited assessment of the ocean dynamics both spatially and temporally. Initially, it was very difficult to detect these propagating waves in the ocean as they have very small signatures over

the sea surface compared to their wavelength. The advent of remote sensing satellites provides a wide opportunity of observing these phenomenon over large spatial domain and at frequent time intervals. TOPEX/Poseidon (T/P) altimetry data is widely utilized by many researchers to identify the propagation of waves in the Indian Ocean (Kindle and Thompson, 1989; Quadfasel and Swallow, 1986; Subrahmanyam *et al.*, 2001; Basu *et al.*, 2000; Gopalan *et al.*, 2000, Brandt *et al.*, 2002). Recently, Hareesh Kumar and Sanilkumar (2004) studied the wave propagation along the coastal regions of the north Indian Ocean using this data sets.

However, many of these studies were either limited only to a selected region or selected years. In this chapter, Sea Surface Height (SSH) anomaly from T/P data is utlized to study the characteristics of the propagating waves along typical zonal sections in the Indian Ocean. Moreover, their inter-annual variability is discussed considering five consecutive years from 1993-1997. The prominent harmonics at selected locations are decomposed using wavelet analysis technique and their confidence level is tested using statistical significance test. Power spectrum analysis is also performed to support the results from the wavelet analysis.

6.2. Data and Methodology

Processed Sea Surface Height anomalies (SSH) from T/P altimetry for the period 1993-1997 are utilized in this study. The United States National Aeronautics and Space Administration and French Space Agency, Centre National d'Etudes Spatials, conducted this mission for studying global ocean circulation from space. T/P satellite was launched on August 10 1992. The satellite orbits at an altitude of 1336 km above the Earth at an inclination of 66°. T/P altimetry with its rapid 10 day repeat cycle and high accuracy gives an opportunity to study the long waves in the ocean using sea level variations (Chelton and Schlax, 1996). The measurement precision for sea surface height is 4.3 cm. These SSH values are used to generate Hovmoller diagrams (longitude/time plots). In these diagrams, propagating waves appear as diagonal strands sloping eastward/westward indicating eastward/westward propagation.

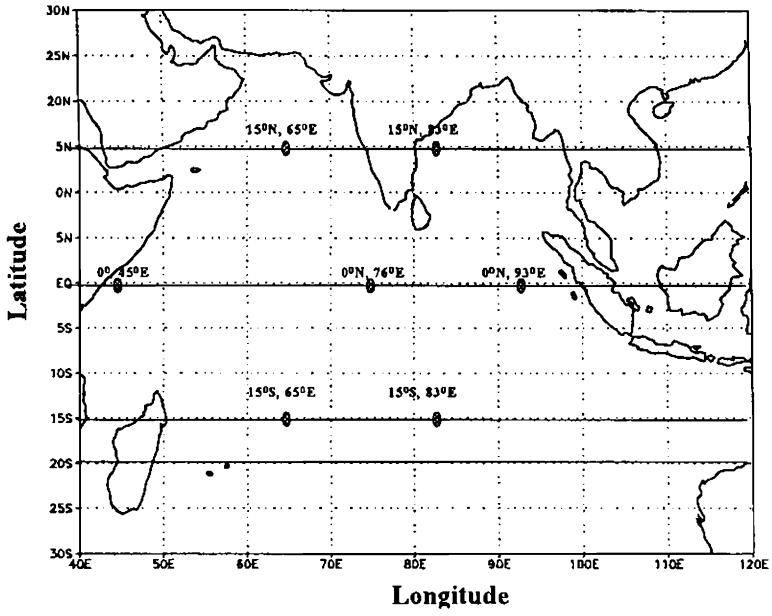

Fig.6.1 Study region

To study the nature of the propagating waves, time series of SSH is retrieved along five latitude tracks viz. along equator, 15°N, 15°S, 20°N, and 20°S (Fig.6.1). The temporal variability and the harmonics embedded in the signals are studied utilizing the time series of SSH retrieved from typical stations. The stations are selected as follows. Two stations are selected in the north Indian Ocean representing Bay of Bengal (15°N, 83°E) and Arabian Sea (15°N, 65°E). Three stations along the equator, represent western (0, 45°E), central (0, 76°E) and eastern equatorial Indian Ocean (0,93°E). Finally, two stations are selected in the southern Indian Ocean (15°S, 65°E; 15°S, 83°E). The missing data gaps in the time series data are filled using three point lagrangian interpolation scheme. The final time series data sets for each station consist of 176 points and is utilized for the wavelet and power spectrum analysis. The prominent harmonics embedded in the time series of SSH are decomposed using the wavelet analysis, which is discussed in the section 6.2.1. Wavelet analysis is an important statistical tool used in the field of Meteorology and Oceanography for studies on multiscale, non-stationary processes occurring over finite, spatial and temporal domain. The confidence level is tested using statistical significance test, also explained in the same section. The power spectrum analysis, discussed in section

6.2.2 is utilized to compare the results from wavelet analysis. In addition, NCEP/NCAR wind at 10 m level for the years 1993-97 are utilized to explain the inter-annual variability in the nature of the propagating waves.

6.2.1 Wavelet analysis.

Wavelet decomposition is a method of time-frequency localization that is scale independent. This method of decomposition can be employed where a predetermined scaling may not be appropriate because of a wide range of dominant frequencies. Wavelet analysis attempts to solve by decomposing the time series signals into time / frequency space simultaneously. This method has the advantage of incorporating a wave of a certain period, as well as being finite in extent. This method of signal decomposition provides information on both the amplitude of any periodic signals within the series, and how this amplitude varies with time.

In this study, Daubechies Wavelet is utilized to obtain the predominant signals embedded in the time series of SSH. This wavelet is slide along the time series data to determine the amplitude of this wave contained in this width for all the data. The scale of this width can be changed which is the advantage of wavelet analysis over Fourier spectrum. Analysis is carried out in MATLAB. The wave decomposition is performed using [C,L] = wavedec (X,N,'*wname*') which, returns the wavelet decomposition of the signal X at level N, using '*wname*'. N is a positive integer. The output decomposition structure contains the wavelet decomposition vector C and bookkeeping vector L. Wrcoef reconstructs the coefficients of a one-dimensional signal, given a wavelet decomposition structure (C and L) and either a specified wavelet. X = wrcoef ('*type*',C,L,'*wname*',N) computes the vector of reconstructed coefficients, based on the wavelet decomposition structure [C,L], at level N.

From the reconstructed coefficients the harmonics can be computed. Then to determine the confidence limits of these periodicities a significance test is also carried out following Torrence and Compo (1998). The red noise spectrum chosen is

$$P_k = \frac{1-\alpha^2}{1+\alpha^2 - 2\alpha\cos(2\pi k / N)}$$

where α □is the lag-1 correlation and k = 0 .... N/2 is the frequency index. The test was carried out at 99%, 95% and 90% confidence levels.

6.2.2 Power spectrum analysis

A given data series consisting of n points can be represented exactly, meaning that a harmonic function can be found that passes through each of the points, by adding together a series of n/2 harmonic functions

$$y_t = \bar{y} + \sum_{k=1}^{n/2}\left\{C_k \cos\left(\frac{2\pi t}{n} - \phi_k\right)\right\}$$

$$= \bar{y} + \sum_{k=1}^{n/2}\left\{A_k \cos\left[\frac{2\pi kt}{n}\right] + B_k \sin\left[\frac{2\pi kt}{n}\right]\right\} \quad \text{(1)}$$

$$A_k = \frac{2}{n}\sum_{t=1}^{n} y_t \cos\left(\frac{2\pi kt}{n}\right) \quad \text{.....(2)}$$

$$B_k = \frac{2}{n}\sum_{t=1}^{n} y_t \sin\left(\frac{2\pi kt}{n}\right) \quad \text{.....(3)}$$

and $C_k = [A_k^2 + B_k^2]^{1/2}$ .....(4)

where C_k is the amplitude

The characteristics of a time series that has been Fourier-transformed into the frequency domain are most often examined graphically, using a plot known as the periodogram or Fourier line spectrum. This plot is sometimes also called the power spectrum, or simply the spectrum of the data series.

In simplest form, this plot of a spectrum consists of the squared amplitudes as a function of the frequency. The vertical axis is sometimes numerically rescaled, in which case the plotted points are proportional to the squared amplitudes. The spectrum conveys the proportion of variation in the original data series accounted for by oscillations at the harmonic frequencies, but does not supply information about time of occurrence of these oscillations. This is carried out in 'MATLAB'. P=SPECTRUM (X,NFFT,NOVERLAP,WIND) estimates the Power Spectral Density of signal vector X using Welch's averaged periodogram method. The signal X is divided into overlapping sections, each of which is detrended and windowed by the WINDOW parameter, then zero padded to length NFFT. The magnitude squared of the length NFFT DFTs of the sections are averaged to form Pxx. P is a two column

matrix P = [Pxx Pxxc]; the second column Pxxc is the 95% confidence interval. The number of rows of P is NFFT/2+1 for NFFT even, (NFFT+1)/2 for NFFT odd, or NFFT if the signal X is complex. If it is specified a scalar for WINDOW, a Hanning window of that length is used. [P,F] = SPECTRUM (X, NFFT, NOVERLAP, WINDOW, Fs) given a sampling frequency Fs returns a vector of frequencies the same length as Pxx at which the PSD is estimated. PLOT(F,P(:,1)) plots the power spectrum estimate versus true frequency. [P, F] = SPECTRUM (X, NFFT, NOVERLAP,WINDOW, Fs, Pr) where Pr is a scalar between 0 and 1, overrides the default 95% confidence interval and returns the Pr*100% confidence interval for Pxx instead. SPECTRUM(X) with no output arguments plots the PSD in the current figure window, with confidence intervals. The default values for the parameters are NFFT = 256 (or LENGTH(X), whichever is smaller), NOVERLAP = 0, WINDOW = HANNING(NFFT), Fs = 2, and Pr = .95. A default parameter can be obtained by leaving it out or inserting an empty matrix [].

6.3. Results and Discussion

In order to study the propagating waves in the Indian Ocean, Hovmoller (Longitude vs. Time) diagrams of SSH are prepared along the equator, along 15°N representing central Arabian Sea and Bay of Bengal and along 15°S and 20°S, representing southern Indian Ocean (Figs.6.2-6.6).

6.3.1 Hovmoller diagram along the equator

Hovmoller diagram along the equator (Fig.6.2) shows the occurrence of alternate positive and negative SSH on an annual cycle with varying magnitude. In the western Indian Ocean and more clearly east of 60°E, the positive SSH is noticed during the transition months, i.e. during March/April and September/October. The high is observed near the eastern Indian Ocean from May and from October onwards. Negative SSH are noticed during June and December in the western Indian Ocean and from August and January in the eastern Indian Ocean. This suggests that the highs and lows (negative) are formed in the western and eastern Indian Ocean with nearly semi-annual periodicity. Wavelet analysis of SSH field (section 6.3.4) also supported this fact. The positive SSH noticed in the western Indian Ocean during April, reached the eastern Indian Ocean (100°E) by May i.e. within a month, suggesting a speed of ~250 $cm.s^{-1}$. This is due to the eastward slope formed at the equatorial region by the

reversal in wind system. Similarly, negative anomaly formed in the western Indian Ocean during December reached the eastern Indian Ocean by January next year, also suggesting a speed of 250 $cm.s^{-1}$. Studies have indicated that the eastward movement of both positive and negative SSH is associated with the Kelvin (downwelling and upwelling) wave (Subrahmanyam *et al.*, 2001). The speed obtained here (250 $cm.s^{-1}$) agrees well with the theoretical phase speed for a baroclinic Kelvin wave (240 $cm.s^{-1}$) for the equatorial Indian Ocean (Yu *et al.*, 1991; McCreary *et al.*, 1993; Unnikrishnan *et al.*, 1997). However, the estimated speed of Kelvin wave in the equatorial Indian Ocean is found to be less compared to the Pacific Ocean (270 cms^{-1}) as reported by Chelton and Schlax (1996).

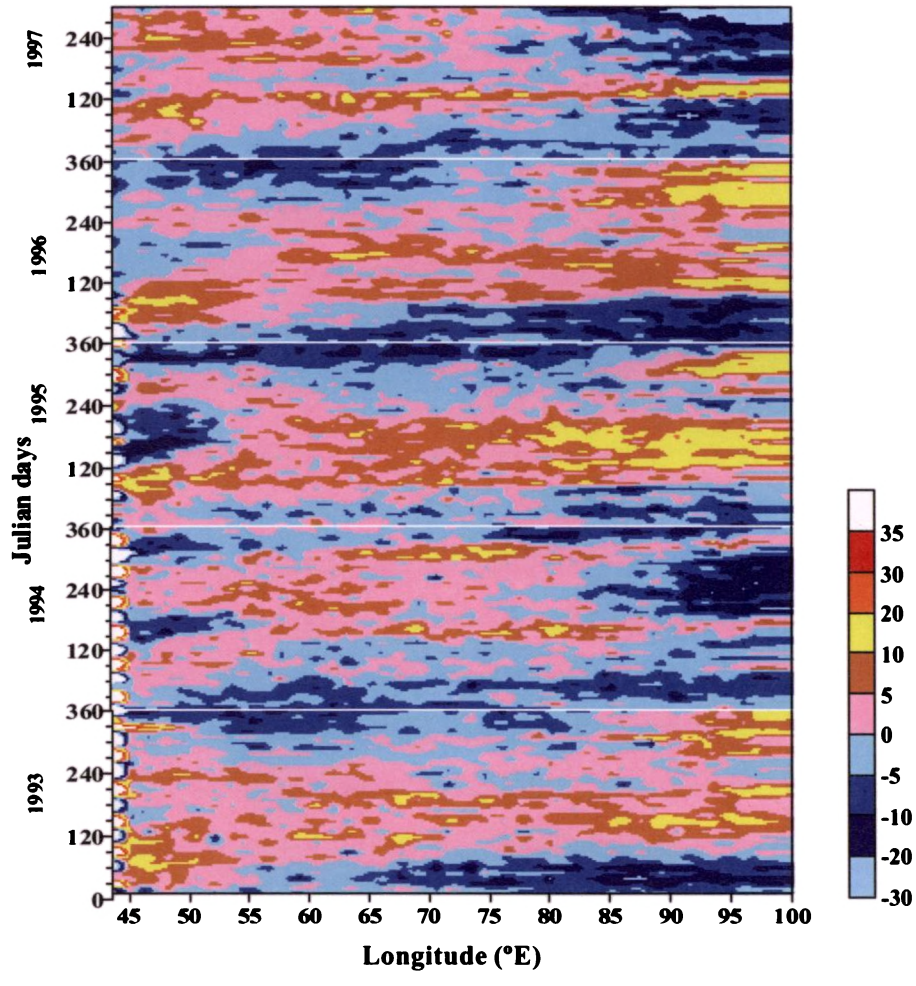

Fig.6.2 Hovmoller diagram of SSH anomalies (cm) along the equator. Y-axis is time in Julian days from January to December for the years 1993-1997.

It is to be noted that the formation and dissipation of positive and negative SSH in the equatorial region is a continuous process, but with a certain periodicity.

Moreover this positive and negative SSH are clearly seen in certain years but not well marked in some other years suggesting their inter-annual variability. In the eastern equatorial region, the inter-annual variability is seen in the appearance of high and low SSH, its duration and magnitude (Fig.6.2). For example, during 1993, two positive and two negative SSH are noticed near the eastern Indian Ocean. The highs (~ 10 cm) persisted from May to August and from October to December while the negative SSH are noticed from January to March/April (-10 cm) and during September (-5 cm). During 1994, two positive SSH and three negative SSH are noticed in the eastern Indian Ocean, with the negative anomaly being more prominent. These negative SSH (-10 cm) appears from January to May, from July to November (–20 cm) and again during December (-5 to -10 cm) in the eastern Indian Ocean. However, positive SSH (~ 5cm) is noticed during June/July and December for less than one month. As the formation of the high and low is mostly associated with the Kelvin waves, their inter-annual variability can be associated with the variability in the Kelvin wave characteristics. It is well known that the downwelling Kelvin waves are generated by the westerly winds, which drive the Wyrtki Jet (Wyrtki, 1973) in the equatorial region. Therefore any variation in the equatorial wind pattern will affect characteristics of the Kelvin wave and hence the SSH field.

From the figure (Fig.6.2) it appears that the variability in SSH for the years 1993, 1995 and 1996 appears similar. During 1993 (Fig.6.2), positive SSH (5-10 cm) from the western/central Indian Ocean reaches the eastern Indian Ocean by May and October respectively. These signals are more discernable in the eastern Indian Ocean and they dissipated by September 1993 and by January 1994 respectively. Similarly, the negative SSH are noticed in the western Indian Ocean during June (-5 cm) and December (-10 cm), and in the eastern Indian Ocean during September and in January next year. The negative anomaly formed during December in the western Indian Ocean is seen continuous and reaches eastern Indian Ocean by January 1994. Similar features are observed during 1995 and 1996 (Fig. 6.2). The positive SSH (5-10 cm) formed in the western equatorial Indian Ocean during March/April 1995 reach the eastern equatorial Indian Ocean by April/May (suggesting a speed of ~250 cms^{-1}) and the high (>10 cm) remains in this region till July. The second high is noticed in the eastern equatorial region from November onwards till mid December. During 1996, the first downwelling signal is noticed in the eastern Indian Ocean from April till July

and the second one between September/October and December. It may be again noted that the sea level variability (Fig.6.2) during the year 1994 and 1997 are typical and distinct compared to other years. These are the El Nino years and Indian Ocean dipole mode event are also reported over the Indian Ocean (Saji *et al.*, 1999). During 1994, the positive SSH is not well marked in the eastern Indian Ocean and is noticed only in June (Fig.6.2). The second high reached the eastern Indian Ocean by November. Positive anomalies are weak (5 cm) in this case compared to 1993, 1995 and 1996 and persisted for less than a month in the eastern Indian Ocean. Similarly, during 1997 also, the weak positive SSH (5 cm) formed in the western regions during April reached eastern equatorial Indian Ocean by May suggesting a speed of ~250 $cm.s^{-1}$. In this case also the positive SSH anomalies persisted only for nearly one month in the eastern equatorial region. The weak positive SSH anomaly and their short duration in the eastern Indian Ocean during these two years may be associated with the weak downwelling Kelvin wave. This can be related to the prevailing wind pattern in the equatorial Indian Ocean. Another noticeable observation during 1994 is the prominent upwelling signals (-10 cm) in the eastern Indian Ocean between July 1994 and March 1995, except during December 1994 when a weak positive sea level (~ 5 cm) is observed. During 1997 also (Fig. 6.2), negative anomalies (-20 cm) prevails in the eastern Indian Ocean from June onwards (data available only upto October).

The analysis clearly indicated that in the equatorial region, the SSH exhibited similar pattern of variability during the years 1993, 1995 and 1996 with prominent positive values (~10 cm) in the eastern and western Indian Ocean. The years 1994 and 1997 are typical and different from other years, with weak positive signals (5 cm) in the western/central Indian Ocean, and lasting for less than a month. Further, anomalous negative values are noticed for a longer duration in the eastern Indian Ocean between June/July and March. The typical ocean behaviour during these years is studied utilizing the surface winds (Figs.5.1-5.5) for the same period.

As mentioned in section 5.3.1, the characteristics of the wind system in the equatorial region during 1993, 1995 and 1996 (Figs.5.1, 5.3 & 5.4) are almost similar. Over the central Indian Ocean weak westerly winds are observed in March/April (2 ms^{-1}) and October (4 ms^{-1}). During 1994 and 1997 (Figs.5.2 & 5.5) the magnitude of westerlies are weak (< 2 ms^{-1}) over the equatorial Indian Ocean especially during March/April and October. Even easterlies are noticed over the equatorial region

during March and October of 1997. Another noticeable observation is the northward extension of the southeasterly winds from the south Indian Ocean over the central and eastern Indian Ocean during 1994 and 1997 from May/June onwards and persisted throughout the year. Semyon *et al.* (2001) reported anomalous climatic event in the Indian Ocean during these years, with a westward gradient of SST and an anomalous reversal of eastward surface current. This could have weakened the downwelling Kelvin wave (Fig.6.2) near the Sumatra region, as indicated by the weak SSH anomaly (~ 5 cm). Murtugudde *et al.* (2000) has also reported strong upwelling in the eastern equatorial region during 1997 and suggested that it was forced locally by alongshore winds and remotely by equatorial and coastal Kelvin waves. Saji *et al.* (1999) reported the occurrence of Indian Ocean Dipole (IOD) events during the years 1994 and 1997 i.e., when cold SST anomalies occur in the southeastern tropical Indian Ocean and warm SST anomalies occurs in the western Indian Ocean. Studies using satellite as well as *in-situ* data (Rao *et al.*, 2002; Feng *et al.*, 2001; Feng and Meyers, 2003) also indicated that IOD events are associated with sea level anomaly having similar structure as SST anomaly, i.e. positive SSH anomaly to warm SST anomaly and vice versa. Therefore the occurrence of the negative SSH anomalies in the eastern Indian Ocean can be linked to the strong upwelling in this region and IOD events.

6.3.2 Hovmoller diagrams along central Arabian Sea and Bay of Bengal

Hovmoller diagrams in the central Arabian Sea (along 15°N) shows alternate positive and negative sea level anomalies sloping westwards (Fig.6.3). Off the west coast of India, positive sea level anomaly is noticed during January each year. Studies have indicated that this high is associated with the arrival of coastally trapped Kelvin waves (Bruce *et al.*, 1994; Shankar and Shetye, 1997; Shenoi *et al.*, 1999). The westward signal represents the offshore radiation of Rossby wave from these Kelvin waves as they propagate northwards along the west coast of India. The positive SSH from the eastern Arabian Sea is noticed upto ~ 65°E by April. In some years, for example in 1997, this positive anomaly extends upto ~ 60°E. During April/May, another high is observed in the western Arabian Sea (Fig.6.3) and remained stationary but protruded into the central Arabian Sea with time. Information on this aspect is quite meagre in the literature. This high is found to limit the westward propagation of the high formed off the west coast of India. With the onset of summer monsoon, i.e. in

June, negative SSH anomalies starts forming in the eastern Arabian Sea, which also shows westward movement. Shankar and Shetye (1997) attributed this westward movement to the propagation of Rossby waves. Thus a high and low in SSH are seen propagating westwards annually from the eastern Arabian Sea towards the central regions. The wavelet analysis of SSH (section 6.3.4) also reveals the dominance of annual periodicity in this region. Subrahmanyam *et al.* (2001) attributed the annual periodicity in the Arabian Sea to the annual Rossby waves.

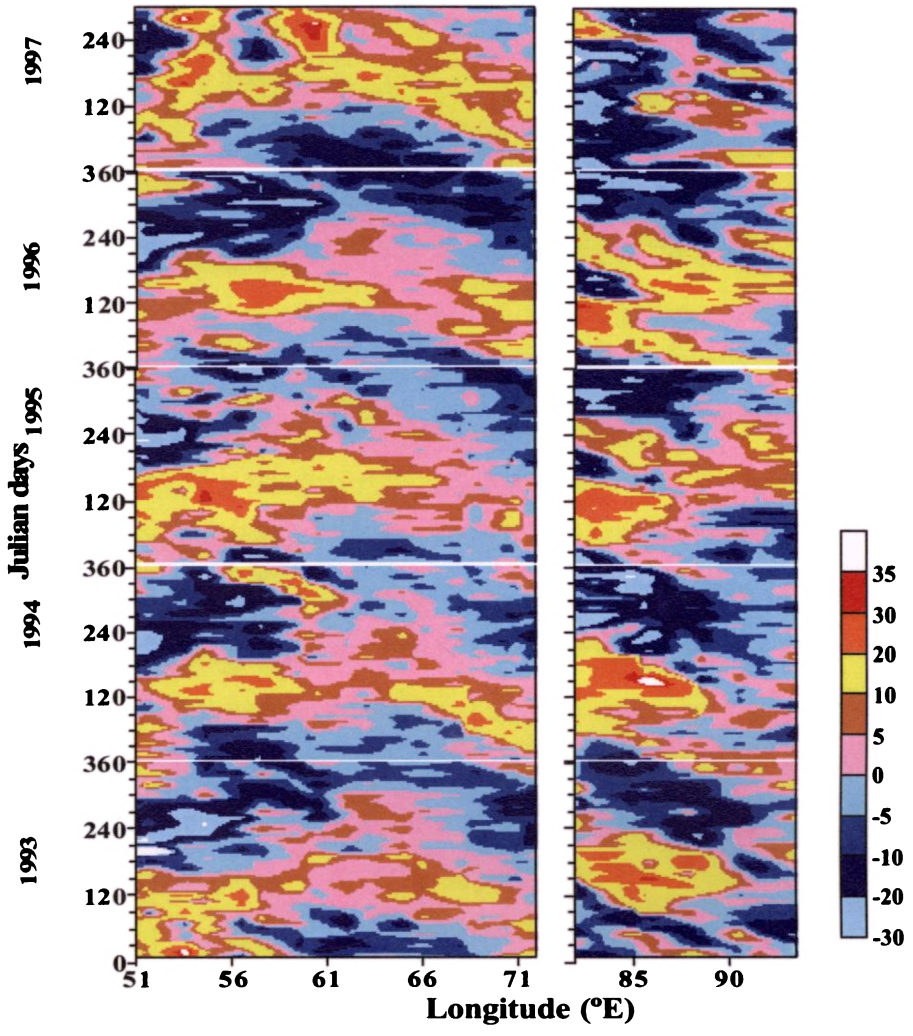

Fig.6.3 Hovmoller diagram of SSH (cm) anomalies along the 15° N. Y-axis is time in Julian days from January to December for the years 1993-1997

It is very difficult to confirm Rossby wave propagation in the Bay of Bengal along 15°N (Fig.6.3) because of the small basin dimension along this latitude. Therefore the features obtained may not be very clear in this region. However, the influence of remote forcing on the Bay circulation has been pointed out earlier (Yu *et*

al., 1991; Potemra *et al.*, 1991; McCreary *et al.*, 1993, 1996). Only in a few years the westward sloping positive SSH anomalies are seen continuous, probably associated with the radiation of Rossby waves (for example in May/June 1995 and 1996, Fig.6.3). In certain years (for example 1994, Fig.6.3), the positive SSH anomalies are seen prominent, either in the western or central Bay of Bengal. According to the model results of Han and Webster (2002), the sea level variability in the eastern and northern boundaries of the Bay were produced predominantly by the propagation of Kelvin wave from the equatorial region. Hareesh Kumar and Sanilkumar (2004) have also reported the same. Moreover, factors like fresh water discharge (UNESCO, 1988), narrow basin and formation of eddies (Sanilkumar *et al.*, 1997) in the northern Bay of Bengal also contributed significantly to the sea level variability. Along the western boundary, the coastal Kelvin waves, radiated Rossby waves and Bay wind (Han and Webster, 2002) contribute to the sea level varaibilty.

In the central Arabian Sea and Bay of Bengal, the SSH exhibited large inter-annual variability. Since the formation of SSH off the eastern boundaries of Ocean and its subsequent westward propagation is associated with the coastal Kelvin waves and Rossby waves, inter-annual variability in SSH can be attributed to the variability associated with these long period waves. These trapped Kelvin waves, which radiate Rossby waves westward from the coastal boundaries, carry energy from the Kelvin waves in the equatorial wave-guide (Potemra *et al.*, 1991; Yu *et al.*, 1991; McCreary *et al.*, 1993; Shankar and Shetye, 1997). Therefore, any changes in the wave characteristics in the equatorial region will reflect in the wave characteristics of central Arabian Sea and Bay of Bengal also. Further it is noted that the changes in the equatorial wave characteristics (Fig.6.2) are induced by the variability in the equatorial wind system (Figs.5.1-5.5), which can be due to El Nino or IOD events. Therefore one factor responsible for the SSH variability in the Arabian Sea and Bay of Bengal is the variability in the equatorial wind system.

The nature of SSH variability in the eastern Arabian Sea during 1994, and 1997 (Fig.6.3) seems to be almost of similar nature, and distinct from other years. The high sea level (>10 cm) associated with downwelling Kelvin wave are noticed from December onwards of the previous year and moves westwards with time. The speed of propagation is estimated to be 8.2 cm s^{-1} (from 72°E to 64°E between January and May) and 10.7 cm s^{-1} (from 72°E to 59°E between January and June) for 1994 and

1997 respectively. During 1993 and 1996, the positive SSH (of 5-10 cm) is noticed in the eastern Arabian Sea but its propagation is noticed upto 68°E from the eastern Arabian Sea. However, during 1995, the SSH is weak (< 5 cm) in the eastern Arabian Sea and propagation is also not clear. Similarly it is interesting to notice variability in the negative anomalies from the eastern Arabian Sea, which forms during June/July. The negative SSH (-10 cm) is prominent during 1996 and with a speed of nearly 8.2 cms^{-1} (from 72° to 58°E during July to February). While in all other years (for example during 1994 and 1997) even though the negative SSH (–10 cm) forms in the eastern Arabian Sea, it weakens (–5 cm) westwards.

The equatorial winds are found to be weak during 1994 (Fig.5.2), which lead to the weak downwelling Kelvin wave during April 1994 as discussed earlier. This weak downwelling Kelvin wave (Fig.6.2), which reach the west coast of India by late 1994 and early 1995, results in weak positive signals (< 5 cm) of the southwest coast of India (Fig.6.3). In spite of weak equatorial winds (< 2 ms^{-1}), IOD events and El Nino events during 1994 and 1997, the positive SSH from the eastern Arabian Sea is found to be prominent due to the strong downwelling Kelvin waves of previous year (i.e. formed in 1993 and 1996). The magnitude of the SSH is also strong in 1996 (Fig.6.3) corresponding to the strong downwelling Kelvin wave of 1995 (Fig.6.2), but confined in the eastern Arabian Sea. Model studies (Shankar and Shetye, 1997) showed that the negative SSH, off the southwest coast of India during the summer monsoon are affected by the upwelling favourable winds along the western Bay, along the southwest coast of India and the winds in the equatorial wave guide. The curl is cyclonic over this region during the summer monsoon. During the 1994 and 1997, the cyclonic curl extension (0.005 $x10^{-5}$-0.01 $x10^{-5}$ Nm^{-3}) over the southern tip of India changes to anti-cyclonic (Figs.5.7 & 5.10) in November, while during other years, its value is higher and remains over the coast and tip of India during October/November (Figs.5.6, 5.8 & 5.9) also. This also could have favoured the positive SSH in 1994 and 1997 in the eastern Arabian Sea. The prominent (< -10 cm) negative SSH in the eastern Arabian Sea during 1996 can also be associated with strong upwelling favourable winds along the west coast of India (Fig.5.4) noticed during 1996 April/May. The cyclonic wind stress curl (Fig.5.9), which favours upwelling, was also found comparatively higher (0.15 $x10^{-5}$-0.02 $x10^{-5}$ Nm^{-3}) during the summer monsoon of 1996 along the southern tip of India upto 15°N.

Thus the inter-annual variability of SSH in the Arabian Sea along 15°N is found to be influenced by the equatorial downwelling Kelvin wave of the previous year, remote and local winds and wind stress curl. Moreover, it is also found that the wind stress curl contributes significantly to the observed variability in the negative SSH during the summer monsoon months.

In the western Arabian Sea (Fig.6.3), high sea level, which is non-propagating, is noticed between November and May. Hareesh Kumar and Sanilkumar (2004) have also noticed the occurrence of a high in the western Indian Ocean during February to May. But in some years, this high is noticed in the offshore region for a short period even after the onset. This high extends into the central Arabian Sea and meets the high propagating from the eastern Arabian Sea during April/May in the central Arabian Sea (around 60°E). As the data is available only from January 1993 onwards, the formation of the high in the western Arabian Sea could not be explained for this year. However, this high is found to extend to 60°E between April and June. For 1993-1994, the high forms in the western Indian Ocean in November 1993, and other features like its duration, extension (~58°E) into the central Arabian Sea remain the same as the case of 1992-1993. During 1994-1995, the high forms only in December 1994, i.e. with a lag of one month compared to the previous year. This high is noticed upto June 1995 and it extends much eastward i.e. upto 67°E. Probably, this may be due to the weak westward propagating signals from the west coast of India during this year (Fig.6.3). The high formed during December 1995 extends to 63°E between April and May 1996, with a comparatively higher sea level (>10 cm). During 1997, the high appears from November onwards and is noticed during June 1997 also and extends only upto 58°E and this year, the high from the eastern Arabian Sea is also prominent. .

So, in the years when the Rossby wave propagation from the west coast of India are strong, the eastward extension of the high is limited to west of 58°E and when it is weak it extends even upto 67°E.

The wind and its curl are utlized to explain the formation of the high. Over the Arabian Sea northeasterly winds (Figs.5.1-5.5) prevailed during the northeast monsoon season weakens by April and is replaced by southwesterlies by May. The wind stress curl suggests negative values in this region during the northeast monsoon

season (Figs.5.6-5.10). This northeasterly winds along with the negative (anti-cylconic) curl favour anticylonic circulation (downwelling) in the western Arabian sea and hence results in the formation of high sea level. With the onset of southwest monsoon, i.e. by June, the curl changes to positive favouring upwelling in this region, which explains why the high sea level disappears by June. However, in certain years, for example in 1994-1995 and 1996-1997, though positive curl is noticed in the coastal regions during June, negative curl is observed in the offshore regions of the Arabian coast. Probably this might have resulted in the occurrence of positive sea level in this region during June 1995 and 1997.

The observed variability in the SSH anomalies along 15°N (Fig.6.3) are more in the Bay of Bengal compared to the Arabian Sea (Fig.6.3). Along this latitude in some years, positive SSH is noticed in the eastern Bay of Bengal, during May/June and November/December and in certain years this is clear only either in May/June or in November/December. The formation of this high can be associated with the arrival of downwelling Kelvin waves formed in the equatorial region during the transition months (Fig.6.2). This high reaches the east coast of India by August/September and February/March next year respectively, suggesting a speed of ~ 12 cms^{-1}. The speed of westward movement of this high corresponds to the speed of Rossby waves of this latitude (Chelton and Schlax, 1996). As discussed earlier, the downwelling Kelvin waves are weak during 1994 and 1997, due to weak equatorial wind field during the transition periods. Moreover, the northeasterly winds over the Bay of Bengal are weak (4 ms^{-1}) and southwesterlies are strong (8 ms^{-1}) in these years (Figs.5.1-5.5). Probably this might have resulted in the weak SSH anomalies in the eastern Bay of Bengal in these years (Fig.6.3). During 1995 and 1996, when the downwelling Kelvin waves are stronger (Fig.6.2), the high anomalies are also comparatively stronger (SSH> 10 cm) and westward movement is prominent from the eastern to western Bay of Bengal.

6.3.3 Hovmoller diagrams along south Indian Ocean

Hovmoller diagram of SSH along 15°S (Fig.6.4) and 20°S (Fig.6.5) latitudes are prepared to study the characteristics of the propagating waves in the southern hemisphere. The wave propagation is clearly seen along both these latitudes. Along 15°S (Fig.6.4), the positive SSH lay as diagonal strands extending from eastern to western Indian Ocean (between 120°-55°E). In the eastern regions, positive SSH is

noticed every year during March. This high sea level shows westward propagation and reaches the western Indian Ocean in January/February of the third year. This shows that this wave takes almost two years to travel from the eastern boundary to the western boundary, which suggests an approximate speed of 12.7 cm s^{-1}. The speed agrees well with the speed of the Rossby waves as reported by Subrahmanyam *et al.* (2001) for the same latitude. In the eastern Indian Ocean, the formation of positive SSH in March and negative SSH in September, suggests an annual periodicity in the SSH anomaly. This fact is supported by the wavelet analysis (section 6.3.4) also. These positive and negative SSH are very prominent in the southern Indian Ocean in certain years, while they are not well developed during other years. Along 20°S (Fig.6.5) positive anomalies are noticed propagating from the eastern Indian Ocean during April/May and reaches the western Indian Ocean in March of the third year taking almost two years to cross the Ocean. Here also, large inter-annual variability is noticed in the SSH anomalies. It is interesting to notice, the propagation of positive anomalies from the eastern Indian Ocean in November/December also during 1995 and 1996. Such signals are noticeable along 15°S also during the same period (Fig.6.4), though it is more clear along 20°S.

The sea level high forms in the eastern Indian Ocean in March/April 1993 (Fig.6.4), reaches the western Indian Ocean in January 1995, suggesting an average speed of 12.6 cm s^{-1}. During 1994, the sea level high starts forming in the eastern Indian Ocean in February, but the westward propagation is noticed only from March/April onwards. The SSH anomaly is found to be less (~5 cm) compared to 1993, especially in the regions between 85° and 100°E and near the western Indian Ocean. The SSH (5 cm) anomaly during 1995 May is weak from the eastern to western Indian Ocean. It is to be noted that compared to other years, the southeast trade winds (Fig.5.3) are weak (6 ms^{-1}) (Fig.5.3) and confined more southward (south of 15°S) between January and pre-monsoon months of 1995. Woodberry *et al.*, (1989) has observed annual Rossby waves propagating in the shear zone between south equatorial current and south equatorial counter current using a wind driven numerical model. Hence, any changes in this wind field can affect the currents and hence the Rossby wave propagation. This could be one possible reason for the weak SSH during 1995. But during 1996, the positive SSH of more than 10 cm are found propagating westward continuously from the eastern boundary. In this year, the magnitude of

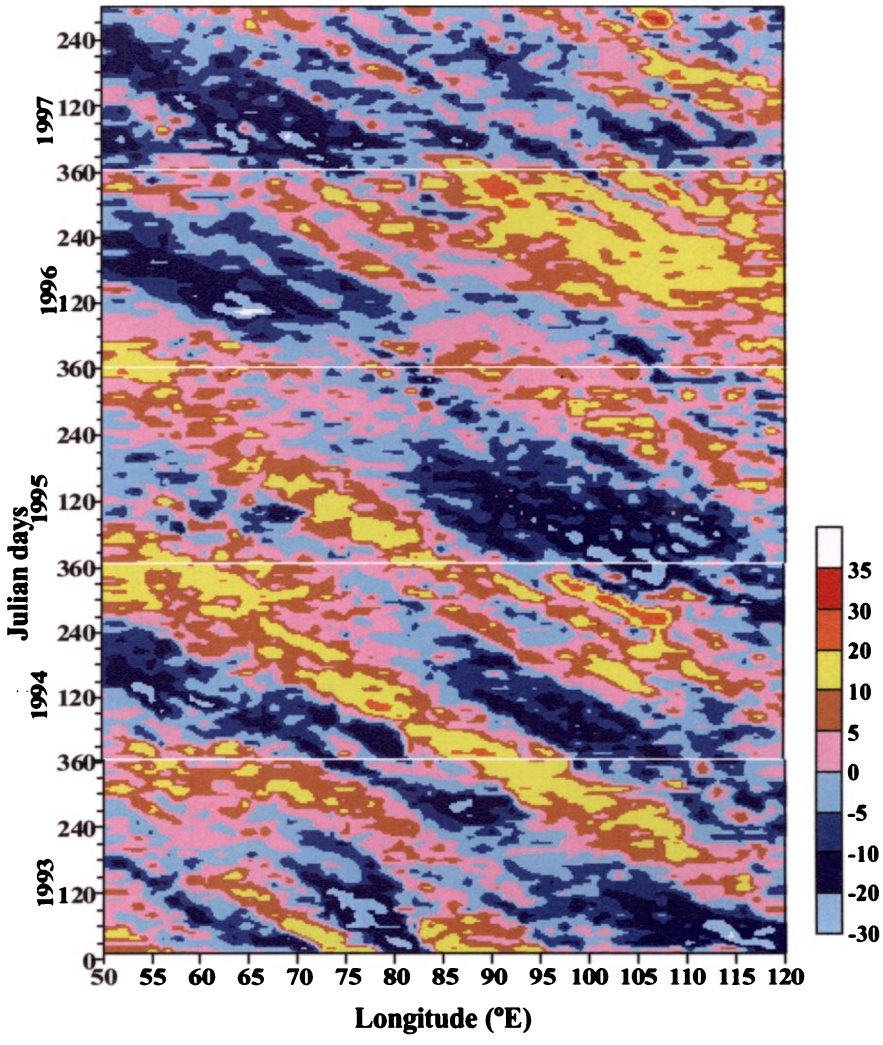

Fig.6.4 Hovmoller diagram SSH (cm) anomalies along the 15°S. Y-axis is time in Julian days from January to December for the years 1993-1997

southeast trade winds (Fig.5.4) are higher (> 7 ms^{-1}) from January onwards compared to other years and also the downwelling Kelvin waves are prominent in the equatorial region during April/May (Fig.6.2). Both this might have contributed together for the high values of positive SSH anomalies in the eastern Indian Ocean during 1996. However, these westward propagating high SSH during 1996 is noticed to be weak in 1997 in the regions west of 85° E. The negative SSH signals (-10 cm) formed in the eastern Indian Ocean during August 1993 (Fig.6.4), reaches the western Indian Ocean by April/May 1995. The negative anomaly weakens west of 85°E (from September 1994). This may be due to decrease in the magnitude of the southeast trade winds (Fig.5.2) during September 1994 (from 8 ms^{-1} in August to 6 ms^{-1} during September). The negative sea level formed during 1994 (August) is more prominent (~-20 cm)

between 115°E to 85°E. Negative SSH anomalies are weak during 1995. The changes noticed around 85°E in almost all the years may be due to the 90 East ridge.

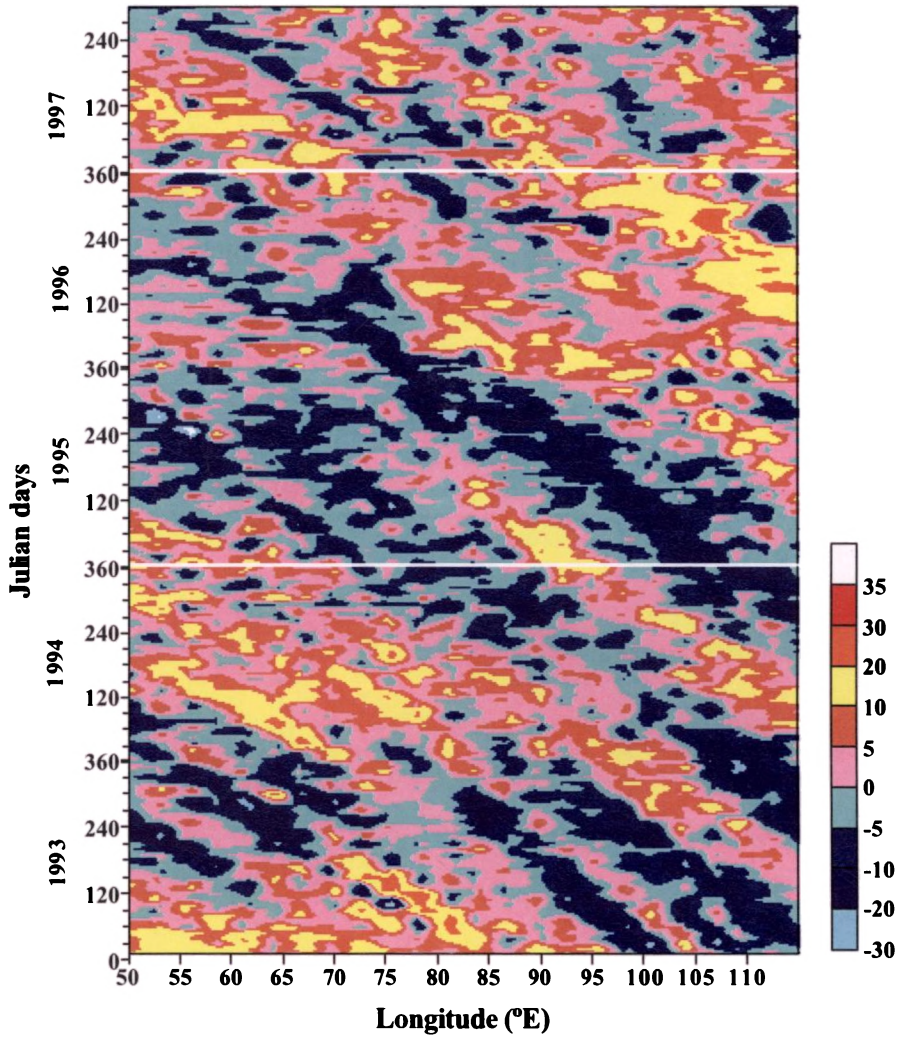

Fig.6.5 Hovmoller diagram of SSH (cm) along the 20° S. Y-axis is time in Julian days from January to December for the years 1993-1997

Along 20°S, the positive and negative SSH propagates westwards from the eastern boundary during April/May and July/August (Fig.6.5) respectively in almost all years. The positive SSH during 1994, appears early from March onwards similar to that along 15°S, but is weak west of 75°E. The negative SSH during July/August 1994, is also strong. The positive SSH from the eastern Indian Ocean during April 1995 is noticed to be prominent along 20°S contrary to that along 15°S. This can be due to the extend of the core of the southeast trades southward during this year (Fig.5.3), discussed earlier, might have favoured the formation and propagation of the

high SSH at this latitude. But the negative SSH is weak and is noticed to propagate in September. However, it is interesting notice the propagation of another positive SSH during November/December 1995 from the eastern boundary. Anomalous positive signals of downwelling Rossby waves similar to that along 15°S are also noticed along 20°S during 1996 and persisted in the eastern Indian Ocean till August.

6.3.4 Time series analysis

Hovmoller diagrams of SSH (Figs.6.2-6.5) clearly revealed the various characteristics of the propagating waves and their large spatio-temporal variability. Some of the variations are found to be rhythmic while some are random. In order to understand the prominent rhythmic oscillations embedded in the SSH at various locations, Wavelet decomposition method is employed (Figs.6.6 & 6.9). The prominent harmonics obtained are in the band of 20-30 day, ~ 60 day, 3-4 months, semi-annual, annual and above annual. Oscillations in the band of 20-60 days are combined together and termed as Intra-seasonal oscillation (ISO). Significance test are also carried out on this data (Figs.6.7 & 6.10). Finally, results from the wavelet analysis are compared with the power spectrum analysis (Figs.6.8 & 6.11).

Along the equator (Fig.6.6) the prominent harmonics are in the bands of ISO, 3-4 months, 6-7 months and ~1.6 year periodicities. In all the harmonics, large spatial as well as temporal variability is noticed, with maximum variability (15 cm) in the eastern (0°, 93°E) and minimum (< 5 cm) in the central Indian Ocean (0°, 76°E). In general, energy in the ISO band is maximum in the eastern equatorial Indian Ocean during 1994 (7.5 cm) and 1997 (15 cm) and minimum (<5 cm) in the western equatorial Indian Ocean in all the years. Both El Nnino and IOD also were reported during 1994 and 1997. The transition winds also shows variability from other years during 1994 and 1997 with weak westerly winds and even easterlies noticed over the equatorial region (Figs.5.1-5.5). This probably explains the large variability observed in the amplitude of the harmonics during these two years from other years. Kindle and Thompson (1989) has reported the 20-30 day oscillations in the ISO band in the equatorial Indian Ocean region due to Yanai waves, related to the instabilities in the western boundary circulation. Sengupta *et al.* (2001) has attributed the ISO in the central equatorial region to unstable currents, the instability occurring when the Rossby waves propagating from the eastern Ocean encountered the local eastward

mean flow. ISO band in the ocean can also arise due to Madden and Julian oscillation (MJO) in the atmosphere (Mysak and Mertz, 1984). In the bands of 3-4 months and semi-annual harmonics, maximum amplitude is noticed in the eastern Indian Ocean during 1995 (>7.5 cm) and minimum during 1994 and 1997 (< 5 cm). In the western Indian Ocean, also the maximum amplitude in the bands of 3-4 month and semi-annual is noticed during 1995 (10 cm) and minimum during 1994 and 1997. This maxima and minima can be clearly seen in the Hovmollor analysis also (Fig.6.2). However, in the central Indian Ocean the 3-4 month harmonic is found to have maximum amplitude during 1994 (7.5 cm).

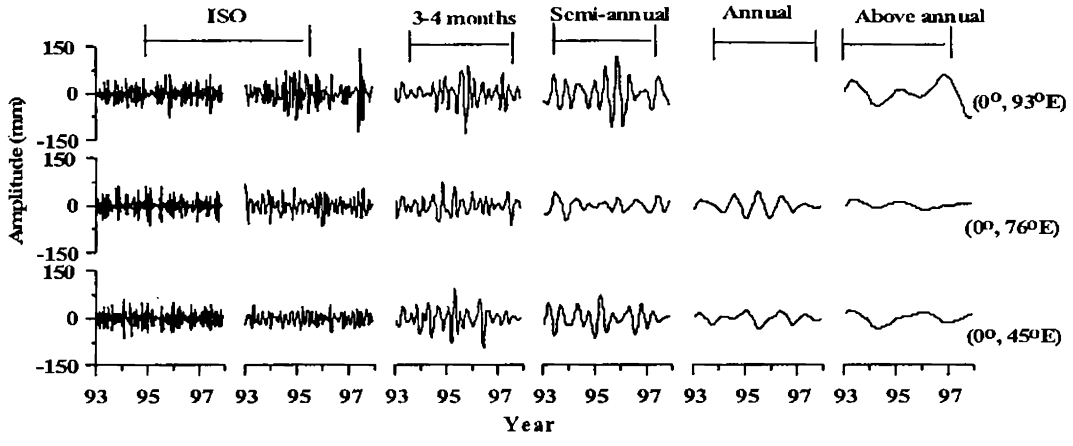

Figure 6.6 Decomposed wavelets in the equatorial region

Semi-annual periodicity is attributed to the semi-annual reversal of winds in the equatorial region during March/April and October, which can lead to the formation of semi-annual downwelling Kelvin waves. In the equatorial region, the 3-4 month harmonic can arise due to the eastward sloping of thermocline caused by semi-annual downwelling Kelvin waves and its restoration to normal after its passage. As explained earlier El Nino and IOD events occur in the years 1994 and 1997. So the minimum variability in the 3-4 month and semi-annual band can be due to prevailing weak wind field and weak equatorial Kelvin waves. Moreover, the equatorial winds are also very weak during the transition period. In the annual band, the maximum variability (5 cm) is found in the central Indian Ocean compared to other regions. The annual signal corresponds to along shore monsoonal winds in the equatorial region (Clarke and Liu, 1993).

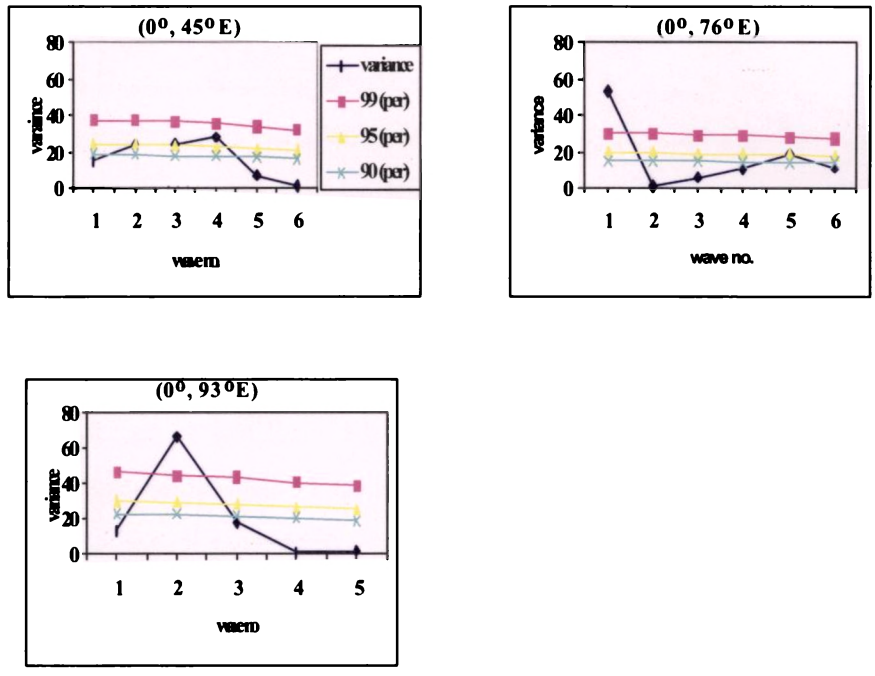

Fig. 6.7 Confidence limits of the prominent harmonics in the equatorial region. X axis represents the prominent harmonics (above annual (1), annual (2), semi-annual (3), 3-4 months (4), 60 day (5) and 30 day (6), annual absent for eastern Indian Ocean)

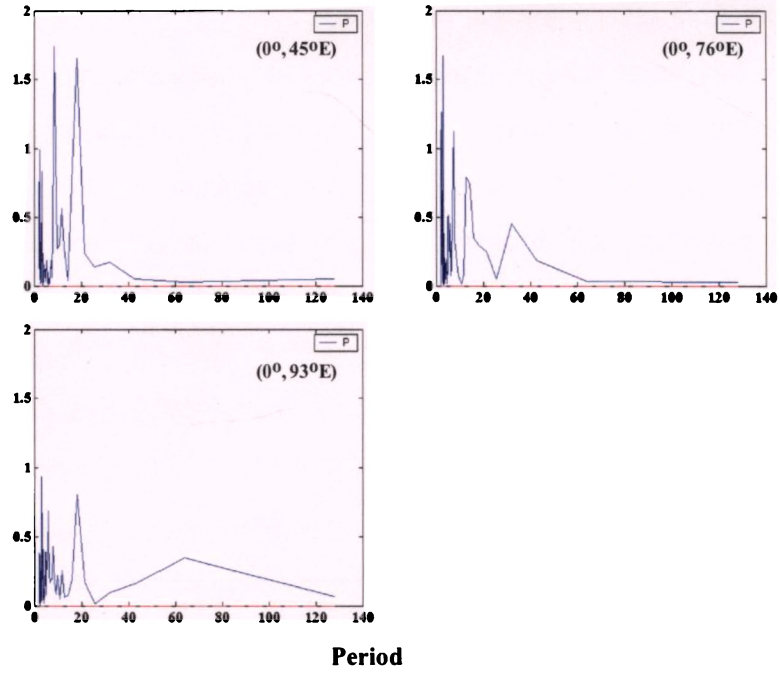

Fig.6.8 Power spectrum estimate of SSH field in the equatorial region

Statistical test (Fig.6.7) reveals the prominence of semi-annual periodicity in the eastern Indian Ocean at 99% confidence limit, which is also supported by power

spectrum (Fig.6.8) analysis. The other signals are found to be less significant below 80% confidence level. This is because the semi-annual component dominated in the signal and contained much energy than any other signals. Therefore, this low frequency was filtered and significance test carried out again. Then, the ISO was found to be significant at 95% confidence level. In the western equatorial Indian Ocean, annual, semi-annual and 3-4 months are dominant at 95% confidence limit, which is supported by the power spectrum also.

In the central Arabian Sea and Bay of Bengal (Fig.6.9) also, prominent harmonics are noticed in the bands of ISO, 3–4 months and 1 year periodicities. In the south Indian Ocean, in addition to these harmonics, another harmonic with biennial periodicity is also observed. In these regions, the most notable observation is the absence of semi-annual periodicity. In all the harmonics, maximum energy is noticed in the Bay of Bengal compared to the central Arabian Sea. Here, annual and 3-4 months harmonics are found to be more prominent.

In the central Arabian Sea, (Fig.6.10) annual periodicity is found prominent at 90% confidence limit, while the power spectrum (Fig.6.11) revealed the dominance of annual and 3-4 month. Brandt *et al.* (2002) attributed the annual periodicity in SSH in the Arabian Sea to the annual Rossby waves. Yu *et al.* (1991) suggested that these annual Rossby waves are produced by the coastally trapped Kelvin waves formed by the equatorial wind and by the Bay winds. In the central Arabian Sea (15°N. 65°E), annual harmonic shows maximum amplitude (5 cm) during 1994, 1995 and 1997 (Fig.6.9). The Hovmoller diagrams (Fig.6.3) revealed the maximum amplitude of positive SSH in the eastern Arabian Sea during 1994 and 1997, and during 1995 in the western Arabian Sea. As seen earlier, the Kelvin waves formed in the equatorial region (Fig.6.2) reached the central Arabian Sea (Fig.6.3) only in the next year. This is the reason why no minima is observed during 1994 and 1997 in the central Arabian Sea corresponding to the El Nino and IOD events. Moreover, strong winds in the equatorial region during the 1993, causing the formation of strong Kelvin waves, reaches the central Arabian Sea in 1994, which can be seen as a significant peak. In the 3-4 month band, maximum variability is noticed during 1993 and 1994 (~10 cm) and minimum during 1996 (< 2 cm). The ISO is having maximum amplitude (>50 mm) during 1994 and 1997 in the Arabian Sea.

In the western Bay of Bengal (Fig.6.9), oscillations in the 3-4 months and annual periodicities dominate. Wavelet analysis revealed 3-4 months to be significant (Fig.6.10) at 95% confidence limits. Power spectrum (Fig.6.11) also supported this with an additional annual periodicity also to be prominent.

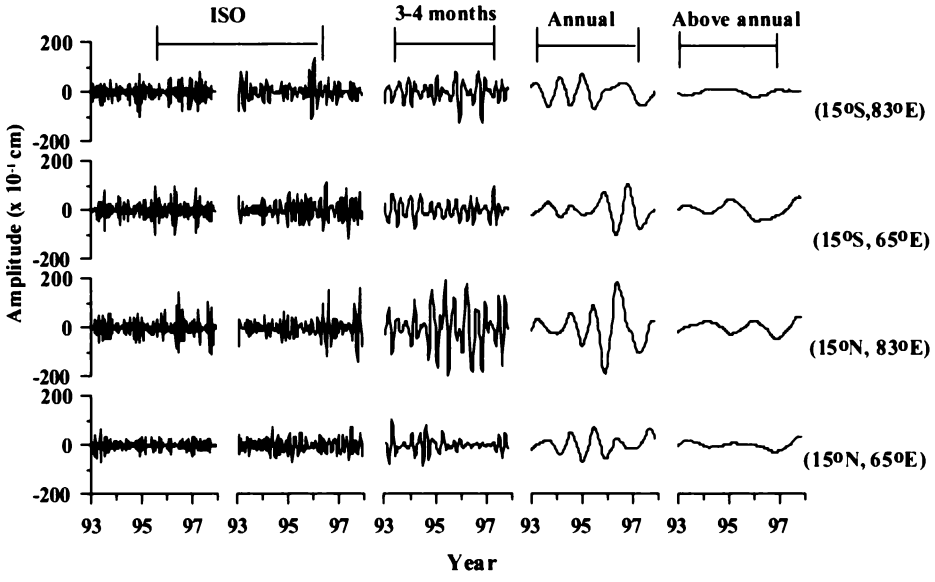

Figure 6.9 Decomposed wavelets in the northern Indian Ocean and southern Indian Ocean

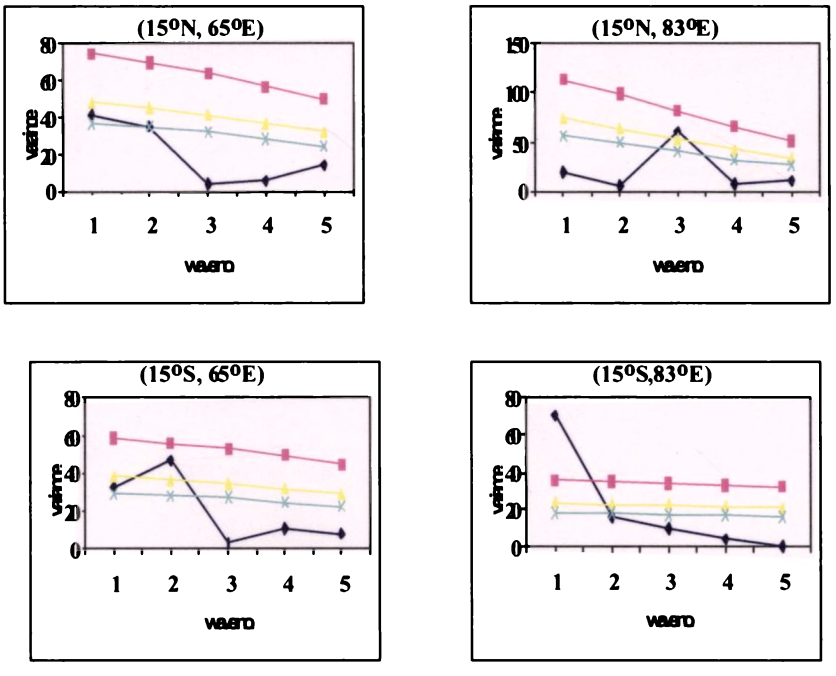

Fig. 6.10 Confidence limits of the prominent harmonics. X axis represents the prominent harmonics (above annual (1), semi-annual (2), 3-4 months (3), 60 day (4) and 30 day (5), annual absent)

In the Bay of Bengal, maximum amplitude is noticed in the annual harmonic during 1996 (~20 cm) and minimum during 1993 (< 5 cm). The 3-4 month band is maximum during 1995-1996 (~20 cm) and minimum during 1993 (< 5 cm). The ISO band shows maximum amplitude during 1996 (15 cm) and 1997 (15 cm).). Bay wind as well as the equatorial wind has a comparable role in causing sea level variability along the western Bay as noticed earlier (Han and Webster, 2002). During 1993, 1995 and 1996, the Bay winds (northeasterlies) and equatorial (westerly) winds were strong (Figs.5.3 & 5.4) compared to other years. These factors act as remote forcing as well as local forcing in causing the sea level variability. In addition the western Bay is very much complicated due to fresh water discharge. All these factors might have contributed here for the observed variability in this location.

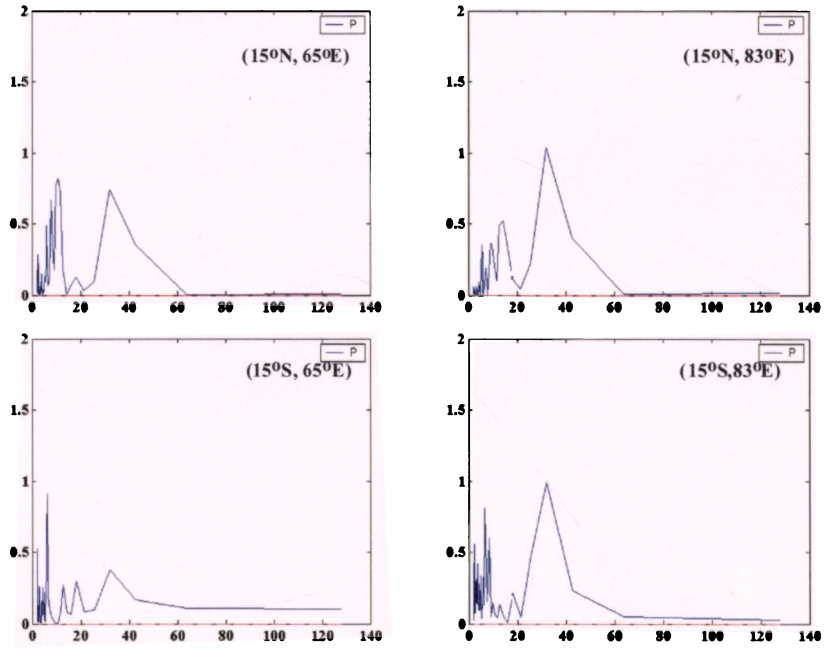

Fig.6.11 Power spectrum estimate of SSH field

Wavelet analysis in the western and central regions of the southern Indian Ocean (Fig.6.10) shows the dominance of annual and nearly two-year periodicity at 90% confidence limits. Power Spectrum (Fig.6.11) analysis also reveals the same. The above annual harmonics are not obtained in power spectrum (Fig.6.11) due to limited number of data sets (less than 5 years). Woodberry *et al.* (1989) and Morrow

and Birol (1997) suggested that the annual periodicity in the southern Indian Ocean corresponds to westward propagating Rossby waves from the eastern Indian Ocean.

Thus in this chapter, the influence of long period propagating Kelvin and Rossby waves in causing the sea level variability is discussed. The intra- and inter-annual variability of these waves are discussed in terms of the prevailing wind pattern in the equatorial and interior ocean. Studies (Potemra *et al.*, 1991; McCreary *et al.*, 1993; Subrahamanyam *et al.*, 2001) have demonstrated that these waves play an influential part in the generation and propagation of eddies in the ocean. The prominent eddies in the Indian Ocean and their inter-annual variability will be discussed in the next chapter.

Chapter 7

Oceanographic features obtained from satellite
Part 11 - Eddies

Chapter 7

Oceanographic features obtained from satellite
Part 11 - Eddies

7.1.Introduction

Arabian Sea and Bay of Bengal are well known for the occurrence of gyral circulation and eddies. During the southwest monsoon, when the Somali current migrates north of the equator, a southward return flow develops offshore and a Southern Gyre (SG), forms between 0°-5°N, 53°E (Bruce, 1973; Swallow *et al.*, 1983). Another eddy, the Great Whirl (GW) develops between 5° and 10°N, 58°E (Bruce, 1973; Swallow *et al.*, 1983). This constitutes the two gyre system in the Somali current region and has been explored earlier by many (Bruce, 1973; Schott, 1983). Local as well as remote forcing has been proposed as the mechanisms for the generation of these gyres and associated eddies. In some years, a third warm core eddy, the Socotra Eddy (SE) forms in late summer (Bruce, 1979; Bruce and Beatty, 1985: Fischer *et al.*, 1996) roughly between 10°-14°N and 54°-58°E. Bruce *et al.* (1994) noticed the formation of an anti-cyclonic eddy in the eastern Arabian Sea during the northeast monsoon period known as the Lakshadweep High (LH). Moreover, a Lakshadweep low (LL) appeared near the southwest coast of India during the southwest monsoon period (Shankar and Shetye, 1997).

Like the western Arabian Sea, the western Bay of Bengal is subjected to strong seasonal reversal of wind, which influences the East India Coastal Current (EICC). Here, compared to local winds, the remote forcing, particularly the Rossby waves propagating westwards from the coastally trapped Kelvin waves from the eastern Bay contribute much to the EICC variability (Shankar *et al.*, 1996; McCreary *et al.*, 1996). This region is also manifested by meso-scale eddies and propagating waves. Babu *et al.* (1991) has identified a subsurface cyclonic eddy in the northern Bay. Gopalan *et al.* (2000) noticed an anti-cyclonic eddy centered at 14°N, 83°E and a cyclonic eddy adjacent to it. They have also observed a cyclonic eddy northeast of Sri Lanka. Studies by Yu *et al.* (1991), McCreary *et al.* (1993) Shankar *et al.* (1996) and Subrahmanyam *et al.* (2001) suggested that planetary waves play major role in the generation and propagation of these eddies.

Earlier studies utilized limited hydrographic data and numerical models to study the meso-scale features in the Indian Ocean. Understanding of these features has considerably increased after the availability of satellite information, as they provide synoptic snapshots over the whole ocean at regular intervals. Studies are still

fragmentary in describing the monthly evolution of these meso-scale features. In this chapter, the main objectives are to map the various eddies in the Indian Ocean using Sea Surface Height (SSH) anomaly data. In addition, evolution of these eddies and their inter-annual variability is also discussed.

7.2.Data

The study region extends from 40° to 100°E and from 0° to 26°N. Details of the data utilized are already described in section 6.2 of Chapter 6. The processed SSH data from TOPEX/Poseidon (T/P) altimetry available at 10-day intervals at 0.5°x0.5° (latitude x longitude) grid is utilized here. The climatology of the region is presented by monthly ensemble averaged SSH for the years 1993-1997. Moreover, monthly anomaly maps for individual years are also prepared to study the evolution of eddies in detail. The wind and wind stress curl discussed in chapter 5 are also used to study their influence on eddies.

7.3.Results and Discussion

The propagating waves and eddies are the major features that influence the

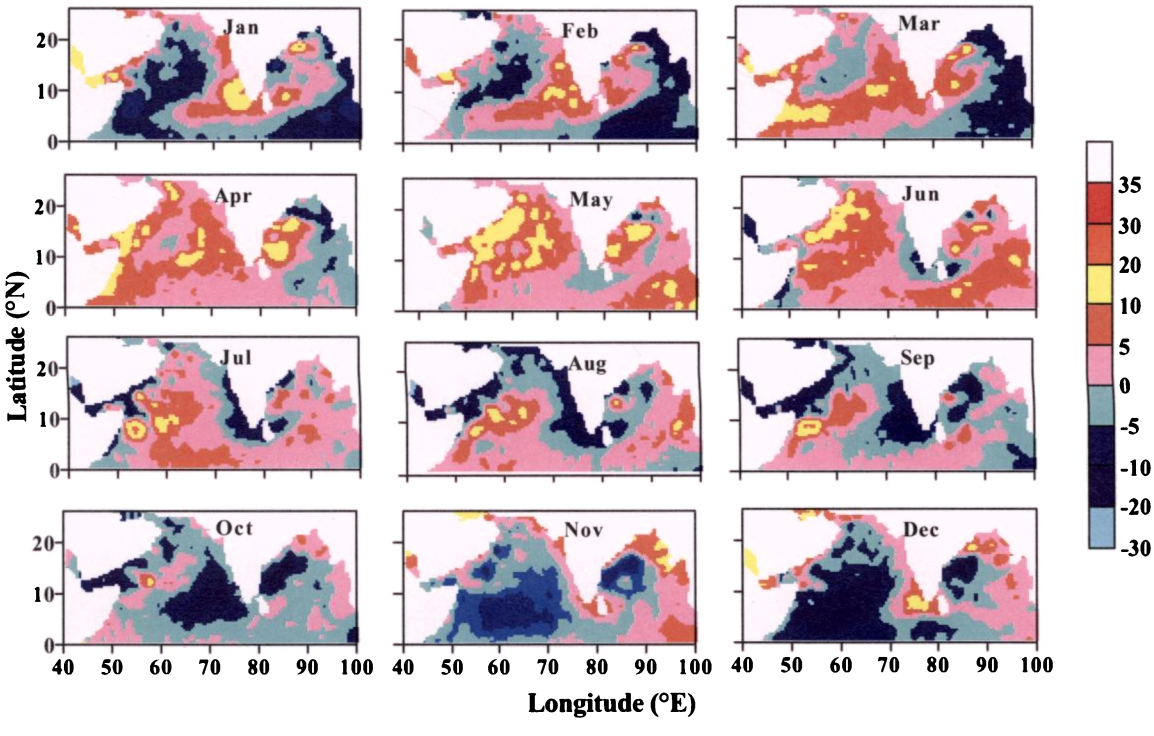

Figure 7.1. Ensemble averages of SSH (cm)

Indian Ocean circulation. In Chapter 6, the long period propagating waves in the Indian Ocean and their inter-annual variability were discussed. Here, main focus is on the various eddies in the Indian Ocean and their inter-annual variability. For this purpose, the monthly mean SSH anomalies in the Indian Ocean are presented Fig.7.1. The figure revealed many features, which include the Lakshadweep High (LH), Lakshadweep Low (LL), the anti-cyclonic high off the coast of Arabia, the anti-cyclonic eddies in the Somali basin and western Bay of Bengal and the cyclonic Sri Lanka dome.

7.3.1 Lakshadweep High (LH) and Lakshadweep Low (LL)

Studies (Bruce *et al.*, 1994, 1998; Shankar and Shetye, 1997; Shenoi *et al.*, 1999) have indicated that the LH, an anti-cyclonic circulating feature, forms off southwest coast of India during the northeast (winter) monsoon season. This high is noticed as a region of positive SSH from November onwards and evident upto April (Fig.7.1). The LH disappears with the formation of negative sea level associated with the LL in May. Similarly during the summer monsoon season, a region of cyclonic circulating feature known as the LL, forms in the eastern Arabian Sea. This region of negative sea level is noticed between May/June and October (Fig.7.1) and start dissipating from the west coast with the formation of LH in November. Both these features exhibit westward movement, associated with the Rossby wave radiation as suggested by Shankar and Shetye (1997). In the following section, the evolution of LH and LL in the eastern Arabian Sea during the years 1993-1997 is discussed.

7.3.1.1 Lakshadweep High

The monthly averaged SSH (Fig.7.1) clearly shows the formation of LH in November, off the southwest coast of India. The negative wind stress curl (< -0.01 $x10^{-5}$ Nm^{-3}) prevails in this region during the northeast monsoon period (Figs.5.6-5.10) favours the formation of this LH. Moreover, the arrival of downwelling Kelvin waves off the southwest coast of India during November can also favour the formation of the LH. This high (SSH>10 cm) is found to have its maximum dimension (>600 km) in January and propagates westwards with the progress of time. This high reaches the Somali coast in March and remains there till May. Studies have indicated that the westward movement of the LH is a consequence of radiation of Rossby waves from the coastally trapped Kelvin waves as they propagate northward

along the west coast of India (Bruce *et al.*, 1994, 1998; Shankar and Shetye, 1997; Shenoi *et al.*, 1999). The propagating anomalies in the Arabian Sea and Bay of Bengal associated with the coastal Kelvin wave showed large inter-annual variability (Fig.6.3, chapter 6). As the formation of LH is associated with these waves and the wind stress curl, their characteristics can also exhibit large inter-annual variability.

To study their inter-annual variability, the SSH anomalies for individual years from 1993 to 1997 are examined. From the figures (Figs.7.2-7.5), it can be seen that in all the years a high in sea level forms off the southwest coast of India during November. However, the region of formation, the dimension and the speed of westward propagation shows large variability. The high (>5 cm) formed off the southwest coast of India during November 1993 (Fig.7.2) is noticed at 8.5°N, 75°E in December 1993 and moves to 9°N, 74°E in January 1994. In January, the dimension of the eddy exceeds 500 km. From the westward movement, the estimated speed is 4.7 cm s^{-1} . This eddy splits into two anti-cylonic eddies of dimension ~ 400 km and 200 km with a cyclonic low in between. This high reaches Somali coast by April and starts dissipation afterwards. Shankar and Shetye (1997) suggested that the westward movement of this high is associated with the radiated Rossby waves. Hence, the westward movement of this high approximated suggests the speed of Rossby wave propagation.

During 1995 (Fig.7.4) and 1996 (Fig.7.5) also, the LH appear off the southwest coast of India in November. This high (Fig.7.4) is noticed at 8°N, 75°E in December 1995 and at 9°N, 73°E in January 1996, suggesting an approximate speed of ~9.4 cm s^{-1}. This anti-cyclonic eddy is having a diameter of more than 500 km in January 1996. The speed of the propagation is much greater than during 1993-94. During 1996 (Fig.7.5), the LH is noticed at 7°N, 76°E in December 1996 and moves to 8°N, 75°E by January 1997, suggesting a speed of ~6 cm s^{-1}. The dimension of this eddy is also found to exceed 500 km in January. Another notable observation during all these years is the formation of multiple eddies, slightly north of the first eddy. One such eddy is noticed during 1993-94 (Fig.7.2), in February 1994 near 15°N, 72°E. Two more anti-cyclonic eddies are noticed during 1995-96, in addition to the main

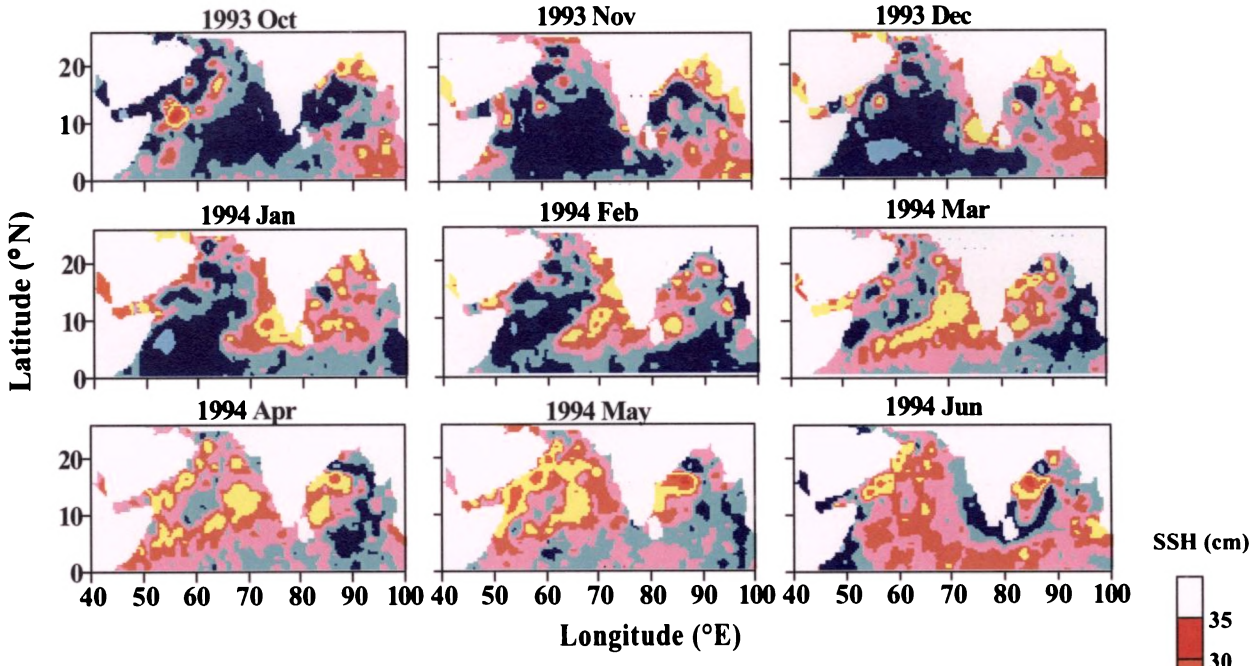

Fig. 7.2 Evolution of LH during 1993-1994

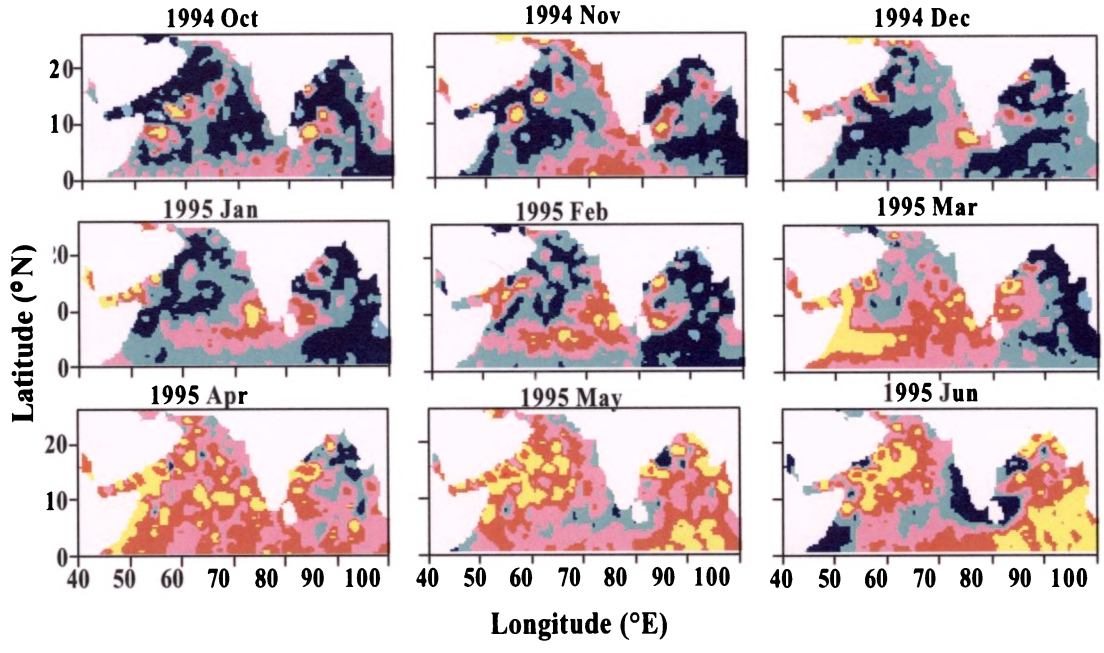

Fig. 7.3 Evolution of LH during 1994-1995

LH, one formed at 16°N in January and other also at 16°N, but in April. However, during 1996-97, the multiple eddies are found to form at different locations i.e. at 15°N, 71°E in January and at 11°N, 75°E in February. All these eddies are found to propagate westward with the progress of time. This propagation is found limiting to west of 68°E. All these highs are found to dissipate by May. Once the main LH

reaches the Somali region, the sea level all along the Somali region increases by more than 5 cm.

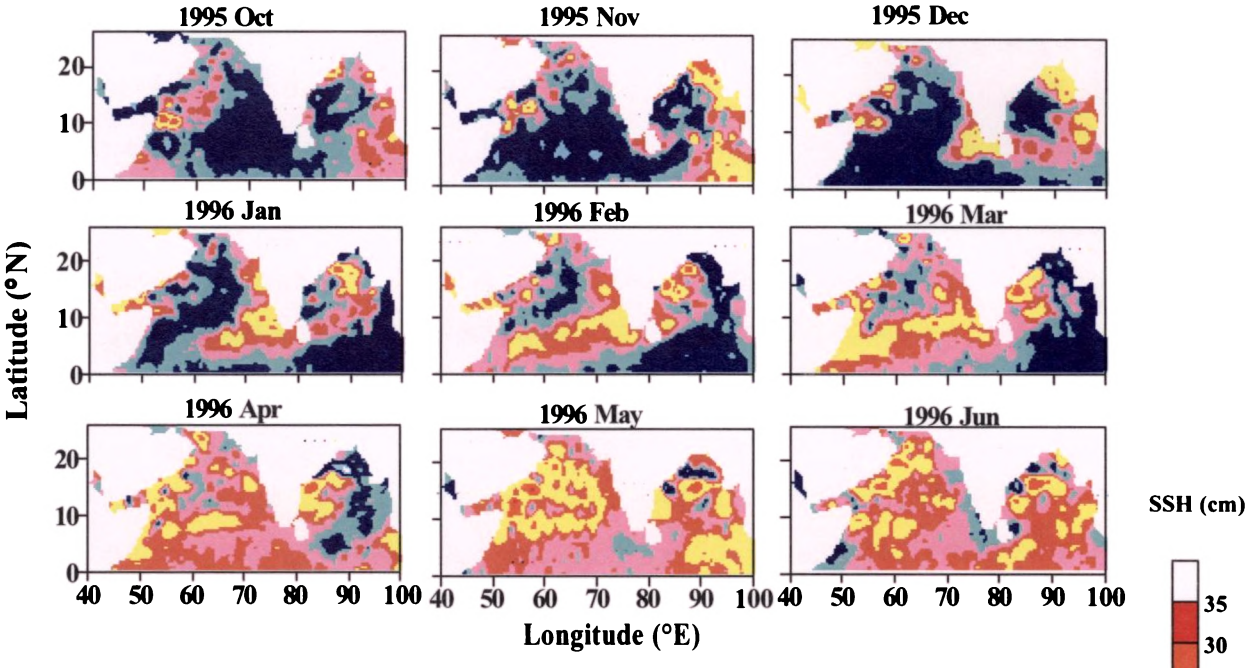

Fig. 7.4 Evolution of LH during 1995-1996

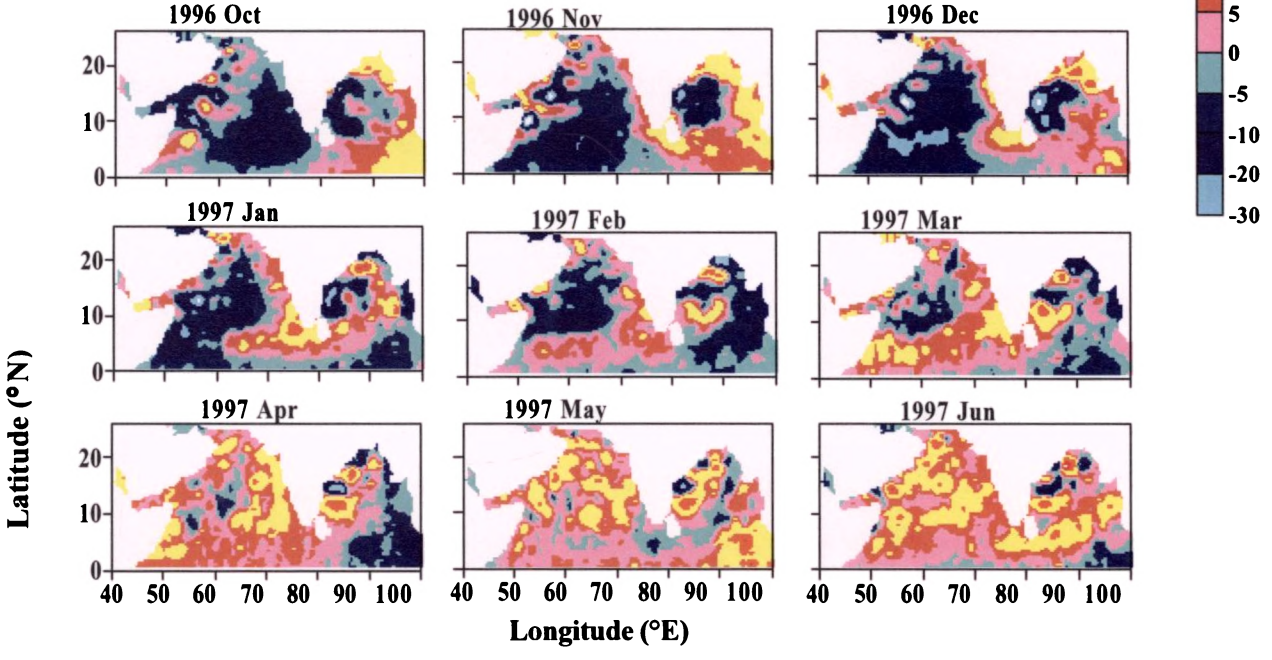

Fig. 7.5 Evolution of LH during 1996-1997

As observed in other years, the LH appears off the southwest coast of India in November 1994 (Fig.7.3) also, even though it is an El Nino year. The speed of propagation is 9.4 cms^{-1} (from 8°N, 75°E in December to 9°N, 73°E in January) is

also comparable to other years. Similarly, multiple eddies are also formed at 9°N, 75°E during February and April. The only difference observed in this year is the smaller dimension of the LH (< 200 km) compared to other years. This can be also be due to the weak coastal Kelvin wave formed from the weak equatorial Kelvin wave of April/May 1994 (Fig.6.2), which reaches there by 1994 November.

7.3.1.2 Lakshadweep Low (LL)

The LL is a region of low sea level formed off the southwest coast of India during the southwest monsoon season. The formation of LL is seen off the southwest coast of India from May onwards (Fig.7.1) from the appearance of negative sea surface anomaly in this region. The Kelvin wave formed during October in the equatorial region and the remote alongshore winds along the northern and eastern boundaries of Bay have a downwelling peak in June along the east coast of India (McCreary *et al.*, 1993). This signal is blocked at the surface by the strong upwelling signal forced by local alongshore winds (McCreary *et al.*, 1996). This upwelling signal also makes it way around the southern tip of India to the west coast. The positive wind stress curl (Figs.5.6-5.10) over the southwest coast of India during the summer monsoon also favours upwelling in the region. Shankar and Shetye (1997) has attributed the alongshore winds of southwest India, cyclonic wind curl off the southern tip of India, winds in the Bay of Bengal and the winds in the equatorial wave-guide to the formation of LL. It is to be noted that the LL also showed westward propagation with progress of time, which is associated with the radiation of Rossby waves from the coastal Kelvin waves (Shankar and Shetye, 1997). This LL starts dissipating from the west coast of India by November, with the formation of positive SSH anomalies associated with the LH (Fig.7.1).

The characteristics of LL shows similar pattern during 1993, 1995 and 1996 (Figs.7.6, 7.8 & 7.9). The years 1994 (Fig.7.7) and 1997 (Fig.7.10) behave typically compared to other years. During 1993, 1994 and 1995 (Figs.7.6-7.8), negative SSH (-5 cm) appears off the west coast of India during May, which intensifies (~ -10 cm) and moves westward. The low sea level extends to 60°E in October and by December, negative SSH occupied the whole Arabian basin (45° to ~75°E). However, during 1996 (Fig.7.9), the formation of the LL is found to be delayed by a month i.e. in June only, but reaches the Somalia region by November itself. In all the cases, the

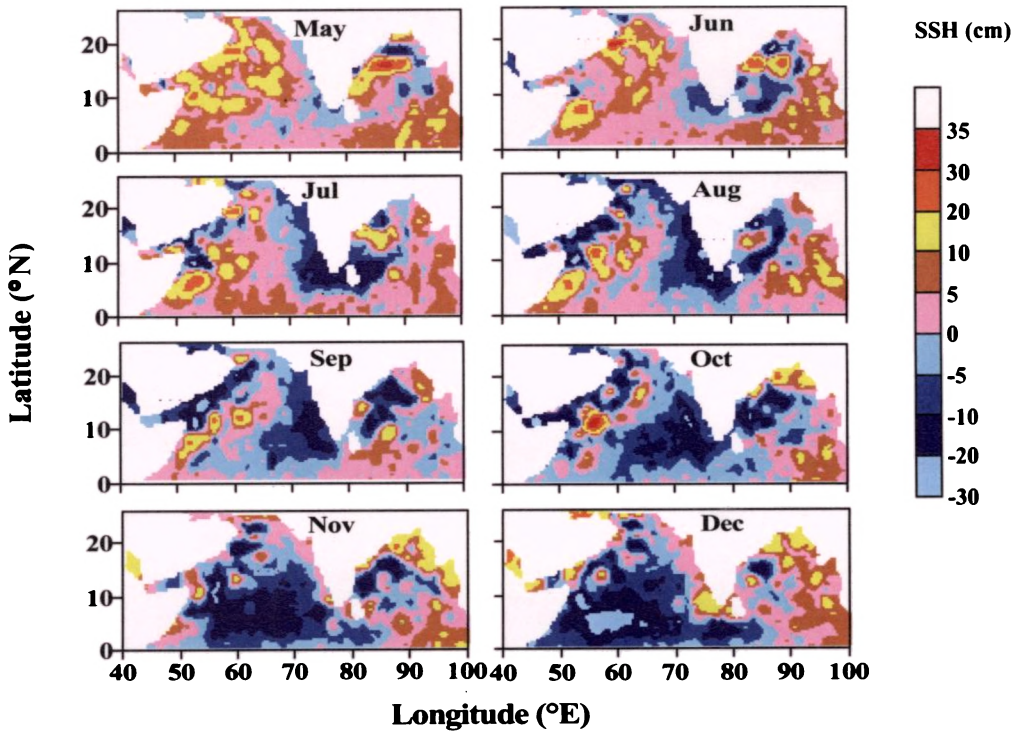

Figure 7.6. Evolution of LL during 1993

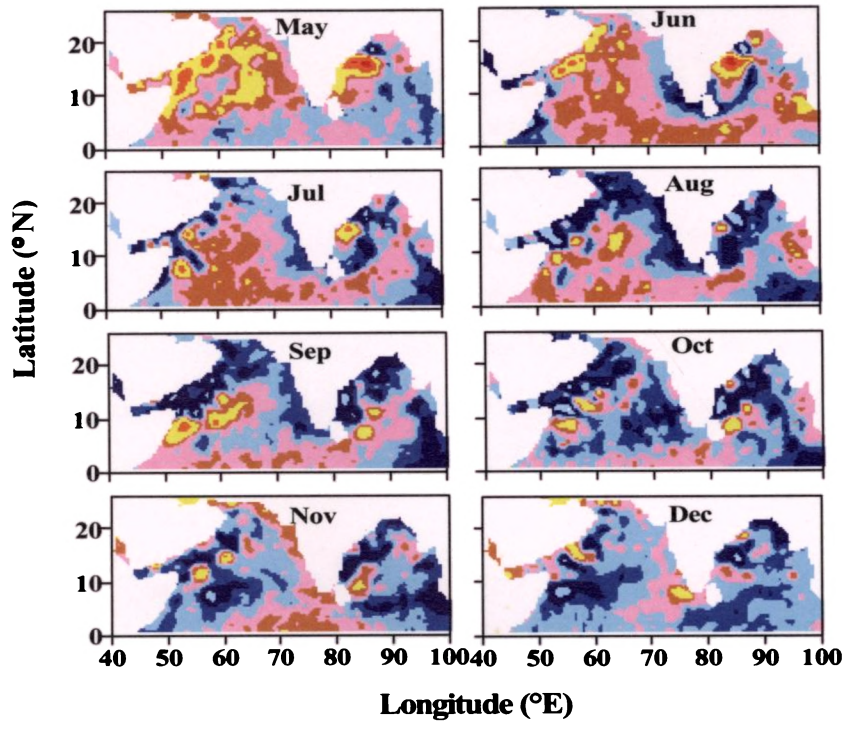

Figure 7.7 Evolution of LL during 1994

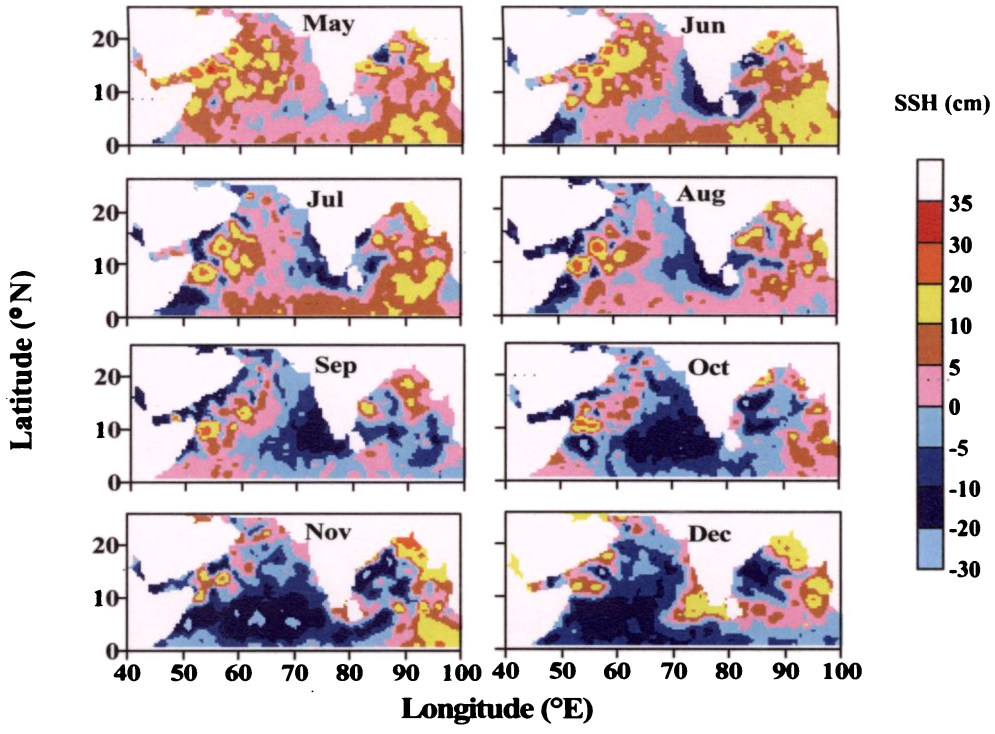

Figure 7.8 Evolution of LL during 1995

dissipation of the LL, starts with the formation of LH off the southwest coast of India, during November every year.

During 1994, LL is noticed between 5°-12°N and 50°-60°E in December, occupying much lesser area compared to other years (Fig.7.7). As the data is available only upto October during 1997, its lateral extension could not be estimated. However, it is seen upto 65°E from the eastern Arabian Sea during October. In all other years, the LL occupied the whole of the Arabian Sea from 40° to ~70°E. Saji and Yamagata (2003) reported considerable warming in the western Indian Ocean during 1994 and 1997, that continue upto September/October associated with the IOD event. This might have limited the westward extension of the LL thereby reducing its dimension in these years.

The wind stress curl for all the years (Figs.5.6-5.10) shows positive curl (0.02 $x10^{-5}$ Nm^{-3}) from May onwards over this region indicating the prevalence of cyclonic circulation, which also extends westward. The curl is positive over the west coast of India also. The change of this cyclonic wind stress curl to negative/anti-cyclonic off the tip of India by November itself also might have limit the westward extension of the low during 1994 and 1997.

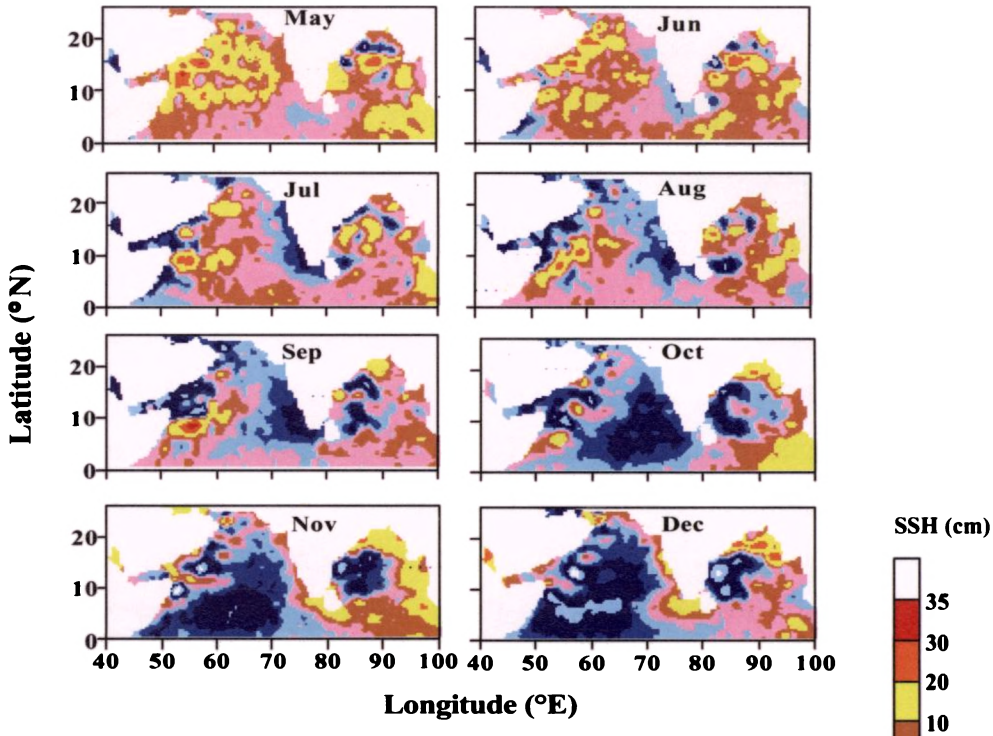

Figure 7.9 Evolution of LL during 1996

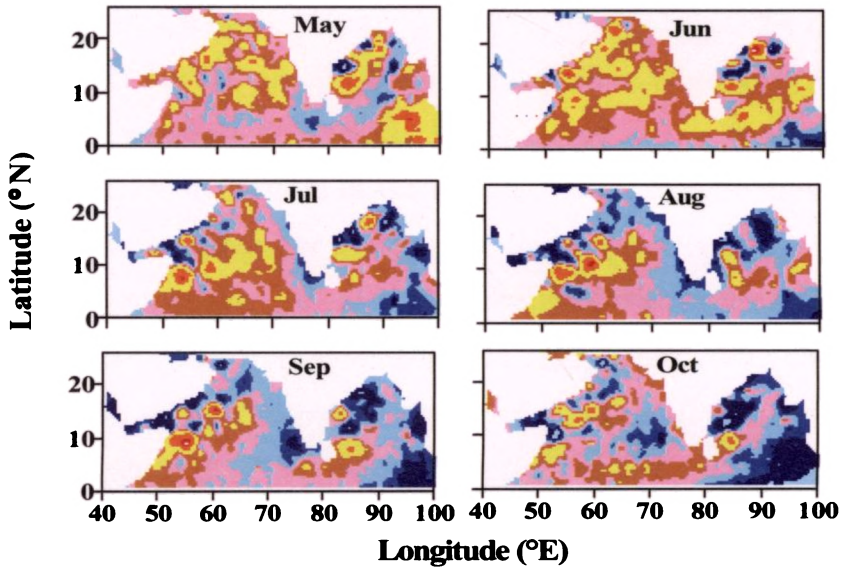

Figure 7.10 Evolution of LL during 1997

7.3.2 Arabian Anti-cyclonic High

In the northwestern Arabian Sea (Fig.7.1), a sea level high (10 cm) is observed from January onwards till May/June with its maximum magnitude during April/May. This is termed as the Arabian Anti-cyclonic High. Not many studies were carried out

to understand this Arabian Anti-cyclonic High. Recently, Hareesh Kumar and Sanil Kumar (2004) reported the occurrence of this high in the western Arabian Sea. This high does not show any propagating nature, but is found stationary. This high extends all along the Arabia coast and laterally up to 65°E (Fig.7.1). The analysis of the wind field (Fig.5.1-5.5) and its curl (Fig.5.6-5.10) during the northeast monsoon, favours downwelling in this area and persisted upto May. This downwelling process cause high sea level in this area resulting in the formation of the Arabian Anti-cyclonic High. The wind stress curl suggested anti-cyclonic circulation over this region during northeast monsoon up to May. Both this favour downwelling process and constitute a reason for the formation of this Arabian Anti-cyclonic High. This high sea level and its subsequent extension towards the interior Arabian Sea, plays a significant role in limiting the westward propagation of the sea level high formed off the west coast of India, as noticed from the Hovmoller diagram along 15°N (Fig. 6.3) The high starts dissipating by the onset of summer monsoon, i.e. in June. The dissipation of this Arabian high might have been initiated by the occurrence strong southwesterly winds during May/June (Fig.5.1-5.5) and associated coastal upwelling.

During 1993, the positive sea level (5-10 cm) appear off the coast of Arabia and Gulf of Aden from January (figure for January not presented) onwards and attains its maximum dimension (15°-20°N and SSH >10 cm) during April/May (Fig.7.11). Many multiple highs are noticed in the western Arabian Sea (north of 10°N) during May. With the onset of summer monsoon i.e. by June, these positive anomalies start dissipating, and are replaced by negative anomaly. Similar pattern is noticed during 1994 and 1996 also. However, during 1995 and 1997, the Arabian Anti-cyclonic High is noticed in June also. The distribution of wind stress curl (Figs.5.6-5.10) suggested the change of negative (-0.015×10^{-5} Nm^{-3}) to positive (0.015×10^{-5} Nm^{-3}) curl during May off the Arabia coast. By June, in all the years, except 1995 and 1997, cyclonic curl extends over the northwestern Arabian Sea. During the years, 1995 and 1997 (Figs.5.3 & 5.5), the anti-cyclonic curl (-0.01×10^{-5} Nm^{-3}) continue to exist in the offshore regions in June also, which might have caused the occurrence of this high in June also.

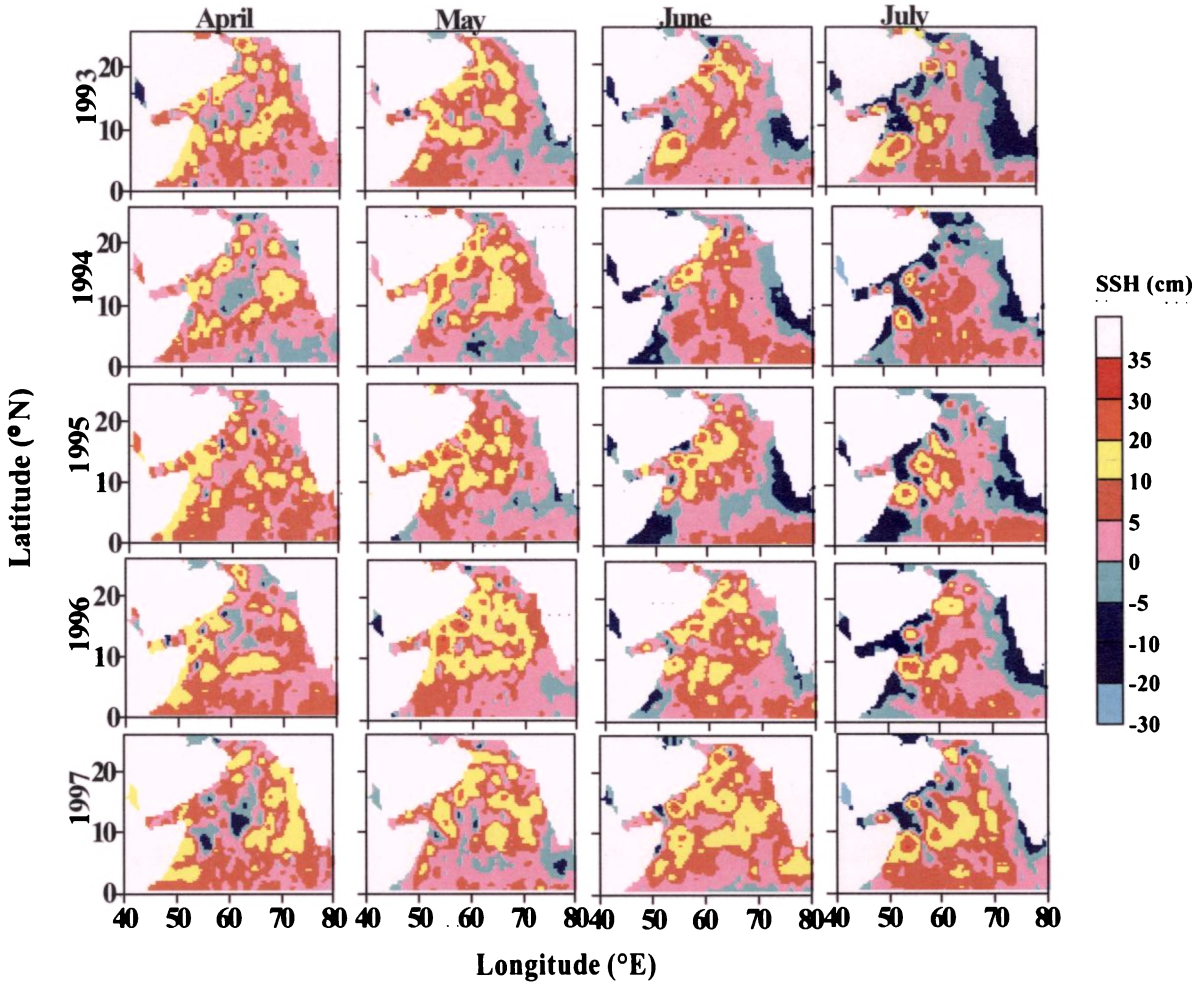

Fig.7.11 Evolution of Arabian Anti-cyclonic High during 1993 -1997

7.3.3 Somali Eddies

The western Arabian Sea is famous for several gyral circulation features. The Southern Gyre (SG) is formed early in June and a second one, the Great Whirl (GW) is formed off the Somali coast with the onset of summer monsoon. Another eddy, whose generation mechanism is still not known clearly, Socotra Eddy (SE), is formed during the late phase of the summer monsoon. Several studies have suggested that the GW can be directly forced by the anti-cyclonic wind curl (Schott and Quadfasel, 1982; Luther *et al.*, 1985) on the eastern side of the Findlater jet. Subrahmanyam *et al.* (2001) has noticed tele-connection between the reflected Rossby waves from eastern Indian Ocean and the Somali eddies. They have also suggested that the radiated Rossby waves from the west coast of India during January reaching the Somali coast by March/April has the possibility of triggering the Somali current and

their meandering before the onset of summer monsoon. A recent study by Wirth *et al.* (2002) has reported that the inter-annual variability in the GW was predominantly by internal processes and not by inter-annual variations of the wind field. The planetary waves are also believed to play an influential part in the generation and propagation of these Somali eddies (Lighthill, 1969; Jensen, 1990; McCreary *et al.*, 1993). The wind stress curl (< -0.025 $x10^{-5}$ Nm^{-3}) during the summer monsoon (June-September) indicates strong anti-cyclonic circulation over the offshore regions of Somali region (Figs.5.6-5.10), favouring the formation of high sea level in these regions.

Eddies near the Somali region are seen as high in sea level from June/July onwards, forming into circular or elliptical shape and seen upto October (Fig.7.1). For convenience, the eddies near Somali are together termed as Somali eddies. The climatology of the region shows the evolution of negative sea level (~-5 cm) south of Somalia during May, which extended northwards by June. This is the cold wedge formed prior to the formation of SG and GW. Schott *et al.* (1990) also reported the same feature. East of this cold wedge, an anti-cyclonic eddy (>10 cm) with diameter of more than 300 km, centered at 7.5°N, 53.5°E is noticed in July. In August, multiple eddies are formed in this region and by September, all these eddies merges to form a single eddy with a lateral diameter of nearly 400 km. These eddies dissipates by October. The negative wind stress curl (> -0.025 $x10^{-5}$ Nm^{-3}) over this region (Fig.5.5-5.10) from May onwards indicate anti-cyclonic circulation over this region and hence high in sea level. The negative curl values intensified during June/July and changes to positive values by November.

In the Somali region, the anti-cyclonic eddies are noticed from June (Fig.7.12) onwards, during the years 1993, 1996 and 1997 (Figs.7.12, 7.15 & 7.16) and from July onwards for 1994 and 1995 (Figs.7.13 &7.14). However, the area of formation, number of eddies and their dimensions vary from year to year. During 1993 (Fig.7.12) core of the anti-cyclonic eddy of 500 km diameter is noticed at 6.5°N, 53°E sandwiched between two cold wedges (SSH ~ 5 cm) along the Somali coast. In August, another anti-cyclonic eddy forms at 12°N, 56°E, northeast of the first eddy. These eddies coalesced to form a single eddy of diameter of nearly 300-400 km in October and is noticed with its core at 11°N, 56°E. A small eddy is noticed at 14°N in December (Fig.7.6) probably be the remnants of Somali eddy.

During 1996, though the anti-cyclonic eddy forms in June, it became prominent in July only, when the eddy is having a diameter in excess of 400 km and noticed at 9°N, 54°E. This eddy stretches along the Somali coast in August and became elliptical by September. Weakening of the eddy is noticed by October. The scenario is slightly different in 1997. Two anti-cyclonic eddies of diameter greater than 400 km is noticed in July centered at 8°N, 53.5°E and near 9°N, 60°E. During August, a southern eddy is also noticed along the Somali coast with its core at 4°N, 50°E. It is to be noted that the negative wind stress curl was found strong in August 1997 compared to other years (Fig.5.10), which might have caused the formation of eddies in August also.

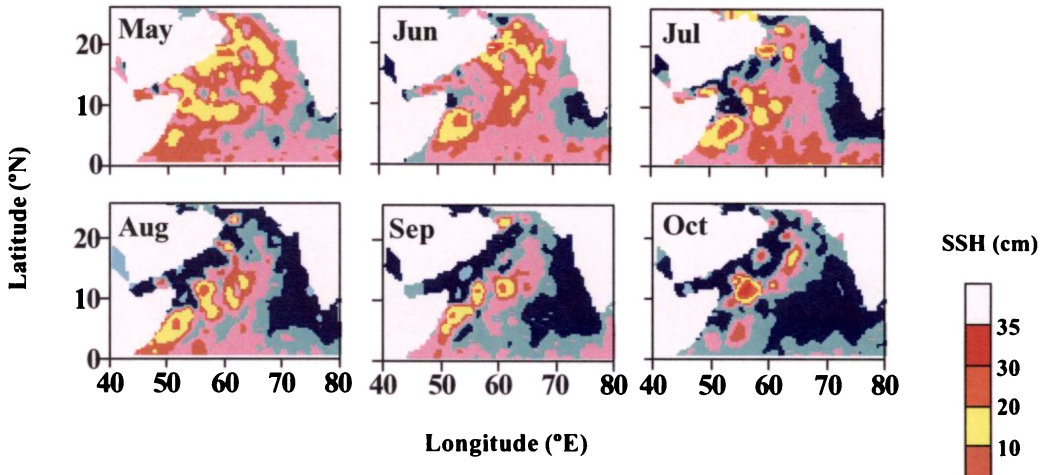

Fig.7.12 Evolution of Somali eddies (SSH in cm) during 1993

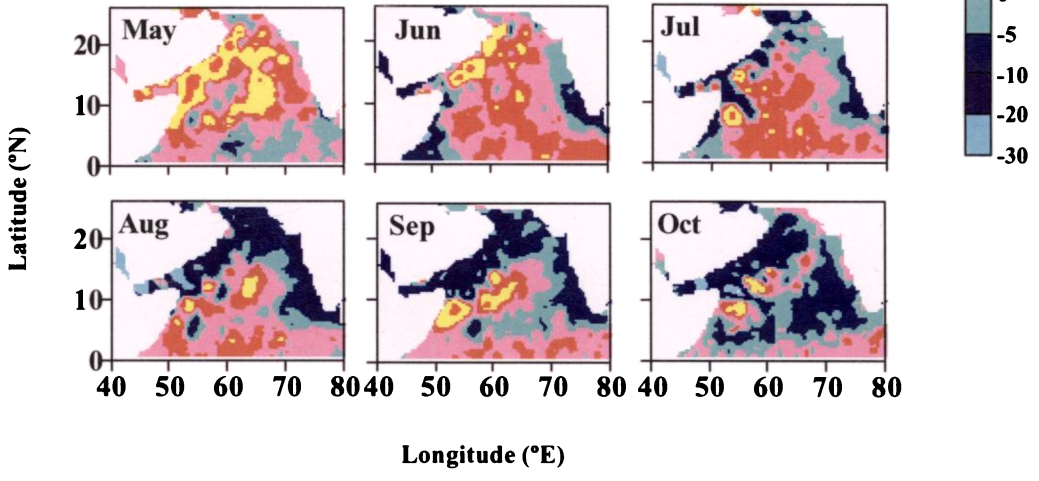

Fig.7.13 Evolution of Somali eddies (SSH in cm) during 1994

The Somali eddies appear weak during the initial phase of 1994 (Fig.7.13), because of strong the negative SSH anomaly that extend more eastward in June. In

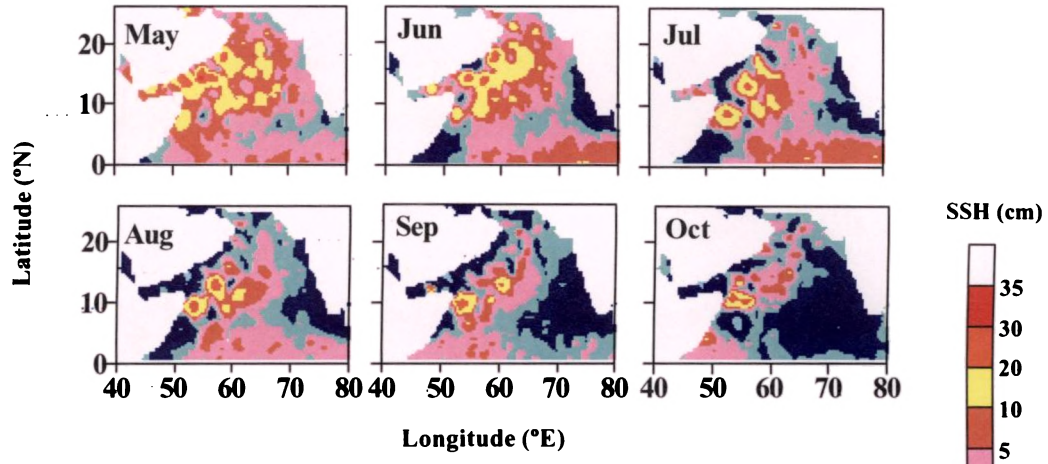

Fig.7.14 Evolution of Somali eddies during 1995

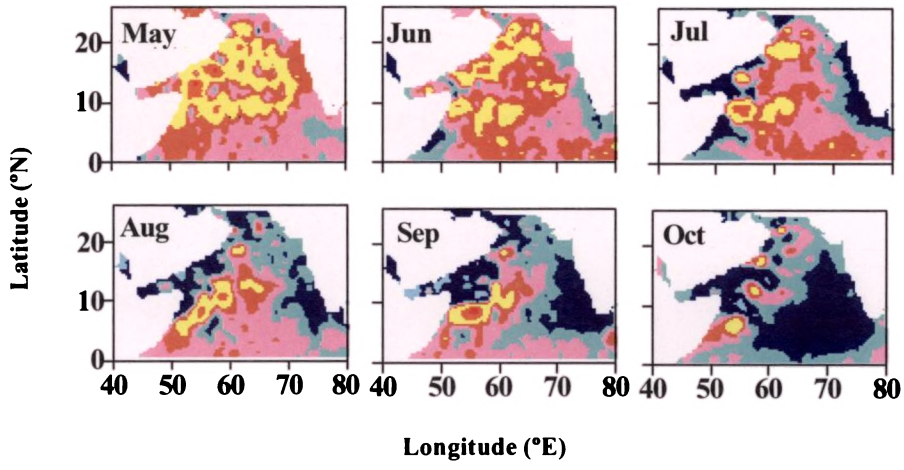

Fig. 7.15 Evolution of Somali eddies during 1996

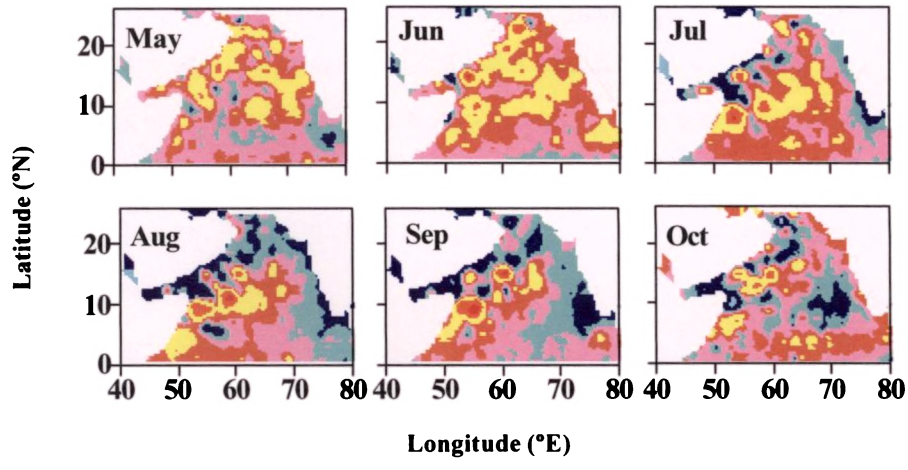

Fig. 7.16 Evolution of Somali eddies during 1997

July, the anti-cyclonic eddy of diameter 200 km is noticed with its centre at 8°N, 53.5°E and attain its maximum dimension of 500 km in September when it is noticed between 6° to 10°N and 50° to 55°E. Another eddy also forms, slightly northeast of first eddy, i.e. at 10°N, 59°E.

During 1995, the negative wind stress curl (Fig.5.8) strengthened only in July, which might have also caused a delay in the occurrence of high SSH. In this year, two eddies one centered at 9°N, 53°E with a diameter of 400 km and other centered at 13.5°N, 56.5°E with a diameter of 200 km are noticed in July. The dimension of these eddies are less compared to all other years. These eddies merge to form a single eddy and is noticed at 10°N, 53°E in November (Fig.7.8). Thus in most of the cases examined here, the variability in the Somali eddies can be explained in terms of the wind stress curl but not completely. Therefore, there seems to be some other mechanisms in addition to wind stress curl, which seems to play role in variability in the characteristics of Somali eddies.

7.3.4 Bay of Bengal Eddies

In the Bay of Bengal, an anti-cyclonic gyre existed in the western region from February to July and a cyclonic gyre the rest of the year (Cutler and Swallow, 1984). Subrahmanyam (1999) has also identified anitcyclonic and cyclonic eddies in the western Bay. The currents along the east coast of India, i.e., EICC reverses direction twice a year, flowing polewards from February to September and equatorward from October to January (Shetye *et al.*, 1993; Cutler and Swallow, 1984). Associated with this current reversal, several eddies are also formed in the western Bay (Shetye *et al.*, 1993). The surface circulation is best organized in the interior of the Bay from February to May, when the EICC forms the western boundary current of a basin wide anti-cyclonic gyre.

Two anti-cyclonic eddies (SSH> 10 cm) are noticed in the western Bay on an annual cycle, one eddy in the northern Bay between January and May and another east of Sri Lanka between October and May (Fig.7.1). These eddies changes their dimension and location (Fig.7.1) with the progress of time. The wind stress curl (Figs.5.6-5.10) was negative over the western Bay from November/December to

March/April favouring the formation of these eddies. The northern eddy exhibits southward movement while the Sri Lankan anti-cyclonic eddy shows northwestward movement (Fig.7.1). Subrahmanyam (1999) has reported that the Sri Lankan anti-cyclonic gyre seems to be receiving energy from the westward propagating Rossby waves from the eastern Bay during October. The maximum dimension of both eddies in the western Bay is noticed during April/May. In between these two highs, a cyclonic low (SSH>-10 cm) is also noticed during January centered at 15°N, 82°E. This seems to have dissipated by March. Another cyclonic low evolves east of Sri Lanka during the summer monsoon period (June to August/September) which is identical with the Sri Lanka dome as reported by Vinayachandran and Yamagata (1998). This dome also shifts northwestwards with time (Fig.7.1).

The wind field (Fig.5.1-5.5) and wind stress curl (Fig.5.6-5.10) showed northeasterly winds and anti-cyclonic curl (-0.02 $x10^{-5}$ ms^{-2}) over the western Bay during the northeast monsoon season favouring downwelling along the coasts. This condition remains in the offshore regions of east coast during April/May also.

In the western Bay, the anti-cyclonic eddies are having dimension less than 100 km during 1995 (Fig.7.19), while they are well developed with dimension in excess of 200 km in all other years (Figs.7.17, 7.18, 7.20 & 7.21). During January 1993, two anti-cyclonic eddies are noticed in the western Bay, one in the northwestern Bay centered at 18°N, 86.5°E, and another east of Sri Lanka centered at 10°N, 84°E with diameter in excess of 300 km and 500 km respectively (Fig.7.17). A cyclonic low is sandwiched between these two eddies, with its core at 15°N, 82.5°E. This cyclonic eddy remains in the western Bay till April. The anti-cyclonic eddies in the western Bay merge together in May to form an elongated anti-cyclonic eddy (SSH > 20 cm) with its core at 16°N. This eddy splits again into two small eddies of ~ 200 km diameter in June and weakens thereafter. However, the signatures of these eddies are noticed till September. During 1994 (Fig.7.18), many small eddies having dimension less than 100 km are noticed in the western Bay. The anti-cyclonic eddy of Sri Lanka (core at 9°N, 84°E) also has lesser dimension this year (~ 200 km). The cyclonic eddy formed in the western Bay (15°N) in January in between the two anti-cyclonic eddies dissipates by February. As observed in 1993, the anti-cyclonic eddy off Sri Lanka moves northward and merges with the northern eddy at 16°N, 83.5°N in May. This merged eddy is having a diameter greater than 500 km. By June this eddy starts

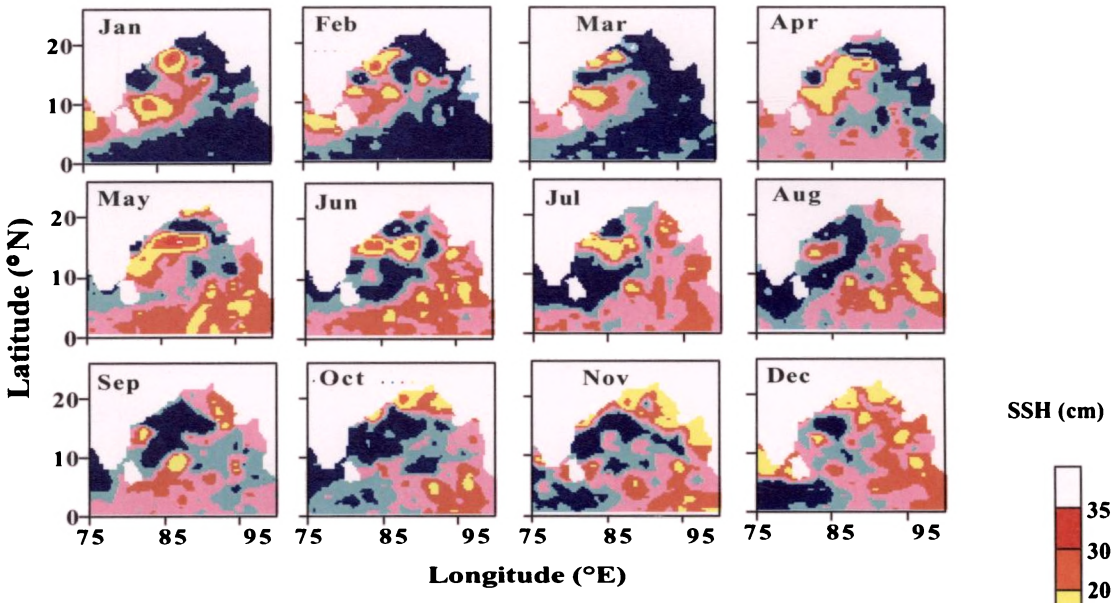

Fig. 7.17 Eddies in the Bay of Bengal during 1993

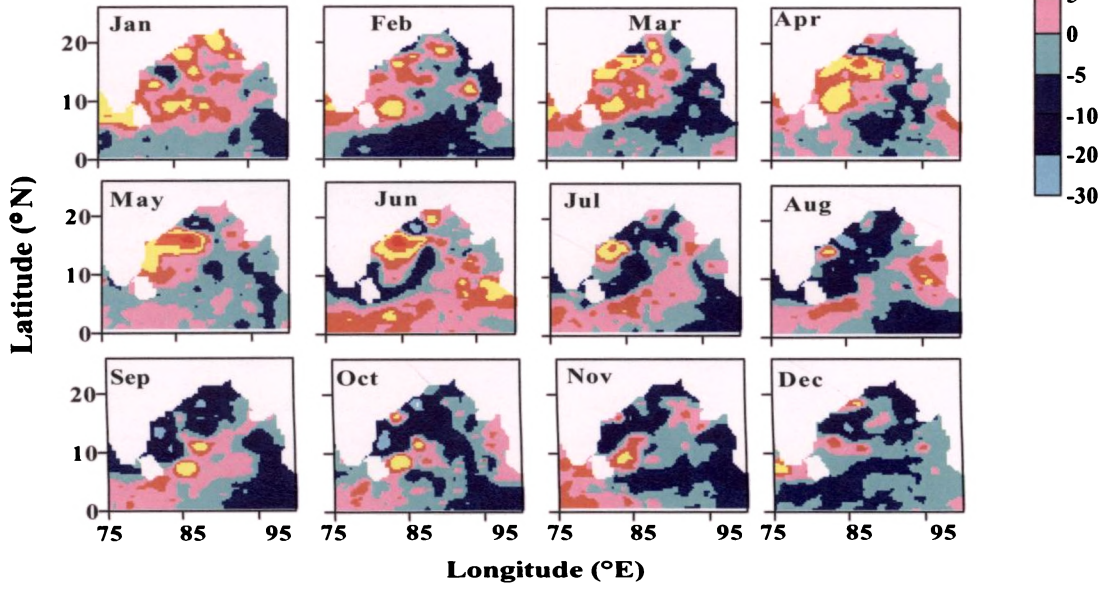

Fig.7.18 Eddies in the Bay of Bengal during 1994

dissipating. Similar situation observed during 1995 also (Fig.7.19). As observed in other years, the anti-cyclonic eddies are noticed in January but with lesser dimension. By February, the eddies off Sri Lanka (8°N, 84°E) and northwestern Bay (16°N, 84°E) attains diameter of ~ 100 km. The eddy near Sri Lanka moves northwestwards while the eddy in the northwestern bay moves southward. These two eddies merges together in April to form an elongated eddy of lateral diameter ~500 km centered at 15°N in the western Bay. The cyclonic low noticed in between these eddies in January dissipated by March. During 1996 (Fig.7.20), the anti-cyclonic eddy in the

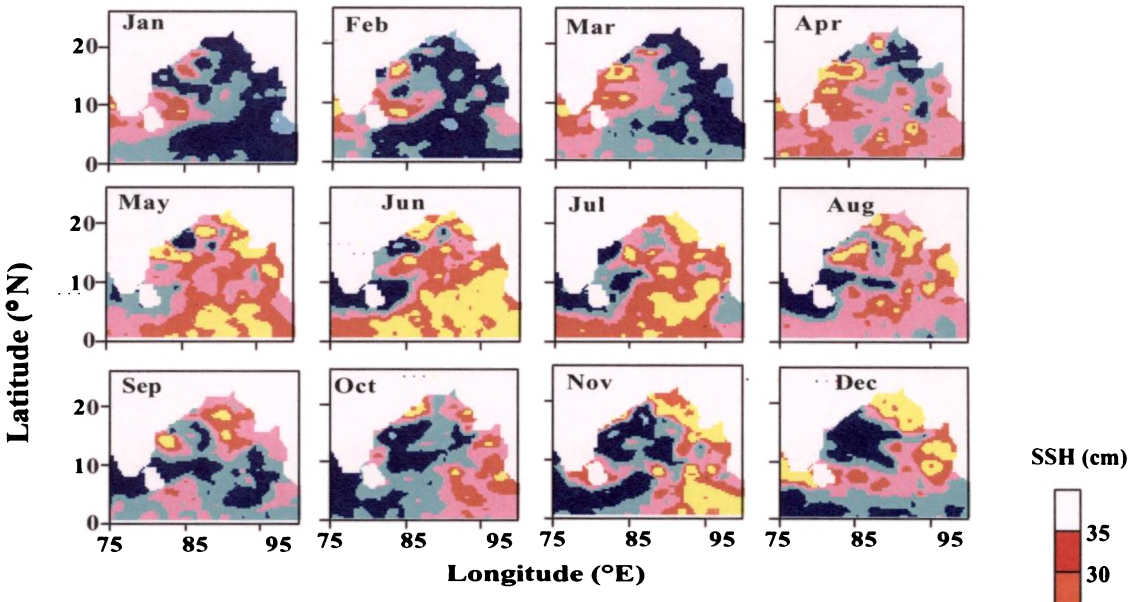

Fig. 7.19 Eddies in the Bay of Bengal during 1995

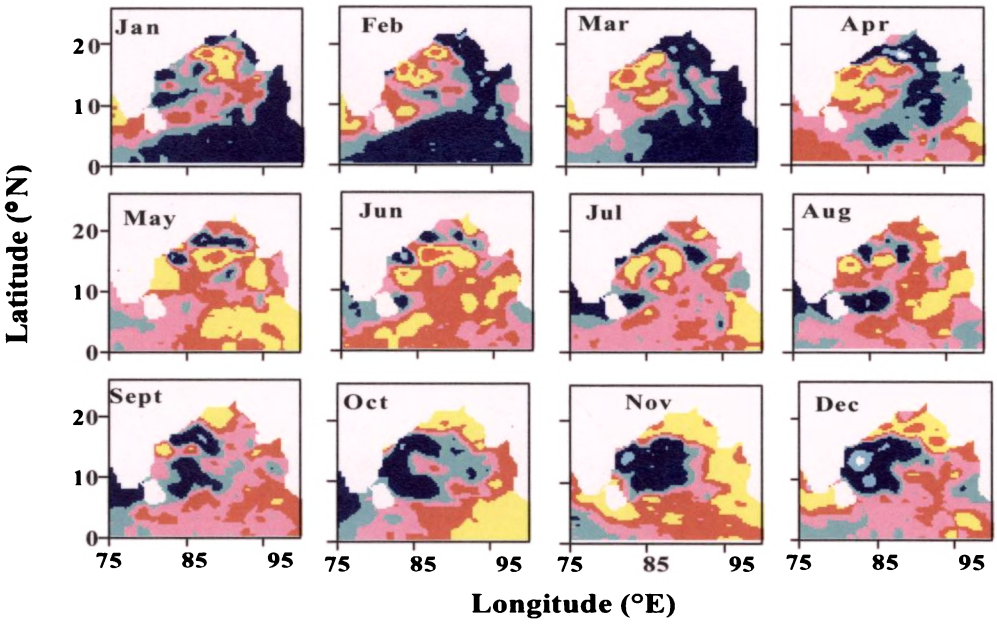

Fig.7.20 Eddies in the Bay of Bengal during 1996

northwestern Bay is found in January slightly northwards (19°N) compared to 1993 and having much larger dimension (500 km). This eddy moves westward in February and splits into multiple eddies. By this time, an anti-cyclonic eddy of dimension ~200 km appears of Sri Lanka (core at 9°N, 84°E). A cyclonic eddy is also noticed in the western Bay in January and dissipates by February. It is to be noted that both the anti-cyclonic eddies merged together in April and a single eddy is noticed in the western

Bay between 10°-17°N and 80°-85°E. In May, though this eddy weakens, two more anti-cyclonic eddies are noticed in the central Bay, with their core at 16°N, 89°E and 13°N, 94°E. These eddies weakens by July. In September only one prominent anti-cyclonic eddy is noticed in the western bay centered at 14°N, 82°E. During January 1997 also (Fig.6.21), the formation of anti-cyclonic eddies are noticed in the western Bay (18.5°N, 88°E) and off Sri Lanka with dimensions, 400 km and 200 km respectively. It is interesting to notice that during March, the dimension of the northern eddy decreases and increases in the case of the eddy observed off Sri Lanka (> 500 km). Another notable observation is the occurrence of strong cyclonic eddy in January in the western Bay between 10° and 16°N. This eddy persists in the western Bay along 15°N till August, though with a reduced dimension.

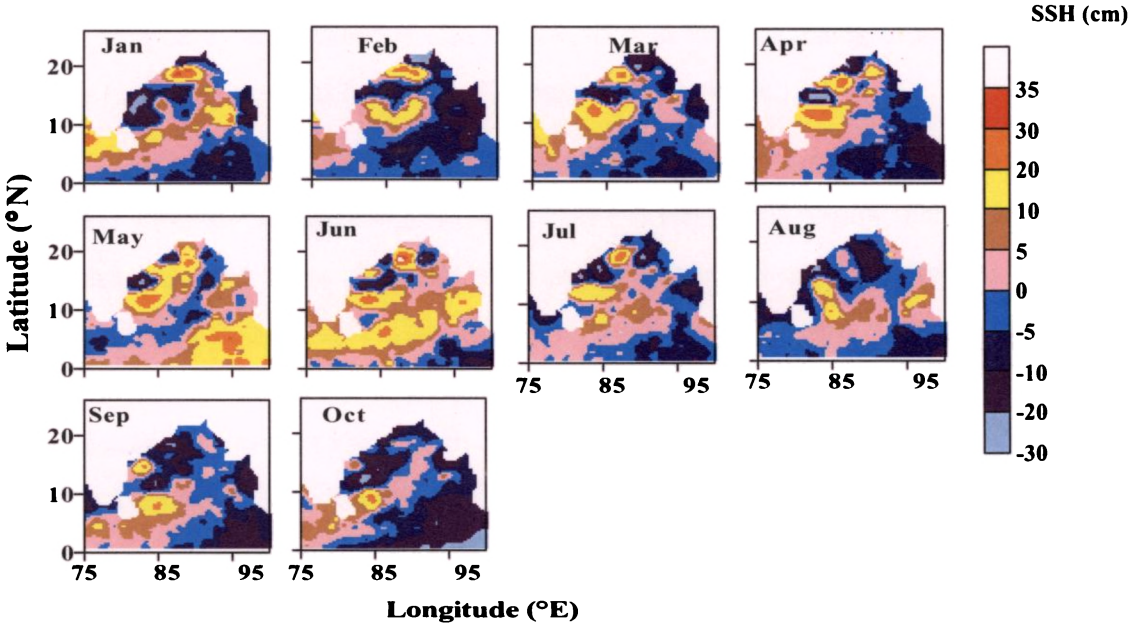

Fig. 7.21 Eddies in the Bay of Bengal during 1997

The above analysis revealed that the anti-cyclonic eddies in the Bay are weak during 1995 and well developed during other years. The wind stress curl (Figs.5.6-5.10) indicated negative values over the western Bay during the northeast monsoon period favouring the formation of the anti-cyclonic eddies. The analysis of winds (Figs.5.1-5.5) indicated weak northeasterly winds ($4ms^{-1}$) in the Bay during 1994 and 1997. Moreover, these are years of El Nino and IOD events. In the equatorial region also weak westerly winds prevailed in these years. These weak winds in 1994 in turn cause the formation of weak Kelvin waves during October 1994, which will reach the

northwestern Bay of Bengal as coastally trapped Kelvin waves in early 1995. Probably the arrival of weak Kelvin waves might have been one of the reason for the reduced dimension of the anti-cyclonic eddies in 1995.

7.3.4.1 Sri Lanka dome (SD)

The climatology of SSH (Fig.7.1) shows the evolution negative SSH anomalies (-5 to -10 cm) from June onwards with an approximate diameter of nearly 400 km in August. With the progress of time, this low sea level shifts northward. The wind stress curl (Figs.5.6-5.10) revealed positive values (0.02 $x10^{-5}$ Nm^{-3}) around southern tip of India and east of Sri Lanka between May and October, indicating cyclonic circulation, which can lead low sea level in this region. The positive curl also showed a northwestward extension during this period. This region of low sea level was termed as the Sri Lanka dome (SD) by Vinayachandran and Yamagata (1998). The dissipation of the dome is also associated with the weakening of the positive wind stress curl in this region from October/November onwards.

The SD forms in June, in the region east of Sri Lanka in all the years, as evident from the appearance of low sea level (-SSH) in this region. The SSH anomaly in this region vary from –5 to –20 cm. The SD is found to move northwestward before its dissipation before September. However, marked year to year variability is noticed in the characteristics of this SD. During 1993 (Fig.7.17), this dome attains its maximum dimension (500 km) in July, when it is noticed between 4°-12°N and 82°-87°E. This low sea level associated with the dome moves northwestward and weaken thereafter. During 1994 (Fig.7.18) also, this dome forms in June, but attains its maximum dimension (>500 km) only in August and then it is noticed more northward compared to 1993, between 7° and 14°N and 82° and 86°E. Similarly in 1995 (Fig.7.19) also, the dome forms in June, its maximum dimension (<350 km), though weak compared to other years, is noticed in the same month itself. During this period, the dome is noticed between 6°-10°N and 82°-85°E. This dome weakens by August. The dome extends between 7°-10°N and 82°-87°E, with an east-west dimension of more than 500 km in August 1996 (Fig.7.20). Compared to all years, the SSH anomaly is found to be weak (~5 cm) in June 1997, when the dome appear east of Sri Lanka centered at 8°N, 83°E (Fig.7.21). The dimension of this SD is found to be the minimum (< 100 km) compared to all other years. Even though, the low sea level

extends all along the east coast of Sri Lanka in August, with a lesser eastward extent. In all the years, the dissipation of the SD is associated with the development of negative curl over the region.

Thus the major eddies noticed in the north Indian Ocean showed large inter-annual variability associated with the long period propagating waves, alongshore winds, remote winds and also on the wind stress curl over the region.

Chapter 8

Summary and Conclusions

The thesis "Salient features of the north Indian Ocean associated with the Indian summer monsoon" primarily focuses on certain aspects of the atmosphere and ocean variability in the North Indian Ocean associated with the monsoon. These include the Arabian sea mini warm pool formed in the eastern Arabian Sea during the pre-monsoon season, variability in the ocean response of central and northern Bay of Bengal to atmospheric systems/disturbances during the summer monsoon 99, the marine boundary layer characteristics during the summer monsoon 99 and the variability induced by the atmospheric systems/disturbances, evolution of propagating waves and eddies and their inter-annual variability.

In the Indian Ocean, an active area of recent research is the Indian Ocean warm pool and associated ocean and atmosphere dynamics. However, not much attention is paid to the Arabian Sea mini warm pool, where the onset vortex is formed. In this thesis, the focus is given on the Arabian Sea mini warm pool, which is a part of the Indian Ocean warm pool and formed in the southeastern Arabian Sea prior to the onset of summer monsoon. Utilizing 45 years of data corresponding to the onset date and corresponding rainfall, it was found that an early onset of monsoon over Kerala favoured a good monsoon rainfall and a late onset leads to below normal rainfall. NCEP/NCAR sea surface temperature (SST) data (1960-1998), from ships of opportunities, high resolution TMI SST for typical years were utilized to study the characteristics of the Arabian Sea mini warm pool. As the temperature in the entire Arabian Sea exceeds 29°C during the pre-monsoon, 30°C isotherm was selected to represent the Arabian Sea mini warm pool in this study. The study revealed in the eastern Arabian Sea, maximum temperature occurred approximately two weeks prior to the onset of summer monsoon over Kerala. However, the extent and the core temperature varied depending on the nature of the forthcoming monsoon. One of the notable result was that the dissipation of the mini warm pool started nearly one-two weeks prior to the onset of summer monsoon over Kerala. This was due to the arrival of monsoon winds to the western and central Arabian Sea, which increased vertical mixing processes. This result was confirmed utilizing TMI SST data for 2001, 2002, 2003. It was also found that the warm pool attained its maximum core temperature (30.5°C) and lateral extent (> 30,00000 km^2) during wet year compared to normal (30.2°C, > 16,94000 km^2) and dry year (< 30°C, in the eastern Arabian sea).

Verification of the results with TMI SST for the years 2001 (below normal), 2002 (dry) and 2003 (above normal) confirmed this conclusion. This suggests that the dissipation of the Arabian Sea mini warm pool, its core temperature and lateral extent can be utilized as a tool to characterize the forthcoming summer monsoon.

The analysis of salinity data indicated the presence of low saline water in the mini warm pool region, with minimum salinity during wet year. Probably, this low saline water might have increased the vertical stratification and thereby causing the occurrence of maximum temperature during wet year. This needs further verification. Two possible sources for the low saline water in the southeastern Arabian Sea have been proposed. One from the Bay of Bengal and other from the western equatorial Indian Ocean.

Information on the marine boundary layer was extremely sparse over the Indian Ocean especially during the monsoon season. The radiosonde data collected during the BOBMEX-99 experimental program onboard the research vessel ORV Sagar Kanya, provided valuable information on the influence of weather systems on the Marine Boundary Layer (MBL) characteristics. The vertical variations of observed parameters such as temperature, humidity, wind speed and direction showed variability with the formation and dissipation of the systems over the Bay of Bengal. Temperature was usually greater than 28°C in the surface layer and decreases with height. Atmosphere was relatively humid (>80%) below 1000 m, throughout the observation period with large variability observed above that till 8000 m. Relative humidity was less than 30% above 11000 m. Wind showed westerlies (1-16 ms^{-1}) below 5000 m and easterlies (>31 ms^{-1}) above 8000 m, with the core around 15000 m. The potential temperature gradient, a measure of the stability of the atmosphere showed negative values indicating unstable situations only in the lower layer below 150 m. The formation of atmospheric systems induced large variations in all these fields. Temperature decreased by the order of 1.5° to 3.5°C below 1000 m, with the maximum gradient below 200 m with the formation of atmospheric systems. No large variation existed above 1000 m. The large variation in humidity values associated with systems were confined in the levels between 1000 and 8000 m. During the formation stage of the systems relative humidity increases to more than 85% in the levels below 7000-8000 m and returned to pre-system values after its dissipation. The

wind speed showed large increase (11-16 ms^{-1}) during convective systems such as rain with the westerlies below 7500 m. Easterlies are noticed above that with the core of the Easterly Jet stream (>31 ms^{-1}) between 15000 and 17000 m. This core was confined to nearly 16000 m after the rainfall event thereby reducing the thickness of the core. Potential temperature gradient showed maximum gradient (-0.01°C m^{-1}) in the lower 50 m, indicating unstable condition associated with the formation of systems.

Wind shear was generally higher above 15000 m and coincided with the Easterly Jet stream. Nearly zero wind shear was noticed in the level between 10000 and 14000 m, where the effect of both the easterly and low level Westerly Jet Streams are minimum. Associated with the rainfall event when the wind increased, wind shear also increased (0.0118 s^{-1}) in the levels between 15000 and 20000 m and below 10000 m. The vertical extent of the wind shear zone in the Jet stream region decreased (~3000 m) after the rainfall event.

Coinciding with weak monsoon condition, temperature was above 28°C in the surface layers and low humidity regime (<60%) extended downwards to ~ 5000 m. The wind speed decreased considerably (1-6 ms^{-1}) during this period and the easterlies also extended downwards to ~5000 m.

The lowering of lifting condensation level below 965-970 mb was also associated with the system formation and the lowest value ~ 997 mb corresponded to the major rain event. A decrease in Boundary Layer Height (BLH) by the order of 1500 m and frictional velocity by the order of more than 0.3 ms^{-1} was also associated with convective activity.

Understanding of the refractive index conditions of the atmosphere is mostly needed for radar ranging and tracking purposes. The refractive index gradient showed large variations with the changing moisture content and temperature of the atmosphere associated with the systems in the lower layers below 400 m and standard conditions existed above this level. The trapping conditions, which is ideal for tracking existed in the lower layers below 70 m associated with the system formation. The sub-refractive condition in the near surface layers coincided with the rainfall event with standard condition just above this layer and below 30 m. Super-refractive conditions were noticed to exist from 50-400 m during the weak monsoon period.

The physical and oceanographical conditions are different in Northern and central Bay of Bengal. Northern Bay of Bengal is less saline due to large freshwater influx from river discharge. During the summer monsoon, the monsoon trough dips into the northern Bay of Bengal and many systems were also formed over this region. Simultaneous observation at these two station locations, during the BOBMEX experimental programme of summer monsoon 1999 provided an opportunity to study the response of the central and northern Bay of Bengal to the summer monsoon and atmospheric systems that formed over this region. The buoy data available at these locations were also utilized in this work. The central Bay and northern Bay responded differently to the summer monsoon and to the atmospheric systems that formed over this region. The pressure and sea surface temperature values were in general higher over the central Bay. The amplitude of the variations was also comparatively less over the central Bay.

Over the northern Bay, prior to the formation of any atmospheric system, atmospheric pressure is of the order of 1000 mb, air-temperature is of the order of 29°C, wind speed is of the order of 7 ms^{-1} and SST of the order 28.7°C. With the formation of system, significant decrease is noticed in the atmospheric pressure (998 mb and below), air temperature and SST (< 26°C, < 28°C), while wind speed increased to above 10 ms^{-1}. Winds were southwesterly during weak monsoon condition and west southwesterly during the depression period. However at the central Bay, amplitude of variations was comparatively less. Effect of the systems were noticed here with reduced magnitude. One reason can be due to most of the systems formed in around northern Bay. The atmospheric pressure and SST were generally above 1005 mb and 28.4°C respectively with wind speed around 7 ms^{-1}. Strong winds 10 ms^{-1} were observed during the active monsoon period. Winds were southwesterly throughout the observation period.

The net heat flux is higher (~400 Wm^{-2}) over the central Bay. Over the northern Bay net heat gain was less under increased cloud cover and associated systems and increased with weak monsoon condition. The SST-DB, an indication of static stability, increased (>2°C) corresponding to system formation and more pronounced over northern Bay. A notable result was the decrease in specific humidity

associated with system formation over northern Bay, from more than 0.022 to less than 0.019.

Another important result was the critical limit for the sea surface temperature. It was noticed that whenever, SST increased beyond 28.7°C over the northern Bay, systems were formed over the Bay of Bengal. The same was true for the convective systems associated with rainfall event also. A lag of 2-3 days was also noticed between the ocean pressure minimum and SST minimum.

The mixed layer depth shoaled/deepened during the period of increased /decreased winds at the central Bay and suggested the role of forcing other than local in controlling the mixed layer variations. A one-dimensional model of Miller (1976) was utilized to simulate the mixed layer characteristics in the northern and central Bay of Bengal. Large disagreement between observation and simulation was noticed at both the stations, suggesting the dominance of remote forcing over local forcing. This can be attributed to rich eddy fields, complex circulation pattern, long period waves and internal waves occurring in this region.

The surface winds over the Indian Ocean are notable for its seasonal reversal. NCEP/NCAR surface winds at 10 m level were utilized to examine the surface wind and wind stress curl for the years 1993-1997 and to study their inter-annual variability. 1994 and 1997 were El Nino years and Indian Ocean Dipole events were also reported during these years. Analysis of surface winds revealed peculiar characteristics during these years. The westerly winds over the equatorial Indian Ocean during the transition period between the monsoons were weak during 1994 and 1997 (<2 ms^{-1}) compared to the other years and even easterlies appeared over the region during this period. The northeasterly winds were stronger and southwesterlies were weaker over the Bay of Bengal during the 1993, 1995 and 1996 winter and summer monsoon respectively. The southeast trade winds over the south Indian Ocean were more prominent during 1994 and 1997, over the eastern Indian Ocean along the Sumatra coast as it extended more northwards over the equatorial region from June to December.

Wind stress curl also reversed seasonally to positive/cyclonic or negative/anti-cyclonic with the monsoon winds. They are also important as they favour cyclonic/anti-cyclonic circulation over the region. The regions of positive/negative

curl were separately discussed for further use of this information in studying the propagating waves and eddies.

The curl of the wind stress were in general negative/anti-cyclonic during the northeast (winter) monsoon period favouring anti-cyclonic circulation in the ocean over the northwestern Arabian Sea, southern tip of India and offshore regions extending westwards, over Sri Lanka region, the western Bay and over the Somali coast. However, in the offshore regions of the Somalia and extending northwards, the curl was positive or cyclonic. The curl value decreases and changes its sign with the progress of season. During the summer monsoon season, the curl became positive/cyclonic favouring cyclonic circulation over the southern tip of India and west coast of India extending westwards and over western Bay, over the coast of Arabia and western Arabian Sea, over the east coast of India and around Sri Lanka. Along the Somali coast during the summer monsoon, the curl was positive and it was negative to the east, extending to the central regions of the Arabian Sea. The large variability in the winds and its curl can cause corresponding variability in the sea level also.

The positive or negative curl over the study region revealed large inter-annual variability during the years 1993-1997. It was found that the negative curl over the southern tip of India during December/January remained there offshore till March/April for all the years and is shifted more southwards during January 1994 and 1997 compared to other years. The positive curl during the summer monsoon over the west coast of India also showed large variability with similar pattern during 1994 and 1997 as the curl became negative earlier by November itself compared to other years. During other years, this positive curl extended over the west coast upto 15°-20°N and remained over the southern tip during October/November also. Over the northwestern Arabian Sea the curl was negative from November/December onwards till May and turned positive by June. But during 1995 and 1997 curl remained negative during June also. Over the Sri Lankan region, the curl was positive through out the summer monsoon season. In the offshore regions of Somalia, the extension of the negative curl during the summer monsoon showed large inter-annual variability. Similar pattern of negative curl was noticed during 1993 and 1994 June but sign changed comparatively earlier in 1994. During 1996, the extension of the negative curl over this region was

higher compared to 1995 and 1997, but less than 1993 and 1994 June. The extension of the negative curl in August 1997 was higher than all other years.

The winds during the transition period between monsoons drive the equatorial Jet, and force the eastward propagating Kelvin waves. On reaching the eastern boundary, a part of it reflects back as Rossby waves and other part propagates northward and southward as coastally trapped Kelvin waves. The TOPEX/Poseidon Sea Surface Height (SSH) anomaly data were utilized to study the propagating waves along typical sections viz. equator (0°), central Arabian sea, Bay of Bengal along (15°N) and in the south Indian Ocean (along 15°S & 20°S). Wavelet analysis technique was also utilized to determine the prominent harmonics embedded in the time-series of SSH field at selected locations. Along the equator, positive SSH, representing downwelling Kelvin wave propagated from the western Indian Ocean during March/April and September/October and reached the eastern Indian Ocean within a gap of one month thus indicating the semi-annual periodicity of these waves. This was supported using wavelet analysis also. The speed of this downwelling Kelvin wave was computed to be ~ 250 cms^{-1}. These SSH anomalies indicating Kelvin wave propagation revealed large inter-annual variability. Another notable result was that corresponding to the weak equatorial westerlies during the transition period of 1994 and 1997, downwelling equatorial Kelvin waves were also weak. In these years, the upwelling signals were more prominent in the eastern equatorial Indian Ocean. During other years, when the equatorial westerlies were strong, equatorial downwelling Kelvin waves were also prominent.

The westward propagation of positive SSH anomalies from the eastern Arabian Sea (along 15°N) during December/January, denoted Rossby waves propagation from their speed (between 8-10 cms^{-1}) and direction of propagation. Wavelet analysis revealed annual harmonic to be significant in this region. This also supported the result, as annual periodicity, westward propagation and its speed coincide with that of the annual Rossby waves propagation in the eastern Arabian Sea along this latitude. It was also interesting to notice these signals to be more prominent during 1994 and 1997, inspite of weak equatorial westerlies, and when El Nino and Indian Ocean Dipole (IOD) events were also reported to have occurred. The prominent wave during 1994 and 1997 can be associated with the previous years

downwelling Kelvin wave i.e. of 1993 and 1996 respectively, which reached there during this period. This analysis also supported the role of equatorial wind (as downwelling Kelvin wave) in causing inter-annual variability in the propagation of waves in the eastern Arabian Sea.

Another interesting feature noticed was the formation of a high of non-propagating nature in the western Arabian Sea, from November to May/June, but extending to the central regions. This was found to be associated with the persisting anti-cyclonic circulation over the northwestern Arabian Sea during this period. This high limited the westward extension of the positive SSH formed in the eastern Arabian Sea. When the Rossby wave propagation from the eastern Arabian Sea was weak especially during 1995, this high extended more eastward.

In the central Bay of Bengal (15°N) also, westward propagating positive signals were noticed from the eastern Bay, during May/June and November/December, but prominent only in certain years. This was also associated with the downwelling Kelvin waves from the equatorial Indian Ocean. The signals were less prominent during 1994 and 1997 when the equatorial downwelling Kelvin wave was weak. The speed of westward propagation of this high ~12 cms^{-1} also corresponds to the Rossby wave speed along this latitude. In 1994 and 1997, when weak northeasterlies occurred over the Bay region, the high anomalies from the eastern Bay also appeared weak, suggesting the role of equatorial as well as Bay winds in causing inter-annual variability in the wave propagation. In the south Indian Ocean (along 15°S & 20°S), the Rossby wave propagation was clearly identified from the eastern Ocean, which took almost two years to reach the western Indian Ocean suggesting a speed of 12.6 cms^{-1}. Large inter-annual variability was noticed in the SSH anomalies in the south Indian Ocean and the southeast trade winds were also noticed to play a major role in the formation and propagation of these SSH anomalies. A major conclusion emerged from this study is the influence of surface winds on wave propagation and its inter-annual variability. Thus the winds form an integral part in controlling the ocean dynamics.

The Daubechies wavelet was utilized to decompose the prominent harmonics embedded in the SSH signals and their confidence level was tested using significance test. In the equatorial region prominent harmonics were in the bands of ISO (intra-

seasonal), 3-4 month, semi-annual, annual and above annual. In the equatorial region prominent harmonics were in the semi-annual band at the western and eastern equatorial Indian Ocean and attributed to semi-annual reversal of winds and associated semi-annual Kelvin waves. In the central Arabian Sea annual periodicity corresponding to annual Rossby waves dominated and in the Bay of Bengal (near the coast), prominent harmonic was in 3-4 month band. In the south Indian Ocean low frequency signal was noticed to be prominent i.e. annual and biennial. Large spatial as well as temporal variability was noticed in all the harmonics.

The T/P SSH data was further utilized to identify the major eddies in the north Indian Ocean and their inter-annual variability. The major eddies in the north Indian Ocean identified were the Lakshadweep High (LH) and Lakshadweep Low (LL), the Arabian Anti-cyclonic high, Somali eddies and the eddies in the Bay of Bengal.

The LH stared forming in the Lakshadweep region with the arrival of equatorial downwelling Kelvin wave (as coastally trapped) of April at the southwest coast of India by November. These coastal Kelvin waves radiate Rossby waves westward. The LH propagated westward, coinciding with the speed of Rossby wave propagation. Thus the Rossby waves were noticed to play a major role in the formation of this LH. The wind stress curl over this region was also negative favouring the formation of high in SSH. A noticeable result from the study was the large inter-annual variability in the dimension, speed, and number of multiple eddies of this LH. The least dimension of the LH was noticed during 1994-1995 (<200 km). This can be associated with the weak equatorial downwelling Kelvin wave of April/May 1994. In all other years, the dimension of this eddy was greater than 500 km. The LH dissipated by May.

The LL, formed off the southwest coast of India, from May onwards and correspondingly wind stress curl was positive/cyclonic favouring the development of low SSH during this period. This also propagated westward at the Rossby wave speed of propagation. The low extended all over the Arabian Sea basin by November/December and started dissipating from the west coast with the formation of LH in November.

The LL also showed large inter-annual variability. The extent of this low was noticed to be least in the Arabian Sea during 1994 and 1997. Corresponding cyclonic

wind stress curl changed to negative/anti-cyclonic earlier in November itself during these years. In addition, in these to two years, El Nino and IOD vents were reported causing considerable warming in these regions, which also might have limited the westward extension of the LL.

The Somali anti-cyclonic eddies formed off the Somali coast during summer monsoon from June/July onwards and corresponding wind stress curl was also found to be anti-cyclonic in the offshore regions, favouring the development of high in SSH. Large inter-annual variability was noticed in the dimension of these eddies in all the years. These eddies merged together in some years and dissipated by October. The dimension of this eddy was the least during the initial phases of the 1994 and increased later in September only. In all other years, dimension of this eddies became greater than 200-500 km during June/July itself.

In the western Bay of Bengal, anti-cyclonic eddies were noticed during January-June period, off Sri Lanka and off northwestern Bay of Bengal. The wind stress curl was negative/anti-cyclonic over this region favouring the formation this high. A cyclonic eddy was also noticed in between these two anti-cyclonic eddies. Both these eddies changed their dimension and position with the progress of time. By April/May, a single eddy probably by the merging of these anti-cyclonic eddies were noticed in the western Bay. The dissipation started from May/June onwards. These eddies showed inter-annual variability in their dimension and center of location. During 1993, 1994, 1996 and 1997, the dimension of these anti-cyclonic eddies of Sri Lanka and northern Bay was higher (200km to 500 km), while in 1995 it was less (~100 km). The winds along with wind stress curl over the region and coastal Kelvin wave from the equatorial region were noticed to play a major role in the development of these eddies. The Sri Lanka dome, a region of low sea level formed east of Sri Lanka during the summer monsoon period. The corresponding wind stress curl was positive/cyclonic favouring the development of negative SSH in the ocean. The dissipation of this dome is associated with the weakening of positive curl in this region.

Scope for future work

In this thesis, attempts were made to understand various aspects of time-scale variability of major features occurring in the Indian Ocean associated with Indian

summer monsoon. The results from the thesis can be utilized as an input for model studies for prediction of monsoon, understanding the ocean dynamics, for radar tracking and ranging etc. Arabian Sea mini warm pool has been studied utilizing limited data sets. The results presented in this thesis can be confirmed by extending the analysis for long period to bring out characteristic features during different types of monsoon. Numerical model studies suggested the importance of remote forcing at northern and central Bay. Hence inclusion of remote forcing can give a better simulation of the major ocean dynamics. The response of the atmospheric systems formed over Bay of Bengal to the characteristics of marine atmospheric boundary layer and upper layer was studied here as a case study. An extension of this work for more years could be used to confirm the results. It has been found that the eddies and propagating waves influence the major ocean dynamics of the Indian Ocean. So, a detailed study in this direction will help for a better understanding of these features and hence the climate over this region.

References

Anjaneyulu TS (1980): A study of the air and sea surface temperatures over the Indian Ocean. *Mausam*, **31**, 551-560.

Arya SP (1988): Introduction to Micrometeorlogy. Academic Press, 307pp.

Babu MT, S Prasanna Kumar and DP Rao (1991): A subsurface cyclonic eddy in the Bay of Bengal. *Journal of Marine Research,* **49**, 404-410.

Basu S, SD Meyers and JJ O'Brien (2000): Annual and inter-annual sea level variations in the Indian Ocean form TOPEX/POSEIDON observations and ocean model simulations. *Journal of Geophysical Research,* **105**, 975-994.

Bhat GS (2001): Near surface atmospheric characteristics over the North Bay of Bengal during the Indian summer monsoon. *Geophysical Research Letter*, **28**, 987-990.

Bhat GS, S Gadgil, PV Hareeshkumar, SR Kalsi, P Madusoodanan, VSN Murty, CVK Prasada Rao, V Ramesh Babu, LVG Rao, M Ravichandran, KG Reddy, P Sanjeeva Rao, D Sengupta, DR Sikka, J Swain and PN Vinayachandran (2001): BOBMEX - the Bay of Bengal Monsoon Experiment. *Bulletin of American Meteorological Society,* **82**, 2217-2243.

Bottomley M., CK Folland, J Hsiung, RE Newell and DE Parker (1990): 'Global ocean surface temperature atlas'. A joint project of the UK Meteorological Office and MIT.

Brandt P, L Stramma, F Schott, J Fischer, M Dengler and D Quadfasel (2002): Annual Rossby waves in the Arabian Sea from TOPEX/POSEIDON altimeter and *insitu* data. *Deep Sea Research* II, **49**, 1197-1210.

Bruce JG (1973): Large scale variations of Somalia current during the southwest monsoon. *Deep-Sea Research*, **20,** 837-846.

Bruce JG (1979): Eddies off the Somali coast during the southwest monsoon. *Journal of Geophysical Research,* **84**, 7742-7748.

Bruce JG (1983): The wind field in the western Indian Ocean and related ocean circulation. *Monthly Weather Review*, **111**, 1442-1453.

Bruce JG and WH Beatty (1985): Some observations of the coalescing of the Somali eddies and a description of the Socotra eddy. *Oceanologia Acta*, **78**, 207-219.

Bruce JG, DR Johnson and JC Kindle (1994) Evidence for eddy formation in the eastern Arabian Sea during northeast monsoon. *Journal of Geophysical Research,* **99**, 7651-7664.

Bruce JG, JC Kindle, LH Kantha, JL Kerling and JF Bailey (1998): Recent observations and modeling in the Arabian Sea Laccadive High region. *Journal of Geophysical Research,* **103**, 7593– 7600.

Bryan K (1969): Climate and the ocean circulation: III The Ocean Model. *Monthly Weather Review*, **97**, 806-827.

Cadet DL and BC Diehl (1984): Inter-annual variability of surface fields over Indian Ocean during recent decades. *Monthly Weather Review*, **112**, 1921-1935.

Cane M (1980): On the dynamics of equatorial currents, with application to the Indian Ocean. *Deep Sea Research*, **27A**, 525-544.

Chelton DB and MG Schlax (1996): Global observations of oceanic Rossby waves. *Science*, **272**, 234-238.

Clarke AJ and X Liu (1993): Observations and dynamics of semi-annual and annual sea levels near the eastern equatorial Indian Ocean boundary. *Journal of Physical Oceanography*, **23**, 386-399.

Cutler AN and JC Swallow (1984): Surface currents of the Indian Ocean (to 25°S, 100°E): compiled from historical data archived by the Meteorological Office, Bracknel, UK, Rep-187, 8pp, 36 charts, institute of Oceanology Science, Wormley, England.

Denman KL (1973): A time-dependent model of the upper ocean. *Journal of Physical Oceanography,* **13**, 173-184.

Denman KL and M Miyake (1973): Upper layer modification at ocean station Papa: observations and simulation. *Journal of Physical Oceanography,* **3**, 185-196.

Düing W (1970): The Monsoon Regime of the Currents in the Indian Ocean, East-West Center press, Honolulu, 68pp.

Düing W and A Leetma (1980): Arabian Sea cooling: A preliminary heat budget, *Journal of Physical Oceanography,* **10**, 307-312.

Düing W and F Schott (1978): Measurements in the source current of the Somali Current during monsoon reversal. *Journal Physical Oceanography*, **8**, 278-289.

Düing W and KH Szekielda (1971): Monsoonal response in the western Indian Ocean. *Journal of Geophysical Research,* **76**, 4181-4187.

Durand F, SR Shetye, J Vialard, D Shankar, SSC Shenoi, C Ethe and G Madec (2004): Impact of temperature inversions on SST evolution in the South-Eastern Arabian Sea during the pre-summer monsoon season. *Geophsyical Research Letters,* **31**, L01305, DOI:10.10.29-2003,GL018906.

Evans, RH and OB Brown (1981): Propagation of thermal fronts in the Somali Current system. *Deep Sea Research.* **28**, 521-527.

Feng M and G Meyers (2003): Interannual variability in the tropical Indian Ocean: A two-year time scale of IOD. *Deep-Sea Research,* in press.

Feng M, G Meyers and S Wijffels, (2001): Interannual upper ocean variability in the tropical Indian Ocean. *Geophysical Research Letter,* **28,** 4151–4154.

Findlater J (1971): Mean monthly airflow at low levels over the western Indian Ocean. *Geophysical Memoirs*, **115**, 55.

Fischer J, F Schott and L Stramma (1996): Currents and transports of the Great Whirl-Socotra Gyre system during the summer monsoon, August 1993. *Journal of Geophysical Research*, **101**, 3573-3587.

Flagg CA and HS Kim (1998): Upper ocean current in the northern Arabian Sea from shipboard ADCP measurements collected during the 1994-1996 U.S. JGOFS and ONR Programs. *Deep Sea Research II*, **45**, 1917-1959.

Gadgil S, PV Joseph and NV Joshi (1984): Ocean - Atmosphere coupling over monsoon regions. *Nature*, **312**,141-143.

Godfrey JS, A Alexiou, AG Ilahude, DM Legler, ME Luther, JP.McCreary, GA Meyers, K Mizuno, RR Rao, SR Shetye, JH Toole, and S Wacongne (1995): The role of the Indian Ocean in the Global Climate System: Recommendations regarding the Global Ocean Observing System. Report of the Ocean Observing System Development Panel, Texas A&M Univ., College Station, TX, *USA Review,* **111**, 46-59.

Gopalan AKS, VV Gopalakrishna, MM Ali and R Sharma (2000): Detection of Bay of Bengal eddies from TOPEX and *insitu* observations. *Journal of Marine Research,* **58**, 721-734.

Graham NE and TP Barnett (1987): Sea surface temperature, surface wind divergence and convection over tropical oceans. *Science*, **238**, 657-659.

Han W (1999): Influence of salinity on dynamics, thermodynamics and mixed-layer physics in the Indian Ocean. Ph.D thesis, Nova Southeastern university, Florida , USA.

Han W, JP McCreary Jr, DLT Anderson and AJ Mariano (1999): On the dynamics of the eastward surface jets in the equatorial Indian Ocean. *Journal of Physical Oceanography,* **29**, 2191-2209.

Han W and PJ Webster (2002): Forcing Mechanisms of Sea Level Interannual Variability in the Bay of Bengal. *Journal of Physical Oceanography*, **32,** 216-239.

Hareesh Kumar PV (1994): "Thermohaline variability in the upper layers of Arabian Sea". Ph. D Thesis. Cochin University of Science & Technology, Cochin, 113 pp.

Hareesh Kumar PV and B Mathew (1997): On the heat budget of the Arabian Sea. *Meteorology and Atmospheric Physics*, **62**, 215-224.

Hareesh Kumar PV, B Mathew and P Madhusoodanan (1996): Upper oceanic variability off Cochin during pre-monsoon heating regime. *Oebalia*, **22**, 119-129.

Hareesh Kumar PV, CVK Prasada Rao, J Swain and P Madhusoodanan (2001): Intra-seasonal oscillations in the central Bay of Bengal during summer monsoon 1999. *Current Science*, **80**, 786-790.

Hareesh Kumar PV and KV Sanilkumar (2004): Long period waves in the coastal regions of the north Indian Ocean. *Indian Journal of Marine Sciences*, **33**, 150-154.

Hastenrath S and PJ Lamb (1979): Climatic atlas of the Indian Ocean, Part I: Surface climate and atmospheric circulation. University of Wisconsin Press, Madison, USA.

Hastenrath, S and L Greischar (1989): Climatic atlas of the Indian Ocean, Part III: Upper-ocean structure. University of Wisconsin Press, Madison, USA.

Hellermann S and M Rosenstein (1983): Normal monthly wind stress over the world ocean with error estimates. *Journal of Physical Oceanography*, **13**, 1093-1105.

Hitney HV (1985): Tropospheric radio propagation assessment. *IEEE proceedings,* **73**, 265-283.

Holt T and Sethuraman (1987): A study of mean boundary layer structures over the Arabian sea and Bay of Bengal during active and break monsoon periods. *Boundary layer meteorology,* **38**, 73-94.

Jensen TG (1990): A numerical study of the seasonal variability of the Somali Current. PhD dissertation, Florida State University, Tallahassee, Florida, USA.

Jerlov NG (1968): Optical Oceanography (Elsevier, London), 194pp.

Joseph MG, PV Hareesh Kumar and B Mathew (1990): Short term pre-onset southwest monsoonal transformations in upper western equatorial Indian Ocean. *Indian Journal of Marine Sciences*, **19**, 251-256.

Joseph PV (1990a): Warm pool over the Indian Ocean and Monsoon Onset. *Tropical Ocean-atmosphere news letter*, **53**, 1-5.

Joseph PV (1990b): Monsoon variability in relation to equatorial trough activity over Indian and West Pacific Oceans. *Mausam*, **41**, 291-296.

Joseph PV and PV Pillai (1984): Air-Sea interaction over north Indian Ocean – Part I: Inter-annual variations of sea surface temperature and Indian summer monsoon rainfall. *Mausam*, **35**, 323-330.

Joseph PV and Raman (1966): Existence of low-level westerly Jet stream over peninsular India. *Indian Journal of Meteorology and Geophysics*, **39**, 360-362.

Joseph PV, JE Eischeid and RJ Pyle (1994): Interannual variability of the onset of the Indian summer monsoon and its association with atmospheric features, El Nino and sea surface temperature anomalies. *Journal of Climate*, **7**, 81-105.

Josey SA, EC Kent, PK Taylor (1999): New insights into the ocean heat budget closure problem from analysis of SOC air-sea flux climatology. *Journal of Climate*, **12**, 2856-2880.

Kalnay E, M Kanamitsu, R Kistler, W Collins, D deaven, L Gandin, M Iredell, S Saha, G White, J Woollen, Y Zhu, A Leetmaa, R Reynolds, M Chelliah, W Ebisuzaki, W Higgins, J Janowiak, KC Mo, C Ropelewski, J Wang, Roy Jenne and Dennis Joseph (1996): The NCEP/NCAR 40 year reanalysis project. *Bulletin of American Meteorological Society*, **77**, 437-471.

Kato H and OM Phillips (1969): On the penetration of a turbulent layer into stratified fluid. *Journal of Fluid Mechanics*, **37**,643-655.

Kershaw R (1988): The effect of sea surface temperature anomaly on a prediction of the south-west monsoon over India. *Quarterly Journal of Royal Meteorological Society*, **114**, 325-345.

Kindle JC and JD Thompson (1989): The 26- and 50- days oscillation in the western Indian Ocean: Model Results. *Journal of Geophysical Research,* **94**, 4721-4736.

Kraus EB and JS Turner (1967): A one-dimensional model of the seasonal thermocline: II, The general theory and its consequences. *Tellus*, **19**, 98-106.

Kumar SP and AS Unnikrishnan (1995): Seasonal cycle of temperature and associated wave phenomena in the upper layers of the Bay of Bengal. *Journal of Geophysical Research,* **100**, 13585-13593.

Lee CM, BH Jones, KH Brink and AS Fischer (2000): The upper ocean response to monsoonal forcing in the Arabian Sea: seasonal and spatial variability. *Deep Sea Research II*, **47**, 1177-1226.

Leetmaa A (1972): The response of the Somali Current to the southwest monsoon of 1970. *Deep Sea Research,* **19**, 397-400.

Leetmaa A (1973): The response of the Somali Current at 2°S to the southwest monsoon of 1971. *Deep Sea Research,* **20**, 319-325.

Legeckis R (1987): Satellite observations of a western boundary current in the Bay of Bengal. *Journal of Geophysical Research*, **92**, 12974-12978.

Levitus S and TP Boyer (1994): World ocean atlas, Vol.4: Temperature. NOAA Atlas NESDIS4. US Dept. of Commerce, Washington DC, USA.

Lighhill MJ (1969): Dynamic response of the Indian Ocean to the onset of the southwest monsoon. *Philosophical Transactions of Royal Society*. **A265**, 45-92.

Lukas R, E Lindstrom (1991): The mixed layer of the western equatorial Pacific Ocean. *Journal of Geophysical Research*, **96**(Supplement), 3343-3358.

Luther ME and JJ O'Brien (1985): A model of the seasonal circulation in the Arabian Sea forced by observed winds. *Progress in Oceanography* , **14**, 353-385.

Luther ME, JJ O'Brien and AH Meng (1985): Morphology of the Somali Current system during the southwest monsoon, in coupled Ocean-Atmosphere Models, edited by JCJ. Nihoul, Elsevier Science, New York, pp.405-437.

Mathew B (1981): Studies on upwelling and sinking in the seas around India. Ph.D Thesis 159pp.

Mathew B, PV Hareesh Kumar and RR Rao (2003): Mixed layer variability at selected locations in the Arabian Sea during pre and summer monsoon seasons: Observations and simulations. *Mausam*, **54,** 917-928.

McCreary JP, W Han, D Shankar and SR Shetye (1996): Dynamics of the East India Coastal Current.2. Numerical solutions. *Journal of Geophysical Research,* **101**, 13993-14010.

McCreary JP, PK Kundu and RL Molinari (1993): A numerical investigation of dynamics, thermodynamics and mixed-layer processes in the Indian Ocean. *Progress in Oceanography,* **31**, 181-244.

Mellor GL and PA Durbin (1975): The structure and dynamics of the ocean surface mixed layer. *Journal of Physical Oceanography*, **5**, 718-728.

Miller JR (1976): The salinity effect in a mixed-layer ocean model. *Journal of Physical Oceanography*, **6**, 29-35.

Mohanty UC and S Das (1986): On the structure of the atmosphere during suppressed and active periods of convection over the Bay of Bengal. *Proceedings of Indian National Science Academy,* **52**, 625–640.

Moore DW and SGH Philander (1977): Modeling of the tropical oceanic circulation, The Sea: Ideas and Observations in the Study of the Sea, edited by E. D. Goldberg et al, Wiley Inter-science New York, **6**, 319-369.

Morrow R and F Birol (1997): Variability in the south-east Indian Ocean from altimetry - forcing mechanisms for the Leeuwin Current. *Journal of Geophysical Research,* **103,** 18529-18544.

Murtugudde R, JP McCreary Jr and AJ Busalacchi (2000) Oceanic processes associated with anomalous events in the Indian Ocean with relevance to 1997-1998. *Journal of Geophysical Research,* **105**, 395-3306.

Murty PGK and PV Hareesh Kumar (1991). Response of coastal waters off Karwar to a deep depression. *Continental Shelf Research*, **11**, 239-250.

Mysak LA and GJ Mertz (1984): A 40- to 60- day oscillation in the source region of the Somali Current during 1976. *Journal of Geophysical Research,* **89,** 711-715.

Niiler PP and Kraus EB (1977): "One dimensional models", In: Modeling and prediction of the upper layer of the oceans. E B Kraus (Ed.) (Pergamon Press, New York) 143-172.

Nimmi R Nair, N Mohankumar and RK Shukla (1997): The boundary layer characteristics over the Arabian Sea. Research Report. RR No. 9/97.

O'BrienJJ and HE Hurlburt (1974): An equatorial jet in the Indian Ocean theory. *Science*, **184**, 1075-1077.

Parthasarathy B, AA Munot, and DR Kothawale (1994): All India monthly and seasonal rainfall series:1871-1993. *Theoretical and Applied Climatology*, **49**, 217-224.

Perigaud C and P Delecluse (1992): Annual sea level variations in the Southern Tropical Indian Ocean from Geosat and shallow-water simulations. *Journal of Geophysical Research,* **97**, 169-178

Picaut J, T Delcroix (1995): Equatorial wave sequence associated with warm pool displacements during the 1986-1989 El Nino-La Nina. *Journal of Geophysical Research*, **100(C9)**, 169-178.

Pickard GL and WJ Emery (1982): Descriptive Physical Oceanography An Introduction. Pergamon Press, 249pp.

Pollard JF, CNK Mooers and JC Van Leer (1973): Observation and simulation of storm induced mixed layer deepening. *Journal of Physical Oceanography*, **8**, 582-599.

Potemra JT, ME Luther and JJ O'Brien (1991) The seasonal circulation of the upper ocean in the Bay of Bengal. *Journal of Geophysical Research,* **96**, 12667-12683.

Price JF, RA Weller and R Pinkel (1986): Diurnal cycling: Observations and models of the upper ocean response to diurnal heating, cooling and wind mixing. *Journal of Geophysical Research*, **91**, 8411-8427.

Quadfasel DR and F Schott (1982): Water-mass distributions at intermediate layers off the Somali coast during the onset of the Southwest Monsoon, 1979. *Journal of Physical. Oceanography, 12*, 1358-1372.

Quadfasel DR and F Schott (1983): Southward subsurface flow below the Somali Current. *Journal of Geophysical Research,* **88,** 5973-5979.

Quadfasel DR and JC Swallow (1986): Evidence for 50-day period planetary waves in the South Equatorial Current of the Indian Ocean. *Deep Sea Research,* **33**, 1307-1312.

Rajeevan M, DS Pai, SK Dikshit and RR Kelkar (2004): IMD's new operational models for long-rangeforecast of southwest monsoon rainfall over India and their verification for 2003. *Current Science*, **86**, 422-431

Raman CRV, YP Rao SK Subrahamaniyam and ZE Shaikh (1978): Wind shear in a monsoon depression. *Nature*, **275**, 53-53.

Ramanathan Y (1978): A study of the atmospheric boundary layer over the Arabian Sea from ISMEX-1973 data. *Indian Journal of Hydrology and Geophysics*, **29**, 613-654.

Ranjit Singh (1983): Study of sea Surface Pressure, sea Surface Temperature and cloudiness patterns over Indian ocean region in some contrasting South West monsoon rainfall in India – Part II. *Mausam*, **34**, 205-212.

Rao AS, SK Behera, Y Masumoto and T Yamagata (2002): Interannual variability in the subsurface tropical Indian Ocean. *Deep-Sea Research,* **49B,** 1549–1572.

Rao DP and VSN Murty (1992): Variability of temperature and water vapour content in the lower troposphere of the northern Bay of Bengal during MONTBLEX-90. In: *Proceedings of workshop on preliminary results of MONTBLEX held at IISC Bangalore during 16-17 January, 1992*, DST & MST, Technology Bhavan, New Delhi, 185pp.

Rao DS and RR Rao (1986): A case study of the genesis of a monsoon low and the thermal structure of the upper northern Bay of Bengal During Monex-79. *Mahasagar-Bulletin of NIO*, **19**, 1-9.

Rao KG and BN Goswami (1988): Interannual variations of SST over the Arabian Sea and the Indian monsoon: A new perspective. *Monthly Weather Review*, **116**, 558-568.

Rao RR (1986): Cooling and deepening of the mixed layer in the central Arabian Sea during MONSOON-77: Observations and simulations. *Deep-Sea Research*, **33**, 1413-1424.

Rao RR (1990): Observed Variability in the thermal response of the upper north central Arabian Sea to the forcing of onset vortex during summer monsoon experiments. *Mausam*, **41,** 439-444.

Rao RR, VV Gopalakrishna and SV Babu (1981): A case study on the northern Bay of Bengal sub-surface thermal structure and ocean mixed layer depth in relation to surface energy processes. *Mausam*, **32**, 85-92.

Rao RR, PV Hareesh Kumar and B Mathew, (1994): Near surface heating in the Arabian Sea during the pre-onset regime of MONEX-79. *Meteorology and Atmospheric Physics*, **53**, 19-31.

Rao RR and B Mathew (1990): A case study on the mixed layer variability in the south central Arabian Sea during the onset phase of MONEX-79. *Deep Sea Research*, **37**, 227-243.

Rao RR, B Mathew and PV Hareesh Kumar (1993): A summary of results on thermohaline variability in the upper layers of the east central Arabian Sea and Bay of Bengal during summer monsoon experiments. *Deep Sea Research*, **40**, 1647-1672.

Rao, RR, RL Molinari and JF Festa (1991): Surface meteorological and subsurface oceanographic atlas of the tropical Indian Ocean. NOAA Tech. Memo, ERL-AOML-69.

Rao RR and R Sivakumar (1999): On the possible mechanisms of the evolution of a mini-warm pool during the pre-summer monsoon season and the genesis of of onset vortex in the south eastern Arabian Sea. *Quarterly Journal of Royal Meteorological Society*, **125**, 787-809.

Rao RR, SVS Somanadhan SSVS Ramakrishna and R Ramanadham (1987): A case study on the genesis of a monsoon depression in the northern Bay of Bengal during Monsoon-77 experiment. *Mausam*, **38**, 387-394.

Rao YP (1976): The southwest monsoon. Indian Meteorological Department Monograph, Synoptic Meteorology, 1/1976, Indian Meteorological Department, 367 pp.

Sadhuram Y, V Ramesh Babu, VV Gopalakrishna and MSS Sharma (1991): Association between Pre-monsoonal Sea Surface Temperature anomaly field in the eastern Arabian sea and subsequent monsoon rainfall over the west coast of India. *Indian Journal of Marine Sciences*, **20**, 106-109.

Saji NH, BN Goswami, PN Vinayachandran and T Yamagata (1999): A dipole mode in the tropical Indian Ocean. *Nature*, **401**, 360-363.

Saji NH and T Yamagata (2003): Structure of SST and Surface Wind Variability during Indian Ocean Dipole Mode Events: COADS Observations. *Journal of Climate*, **16**, 2735-2751

Sanilkumar KV, P Madhusoodanan, MG Joseph and B Mathew (1991): Mixed layer variability in east central Arabian Sea during the onset phase of MONEX-79". *Deep Sea Research*, **37**, 227-243.

Sanilkumar KV, PV Hareesh Kumar and MX Joseph (1993): Observations and simulations of the mixed layer characteristics off Bombay, west coast of India during the summer monsoon of 1988. *Estuarine Coastal and Shelf Sciences*, **36**, 59-69.

Sanilkumar KV, PV Hareesh Kumar, JK Joseph and JK Panigrahi (2004): Arabian Sea mini warm pool in the eastern Arabian Sea during May 2000. *Current Science*, **86**, 180-184

Sanilkumar KV, TV Kuruvilla, D Jogendranath and RR Rao (1997): Observations of the western boundary current of the Bay of Bengal from a hydrographic survey during March 1993. *Deep Sea Research*, **44**, 135-145.

Sanilkumar KV, P Madhusoodanan, MG Joseph and B Mathew (1991): Mixed layer variability in east central Arabian Sea during premonsoon season of 1979. *Indian Journal of Marine Sciences*, **20**,239-243.

Sanilkumar KV, N Mohankumar, MX Joseph and RR Rao (1994): Genesis of meteorological disturbances and thermohaline variability of the upper layers in the head of the Bay of Bengal during MONsoon Trough Boundary Layer Experiment. *Deep Sea Research*, **41**,1569-1581.

Schott F (1983): Monsoon response of the Somali Current and the associated upwelling. *Progressive Oceanography*, **12**, 1343-1357.

Schott F, M Fieux, J Kindle, J Swallow and R Zantopp (1988): The boundary currents east and north of Madagascar, 2, Direct measurements and model comparisons. *Journal of Geophysical Research*, **93**, 4963-4974.

Schott F and JP McCreary Jr. (2001): The monsoon circulation of the Indian Ocean. *Progress in Oceanography*, **51**, 1-123.

Schott F and D Quadfasel (1982): Varaibilty of the Somali Current and associated upwelling. *Progress in Oceanography*, **12**, 357-381.

Schott F, J Swallow and M Fieux (1990): The Somali Current at the equator: annual cycle of currents and transports in the upper 1000 m and connection to neighbouring latitudes. *Deep sea Research*, **37A**, 1825-1848.

Seetharamayya P and A Master (1984): Observed air-sea interface conditions and a monsoon depression during MONEX-1979. *Archives for Meteorology Geophysics and Bioclimatology*, **33**, 61-67.

Semyon AG, JA Carton, and R Murtugudde (2001): Anomalous surface currents in the tropical Indian Ocean. *Geophysical Research Letters,* **28,** 4207-4210.

Sengupta D, R Senan and BN Goswami (2001): Origin of intra-seasonal variability of circulation in the tropical central Indian Ocean. *Geophysical Research Letter*, **28**, 1267-1270, 2001.

Shankar D (1998): Low frequency variability of sea level along the coast of India. PhD thesis, Goa University, Goa, India.

Shankar D (2000): Seasonal cycle of sea level and currents along the coast of India. *Current Science*, **78**, 279-288.

Shankar D, VV Gopalakrishna, SSC Shenoi, F Durand, SR Shetye, CK Rajan, Z Johnson, N Araligidad and GS Michael (2004): Observational evidence for westward propagation of temperature inversions in the southeastern Arabian Sea. *Geophsyical Research Letters,* **31**, L08305, DOI:10.1029-2004 GL019652.

Shankar D, JP McCreary, W Han and SR Shetye (1996), Dynamics of the East India Coastal Current1; Analytical solutions forced by interior Ekman pumping and local alongshore winds. *Journal of Geophysical Research*, **101**, 13975-13991.

Shankar D and SR Shetye (1997): On the dynamics of the Lakshadweep high and low in the southeastern Arabian Sea. *Journal of Geophysical Research,* **102**, 12551-12562.

Shea DJ, KE Trenberth and RW Reynolds (1990): A global monthly sea surface temperature climatology. Tech. Note TN-345+STR. NCAR, Boulder, Colorado, USA.

Shenoi SSC, D Shankar, and SR Shetye (1999): The sea surface temperature high in the Lakshadweep sea before the onset of the southwest monsoon. *Journal of Geophysical Research*, **104**, 703-712.

Shetye SR (1986): A model study of the seasonal cycle of the Arabian Sea surface temperature. *Journal of Marine Research.* **44**, 521-542.

Shetye SR, AD Gouveia, D Shankar, SSC Shenoi, PN Vinayachandran, D Sundar, GS Michael and G Nampoothiri (1996): Hydrography and circulation in the western Bay of Bengal during the northeast monsoon. *Journal of Geophysical Research*, **101**, 14011-14025.

Shetye SR, AD Gouveia, SSC Shenoi, D Sundar, GS Michael and G Nampoothiri (1993): The western boundary current of the seasonal subtropical gyre in the Bay of Bengal. *Journal of Geophysical Research*, **98**, 945– 954.

Shetye SR, AD Gouveia, SSC Shenoi, D Sunder, GS Michael, AM Almeida and K Santanam (1990): Hydrography and circulation off the west coast of India during the southwest monsoon 1987. *Journal of Marine Research.* **48**, 359-378.

Shetye SR, SSC Shenoi, AD Gouveia, GS Michael, D Sundar and G Nampoothiri (1991): Wind-driven coastal upwelling along the western boundary of the Bay of Bengal during the southwest monsoon. *Continental Shelf Research*, **11**, 1397-1408.

Shi W, JM Morrison, E Bohm and V Manghnani (2000): The Oman upwelling zone during 1993, 1994 and 1995. *Deep Sea Research II*, **47**, 1227-1247.

Shukla J (1975): Effect of Arabian Sea surface temperature anomaly on Indian summer monsoon, a numerical experiment with the GFDL model. *Journal of Atmospheric Sciences*, **32**, 503-511.

Shukla J and BM Misra (1977): Relationships between sea surface temperature and wind speed over central Arabian Sea and monsoon rainfall over India. *Monthly Weather Review*, **105**, 998-1002.

Stull RB (1993): An introduction to boundary layer meteorology. Kluwer Academic publishers.

Stull RB (1997): An introduction to boundary layer meteorology. Kluwer Academic Publishers, 664 pp.

Stull R (2000):Meteorology for Scientists and Engineers. Brooks/Cole press, 502 pp

Subrahmanyam B (1999): A study of the Indian Ocean circulation using satellite observations and model simulations. Ph.D thesis. Southampton University.

Subrahmanyam B, IS Robinson, JR Blundell and PG. Challenor (2001): Indian Ocean Rossby waves observed in TOPEX/POSEIDON altimeter data and in model simulations. *International Journal of Remote Sensing*, **22**, 141-167.

Subrahmanyam B, V Ramesh Babu, VSN Murty and LV Gangadhara Rao (1996): Surface circulation off Somali and western equatorial Indian Ocean during summer monsoon of 1988 from Geosat altimeter data. *International Journal Remote Sensing*, **17**, 761-770.

Swallow JC and JC Bruce (1966): Current measurements off the Somali coast during the southwest monsoon of 1964. *Deep Sea Research*, **13**, 861-888.

Swallow JC and M Fieux (1982): Historical evidence for two gyres in the Somali Current, *Journal of Marine Research*, **40**, 747-755.

Swallow JC, M Fieux and F Schott (1988): The boundary currents east and north of Madagascar, 1, Geostrophic currents and transports. *Journal of Geophysical Research*, **93**, 4951-4962.

Swallow JC, RL Molinari, JG Bruce, OB Brown and RH Evans (1983): Development of near surface flow pattern and water mass distribution in the Somali Basin in response to the southwest monsoon of 1979. *Journal of Physical Oceanography*, **13**, 1398-1415.

Thompson R (1976): Climatological numerical model of the surface mixed layer of the ocean. *Journal of Physical Oceanography*, **6**, 496-503.

Torrence C and GP Compo (1998): A practical guide to wavelet analysis. *Bulletin of American Meteorological Society*, **79**, 61-78.

Turner JS (1969): A note on wind mixing at the seasonal thermocline. *Deep-Sea Research*, **19**, 297-300.

UNESCO (1988): River inputs to ocean systems: status and recommendations for research. Unesco Technical Papers in Marine Science, No.55, Final reprt of SCOR Working Group 46, Paris, 25pp.

Unnikrishnan AS, S Prasanna Kumar and G Navelkar (1997): Large-scale processes in the upper layers of the Indian Ocean inferred from temperature climatology. *Journal of Marine Research*, **55**, 93-95.

Vinayachandran PN, Y Masumoto, T Mikawa and T Yamagata (1999): Intrusion of the southwest monsoon current into the Bay of Bengal. *Journal of Geophysical Research*, **104**, 11077-11085.

Vinayachandran PN and SR Shetye (1991): The warm pool in the Indian Ocean. *Proceedings Indian Academy of Sciences (Earth and Planetary Sciences),* **100,** 165-175.

Vinayachandran PN, SR Shetye, D Sengupta and S Gadgil (1996): Forcing mechanisms of the Bay of Bengal circulation. *Current Science,* **71,** 753-763.

Vinayachandran PN and T Yamagata (1998): Monsoon response of the sea around Srilanka: generation of domes and anticyclonic vortices. *Journal of Physical Oceanography,* **28,** 1946-1960.

Weare BC (1979): A statistical study of the relationship between ocean surface temperatures and Indian monsoon. *Journal of Atmospheric Science,* **26,** 2279-2291.

Webster PJ and collaborators (2000): An overview of the Joint Air-sea Monsoon Interaction Experiment JASMINE.

Weller RA, MA Baumgartner, SA Josey, AS Fischer and JC Kindle (1998): Atmospheric forcing in the Arabian Sea during 1994-1995: observations and comparisons with climatology models. *Deep Sea Research,* **45,** 1961-1999.

Wirth A, J Willebrandt and F Schott (2002): Variability of the Great Whirl from observations and models. *Deep-Sea Research II,* **49,** 1279–1295.

Woodberry KE, ME Luther and JJ O'Brien (1989): The wind-driven seasonal circulation in the southern tropical Indian Ocean. *Journal of Geophysical Research,* **94,** 17985-18002.

Wyrtki K (1971): Oceanographic Atlas of the International Indian Ocean Expedition. National Science Foundation, Washington, D C, 531pp.

Wyrtki K (1973b): Physical Oceanography of the Indian Ocean. In B. Zeitschel and S. A. Gerlach, Editors, Biology Lee CM, Johns BHof the Indian Ocean, volume 3of Ecological studies: analysis and synthesis, pages 18-36. Chapman and Hall Limited, London.

Wyrtki K (1973): An equatorial jet in the Indian Ocean, *Science,* **181,** 262-264.

Xie SP, H Annamalai, FA Schott and JP McCreary Jr (2002): Structure and mechanisms of south Indian Ocean climate variability. *Journal of Climate,* **15,** 864-878.

Yu L, JJ O'Brien and J Yang (1991): On the remote forcing of the circulation in the Bay of Bengal. *Journal of Geophysical Research,* **96,** 20449-20454 .